INFORMATION TO USERS

This manuscript has been reproduced from the microfilm master. UMI films the text directly from the original or copy submitted. Thus, some thesis and dissertation copies are in typewriter face, while others may be from any type of computer printer.

The quality of this reproduction is dependent upon the quality of the copy submitted. Broken or indistinct print, colored or poor quality illustrations and photographs, print bleedthrough, substandard margins, and improper alignment can adversely affect reproduction.

In the unlikely event that the author did not send UMI a complete manuscript and there are missing pages, these will be noted. Also, if unauthorized copyright material had to be removed, a note will indicate the deletion.

Oversize materials (e.g., maps, drawings, charts) are reproduced by sectioning the original, beginning at the upper left-hand corner and continuing from left to right in equal sections with small overlaps.

Photographs included in the original manuscript have been reproduced xerographically in this copy. Higher quality 6" x 9" black and white photographic prints are available for any photographs or illustrations appearing in this copy for an additional charge. Contact UMI directly to order.

ProQuest Information and Learning
300 North Zeeb Road, Ann Arbor, MI 48106-1346 USA
800-521-0600

UMI®

NOTE TO USERS

This reproduction is the best copy available.

UMI®

DISSERTATION

LONG RANGE FORECASTING OF THE NILE RIVER FLOW USING LARGE SCALE OCEANIC ATMOSPHERIC FORCINGS

Submitted by

Ahmed Khalid Eldaw

Department of Civil Engineering

In partial fulfillment of the requirements

for the degree of Doctor of Philosophy

Colorado State University

Fort Collins, Colorado

Fall 2001

COLORADO STATE UNIVERSITY

August 21, 2001

WE HEREBY RECOMMEND THAT THE DISSERTATION PREPARED UNDER OUR SUPERVISION BY AHMED KHALID ELDAW ENTITLED LONG RANGE FORECASTING OF THE NILE RIVER FLOW USING LARGE SCALE OCEANIC-ATMOSPHERIC FORCINGS BE ACCEPTED AS FULFILLING IN PART REQUIREMENTS FOR THE DEGREE OF DOCTOR OF PHILOSOPHY.

Committee on Graduate Work

Adviser

Co-Adviser

Department Head

ABSTRACT OF THE DISSERTATION

LONG RANGE FORECASTING OF THE NILE RIVER FLOW USING LARGE SCALE OCEANIC ATMOSPHERIC FORCINGS

Forecasting the Nile River flow is of vital interest for African nations such as Sudan and Egypt. These nations use the Nile's water for agriculture and hydropower. An accurate forecast of water availability would be beneficial for efficient management of water resources facilities such as reservoirs and diversions. Any improvement in the forecast accuracy or increase in prediction horizon will have a significant influence on improving the water management in these nations.

This research makes intensive use of sea surface temperatures as predictors. Linear correlation analysis was used to establish the connection between the Nile River flows and the leading climatic indicators. Multiple linear regression, principal component regression, canonical correlation analysis and artificial neural network were used to develop the forecast models. The statistics for equations based on principal component analysis showed improvement in the forecasting accuracy over the equations developed using original variables. Multivariate models improved the performance measures over univariate models.

A crucial step in developing empirical formulae for long-range forecasting requires the selection of appropriate predictors. This dissertation has been guided by an objective

search among a large number of predictors. The sea surface temperature gradient between two locations (referred to as oscillation, dipole, or seesaw) emerged as stable and consistent predictors.

In comparison with the Atlantic and Indian Oceans, the Pacific Ocean shows the highest contribution to the variability of the Blue Nile River flows. Its contribution is as high as the contribution from the three oceans combined. The Nile River flows at Aswan, as expected, show similar patterns with lower adjusted R^2 magnitudes. The Atbara River shows higher response the large-scale variables, followed by the Blue Nile River, the Nile River at Aswan and the Sobat River.

The major contribution of this research is the development of further knowledge in the field of hydroclimatology, and in doing so, the development of long-range streamflow forecasting models. Future work includes the incorporation of the real time operation and investigation of the stable predictors in relation with large-scale phenomenon and other hydroclimatic variables. Further, tests should be on large rivers flows, such as the Mississippi and the Amazon.

Ahmed Khlaid Eldaw
Department of Civil Engineering
Colorado State University
Fort Collins, CO 80523
Fall, 2001

ACKNOWLEDGEMENTS

Accomplishing a Ph.D. in fact is not possible by the efforts of an individual alone. In the long process of finishing and writing a dissertation the support of many is required. I must apologize for not mentioning all of them who deserve my eternal gratitude. Firstly, all thanks are to ALLAH the merciful, for his compassion and mercy. Next, I am deeply indebted to my graduate committee for their guidance and support. I am particularly very thankful to Prof. Jose D. Salas, who remained my adviser for my Master's as well as Ph.D. program and his invaluable time and advice. I am extremely thankful to my co-adviser, Dr. Luis A. Garcia, whose support was very crucial during this research. I find myself in awe of his dedication to his students and his caring. I am honored to work under his supervision and to know him as a friend. I am also thankful to Prof. Maurice L. Albertson for agreeing to serve on my graduate committee at a very critical time, and for his invaluable advice and encouragement. I am thankful to Dr. Jorge A. Ramírez for his patience, advice and time. Thanks to my committee member Prof. Paul W. Mielke, Jr. for his comments and suggestions and Prof. Freeman M. Smith for serving in my Master's and Ph.D. graduate committees.

I am grateful to the Ministry of Irrigation and Water Resources of the Republic of the Sudan for funding my graduate studies both for my MS and Ph.D. and to my friends and staff in the ministry. Special thanks to the first undersecretary for his encouragement and being patient with my long absence. A special thanks to my father and mother,

brothers and sisters, relatives and friends, for their prayers and sacrifices. I would also like to acknowledge the Muslim community in the Fort Collins Islamic Center. Thanks to my friends at the Hydrologic Computing Laboratory and the CSU-IDS for providing a friendly and cooperative research environment. Last but not least a very special thanks to my wonderful wife who deserves all my gratitude for showing extraordinary patience and support during the long time that took to complete this degree which kept me away from her and from many joyful moments with my son Mohammed.

To my parents, my wife, and to the joy of my life….. my son Mohammed

TABLE OF CONTENTS

LIST OF TABLES

LIST OF FIGURES

1. INTRODUCTION

1.1 General

Water availability is becoming a national and international concern. In many parts of the world, rapid population growth, urbanization, deforestation, and industrialization have increased the demand and competition for water even under normal flow conditions. The increasing demand for water is necessitating a change in approaches to water resources management. Human beings face the very real possibility of a serious water deficit in the future. Therefore, it is becoming increasingly critical to plan, design, and manage water resources systems carefully and intelligently. Water resources managers are faced with the responsibility of developing policies that help in the operation of these systems. Effective design of long-term policies will require an understanding of the existing relationship of climate to water resources, the nature of potential changes, the source of uncertainty, and the prospects for resolving the uncertainties. It was pointed out by Guetter and Georgakakas (1996), that the association of EL Niño Southern Oscillation (ENSO) with extra-tropical hydrologic processes carries considerable uncertainty due to continental and regional atmospheric-to-land surface forcing and feedback mechanisms that are unrelated to ENSO. A question of considerable importance for water resources management and environmental concerns is

whether floods and droughts can be related to long-lived oceanic and atmospheric anomalies occurring prior to these extreme hydrologic events.

Seasonal forecasting of river flows is important in water resources development for public safety, environmental issues, water management, and other purposes. Long-range forecasting of hydro-meteorological variables has recently become a popular and economically necessary exercise, commonly tackled by large-scale variables between predictands (the hydro-meteorological variables to predict) and predictors (the large-scale indices).

Recent advances in the understanding of global teleconnections between weather and climate make it feasible to extend the lead-time of streamflow forecasts further. Teleconnections are represented as statistical associations among climatic variables separated by large distances, (Zhang and Trimble, 1996). For decades the possibility of predicting hydro-meteorological variables has intrigued hydrologists, who are now beginning to understand the correlation between these various anomalies and changes in large-scale atmospheric circulation patterns. Large-scale circulation patterns are affected by ocean-atmospheric phenomena. A particularly a well-documented phenomenon is the EL Niño-Southern Oscillation (Piechota et al., 1998). Recently, there has been considerable interest in describing climate variability over the Pacific on decadal and longer time-scales. Many of these investigations have been motivated by the desire to understand the role of natural variability in explaining recent significant changes in the Pacific sea surface temperature (SST), for example, cooling in the North Pacific and warming in the tropical regions. Most of these studies have shown a strong teleconnection between a particular oceanic-atmospheric phenomenon in the tropical

Pacific Ocean, known as EL Niño-Southern Oscillation (ENSO) and the hydroclimatic variations in many places of the Globe. In fact, SST distribution over the world's oceans is now accepted to be one of the decisive factors that govern the level of global atmospheric activity. The monthly distributions of SST anomalies around the globe appear to directly influence the monthly anomalies of the global atmosphere general circulation (Pan and Oort, 1990). Therefore, it is important to study the spatial and temporal relationship of the Nile River flows with SST anomalies.

Ropelewski and Halpert's (1987) maps of harmonic analysis vectors suggest areas of ENSO-related precipitation over tropical Africa and South Africa. The equatorial eastern African region encompasses parts of Kenya, Uganda, Rwanda, Burundi and Tanzania, while the southern Africa region includes portions of all African nations south of latitude 15° S. This analysis does not suggest any large coherent areas of ENSO-related precipitation in the Sahel region. They attribute this to interannual variations in Sahelian rainfall which have been linked to Atlantic ocean SST anomaly patterns (e.g. Gray et al., 1993, 1994), and thus ENSO-precipitation relationships, if they exist, would be difficult to separate from the Atlantic SST relationships, (Ropelewski and Halpert, 1987). Further, they suggested ENSO-related African precipitation in these regions might have some predictability. Latif et al. (1999) investigated by means of atmosphere model experiments the role of Indian Ocean SST anomalies in driving eastern equatorial African rainfall anomalies during December-January 1997/98. They found that SST is an important factor in inforcing climate anomalies over eastern Africa. This link between the Indian Ocean SST and climate over eastern Africa provides some hope for seasonal climate forecasting in this region.

Currently few large-scale circulation indices have been identified to operate as predictors for the Nile River flows. Wang and Eltahir (1999) used the Bayesian theorem to develop a discriminate forecasting algorithm, and conditional categorical probabilities were used to describe the flood forecasting for the naturalized Nile River flow at Aswan. A predicted ENSO index was used as one of the Nile discharge predictors besides rainfall and persistence. However, the study presented here is looking for leading indices to forecast the Nile hydrology rather than using predicted indices that may encounter prediction errors. Eltahir (1996) determined that the ENSO cycle accounted for 25% of the natural variability in the Nile River. When equatorial SSTs are warm (EL Niño), there is a low probability (8%) of the annual Nile River flow being above normal. During periods of cold SSTs, there is a high probability (58%) of the annual Nile River flow being above normal. Influence from oceans on the Nile River flow has been documented by Eltahir (1996), Awadalla and Rousselle (2000), Amaraskera et al. (1997), and Wang and Eltahir (1999) suggesting a teleconnection between SST anomalies and the seasonal flows. Awadalla and Rousselle (2000) best model explains 63% of the variability of the Nile flood with a maximum lead period of three months prior to the flood peak (September).

The current research is divided into three general objectives. The first objective is to look for signals from global scale ocean-atmosphere climatic variables that can be related to the Nile River flow. Links between SST variability and seasonal Nile River flow can be expected because of the strong spatial coherence of SST anomalies which often persists for several months and can result in large anomalous heat fluxes from the sea to the atmosphere. The second objective is to identify consistent, robust, and stable

predictors for the Nile River flow and tributaries. The third objective is to set up a long lead forecast model for the seasonal streamflow of the Nile River that could be used by water resources planners. Predicting hydrological variables (e.g. streamflow) patterns on seasonal time scales requires a methodology that is capable of finding multivariate relationships given a set of predictors and predictand anomalies. In this study, linear and nonlinear approaches will be followed to construct a forecast model for seasonal streamflow. The Nile River was selected for this study because of its geographical extent and the number of countries it serves.

1.2 Description of the Problem

Survival in the Nile basin hinges on irrigated and rain-fed agriculture. Poor crop yields and water shortages in the last two decades (e.g. 1984, 1987) have brought considerable hardship to the region. The impact of droughts could be partially alleviated through better planning based on reliable long-range hydrological forecasts. To improve forecast skill, additional available information including sea surface temperature (SST), sea level pressure (SLP), oscillations (e.g. SOI, NAO, PDO), precipitation over the basin and past river flows should be incorporated into the forecasting process. Evidence suggests that global warming may lead to substantial changes in mean annual streamflows, the seasonal distribution of flows, and increase the possibility of extreme high or low flow conditions, (Miller, 1997).

Long range forecasts of the Nile River flow (July-October) have been crucial for proper agricultural planning and power generation in Sudan. Over the last one hundred years there have been considerable Nile River flow variations (Conway and Hulme, 1993). The variability of the flows in the Nile River is of vital interest to any of the ten

nations in its basin, (Eritrea, Ethiopia, Kenya, Tanzania, Uganda, Rwanda, Burundi, Zaire, Sudan, and Egypt). The variation in the Nile River flow can be illustrated by the fact that 80% of its annual flow occurs from August to October and only about 20% occurs during the remaining nine months.

The idea for this research stems from other studies that have identified the ENSO phenomenon as being an important factor in long-range climate forecasting. The mechanism by which the Pacific EL Niño is transmitted to the Nile basin hydrology is not fully understood, although its effects on the flow have been identified (e.g. Eltahir, 1996). It was shown that anomalously warm (cold) equatorial Pacific Ocean surface temperatures coincide with anomalously low (high) Nile River flow. However, not every low (high) flow in the Nile River is EL Niño (La Niña) induced. For example, the years 1913, 1915, 1940, 1979 and 1984 were low Nile River flow years and not EL Niño years. Likewise, the years 1917, 1929, 1946, and 1969 were high Nile River flow years and not classified as La Niña years (the referred classification for El Niño and La Niña was according to Fraedrich and Muller 1992). This doesn't mean that the ENSO doesn't influence the Nile Basin hydrology. It may be that it doesn't always influence the Nile hydrology in the same way. Other large-scale oceanic-atmospheric systems may exert a significant influence on the climate of the Nile basin as well. Therefore, more useful additional information may be discovered if ENSO conditions are taken into consideration along with other large-scale climate systems that affect the basin hydrology. This will help to find signals that may account for the remaining variability of the Nile River flow which may improve the forecasting skill and increase the forecasting lead time.

In most of the previous studies i.e. Eltahir (1996) and Awadalla and Rousselle (2000) only a single time series and a limited number of predictors were used. Awadalla and Rousselle forecasted the Nile River flow for three months lead-time before the occurrence of the flood peak (September) and Eltahir used concurrent SST values to relate the Nile flow to SST. Wang and Eltahir (1999) adopted the forecasted ENSO indicator to forecast the Nile River flow. More information, a longer forecasting horizon and better forecasting skills will be beneficial for water resources planners and managers.

The aim of this study is to improve the accuracy of the flow forecast and to extend the forecast lead time of the Nile River flows by incorporating new regions of SST in the three oceans and other predictors such as the Guinea precipitation in Western Africa. This study focuses on extending the forecast horizon beyond the previously used time scales (i.e. beyond 3 months). The approach that was taken in this research uses correlation analysis, linear and nonlinear methods and incorporates other potential sources of information. Incorporating several sources of information seems to improve the length of the forecast range and its reliability.

In the last decade, a nonlinear empirical modeling technique has emerged in the field of artificial intelligence; neural network models are now widely applied to numerous scientific fields. One of the objectives of the present work is to study the applicability of artificial neural network (ANN) in the Nile basin hydrology prediction. The research presented here evaluates seasonal forecasting of the Nile River flow. Large scale oceanic and atmospheric variables will be used as predictors. The main focus of the research is to obtain a reliable long-range hydrological forecast (the longest lead period attainable).

1.3 Research Objectives

Many hydroclimatic forcing mechanisms such as atmospheric and ocean circulation, atmospheric pressure, and air and sea-water temperature, influence river basin hydrology. The main goal of the proposed research is to improve the forecasting of the Nile River flow system (skill and lead time horizon) by using a number of large-scale atmospheric ocean indicators such as, sea surface temperature (SST), sea level pressure (SLP) and by using linear and non-linear models. The aim is long range forecasting, i.e. several months to a year or more in advance. The specific objectives of this research could be summarized as follows:

1. To investigate the connections that may exist between large-scale climatic variables such as sea surface temperature, sea level pressure, southern oscillation index (SOI), and North Atlantic oscillation (NAO) and the Nile River system seasonal flow data.
2. To identify consistent, stable and robust predictors at the main sites on the Nile River guided by an objective search.
3. To identify the contribution of the different oceans in the variability of the Nile River flows.
4. To investigate the capability (potential) of using linear models to improve the long range forecasting of the Nile River flows. For this purpose, multiple linear regression (MLR) and principal component analysis (PCA) will be utilized for developing forecast models of the Nile River flows at several sites in the system.
5. To investigate the capability (potential) of using multivariate models to improve long-range forecasting of the Nile River flows. For this purpose, canonical correlation analysis (CCA) will be utilized.

6. To investigate the capability (potential) of using non-linear models to improve the long range forecasting of the Nile River flows. For this purpose, artificial neural networks (ANN) will be applied. Comparisons will be made between linear and non-linear models and single site and multi-site models.

This research is divided into eight chapters. This chapter is an introduction that includes a description of the research problem and research objectives. The second chapter offers a literature review of the research areas related to this study. The third chapter contains a description of the Nile River and its tributaries used as the case study for this research. The fourth chapter features the methodology used. The fifth and the seventh chapters contain the forecasting models, single site and multisite models, respectively. Chapter six explores the stable predictors for the Nile River and its tributaries. The final chapter contains a general discussion of the problem, conclusions based on the research and ideas for future research.

2. LITERATURE REVIEW

Increased understanding of the links between climate and oceanographic features has developed in recent years (McKerchar and Pearson, 1994). The North Atlantic Oscillation (NAO) and the Southern Oscillation (SO) are the two large scale alterations in atmospheric mass discovered by Sir Walker in the 1920's (Dugam et al., 1997). The Southern Oscillation is an irregular inter-annual fluctuation in global climate and the tropical Pacific Ocean and atmospheric circulation (McKerchar et al., 1996). The North Atlantic Oscillation is the pressure difference between the Azores high and the Iceland low. The pressure gradient between the two centers of action, the Iceland low (IL) and Azores high (AH) is the measure of the intensity of the westernly winds in the middle latitudes (Dugan et al., 1997). The Southern Oscillation has been the subject of intensive investigation during the past two decades (Kilades and Diaz, 1989), but few studies have been conducted on the NAO (Dugam et al., 1997). EL Niño southern oscillation (ENSO) phenomenon has been linked to climatic anomalies throughout the world and is now summarized and referred to in standard climatology texts (Philander, 1990; Diaz and Markgraf, 1992). Several analysts have attempted to discover consistent relationships between the ENSO and the hydro-meteorological variables, e.g. precipitation, streamflow, temperature, etc. Many of these studies show that various regions of the global tropics and subtropics exhibit climate anomalies that correlate with

the SO. These studies are complicated by the fact that no two EL Niño events are exactly alike and each has it's own characteristics (Wang, 1995) which indicates that the ENSO cycle is highly non-stationary. They vary with respect to frequency, magnitude, duration and onset (Guetter et al., 1996). The influence of EL Niño on the timing and location of precipitation anomalies depends on the strength of the event, the timing of its onset and decay, and the exact location of the pool of unusually warm ocean water (Miller, 1997). This also may influence other hydro-climatic variables (e.g. temperature) in a similar way. Wang (1995) suggested that it is more meaningful to investigate the evolution of ENSO event by event.

The efforts to study the influence of ENSO on hydroclimatic variables have been investigated in several parts of the world, for example, Australia (Simpson et al., 1993); U.S. (Dracup and Kahya, 1994, Kahya and Dracup, 1993; Redmond and Koch, 1991); South America (Pisciottando et al., 1994, Hastenrath 1990; Mechoso and Iribarren, 1992); Africa (Eltahir, 1996); Asia (Nicholls, 1995), to mention a few. Remond and Koch (1991) and Kahya and Dracup (1993) reported on patterns between US streamflows and ENSO. Simpson et al. (1993) showed that the index of the southern oscillation (SO) based on SSTs in the tropical Pacific Ocean provides useful information for the expected annual discharges in the Darling and Murray Rivers in Australia. Nicholls (1995) provided a method of monsoon prediction based on April SST and SLP changes at Darwin from January to April. Navone and Ceccatto (1994) used a neutral network approach to predict the monsoon based on spring precursors.

Simpson et al (1993) summarized some of the correlation of river flows and ENSO as: $r^2 = 0.22$ (Krishna River, India); $r^2 = 0.12$ (Nile River, Egypt); $r^2 = 0.06$

(Senegal River, Senegal); $r^2 = 0.14$ to $r^2 = 0.24$ (Lachlan, Lodden, Upper Murray, and Murrumbidgen, Australia); $r^2 = 0.31$ (Parana River, Argentina). Amarasekera et al. (1997) found that Amazon and Congo River flows, are weakly and negatively correlated with the equatorial Pacific SST, while the Nile River flow is negatively correlated and Parana River flows shows a positive relation. Eltahir (1996) determined that the ENSO cycle accounted for 25% of the natural variability in the Nile River flow. Statistical analysis proves that EL Niño and La Niña are responsible for up to 40% of annual precipitation variations and up to 30%, of river discharge variations in Florida (Sun and Frurbis, 1997). Mechosso and Irbarren (1992) recognized correlations between the SO and the streamflow of rivers flowing in the tropics and extra-tropics of South America. They found a clear tendency for the streamflow in the Negro and the Uruguay rivers to be below the median during the period June to December in years with a high southern oscillation index (SOI) and a slight tendency to be above the median during the period November to February in EL Niño years. In the same part of the globe, Kildas and Diaz (1989) analyzed the difference in rainfall between warm and cold events for each of the three-month-long standard seasons. Their results confirm that in southeastern South America (southern Brazil, Uruguay, north-eastern Argentina), in the period from September through November it rains more during warm SST events than during cold SST events. They also found hints of similar behavior in a small region of eastern Argentina during the periods of December through February and March through May.

In developing a consensus rainfall forecast in Australia, Casey (1995) proposed a statistical procedure based on an optimal linear combination of four forecast models: two of the models use SOI as a predictor of rainfall, one uses the serial correlation of

rainfall between seasons, and another uses the climatology probabilities. Subsequently, this forecasting research was extended by Piechota (1997) using six individual forecast models (climatology, persistence, SOI-linear-discriminent-analysis (SOI-LDA), SOI-Phase, SST_w-LDA, and SST_w-Phase). Then Piechota et al. (1998) adopted a similar approach, but added SSTs as a predictor of eastern Australia seasonal streamflow. McKerchar and Pearson (1994) report a significant relationship between the SOI in the austral spring (September to November) and flows in one catchment (the Clutha River) of the southern Alps (New Zealand), in the austral summer (December to February). The relationship was not homoscedastic (i.e. variance of one variable depend on the other), as required by ordinary least-squared regression (McKerchare et al., 1996). To overcome this technical problem, a Bayesian scheme (Moss et al., 1994) was developed to estimate the probabilities of summer inflows given the precursor spring SOI.

A series of complementary studies by Ropelewski and Halpert (1986, 1987, 1989) examined and documented large-scale patterns of above- and below-average standardized precipitation associated with both the high and low phases of the SO. In these studies, seasons and regions of strong, consistent ENSO-precipitation relationships were identified, using surface meteorological data, for 19 regions of the globe. Of these 15 were found to have precipitation relationships with the high index (cold) phase of the SO as well. Ropelewski and Halpert (1987), indicated that Southern Africa tends to undergo dry conditions during approximately the same season when equatorial eastern Africa has a wetter than normal season. Klopper et al. (1998) used SSTs as the only predictor sets for mean seasonal maximum temperature over South Africa. From this analysis they concluded that, seasonal maximum temperatures over South Africa do

respond to variations in global scale SSTs. They suggested other predictors to be investigated to find signals that may account for the remaining variance such as persistence and pressure anomalies. Subsequently, this research was supported by Landman and Mason (1999), who used SSTs as the only predictors for seasonal rainfall in South Africa. The SSTs of four consecutive 3-month mean periods are considered, and a canonical correlation analysis (CCA) model was constructed to provide operational (real time) rainfall forecasts for the austral summer rainfall region of South Africa.

The interannual and decadal scale variability in the North Atlantic Oscillation (NAO) and its relationship with Indian summer monsoon rainfall has been investigated by Dugam et al. (1997). The analysis reveals that the NAO during January of the preceding year has a statistically significant inverse relationship with the summer monsoon rainfall for the whole of India and Peninsular India, except for the rainfall of northwest India.

Gray and collaborators (Landsea et al., 1993, 1994) took an interest in West African climate prediction as a direct outgrowth from their work on the long-range forecasting of North Atlantic hurricane activity. Predictands are the June to September rainfall in the western, central and eastern portion of the Sahel zone. As input to "least sums of absolute deviations" (LAD) regressions a pool of 13 predictors are used, of which (a) three pertain to the stratospheric quasi-biennial oscillation (QBO), (b) four pertain to the preceding rainfall, pressure, and temperature gradients in the region, and (c) six pertain to ENSO, and surface pressure and upper-tropospheric wind conditions in the Caribbean basin. The previous year's rainfall in Guinea from August to November

was included in the hurricane prediction models by Gray et al. (1992a, 1992b, 1994), Gray and Landsea (1993), Elsner and Schmertmann (1993). Among these variables are potential predictors used by Gray et al. (1994a) to forecast seasonal Sahelian rainfall, and Gray et al. (1994) to predict ENSO. These variables and others will be investigated here for possible connections with the Nile basin hydrology.

Other large-scale phenomenon in the Pacific are the Pacific Decadal Oscillation (PDO) and Pacific North American (PNA). PDO is a climate phenomenon associated with persistent, bimodal climate patterns in the North Pacific Ocean that oscillate within a characteristic period on the order of 50 years. A particular phase of the PDO will typically persist for about 25 years (Hamlet and Lettenmaier, 1999). The PDO also refers to a numerical climate index based on sea surface temperatures in a particular region of the North Pacific (Mantua, 1997), which has an interannual signature (Hamlet and Lettenmaier, 1999). The latter authors developed a simple method to incorporate the ENSO and PDO climate signals into the extended streamflow prediction. Their forecast extends the lead time by about six months over current streamflow forecasting practices. Garnett et al. (1998) investigated the possible predictive signal in ENSO and PNA indices for long–lead forecasting of summer weather over the cropping region of the Canadian prairies. They defined the PNA as a linear combination of normalized geopotential height anomalies at the 700 mb level at four selected locations. They developed a skillful forecast of summer weather over the Canadian prairies with a lead time of two to four months.

Simpson et al. (1993 a,b) used ENSO to forecast annual discharge of Australian rivers. They showed that up to one year advanced forecasts of the Pacific Ocean SST

provide a mechanism for estimating probabilities of annual river discharge. These improvements in the understanding of global teleconnections of weather and climate have made it feasible to extend the lead-time of streamflow forecasts further for the Nile River flow. Over the last few years, several Nile flow precursors have been identified and prediction tests performed. For example, Attia and Abulhoda (1992) and Eltahir (1996) found a prediction flow signal in the Pacific Ocean. Amaraskera et al. (1997) found that ENSO explains 25% of the Nile flow variability. Wang and Eltahir (1999), used Bayesian theorem in developing a discriminant flow forecasting algorithm based on forecasted ENSO, rainfall, and recent flows for a lead-time of 2-3 months. Awadalla and Rousselle (2000) developed a neural network and transfer functions model to predict the Nile River inflows to the High Aswan Dam (HAD). They found significant improvement in model skill by incorporating SST in three locations of the Pacific, Indian, and Atlantic oceans. The variance explained was about 63% for a 3-month forecasting horizon. These studies and others brought a new perspective to the Nile River flow forecasting.

The above mentioned studies and others prove the teleconnection between the various large scales indices and the hydro-meteorological variables. Although significant, the correlation coefficients found in some cases are relatively small, and thus the percentages of the variances of the hydro-meteorological variables that are explained in this manner are small as well. This indicates that only a portion of the variance can be explained by the SOI alone. The remainder of the variance presumably reflects some other influences on the hydro-meteorological variables, which indicates that, it is not surprising if the oscillation influence is superceded by other effects. However, these

effects may be other oscillations in the Atlantic, the Indian Ocean or even due to some local conditions (e.g. soil moisture). Miller (1997) found considerable evidence that ENSO affects streamflows in the Western United States although ENSO is not the only source of variability. Diaz et al. (1998) studied the Atlantic SST effects on rainfall in South America and found that there are significant relationships between anomalies in rainfall and the SST in the Pacific and the Atlantic.

In recent years, artificial neural networks (ANN) methods have been successfully applied to a number of multivariate forecasting problems in the field of hydrology and water resources engineering. In this study we explore the combined effects of oscillations and SST in the Pacific, Atlantic, Indian Ocean and/or other variables. The input patterns considered in this study are the large-scale indices while the output are the Nile River flow. In this approach, a successfully trained network tries to capture the interrelationship between the trained data sets, which closely approximate the target values. The learning process or training forms, the interconnection between neurons and is accomplished by using known inputs and outputs and presenting these to the ANN in some ordered manner. The proposed neural network with a back-propagation algorithm (BP) is based on the feed-forward or cascade-forward approach or any other efficient training algorithm. The network is presented a set of input-output pairs called patterns. Neurons that constitute the network are described by an activation function (which is nonlinear), and they are interconnected by means of weights. Back-propagation is the most commonly used supervised training algorithm in multi-layer feed-forward networks (Tokar and Johnson, 1999). Tokar and Johnson indicated that the sigmoid and hyperbolic tangent functions are the most commonly used continuous transformations in

the back-propagation networks. It is worth mentioning that other functions besides the sigmoid function and hyperbolic tangent function are available, such as the linear method. The back-propagation algorithm is a gradient descent method in which weights of the connections are updated using partial derivatives of error with respect to weights. Through training, these weights are readjusted by the algorithm to implement a mapping that matches the examples or patterns as closely as possible (Raman and Chandramouli, 1996). A detailed description of ANN will be discussed in chapter 4.

In this study, we examine the correlation between large-scale indices and the Nile River flow. Such correlation would be of obvious benefit in forecasting streamflow. The results of this study will serve as a foundation for improved hydrological variable forecast. This will help to manage water resources better and to design and operate future water systems properly. Previous studies will serve as a foundation from which this study has been built. The results of this study will be checked for consistency against the available results of previous research.

3. DESCRIPTION OF THE NILE BASIN HYDROLOGY

3.1 Introduction

3.1.1 Physical Description

The Nile Basin is one of the most important river basins on the planet, due to its extension (more than 2,900,000 km^2) and length of 6,500 km, it extends from latitude 4° S to latitude 31° N. It extends from east and central Africa to the Mediterranean Sea. Its main lakes have a total area of 81,550 km^2, and its swampy reaches amount to 67,700 km^2. The Nile basin covers parts of ten countries (Eritrea, Ethiopia, Kenya, Tanzania, Uganda, Rwanda, Burundi, Zaire, Sudan, and Egypt). Figure 3-1 shows schematic representation of the Nile River hydrological components. Over its great basin (10% of the African continent) there are large variations in climate, topography, geography and hydrology. However, in spite of its extension and geographical distribution, more than 90% of the Nile River discharge originates from only four of the sub-basins: lake Victoria, the Blue Nile River, the Atbara River and the Sobat River (Conways amd Hulme, 1993). The annual streamflow of the Nile River averages 84 BM^3, as measured at the High Aswan Dam (HAD). The main control structures on the Nile River are: Sennar Dam 1925 (Sudan), Owen Dam 1957 (Uganda), Jebel Aulia Dam 1937 (Sudan), Roseires Dam 1967 (Sudan), Khasm El Girba Dam 1964 (Sudan), and High Aswan Dam 1970 (Egypt).

3.1.2 Climatic Description

The Nile River extends over four climatic zones: equatorial, tropical, semi-arid and arid. The rainfall in Ethiopia is brought by the southeasternly winds which are driven over the African continent and which, upon reaching the Ethiopian highlands, are forced to rise and become cooler, depositing their moisture as rainfall from June to September. The Ethiopian High Plateau lies in the interaction zone of two monsoon regimes: the African (Sahelian) moisture flux having its moisture originating far in the South Atlantic, and the Indian circulation coming from the Indian Ocean (Awadallah and Rousselle, 2000). The big rains of Ethiopia are also said to rely on moisture advection from the Congo Basin through the southwesternly monsoon (Camberlin, 1997). Convective instability, due to the intense heating of high plateau land, is also the cause of a great percentage of the rainfall (Seleshi, 1991). Seleshi also indicated that the cause of the Ethiopian rainfall is the strong movement of moist air from the southwest (Gulf of Guinea, high) to the northeast (center of Arabia, low). The high pressure system builds up over the south Atlantic and the Gulf of Guinea in July, causing the air movement toward the low pressure centers of the continent producing the monsoon and giving the trades an easterly direction as they move from the south of the equator to the north of the equator (Said, 1993).

The northeastern trades of the Southern Hemisphere and the southeastern trades of the Southern Hemisphere flow toward the low pressure region of the equator from the subtropical high pressure belts located at about latitudes 18° North and South (Said, 1993). Where the trades meet is termed the Intertropical Convergence Zone (ITCZ) and

that is the region where the rain falls. The yearly north-south-north passage of the sun is accompanied by a similar movement of these weather systems in the region.

The White Nile is fed from equatorial rains which posses a weak bimodal seasonal distribution, while the Blue Nile and Atbara rivers are supplied from a seasonally arid regime over the Ethiopian highlands. There is effectively zero correlation between these two regimes (Hulme, 1992). Hydrological studies of the White Nile suggest that its behavior is dominated by the influence of Lake Victoria (e.g. Kite, 1981). Owing to the huge surface area of the lake, small natural variations in rainfall have a major effect on the lake outflow, and hence on flows into the other lakes further downstream (Piper et al., 1986). Another notable feature is that many of these flow variations are compensated for by changes in the surface area, and hence evaporation losses, in the Sudd swamps, with the result that the annual flow out of these swamps has remained almost constant for long periods during the observational record despite large variations in inflows (Sene, 2000).

3.1.3 Hydrological Description

The Nile River receives its water from two major sources: the Equatorial lakes plateau with its year round rains and the Ethiopian plateau with its summer rains. It is worth noting that the flow contribution of the main tributaries of the Nile River from the Ethiopian highlands is 86% (Blue Nile 59%, Baro-Adobo 14% and Tekezze-Atbara 13%) and that from equatorial lakes is 14%. During flooding (July to October) over 90% of the Nile River flow is from Ethiopia and less than 10% from the Equatorial lakes. The low contribution of the Equatorial lakes basin to the Nile River is attributed to the fact that a great amount of water is lost by evaporation in the Swamps while the Ethiopian

plateau with steep slopes drains effectively into the Nile River. A simple calculation for the period 1913-1989 shows that the period of July to October accounts for about 68% of the Nile River annual flows at Aswan and about 84% of the Blue Nile River annual flows (Table 3.1). Table 3.1 shows that most of the Nile River tributaries have a higher percentage of their flows during the period July to October. Table 3.1 gives the total seasonal (column 2) and annual river discharges (column 3) for the period 1913-1989. It also shows the ratios of the seasonal flows at a given tributary to its annual flows (column 4) and the annual flows at a given tributary to the annual flows at Aswan (column 5). Column 6 shows the fraction of the seasonal discharges at a given location to the annual Aswan flows while column 7 shows the seasonal flows at a given location to the seasonal flows at Aswan. It is clear from these computations that the Ethiopian Plateau contribution highly dominates the Nile River flows. The Blue Nile River and Atbara River contribute about 73% of the annual river flows measured at Aswan. It is also clear that a high portion of the Nile River flows occur in the July to October season.

The Nile River has three main tributaries: the Blue Nile (plus Rahad and Dinder), the White Nile, and the Atbara River. The Atbara River originates from the Ethiopian Plateau (Setit and Atbara branches), about 96% of the 12 BM^3 annual average discharge is received during July to October and dries out during January to May. The Blue Nile River is the largest tributary of the Nile River and it originates from Lake Tana (3,150 km^2) in the Ethiopian Plateau. With an approximate drainage area of 325,000 km^2, about 84% of the 48 BM^3 average annual discharge comes during the flood period (July to October), which represents 48% of the annual contribution of the Nile River flow at Aswan, Fig. 3-2. The Blue Nile River flow regime is characterized by a strong annual

cycle and interannual variability depicted in Fig. 3-2, with a dominant peak in September. Figure 3.2 further indicates that the summer season is more variable than other seasons. The Sobat River comprises two major tributaries: Baro River which originates from the Ethiopian Plateau and the Pibor River which originates from east Africa. The Sobat River contributes 16% of the Nile River flows at Aswan (Table 3-1). The three tributaries (the Sobat River, the Blue Nile River, and the Atbara River) contribute about 85% of the annual flow of the Nile River at Aswan. Therefore, this justifies the selection of these three tributaries and the season July to October for further analysis.

Table 3-1 Seasonal and annual flows of the Nile River and Tributaries, for the period 1913-1989. * Description of the columns

(1) RIVER	(2) JASO MM^3	(3) JAN-DEC MM^3	(4) $\frac{(2)}{(3)}$	(5) $\frac{(3)}{(3)Aswan}$	(6) $\frac{(2)}{(3)Aswan}$	(7) $\frac{(2)}{(2)Aswan}$
Aswan	57,396	83,953	0.68	1.00	0.68	1.00
Blue Nile	40,506	48,312	0.84	0.58	0.48	0.70
Atbara	12,023	12,466	0.96	0.15	0.14	0.21
Malakal	12,087	29,796	0.40	0.35	0.14	0.21
Sobat	6,454	13,298	0.48	0.16	0.08	0.11
Rahad & Dinder	3,678	3,761	0.98	0.04	0.04	0.06

- * Column 2: annual flows (January to December) in million m^3, column 3: seasonal flows (July to October) in million m^3, column 4: is the ratio of seasonal to annual flow, column 5: is the ratio of annual flows to Aswan annual flows, column 6: is the ratio of seasonal flows to Aswan annual flows, and column 7: is the ratio of seasonal flows to Aswan seasonal flows

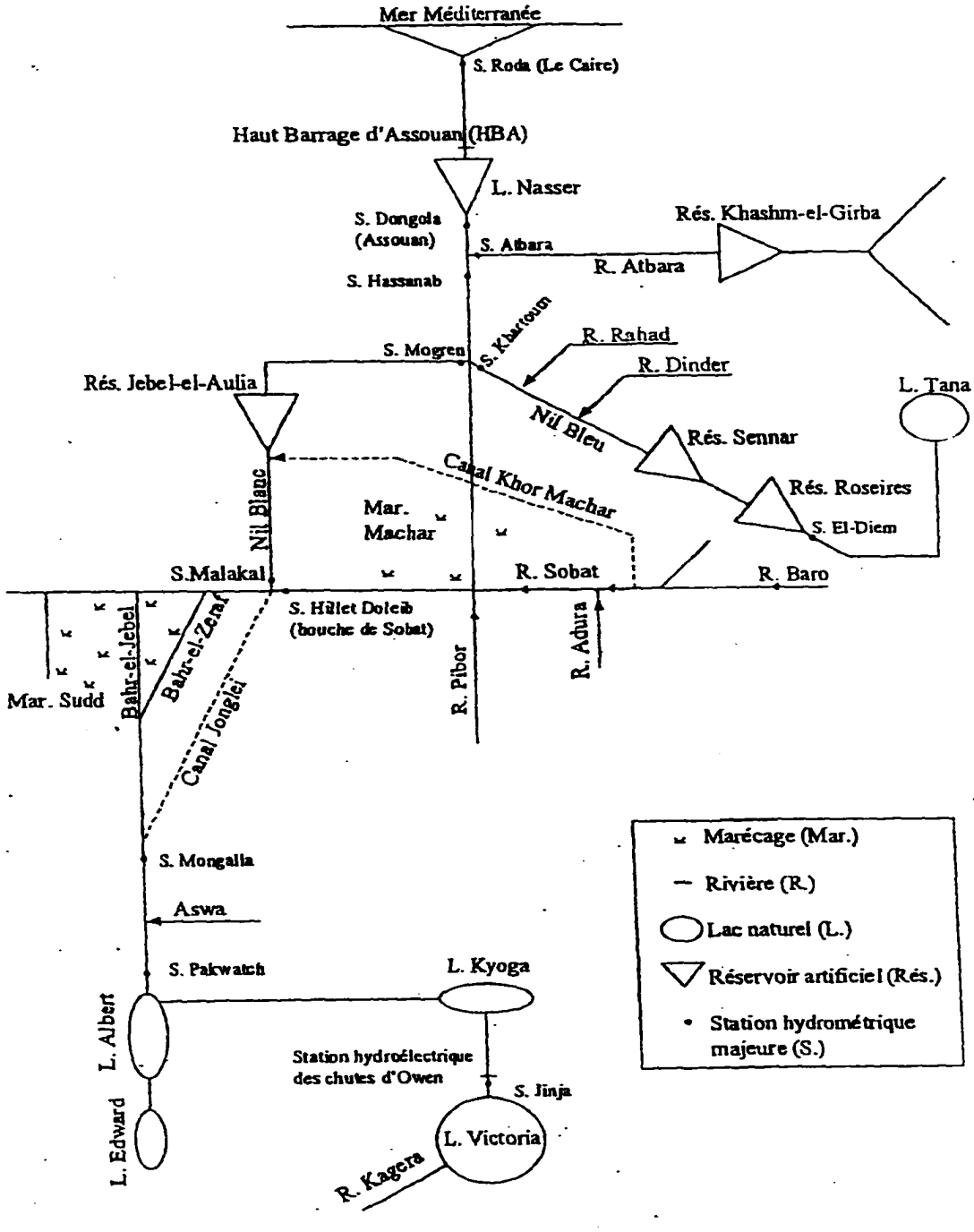

Fig. 3-1 Schematic representation of the Nile basin components (source: Awadalla, 2000)

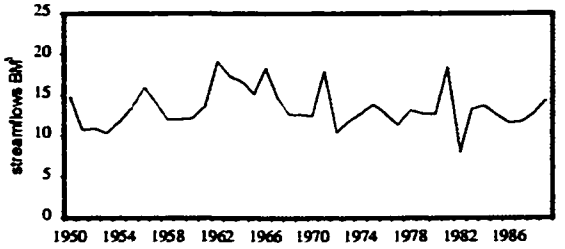

Fig. 3-2a The Sobat River flows (1950-1989)

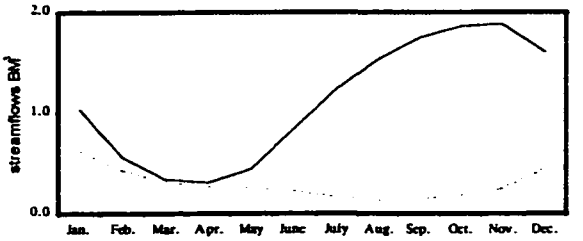

Fig. 3-2b Monthly Sobat River average flows and standard deviation for the period (1950-1989)

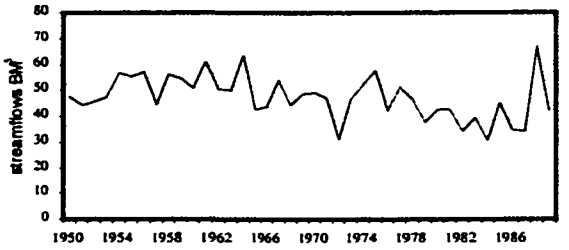

Fig. 3-2c The Blue Nile River flows (1950-1989)

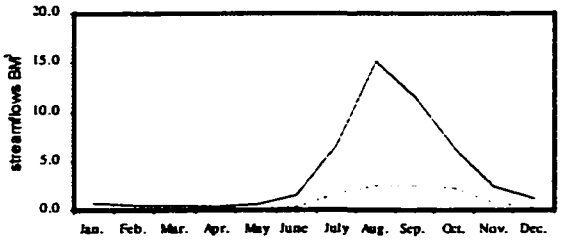

Fig. 3-2d Monthly Blue Nile River average flows and standard deviation for the period (1950-1989)

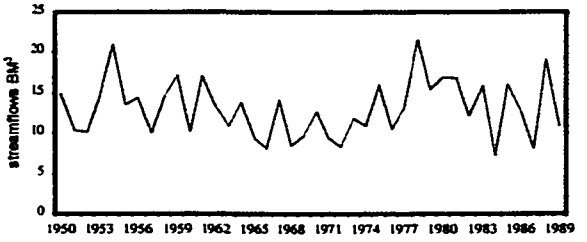

Fig. 3-2e The Atbara River flows (1950-1989)

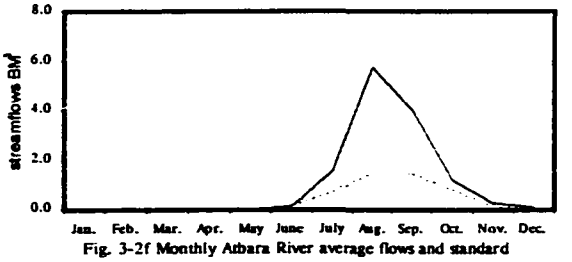

Fig. 3-2f Monthly Atbara River average flows and standard deviation for the period (1950-1989)

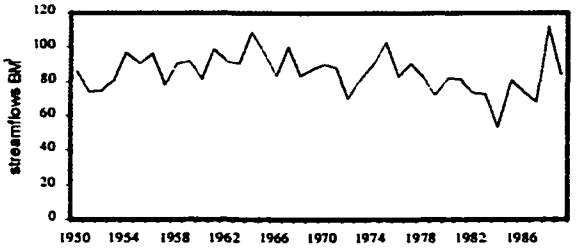

Fig. 3-2g The Nile River flows at Aswan (1950-1989)

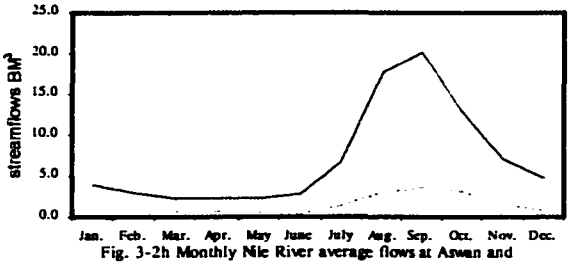

Fig. 3-2h Monthly Nile River average flows at Aswan and standard deviation for the period (1950-1989)

Fig. 3-2 Annual and seasonal flows at the selected Nile River hydrologic stations

The White Nile originates from the Equatorial lakes, from Lake Victoria and through its outlet at Jinja, the river known as the Victoria Nile, enters Lake Kyoga after a series of falls. From Lake Kyoga, the river passes through another series of rapids and falls before entering Lake Albert which also receives water from the Similiki River. The Nile River leaves Lake Albert with an annual average of 30.8 BM^3 as Bahr-el Gebel enters the Sudan at Nimuli and reaches Mongalla with an average annual discharge of 33.7 BM^3 after receiving further discharges from the Torrents River between Lake Albert and Mongalla. From Mongalla the river enters the vast swampy Sudd area loosing large amount of its discharge to evapotranspiration (~50%). Then a very swampy Bahr El Ghazal with a small contribution of 0.5 BM^2 joins Bahr-el Gebel and flows to Malakal where it joins the Sobat River (Baro and Pibor) which adds an annual average of 13.3 BM^3. Thus, the total amount of water provided by the White Nile at Malakal with an annually averages 30 BM^3.

Figures 3-3, 3-4 and 3-5 show the lag1-autocorrelation coefficients, the coefficients of variation and the standard deviation of precipitation and runoff for the eight Nile sub-basins (Coway and Hulme, 1993). The six sub-basins are Lake Victoria, Equatorial lakes, Sudd, Bahr-el Ghazal, Sobat, Central Sudan, Blue Nile, and Atbara. It is clear that the auto-correlation coefficient increases as the area of the basin increases. This is due to the storage characteristics of large basins as well as recycling processes. Variability of annual precipitation given by the coefficient of variation (CV), the standard deviation divided by the mean, decreases with the area of the basin. High variability is observed in the small basins compared to the larger ones, and this may be due to the storage characteristic of the larger watershed.

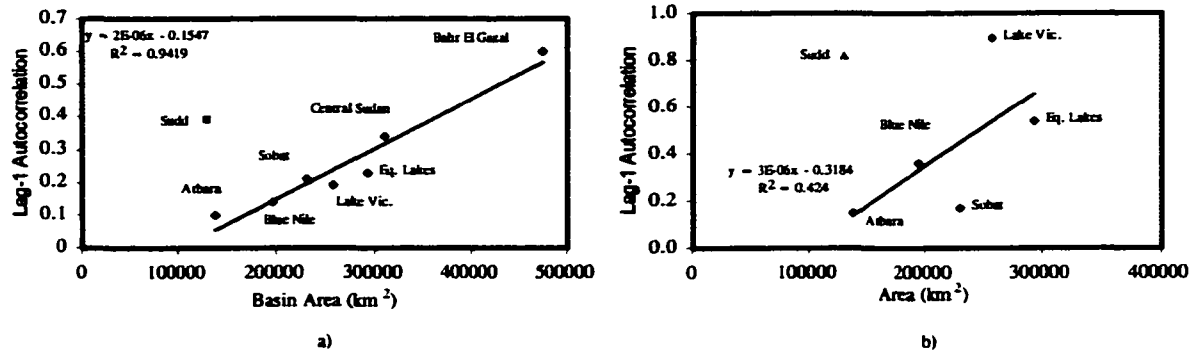

Fig. 3-3 The Nile River sub-basin area and Lag 1 autocorrelation of a) of precipitation b) for streamflow

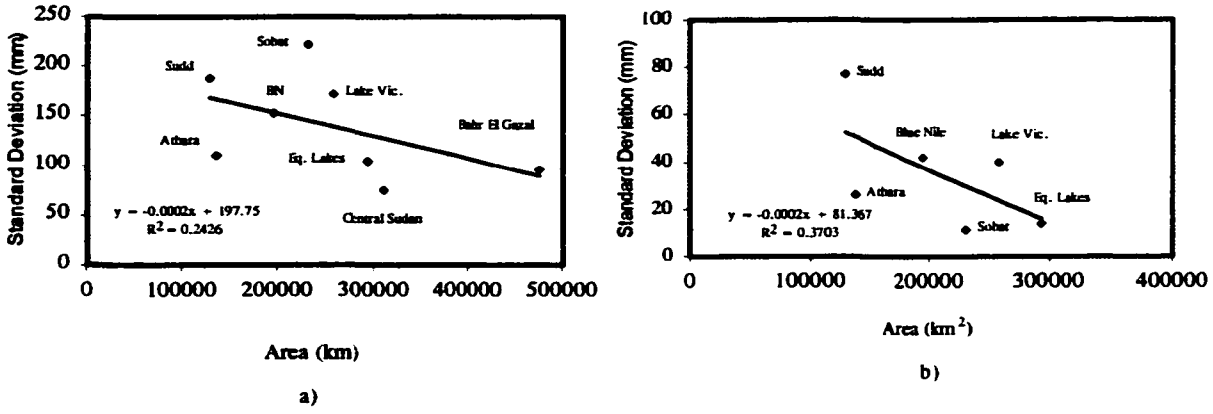

Fig. 3-4 The Nile River sub-basin area and standard deviation of a) precipitation b) streamflow

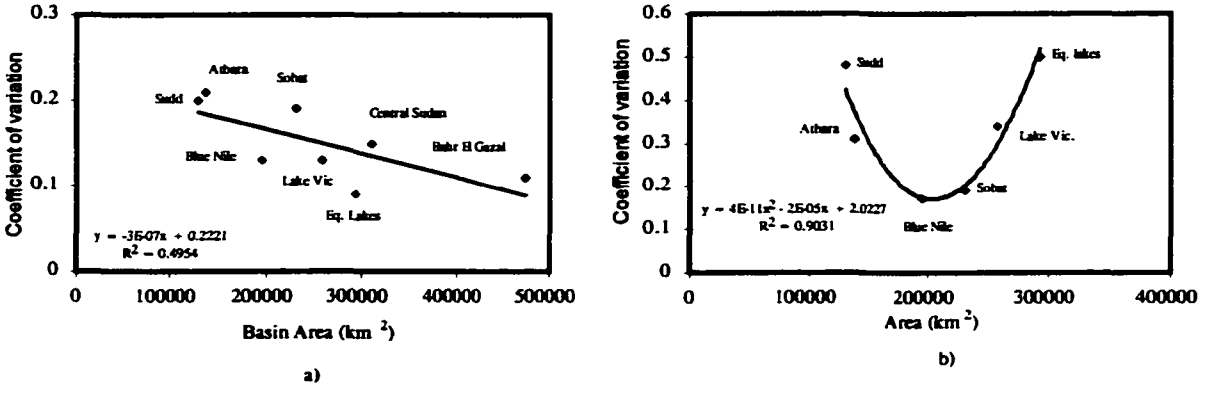

Fig. 3-5 The Nile River sub-basin area and coefficient of variation of a) precipitation b) streamflow

3.1.4 The Nile River Lakes

The three major Equatorial lakes: Victoria, Kyoga, and Albert (or Mobuto Sese Seko), are connected and form a cascaded system containing enormous quantities of fresh water (~ 3,200 km^3) (Georgakakas and Marks, 1987). The hydrology of the Equatorial Lakes system is dominated by the role of the lakes which occupy about 35% of the catchment area and thus have a very significant effect on its water balance, Fig. 3-1. The hydrology of the catchment of the African lakes can thus be considered in two parts: the hydrology of the Lakes, and the hydrology of the catchments that drain into them. Like the majority of the reservoir systems, the regulation of Equatorial lakes and particularly Lake Victoria are multi-objective systems i.e. power generation, navigation, and downstream requirements, which are in conflict most of the time. Lake Tana, at the head of the Blue Nile River is a natural lake with an area of about 3,150 km^2, Fig. 3-1. Because of the large storage capacity and the restriction at its outlet, the lake outflows peak (September) two months after the maximum rainfall (July) and one month after the maximum flows at Roseires (August) (Conway, 1997)

The average annual outflow from Lake Victoria over the period 1946-1961 was 20 BM^3, while for the period 1962-1970 the average increased to 44 BM^3, more than double. The standard deviation of the annual flows from 1962-1970 is 3.92 BM^3, which is more than the standard deviation, 2.71 BM^3 for the period 1946-1961. The average for the lake level at Jinja for the two periods was 11.72 m and 12.55 m, respectively. This shows a drastic increase in the lake levels in the second period, Fig. 3-6. This is most likely attributed to the hydro-climatic change.

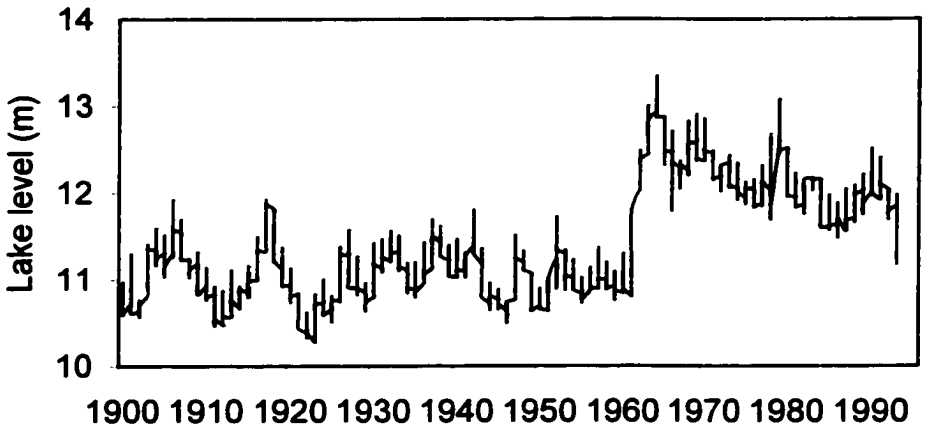

Fig. 3-6 Lake Victoria monthly levels at Jinja (m) 1900-1993

3.2 Data Description

3.2.1 General

Three types of data have been used: the seasonal discharge at the Nile River and the its four tributaries (the Blue Nile, the Atbara, the Sobat and the White Nile), sea surface temperature (SST) data at some regions in the oceans, and other pressure and temperature variables. The SST data were extracted using the software CLIMLAB2000 (Tanco and Berri, 1999) for the region 60° N – 44° S, 180° W – 180° E.

The Nile hydrological variables were averaged over three periods (4-month intervals) (November to February (NDJF), March to June (MAMJ), and July to October (JASO)). The first period is a critical period for winter crops in the Sudan, the second period is critical for hydropower generation (low head and low flow), and the third period is considered to be the main agricultural season in the Sudan and the season of drought and flood concerns. The SSTs were then computed for each of the seasons mentioned above. All the data used in the forecasting study are for the period 1950-1989, which is the overlapping period for all the variables.

3.2.2 Mean sea level temperatures

Mean monthly sea surfaces temperatures are the primary predictors used in this study. SST of the Pacific, Atlantic and Indian Oceans were extracted from CLIMLAB2000, taken from the comprehensive ocean-atmosphere data set (COADS). SSTs are available for the period 1950-1997 for the oceans between latitudes 50° N to 44° S and longitudes 00° to 360°. Cold tongue index as the average temperature in the Pacific Ocean was also used which is another measure of the ENSO index.

3.2.3 Mean sea level pressures

The North Atlantic is an important element of the global climate system (Efimov et al., 1999). The pressure gradient between the two centers of action, the Iceland low (IL) and Azores high (AH), is the measure of the intensity of the westerly winds in the middle latitudes, Dugam et al. (1997). Positive (negative) numerical values of the index are associated with strong (weak) zonal flow between the stations (Rogers, 1984). In this study the North-South gradient and the pressure at each station (seasonal standardized time series for NAO, pressure at Gibralter, and pressure at Azores, Ponta Delegada), 30° N - 40° N, 35° W-25° W were used. Similarly, other indices in the Atlantic Ocean: North Atlantic (5°-20° N, 60°-30° W), South Atlantic (0 - 20° S, 30° W-10° E), and global tropics (10° S-10° N, 0-360°) were examined as well.

Owing to the importance of the ENSO phenomenon on climate variability in the tropics and over other regions of the globe, many predictors have been developed representing the strengths of both its atmospheric component, the southern oscillation (SO), and its occurrence component, EL Niño. The EL Niño Southern Oscillation

(ENSO) is defined as the difference of monthly atmosphere at Tahiti (18° S, 150° W) and Darwin (12° S, 131° E). The positive/negative phase of the SO is defined by high/low pressures at Tahiti/ Darwin. In this study the gradient of Tahiti-Darwin SLP and the SLP at each station were included as well. Similarly, the monthly sea level pressures of Jakarata were also used in this study, available from Konnen et al. (1998). The North Pacific Pattern (NPP) defined as the area weighted sea level pressure over the region (30°N-65°N, 160°E-140°W) was also used.

3.2.4 Surface air temperatures

Monthly mean surface air temperatures anomalies over the North and South Hemispheric regions were used as predictors. These series run from 1882 to 1988 and were obtained as the simple average of Northern Hemisphere (0-90° N) and Southern Hemisphere (0-60° S) values derived and published in Vinnikov et al. (1990). These values are departures from the 1951-1975 period. Other sources of the regional and global surface air temperatures are available in Jones et al. (1986a, 1986b and 1982) and for specific regions in Hansen and Lesedeff (1987).

3.2.5 West Africa precipitation

Gray and collaborators at Colorado State University incorporated the Western Africa region rainfall as predictor to their Hurricane forecast model. Precipitation in Guinea (West Africa) during the previous year August to November was used as a potential predictor for the Nile River flow, available from Gray et al. (1992, 1994).

4. RESEARCH METHODS

4.1 Introduction

Extensive use of linear correlation analysis, multiple linear regression (MLR), and principal component regression techniques (PCR) were made. The goals in the model development were to: 1) maximize the adjusted R^2, 2) minimize the prediction error measured by adjusted RMSE and 3) include uncorrelated variables while keeping the number of predictors used to a minimum. Numerous data sets were employed to extract predictors. Part of the results presented in this research were based on classic correlation analysis, which considers the relationship between the variability of two variables. In this case, the variables are the seasonal streamflow amounts at 5 locations, the SST in some regions in the oceans and other hydroclimatological variables. It is likely that the indices constructed from multiple months represent a more stable target than individual months. Thus, the seasons used were November through February (NDJF), March through June (MAMJ), and July through October (JASO). Also a transformation of variables into a new, reduced, and independent set of variables (so called Principal Components – PCs) was used and principal components regression models were developed. A further step is the development of multivariate models to measure the potential predictability, for this purpose canonical correlation analysis (CCA) was used. Neural network models were also developed.

The stability and consistency of the relationship between the Nile River flows and the predictors have been examined over sliding 31-, 25-, 21-, and 15-year windows, and the stable predictors were defined at the 5% significance level.

The lead-time here is defined as the time from the end of the latest predictor to the end of the predictand period. For example, if the latest predictor is from NDJF(0) and the predictand is from JASO(0), then the lead-time is eight months (March, April, May, June, July, August, September, and October). This is different from that of Chen (1995) and Tang et al. (2000) who defined the lead-time as the time from the center of the period of the latest predictor to the center of the predictand period. Barnston et al. (1994) defined the lead-time as the time from the end of the latest predictor to the center of the predictand period. With the above example, their lead-times would be eight months and six months, respectively.

4.2 Linear Correlation Analysis

Although correlation coefficients are simple by definition, they can indicate a physical relationship between two or more variables (Pabdzic and Trinin, 1998). The use of correlation indices in the study of hydrometeorological phenomena makes sense, especially if variable-to-variable relationships are considered, as in this case. Correlation coefficients (CCs) between the various variables and the Nile River flows were computed and statistical significance was evaluated. Correlation coefficients were calculated for over three years prior to the onset of the forecast target season (JASO). The association between the predictands and predictors was measured by means of the linear correlation coefficient (R) between the forecast (Y_t) and the observed (X_t) and was computed as:

$$R = \frac{\sum_{1}^{N}(Y_t - \bar{Y})(X_t - \bar{X})}{\sqrt{\sum_{1}^{N}(Y_t - \bar{Y})^2 \sum_{1}^{N}(X_t - \bar{X})^2}} \qquad [4\text{-}1]$$

Earlier correlation studies by Parthasarathy (1984) and Hastenrath (1987) of the relationship between Indian rainfall and regional/global circulation parameters have shown that to obtain a stable correlation coefficeints about 20-30 years of record are required. In this study the correlation coefficients at different lead times are computed for 37 years, 1953-1989.

4.3 Multiple Linear Regression (MLR)

In this research the MLR uses both the ordinary least square technique (OLS) and the least absolute difference technique (LAD). A multiple linear regression model was developed as discussed in many texts. In the general multiple linear regression, the predictand Y is expressed as a function of n predictors:

$$\hat{Y} = b_0 + b_1 x_1 + b_2 x_2 + \ldots\ldots\ldots\ldots\ldots + b_n x_n \qquad [4\text{-}2]$$

where Y is the predictand, the b_i's are the regression coefficients that are derived from the observed data (b_o is the intercept), and the x_i's are the regressors, representing the predictors. The predictors are selected by identifying the variable that yields the highest correlation with the predictand and independent of each other. The regression coefficients are determined by using the method of least squares. If a given coefficient

dropped below the 5% significance level then the predictor was removed from the equation. After the selection of predictors, the regression coefficient b_n is computed with the least squares fitting (MSE), which minimizes the objective function:

$$MSE = \frac{1}{N}\sum_{1}^{N}(Y_i - \hat{Y})^2 \qquad [4\text{-}3]$$

The least absolute difference (LAD) used in this study was developed by Prof. Mielke P. W. (CSU, Department of Statistics) and has been detailed in Gray et al. (1993, 1992). A general description of the LAD algorithm will be discussed below, and further details can be obtained from the references. The LAD is preferable to OLS regression since LAD is based on the absolute difference when computing the regression line rather than the square of the difference as OLS does, which emphasizes outliers, Gray et al. (1993). LAD is analogous to using the median in a univariate analysis to estimate the location of a distribution. The median minimizes the sum of the absolute values of the residuals OLS regression analysis yields efficient and unbiased estimates of population regression parameters and their associated standard errors when the population is Gaussian (or multivariate Gaussian) with equal variances (Gray et al., 1992).

The cross-validated prediction values and the observed values for each of the N years are compared by calculating a measure of agreement. The probability of the measure of agreement is obtained under the null hypothesis. If y and $\hat{y}$ denote the observed and the predicted dependent variables, respectively, then the agreement coefficient (ρ) is defined by:

$$\rho = \frac{\mu_\delta - \delta}{\mu_\delta} \qquad [4\text{-}4]$$

$$\text{where } \delta = \frac{1}{N}\sum_{i=1}^{N}|y_i - \hat{y}_i| \qquad [4\text{-}5]$$

and μ_δ is the average value of δ over all N! equally likely permutations of $y_1, \ldots\ldots, y_N$ relative to $\hat{y}_1, \ldots\ldots, \hat{y}_N$ under the null hypothesis that the N pairs (y_i and $\hat{y}_i$ for $i = 1, \ldots\ldots\ldots, N$) are merely the result of random assignment (Gray et al., 1993).

4.4 Principal Component Analysis

Multiple linear regression and principal component analysis (PCA) have been the main techniques used in this research. Linear correlation was used to ascertain the connections between the river discharge and the three Oceans SSTs and Guinea precipitation and other hydroclimatic variables. The linear regression equation may be expressed as in equation (4-2). One problem with multiple linear regression is the multicollinearity of the prediction variables, which is common in hydrometeorological variables. This can be minimized by choosing the predictors carefully and checking for independence of the predictors. Alternatively, one could use a principal component analysis (PCA) model by determining orthogonal variables in order to reduce the dimensionality of the predictors and retain the time series of the principal components.

Principal component analysis is a widely used technique in meteorology and climatology. One objective of PCA is to find a small number of linear functions or a set of variables that successively accounts for the maximum amount of variation in the original variables. When one is faced with a large dataset, one may like to reduce its size, while minimizing any loss of information, with the aim of better understanding and

interpreting the structure of the data. Another objective is to remove the multicollinearity that may be present in the independent variables. The principal component PC_k may be expressed as:

$$PC_k = c_{k1}x_1 + c_{k2}x_2 + \ldots\ldots + c_{kv}x_v \qquad [4\text{-}6]$$

here c_{k1}, $c_{k2},\ldots,c_{kv}$ are coefficients (loadings) of the v-variables for the k^{th} PC. The first principal component PC_1 is a linear function with the maximum possible variance. Then, PC_2 is a linear function with a maximum variance and not correlated with PC_1; the same applies to any PC_k. The first eigenvector is the set of coefficients contained in PC_1. The eigenvalue corresponds to the variance of each PC_k and is therefore a measure of its importance in explaining variation. Garen (1992) included the PCs in sequence, while others (Marsden and Davis, 1968 and Wortman, 1989) allow models to skip PCs. The latter procedure has been adopted in this study. As explained below, the first 10 PCs will be retained and up to 5 PCs with significant regression coefficients will be included in the multiple linear regression models. Computations were done using the CLIMLAB2000 version 1.0 model, developed by Tanco and Berri (1999). Those PC_k's that make a meaningful contribution to the total variance, and significant regression coefficients will be retained. The regression model in terms of the principal component is:

$$Y = a_0 + a_i PC_i + a_j PC_j + a_l PC_l + a_m PC_m + a_n PC_n \qquad [4\text{-}7]$$

where i, j, l, m, and n are the retained components ($i \neq j \neq l \neq m \neq n$) with significant regression coefficients, a_i, a_j, a_l, a_m, and a_n, respectively. To limit artificial skill, predictors are limited to four for the original variable models and five for the PCs models. This is done in order to prevent redundancy and instability of the multiple regression equation and to ensure good results when applying it to new data (Bhalme et al., 1986). A screening procedure is conducted in order to select from a large set of possible predictors only those that contribute significantly and independently to forecast the river flow.

4.5 Canonical Correlation Analysis

Canonical correlation analysis (CCA) is a multivariate statistical methodology to determine linear combinations of two data sets (the predictor data and the predictand data set), i.e. multicomponent predictors are linearly related to multicomponent predictands such that the sum of the squared errors is minimized. The technique is a generalization of the multiple regression analysis that allows one field to be regressed on another field and depicts the major patterns of covariance between the fields analyzed (Graham et al., 1987b). Barnett and Preisendorfer (1987) characterized CCA to be at the top of the regression modeling hierarchy. CCA is used as a forecast technique in many studies (Graham et al., 1987a, 1987b; Barnston, 1994; Barnett and Preisendorfer, 1987; Prasad and Singh, 1996; Yu, 1997; Chu and He, 1994). The technique was used for ENSO predictions (Barnston and Ropeleweski, 1992), for prediction of the United States seasonal temperature and precipitation (Barnston, 1994) at the climate prediction center

in the United States and applied to meteorological data (Barnett and Preisendorfer, 1987).

The CCA technique is considered as an extension of multivariate regression and correlation analysis, and closely related to MLR and PCA. The idea was to examine the relationship between a set of variables X and a set of variables Y. Given that $X = (X_1, X_2,.....,X_i)'$ and $Y = (Y_1, Y_2,.....,Y_j)'$ as the predictors set and predictands set, respectively, where Z and W represent a linear combination of the predictors (X) and the predictands (Y) known as canonical variables, respectively, where i and j represent the number of each set of variables, respectively. Canonical correlation analysis attempts to determine the optimum linear combinations between the two sets of canonical variables with the maximum correlation being produced. The CCA finds canonical eigenvectors (u, v), to produce linear combinations of $Z = u'X_{i,t}$ and $W = v'Y_{j,t}$ (prime denotes transpose) such that canonical variables Z and W have the largest possible correlation. After the first pair of linear combinations (Z_1 the first canonical variable of X's and W_1 the first canonical variable of Y's) has been found, one can proceed to find other pairs of linear combinations that have the strongest correlations, subject to the constraint that the new canonical variable pair is orthogonal to the pairs found earlier (Z_2 and W_2 are uncorrelated with the Z_1 and W_1).

The theory of CCA is described extensively in the literature and further details can be provided by the references cited in this section. Useful discussion of the CCA method is provided by Barnett and Preisendorfer (1987) and for brevity a general description as given by Yu (1997) was presented here. The final forecasting model can be presented as:

$$\hat{Y} = (V')^{-1} AU'X \qquad [4\text{-}8]$$

where $\hat{Y}$ is the predicted values (prime denotes transpose) and the variable A is defined as:

$$A = \begin{pmatrix} a_1 & & & \\ & a & & \\ & & . & \\ & & & a_q \end{pmatrix} \qquad [4\text{-}9]$$

where $a_1 \geq a_2 \geq \ldots\ldots\ldots\ldots \geq a_q$ are the canonical correlations (the square of the canonical correlation is often called the eigenvalue) between Z and W, and q is equal to i or j, which ever is smaller, and Z and W have the largest possible correlation. U and V are called the eigenvectors (the loading patterns).

$$U' = \begin{pmatrix} u_1' \\ u_2' \\ . \\ u_q' \end{pmatrix} \qquad V' = \begin{pmatrix} v_1' \\ v_2' \\ . \\ v_q' \end{pmatrix} \qquad [4\text{-}10]$$

To control for artificial skill produced by the overfitting of random data variability in the relatively short period of record, cross-validation (Michaelsen, 1987) is used in evaluating forecast skill and further details about the forecast skill measures are presented in section 4.7. The drop-one Jackknifing procedure was used. That is, each of the 37 years is held out in turn, and CCA is used to develop a prediction model from the remaining 36 years. The predictor data for the withheld are then projected onto the prediction CCA loading pattern, and predictand values are generated and verified against observed data for the withheld year.

4.6 Artificial Neural Network Analysis (ANN)

4.6.1 ANN: Overview

The roots of all work on neural networks (NN) are in neurobiological studies that date back to about a century ago (Mehrota et al., 1997). Artificial neural networks are computational methods inspired by studies of the brain and nervous systems in biological organisms (Karunanithi et al., 1994). The ability of the brain to perform difficult operations and to recognize complex patterns, even if those patterns are distorted with a high degree of noise, has fascinated scientists for centuries (Minns and Hall, 1996) and has always been a great motivator for modeling the brain. However, most current neural network architectures do not try to closely imitate their biological model, but rather can be regarded simply as a class of parallel algorithms (SNNSv4.1 Mannual, 1995).

The growing interest in neural networks among researchers is due to their excellent performance in modeling nonlinear relationships (Goh, 1995). French et al. (1992) discussed the advantages which are characteristic of an ANN approach to problem solving: (1) application of a NN does not require priori knowledge of the underlying process; (2) one may not recognize all of the existing complex relationships between various aspects of the process under investigation; (3) a standard optimization approach or statistical model provides a solution only when allowed to run to completion whereas a neural network always converges to an optimal (or sub-optimal) solution and need not run to any pre-specified solution condition; (4) and neither constraints nor an a priori solution structure is necessarily assumed or strictly enforced in the ANN development. One of the major advantages of neural nets is their ability to generalize. Learning is the process in which the weights are adjusted in response to training data

provided at the input layer and, depending on the learning rule, at the output layer. The learning process enables the neural network to find a set of weights that will produce the best possible input/output mapping (Maier and Dandy, 1996).

4.6.2 ANN: Applications

Recently, neural networks have been successfully applied to many applications. The area addressed by ANN techniques includes pattern matching, optimization, data compression and function optimization (Raman and Sunilkumar, 1995). Many of the problems that engineers must deal with are exactly the types of the problems for which ANN appear to be most applicable (Garrett, 1994). Flood and Kartam (1994) presented two papers for understanding the usage and potential for application of ANN in Civil Engineering.

In water resources and hydrology, ANNs have been used for flow predictions, flow/pollution simulation, parameter identification, and complex nonlinear input-output time series models (Jain et al., 1999. Previous work has demonstrated that ANN are adequate to model rainfall-runoff (Smith and Eli, 1995; Tokar and Johnson, 1999; Hsu et al., and 1995; Shamseldin, 1997), to forecast river floods (Campolo et al., 1999; and Zealand et al., 1999) to forecast sea surface temperature anomalies (SSTA) (Tangang et al., 1999), flow prediction (Karunanithi et al., 1994), prediction and data analysis (Hsieh and Tang, 1998; Nam et al., 1998; and Sureerattanan and Phien, 1997), reservoir operation (Raman and chandramorti, 1996; Saad et al, 1994), to estimate missing data (Kuligowski and Barros, 1998), for climate zonation (Malmgreen and Winter, 1999), modeling soil moisture correlation (Goh, 1995), water quality (Maier and Dandy, 1996), and solving inverse problem (Davis and Hwang, 1997; and Shigidi, 2000). An ANN has

been integrated with a geographical Information system by Gangopadhyay et al. (1999), to generate subsurface profile and material distribution. Raman and Sunilkumar (1995) successfully used an ANN for multivariate modeling for the synthesis of inflows. Minns and Hall (1996) used ANNs to generate flow data from synthetic storm sequences. French et al., (1992) developed a three layer feed-forward neural network to forecast rainfall intensity in space and time and compared the result with two other methods of short-term forecasting. Awadalla and Rousselle (1999) developed a neural network model and transfer function model to predict the Nile River flow at Aswan dam. Chakraborty et al., (1992) used an ANN to develop multivariate indices for flour prices in three cities. A comparison between ANN models and traditional models has been made by Hsu et al., (1995), multi-layer feed-forward networks have been found to have the best performance with regard to input-output function approximation. Hsu et al., (1995), concluded that the ANN approach is more efficient whenever explicit knowledge of the hydrological sub-process is not required and when the object is to predict streamflow behavior from customary monitored time series of rainfall and flow rate.

In these models, knowledge is usually distributed throughout the net and is stored in the structure of the topology and the weights of the links. The network consists of units (neurons) and directed weighted links (connections) between them. Depending on their function in the net, one can classify three types of units: input units, hidden units, and output units, within three layers: the input layer, the hidden layer, and the output layer, respectively. Connections show the direction of the transfer activation, starts from a source unit to the output unit and each has a weight (strength). To reach the best generalization, the data set should be split into a training set (to minimize the error) and a

test set (to check the performance). The set for activation of all input units is called input pattern, and that for all output units is called output pattern. The input pattern and its corresponding output pattern is simply called pattern. This definition implies that all patterns for a particular network have the same size.

4.6.3 ANN: Configuration

A neural network structure consists of processing elements (nodes), links that connect the elements, and information processing, Fig. 4.1 and 4.2. A layer represents a set of parallel nodes. The interconnection between nodes is controlled by the training algorithm and the nature of the problem. The number of nodes in the input and the output layers are dictated by the dimension of input and output sets presented to the network for training. The number of hidden layers and neurons are a quantity that must be determined empirically for each separate situation due to the complexity of the problem.

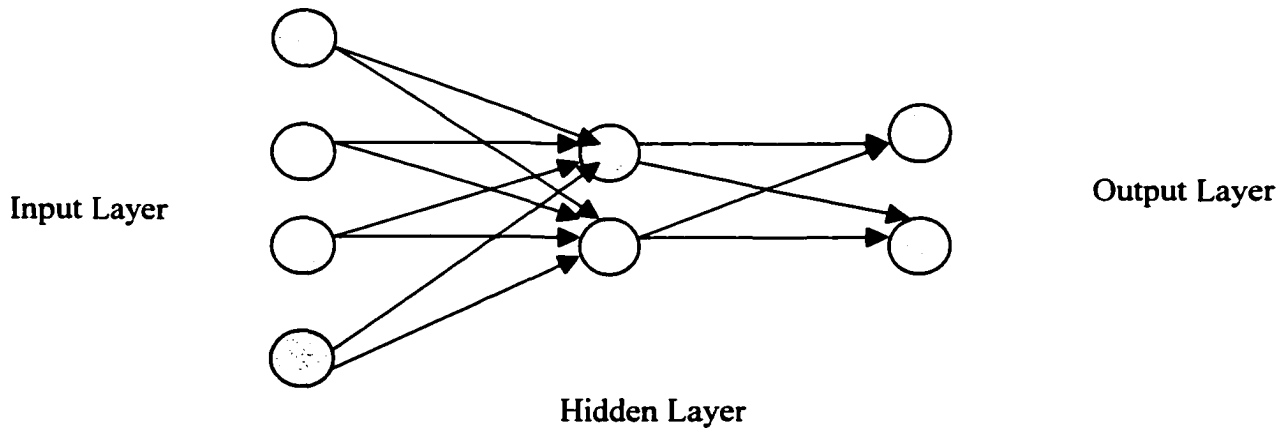

Fig.4.1. Schematic diagram for a Neural Network

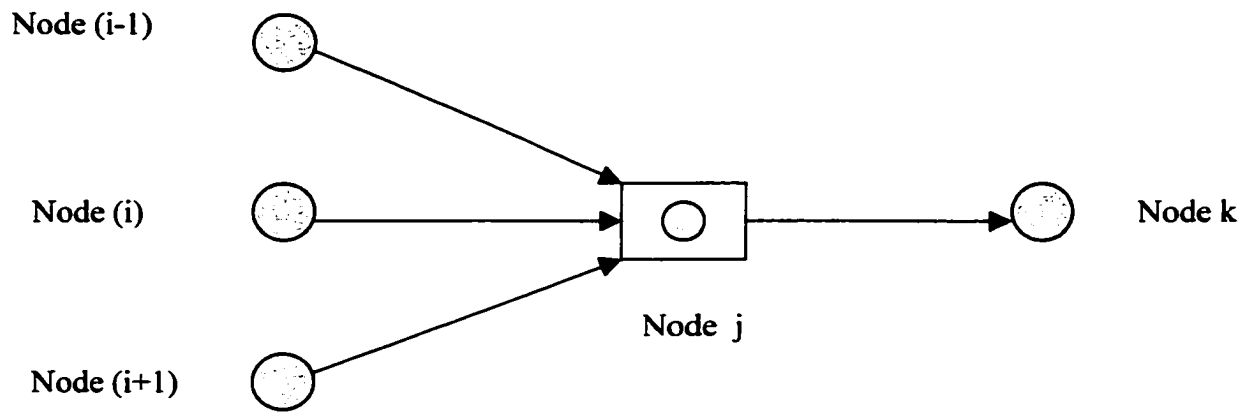

Fig. 4.2. Schematic diagram for neurons connections

4.6.4 ANN: Training

Training is a calibration process by which ANN computes the connection weights "parameters". Training of the ANN is accomplished by providing inputs to the model, computing the outputs, and adjusting the interconnection weights until the desired output is reached at the adopted minimum error or any other stopping criteria. The initial set of weights are assigned random values. The network is designated as trained when the predefined convergence criteria is satisfied, i.e. execution of the maximum number of iterations (epochs) or the optimal solution is reached, whichever comes first. If the maximum number of epochs is executed before an optimal solution is reached, the training algorithm does not converge, therefore a new set of initial weights is generated and the training algorithm is repeated. If after several trials, convergence cannot be achieved, one must change the structure of the network itself. In the testing or validation stage, the network (after having been trained) is used to check if it still performs

satisfactorily with the data that have not been used during the training. The following training algorithms were tested:

Back-propagation (BP) is an iterative technique commonly used for ANN learning (French et al., 1999; Tokar and Johnson, 1999), which is a gradient descent procedure. Training of the network using the BP algorithm requires several epochs or iterations (Gangopachlyay et al., 1998). This algorithm updates the interconnection weights at time t+1 from the weights at time t, as follows:

$$w_{ji}(t+1) = w_{ji}(t) + \Delta w_{ji}(t+1) \qquad [4\text{-}11]$$

The error is propagated backwards through the network to each node, and correspondingly the connection weights are adjusted based on the following equation:

$$\Delta_{ji} w_{ji}(t+1) = -\eta \frac{\delta E_p}{\delta w_{yz}} + \alpha \Delta w_{ji}(t) \qquad [4\text{-}12]$$

Where η = learning rate, specifies the step width of the gradient descent (typically 0.1-1.0); α = momentum factor (between 0.01and 0.99), used to improve convergence by including the previous weight changes on the present change in the weight space; t = time step. With o_{observ} denoting the observed data and o_{pred} denoting the predicted or the simulated output, the ANN is trained by finding the optimal values of the weight and bias parameters (w_{ji}, β_j) which will minimize the cost function, $E_p = \sum (o_{pred} - o_{observ})^2$, where the right hand side of the equation is the sum-squared error of the output. During training, the weights are adjusted by the back-propagation

algorithm so as to reduce the residual error of the training set. There are several methods for finding the weight increment, Δw_{ji} of which the gradient descent method is the most common. The gradient descent method results in weights being changed in the direction of the steepest descent down the error surface. The size of the step used in searching for the minimum value of the objective function is determined by the learning rate η.

Cascade-Correlation is characterized as a constructive learning rule (SNNS4.1, 1995). It starts with a minimal network consisting only of an input and output layer, equivalent to a linear model. Minimizing the overall error of a network, it adds step-by-step new hidden units to the hidden layer. When a node is added, its input weights are trained first. Then all the weights on the connections to the output layer are trained while leaving other weights unchanged. Weights associated with the potential hidden units are optimized by a gradient ascent method so as to maximize the correlation between its output and the residual error of the network. Once a new hidden node has been added to the network, its input-side weights are frozen. The hidden nodes are trained in order to maximize the correlation between the new unit output and the residual error signal of the network. The sign of the correlation coefficient will determine the sign of the weight on the connection from this hidden node to the output node. The addition of new hidden nodes is continued until maximum correlation between the hidden nodes and the error is attained.

The neurons in the hidden and the output layers are called activation function to transfer the signal. The activation function used in the hidden nodes is a tangent hyperbolic function and a linear function in the output nodes. The use of the tangent hyperbolic function introduces non-linearity to the network. Each hidden and output

neuron takes the linear combination of all values of the previous layer and transforms it with the activation function. The input to each neuron j in the hidden layer is the sum of the weighted input signal x_i, ($\Sigma w_{ji}x_i + \alpha_j$) in which w_{ji} is the interconnecting weight between neuron j in the hidden layer and neuron i in the input layer and α is a biased value). The output y_j from a hidden neuron is given by:

$$y_j = \tanh(\sum_i w_{ji}x_i + \alpha_j) \qquad [4\text{-}13]$$

The weight w reflects the relative importance of each input to the neuron. The tangent hyperbolic function shape is determined by the weights, w, and the bias (threshold), α. This function has values that range from –1.0 and +1.0 thus, the input and the output patterns are transformed to be in the function range. The output of neurons in the output layer is computed similarly with the linear function:

$$z_k = \sum_j w_{kj}y_j + \beta_k \qquad [4\text{-}14]$$

In general, for a network with I inputs, J hidden nodes and K output nodes and an activation function S, the final output could be written in the following form:

$$z_k = S_1(\sum_{j=1}^{J} S_2(\sum_{i=1}^{I} w_i x_i) \qquad [4\text{-}15]$$

The architecture of the network is finalized after a trial-and-error procedure. Trial and error, based on systematic studies using different training procedures, is still the preferred choice of most users, (e.g. Abrachart and See, 2000). If the architecture is too small, the network may not have sufficient degrees of freedom to learn the process correctly. On the other hand if the network is too large, it may not converge during training or it may overfit the data (Karunanithi et al., 1994). To improve generalization

of the network and to avoid overfitting, two methods defined in MATLAB are used: regularization and early stopping. Regularization involves modifying the performance function, which is chosen to be the mean of squares of the network errors on the training set (mse).

$$F = mse = \frac{1}{N}\sum_{i=1}^{N}(e_i)^2 = \frac{1}{N}\sum(Y - \tilde{Y})^2 \qquad [4\text{-}16]$$

It is possible to improve generalization if the performance objective function is modified by adding a term that consists of the mean of the sum of squares of the network weights and biases:

$$msereg = \gamma mse + (1-\gamma)msw \qquad [4\text{-}17]$$

where γ is the performance ratio, and

$$msw = \frac{1}{N}\sum_{j=1}^{N} w_j^{\,2} \qquad [4\text{-}18]$$

Using this performance function will cause the network to have smaller weights and biases, and this will force the network response to be smoother and less likely to overfit, (Matlab Neural Network Tool Box, Version 4, 1995).

The early stopping technique provides an efficient way to constrain the training of an ANN. In the early stopping method, the available data is partitioned into two subsets, the training set and the validation set (testing set). The first subset, the training set, is used for computing and updating the network weights and biases. The training subset is further partitioned into two subsets: a subset used for training the model and a subset used for evaluation (monitoring the performance of the model). The evaluation subset is used to check the progress of the network in order to define the epoch at which training should be stopped. The error on the evaluation set is monitored during the training

process. The evaluation error will normally decrease during the initial phase of training, as does the training set error. However, when the network begins to overfit the data, the error on the evaluation set will typically begin to rise. When the evaluation error increases for a specified number of iterations, the training is stopped, and the weights and biases at the minimum of the evaluation error are returned. At this point the network has activated the best generalization. If training is not stopped, the network will be over-trained and the performance of the network over the validation set will deteriorate despite the error of the training data still decreasing. The validation set error is not used during the training, but it is used to compare different models.

4.7 Forecasting Assessment and Validation

This study is unique with regard to the length of the lead season and to the input data used, so no other model results are available with which to compare accuracy improvement. Model results can only be compared with the observed values and the performance skill measures will be used to evaluate the models. However, there was a previous study (Awadalla and Rousselle, 1999) with relatively short lead-time (3 months before the flood peak in September), which is compared with the research results at that particular lead-time.

A number of statistics are used to measure the forecast potential. They include the association between two data sets calculated by means of the linear correlation coefficient (R) between the forecast ($\hat{Y}_t$) and the observed value (Y_t), the root-mean-square-error (RMSE), the mean absolute error (MAE), and the bias (BIAS). The referred four statistics may be determined as:

$$RMSE = \sqrt{\frac{1}{N}\sum_{1}^{N}(Y_t - \hat{Y}_t)^2} \qquad (4-19a)$$

$$MAE = \frac{1}{N}\sum_{1}^{N}\left|Y_t - \hat{Y}_t\right| \qquad (4-19b)$$

$$BIAS = \frac{1}{N}\sum_{1}^{N}(Y_t - \hat{Y}_t) \qquad (4-19c)$$

$$R = \frac{\sum_{1}^{N}(Y_t - \bar{Y})(\hat{Y}_t - \bar{\hat{Y}})}{\sqrt{\sum_{1}^{N}(Y_t - \bar{Y})^2 \sum_{1}^{N}(\hat{Y}_t - \bar{\hat{Y}})^2}} \qquad (4-19d)$$

in which $\bar{Y}$ is the mean of the observed data $Y_1, Y_2, \ldots\ldots, Y_N$; $\bar{\hat{Y}}$ is the mean of the predicted values $\hat{Y}_1, \hat{Y}_2, \ldots\ldots\ldots\ldots, \hat{Y}_N$; and N is the sample size.

For a given regression model, the coefficient R^2 is bounded between 0 and 1, with values closer to 1 denoting a better fitting model. However, increasing the number of regressor variables in the model i.e. increasing the number of parameters, can only increase the value of R^2 or leave it unchanged (Garnett et al., 1998). For this reason, a modified measure called the adjusted coefficient R^2 for a p order model is defined as:

$$Adjusted\ R^2 = 1 - [(1 - R^2)(N - 1)/(N - p)] \qquad [4\text{-}20]$$

Similarly, the adjusted root mean squares error is defined by:

$$Adjusted\_RMSE = \sqrt{\frac{1}{N - p - 1}\sum_{1}^{N}(Y_t - \hat{Y}_t)^2} \qquad [4\text{-}21]$$

The adjusted R^2 takes into account the degrees of freedom of the model and introduces a slight penalty for each regressor variable in the model. It may decrease in value if too many regressor variables are included in the model. The adjusted R^2 is the

statistic used in this study for determining the degree of explained variance in a model. In the following analyses the predictors and predictand are standardized respectively by subtracting the mean and dividing by the standard deviation. Thus, each standardized series will have zero mean and unit standard deviation i.e. fluctuations in the series are non-dimensional and can be compared easily among each other. For example, an advantage of standardizing the data is not to allow principal components analysis to give more weight to one variable over others.

In the construction of any forecast model, it is essential that the model be developed on a subset of the data and then be independently tested on a different subset of the data not used in the model calibration. This procedure is known as split sample testing. It has been widely used for model validation with conceptual and statistical hydrologic models. However, Wortman (1989) listed some shortcomings of this scheme such as withholding critical information from the calibration step and providing unstable error statistics highly dependent on the subset size and information content. Thus, a variation on the Jackknife procedure was recommended as a reasonable and robust approach for model validation. The validation of a forecast model may be accomplished by means of a drop-one Jackknife procedure that assures that the prediction for any year is independent of the predicted observations for that year (Gray et al., 1993). In this case each model is formulated based on N-1 years and tested on the remaining year not used in the construction of the model. In this scheme a minimum amount of information is withheld from each fitted model. However, for comparison with the ANN models and to check the stability of the predictors split sample technique was also used.

5. SINGLE SITE ANALYSIS

5.1 Blue Nile River

5.1.1 Lead-Lag SST streamflow Relationship

In this section, lead-lag relationships between the Blue Nile River flows and SST are investigated by means of linear correlation analysis. The correlation coefficients between the July to October (JASO) river flows and the 4-month averaged SST data defined as, November to February (NDJF), March to June (MAMJ), and July to October (JASO) are calculated for each region of the oceans and for different lead-lags. NDJF is dated by the year in which January occurs. In addition, in this research we refer to years leading, concomitant and lagging the central year as year (-1), year (0), and year (+1), respectively. The seasons for each year are defined in a similar way. Some studies have used the forecast of large-scale variables such as ENSO indices to forecast hydro-climatological variables. However, the forecast of ENSO is difficult and still in the experimental stage and need to be further improved (Chen and Wu, 2000). In this study the leading indicators such as SST were used to build the forecasting models. Assuming that the data have a Gaussian distribution, then the computed correlations are considered to be significant if they exceed 0.32 at 5% confidence level and then check for normality for the selected predictors.

Appendix A_2 shows the variation of correlation coefficients between the averaged Blue Nile River flows during July to October of a given year, denoted as JASO (0) and SSTs for MAMJ (-5) to NDJF (+2). The maps of correlations were computed for successive seasons beginning at MAMJ (-5) through NDJF (+2). These long lead-lags may help track the effect of the evolution of large-scale climatic variables such as ENSO. It is clear from the correlation maps that, as the lead time becomes smaller the magnitudes increase as well as the corresponding areas or regions in the sea. The highest positive correlations (of the order of 0.6) has been observed for NDJF (0) in the tropical North Atlantic. The highest negative correlations (of about -0.60) are observed for MAMJ (0) in the tropical eastern South Pacific. The North Atlantic (north of 40° N) and around the mid latitudes of the North and South Pacific consistently maintain a positive correlation with the Blue Nile River flow in all seasons while the South Atlantic is generally negatively correlated. Except for the Arabian Sea and north-Australian-Indonesian region in year (0), the Indian Ocean SSTs maintains a negative correlation with the Blue Nile River flows. Quin (1992) explained that in the summer a large low pressure system over India and the Arabian Sea dominates the airflow and brings strong, persistent southwesterlies to the southern part of the region. He further indicated that, at the same time, the intertropical convergence zone (ITCZ) lies just to the north of Eritrea so that the resulting convergence may bring significant precipitation over the headwaters of the Blue Nile River basin. It may also influence the direction and the amount of moisture fluxes from the Atlantic Ocean and the Congo basin. In addition, warm SSTs in north-Australia-Indonesia are generally associated with high Blue Nile River flows, while low river flows are usually accompanied and preceded by cold SSTs. The northern

Australia-Indonesia region is clearly an important component in the large-scale interaction between SSTs and the Blue Nile River hydrology.

Significant negative correlations were found in the southwest Indian Ocean in the regions east and/or south of Mauritius in the seasons MAMJ (-3), NDJF (-2), MAMJ (-2), JASO (-2), MAMJ (-1) and JASO (-1). Jury (1993) explained that, 14% of the world's known tropical cyclones taken place in the southwest Indian Ocean region (5° S - 30° S, 40° E - 80° E) during the austral summer, November to April. Also, Jury and Pathack (1991) indicated that, the Southwest Indian Ocean experiences regular organized convective activity leading to an average of 11 disturbances reaching tropical depression intensity each summer. This may indicate that cyclone frequency and intensity may contribute to the Blue Nile River flow variability. Generally, negative correlations dominate the Southern Hemisphere while positive correlations prevail in the Northern Hemisphere although remarkable negative and positive correlations can also be found in the northern and Southern Hemisphere, respectively.

Based on a composite scenario derived from six warm SST events that occurred during 1950-1976, Rasmusson and Carpenter (1982) defined five phases for a warm event: Antecedent (June to October of year (-1)), onset (November of year (-1) to January of year (0)), peak (March to May of year (0)), transition (June to October of year (0)), and mature (November of year (0) to February of year (+1)). They named March to May of year (0) as the peak phase because the South American western coast reached its peak warming during that period for the pre-1977 events, (Wang, 1995). The definition of seasons in this study is almost identical to the foregoing definition of the stage duration by Rasmusson and Carpenter, which helps to compare the regions and the seasons. For

example, negative correlations emerge in the southern part of the eastern Pacific Ocean centered around, 100° W, 35° S in MAMJ (-1). In JASO (-1) the area expands west to 140° W, north to 20° S, and east to the South American coast, and in NDJF (0) further expands along the South American coast. The signal migrates north-westward to the tropical eastern Pacific Ocean in MAMJ (0) and then intensifies and spreads westward in JASO (0) and NDJF (+1) covering a vast area of the central and eastern tropical Pacific Ocean (the whole ENSO region) as shown in Appendix A_2. Rasmusson and Carpenter (1982) presented evidence of a westward migration of SST anomalies that appear along the Ecuador-Peru coast. At each ENSO stage significant correlation regions between SST and Blue Nile River flows are consistent with the ENSO development, which suggests that the evolution of ENSO signal is clearly an important component in the large-scale interaction between SST and the Blue Nile River hydrology.

In NDJF (0) a dipole is established over the Indo-Pacific (Indonesian region) and eastern North Pacific Ocean. Then, in MAMJ (0) the sign of correlations changes in the eastern North Pacific Ocean from negative to positive. Also MAMJ (0) is the season when the central/western North Pacific Ocean and central/western South Pacific Ocean have high positive correlations. As expected, the correlations are stronger (negative) over the central and eastern Pacific basin during JASO (0) and NDJF (+1) as shown in Appendix A_2. The two seasons lie within the definition of the transition and mature stages of ENSO, respectively. The correlation for both seasons reaches –0.6 in the region (5° N-10° S, 165° E -75° W). This is in agreement with the previous studies of Eltahir (1996) and Amarasekera et al. (1997) which were carried out on a monthly basis. During these seasons the negative correlation field region decreases from the east equatorial

Pacific Ocean along the South American Pacific coast to the west equatorial Pacific Ocean near Indonesia. This area includes the Niño12 (0°-10° S, 90° W-80° W), Niño3 (5° N-5° S, 150° W-90° W), Niño34 (5° N-5° S, 170° W-120° W), and Niño4 (5° N-5° S, 160° E-150° W) regions. Correlations remain strongly negative over most of the oceans at the tropics during NDJF (+1) and strongly positive in the subtropics. In MAMJ (-2) and NDJF (0) a dipole is established over the subtropical North Atlantic Ocean and tropical North Atlantic Ocean resembling a NAO episode.

It is worth mentioning that some of these highly correlated regions, in the three oceans, at times appear to be associated with well defined developments in the oceanic-atmospheric system such as the North Pacific Pattern (NPP) SST region (30° N°-65, 100° E-140° W), Niño3 (5° N-5° S, 150° W-90° W), and cyclone source regions. Sea surface temperature in the Caribbean Sea region and the East Pacific Ocean show positive correlation (0.5) with the Blue Nile River flow for lead season JASO (-1). Elsner and Kara (1999) define an area that extends from the Caribbean Sea into the east Pacific Ocean as the tropical cyclone source region. This suggests that it may be worth considering other climatic variables as driving forces in the Nile River hydrology.

The main conclusion that can be drawn from the foregoing correlation analysis is the existence of a number of potential predictors for long-range forecasting of the Nile River flow based on SSTs. This analysis indicates that significant lead-lag correlations exist between the Blue Nile River flows and the oceanic surface temperatures. Significant correlations are found for various lag times between the Blue Nile River flows and various regions of the Pacific, Atlantic and Indian Oceans. Based on the

correlations maps, key regions of largest correlations are identified, and averaged seasonal SST over each of these regions are extracted for all seasons.

5.1.2 Multiple Linear Regression Analysis

The main statistical tool used in this study is multiple linear regression (MLR). Linear regression is a useful empirical approach to long-range forecasting of large-scale events such as monsoon rainfall and ENSO (Parthasarathy et al., 1988). Although atmospheric processes are basically nonlinear, use of statistical forecast models can contribute toward understanding of the mechanisms associated with the large-scale teleconnection patterns of the general circulation (Kung and Sharif, 1980). After the relevant predictors are determined, multiple linear regression is employed to relate these predictors with the Blue Nile River flows in order to find the smallest set of predictor variables that still does an adequate job of predicting the value of the dependent variable.

Out of the 84 regions initially identified 21 regions having serially independent SSTs series (to avoid miss-leading results) were selected for multiple linear regression. In addition, the previous year's August to November (ASON) Guinea precipitation was also incorporated as a predictor. The previous year August to November rainfall over Guinea is strongly and positively correlated with the Blue Nile River flow ($r = 0.63$) for the period 1953-1989. This association appears to be the strongest of any of the individual predictors shown in Table 5-1. This indicates that Guinea rainfall is a potential predictor for the Nile River flow with a 7-month lead-time before the flood season (JASO). Table 5-1 lists all the predictors which satisfy the above criteria and their corresponding location and lead season. It is worth mentioning that some of these highly correlated regions, in the three oceans, are thought to be associated (at times) with quite

well defined developments in the oceanic-atmospheric system. For example, region 4 lies within the North Pacific Pattern (NPP) SST region (30° N-65° N, 100° E-140° W); region 18 is located within the Niño3 (5° N°-5° S, 150° W-90° W). This will allow us to consider further climatic variables to be used as driving forces in Nile hydrology.

Figure 5-1 plots the standardized Blue Nile River flow (JASO) and that of the previous year (August-November) precipitation of Guinea. As shown in Fig. 5-1, in 65% of the years the river flow and the precipitation are positively connected (24 times out of 37). Table 5-1 summarizes the results obtained including the locations of the predictors and their respective correlation coefficient with the Blue Nile River flow (JASO) at various leading seasons.

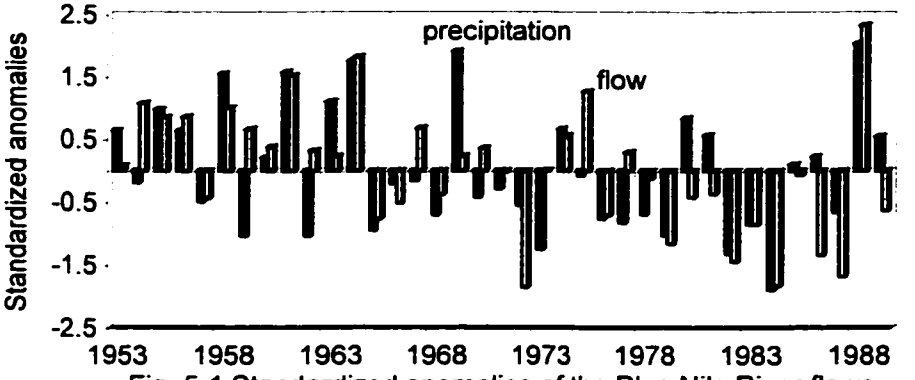

Fig. 5-1 Standardized anomalies of the Blue Nile River flows (JASO) and previous year Guinea precipitation ASON (-1)

Many combinations of these regions (Table 5-1) were used to forecast the Blue Nile River flows at different lead times. Table 5-2 shows five multiple linear regression models developed to forecast the Blue Nile River flows (JASO) as a function of SST and Guinea precipitation. The subscripts stand for the region number as shown in Table 5-1. The performance measures shown in Table 5-2 help in judging the performance measures of the various models. In general, as shown in Fig. 5-2, the variability of the forecast

flows through the years resemble the observed data quite well. Table 5-2 shows that for a 4-month lead time (Model A_1) the adjusted R^2 for validation reaches 64% while it becomes 48% for a 16-month lead time forecast (model A_5). As expected, the shorter the lead time the higher the forecast performance results.

Table 5-1. Locations of the SST predictors and their respective correlation coefficients with the Blue Nile River flow (JASO) for various leading seasons. The correlation with the Guinea precipitation is also shown

NO.	LEAD- SEASON	LOCATION	LATITUDE	LONGITUDE	CORR. COEFF.
1	MAMJ (-3)	Pacific	20° S→30° S	170° W→145° W	0.48
2	JASO (-3)	Pacific	20° N→05° N	130° E→130° E	-0.52
3	NDJF (-2)	Atlantic	30° N→20° N	90° W→70° W	0.42
4	NDJF (-2)	Pacific	50° N→35° N	160° W→140° W	0.54
5	NDJF (-2)	Pacific	10° N→00°	148° E→155° E	-0.39
6	MAMJ (-2)	Atlantic	45° N→35° N	50° W→35° W	0.41
7	NDJF (-1)	Pacific	15° S→25° S	175° W→165° W	0.32
8	MAMJ (-1)	Indian	35° S→44° S	115° E→130° E	-0.43
9	MAMJ (-1)	Pacific	30° S→44° S	110° W→90° W	-0.46
10	JASO (-1)	Atlantic	15° N→10° N	75° W→65° W	0.42
11	JASO (-1)	Indian	00° →07° S	90° E→130° E	-0.39
12	JASO (-1)	Pacific	20° S→35° S	140° W→100° W	-0.43
13	JASO (-1)	Pacific	15° N→10° N	120° W→100° W	0.52
14	ASON (-1)	$Guinea_p$			0.63
15	NDJF (0)	Atlantic	10° N→00°	60° W→40° W	0.52
16	NDJF (0)	Indian	35° S→44° S	20° E→60° E	-0.42
17	MAMJ (0)	Indian	10° S→20° S	110° E→125° E	0.40
18	MAMJ (0)	Pacific	02° N→05° S	130° W→90° W	-0.55
19	MAMJ (0)	Pacific	05° N→20° S	120° W→80° W	-0.52
20	MAMJ (0)	Pacific	30° N→25° N	140° E→160° E	0.57
21	MAMJ (0)	Pacific	25° N→35° N	179° W→160° W	0.44
22	MAMJ (0)	Pacific	20° S→35° S	179° W→160° W	0.45

Table 5-2. Assessment and validation statistics for various forecast models based on multiple linear regression (MLR-OLS). Values in parentheses in the second rows are for the validation phase (category A)

LEAD SEASON	REGRESSION EQUATION	ρ	R	R^2	ADJ_R^2	ADJ_RMSE	RMSE	MAE	BIAS
A_1) MAMJ(0)	$Q_{BN(0)} = 0.05 + 0.28SST_3 + 0.54SST_{13} + 0.31Guinea_p + 0.48SST_{21}$	0.65	0.88 (0.82)	0.77 (0.67)	0.75 (0.64)	0.53 (0.63)	0.50 (0.59)	0.40 (0.49)	0.00 (0.00)
A_2) NDJF(0)	$Q_{BN(0)} = 0.06 + 0.34SST_1 + 0.31SST_{13} + 0.51Guinea_p - 0.29SST_{16}$	0.60	0.84 (0.79)	0.71 (0.63)	0.67 (0.60)	0.59 (0.67)	0.55 (0.63)	0.42 (0.49)	0.00 (0.00)
A_3) ASON(-1)	$Q_{BN(0)} = 0.06 + 0.37SST_1 + 0.46SST_4 + 0.26SST_7 + 0.52Guinea_p$	0.61	0.87 (0.82)	0.75 (0.68)	0.72 (0.65)	0.55 (0.63)	0.51 (0.58)	0.42 (0.48)	0.00 (-0.01)
A_4) JASO(-1)	$Q_{BN(0)} = 0.04 + 0.48SST_1 + 0.46SST_3 + 0.33SST_7 + 0.49SST_{13}$	0.61	0.85 (0.79)	0.72 (0.63)	0.68 (0.60)	0.58 (0.67)	0.54 (0.63)	0.44 (0.51)	0.00 (0.00)
A_5) MAMJ(-1)	$Q_{BN(0)} = 0.02 + 0.39SST_1 + 0.51SST_4 + 0.30SST_7 - 0.35SST_8$	0.55	0.79 (0.72)	0.63 (0.52)	0.58 (0.48)	0.67 (0.77)	0.62 (0.71)	0.47 (0.54)	0.00 (0.01)

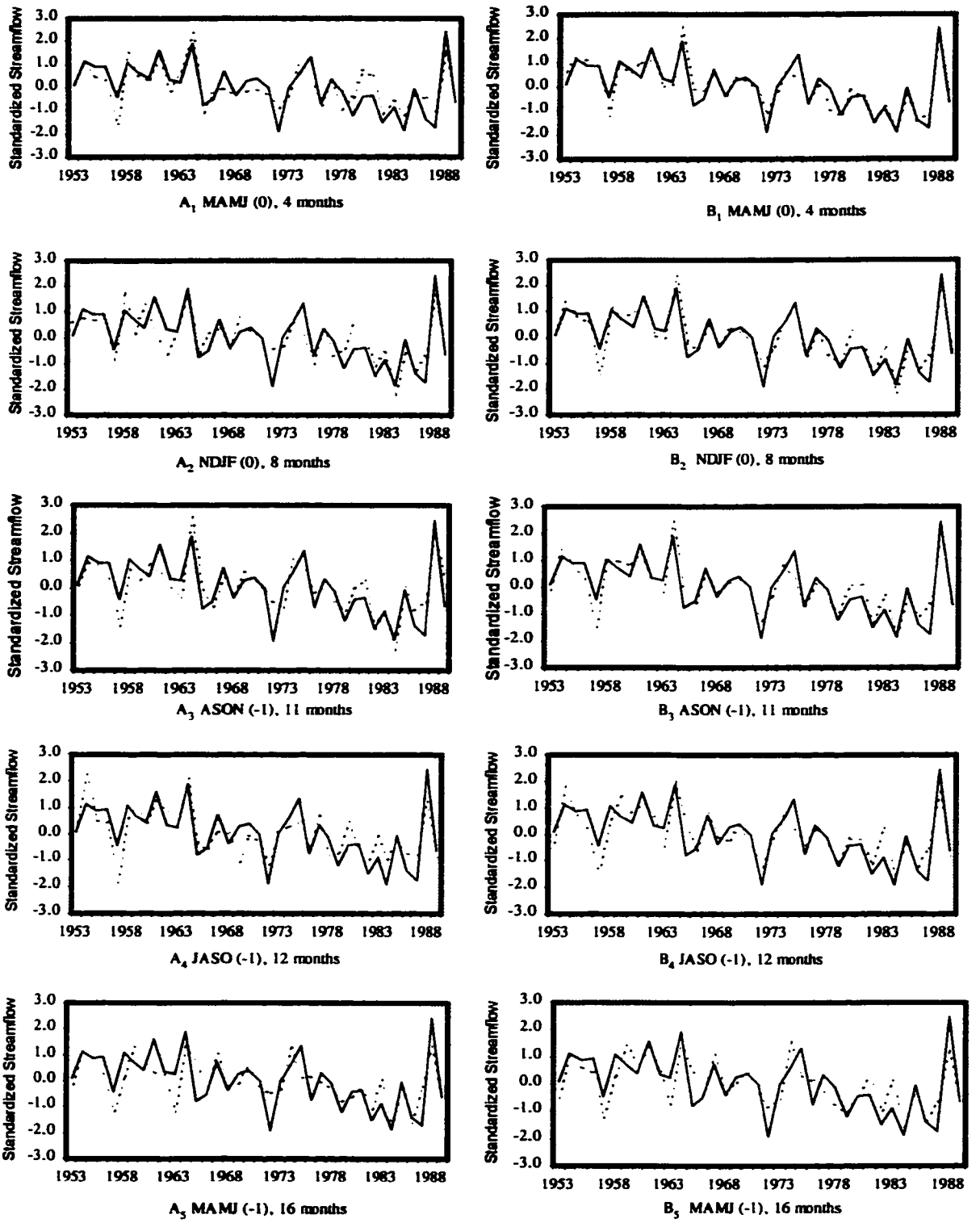

Fig. 5-2 Comparison between the observed Blue Nile River flows (solid line) and the forecasted flows (dotted line) for the 5 models listed in Table 5-2 (category A) and the models listed in Table 5-4 (category C). The figures listed on the left column correspond to category A and those listed on the right to category C

The forecast results for the five models shown in Fig. 5-2 and Table 5-2 indicate potential predictability of the Blue Nile River flows based on SST at various locations in the oceans and Guinea precipitation, for different forecast lead periods. The multiple linear regression requires that the predictors are uncorrelated. In order to guarantee this requirement multiple linear regression analysis was performed between every predictor (for each model) and the rest of the predictors, and the adjusted R^2 coefficients were computed. The percentage of variance of any given predictor that is explained by other predictors ranges between 0% and 15%. Thus, it is assumed that the predictors are independent, and consequently, there is no change in the number of degrees of freedom required for testing the significance of the correlations between the data sets. A similar procedure was also followed by Berri and Flamenco (1999). The hypothesis of normality for the all the original variables used in the models presented (Table 5-2) was not rejected. In addition, the sign test of the regression coefficients agrees with the correlation coefficients sign of the individual predictor and the predictand. Figure 5-3 shows the individual lagged standardized time series for the predictors used in the models of Table 5-2.

5.1.3 Hybrid PC Multiple Linear Regression Model

One of the purposes of PCs regression is to make sure that any intercorrelation among the original variables is removed. High correlation among the independent variables would result in computational error or a singular matrix if regression on these variables is attempted (Marsden and Davis, 1968). Because some of these predictors are interconnected, principal component analysis on these predictors was conducted.

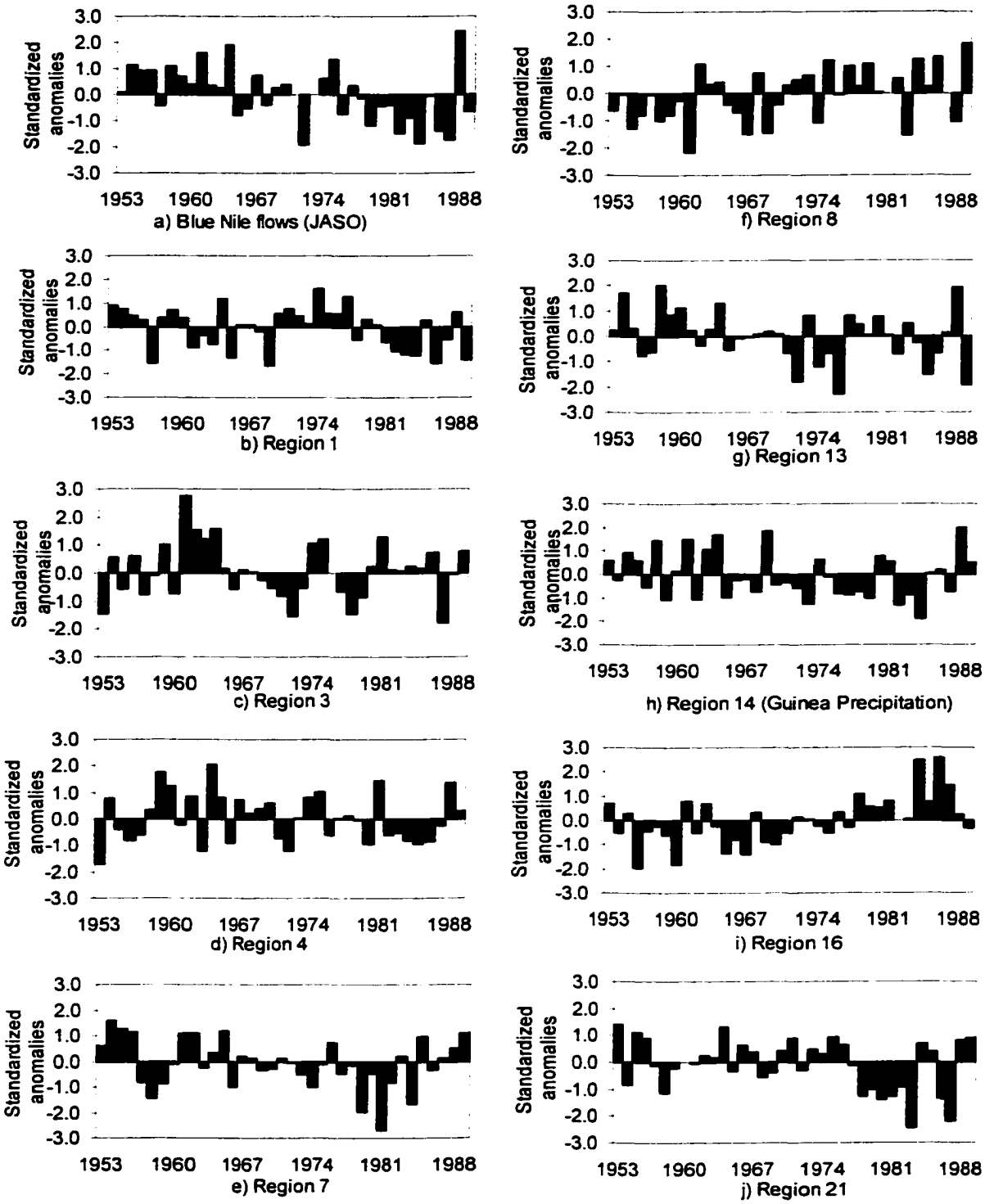

Fig. 5-3 Lagged time series for the original variables predictors and predictand included in the models of Table 5-2 for seasons and locations shown in Table 5-1 for the period 1953-1989

Interannual modes of SST variation at 84 locations from the lead correlation analysis across the oceans and the previous year Guinea precipitation during the period 1953-1989 were defined by using principal components for lead seasons MAMJ (-3) to MAMJ (0). The first 10 PCs were retained, and up to 5 PCs with significant regression coefficients for each lead season were taken as input to the multivariate linear regression model. Figure 5-4 illustrates the declining variance explained by successive PCs, and supports the retention of the first 10 PCs. Most of the explained variance is contained in the first four components. Regression equations as shown in Table 5-3 were determined based on the principal components, and nonsignificant coefficients were set equal to zero.

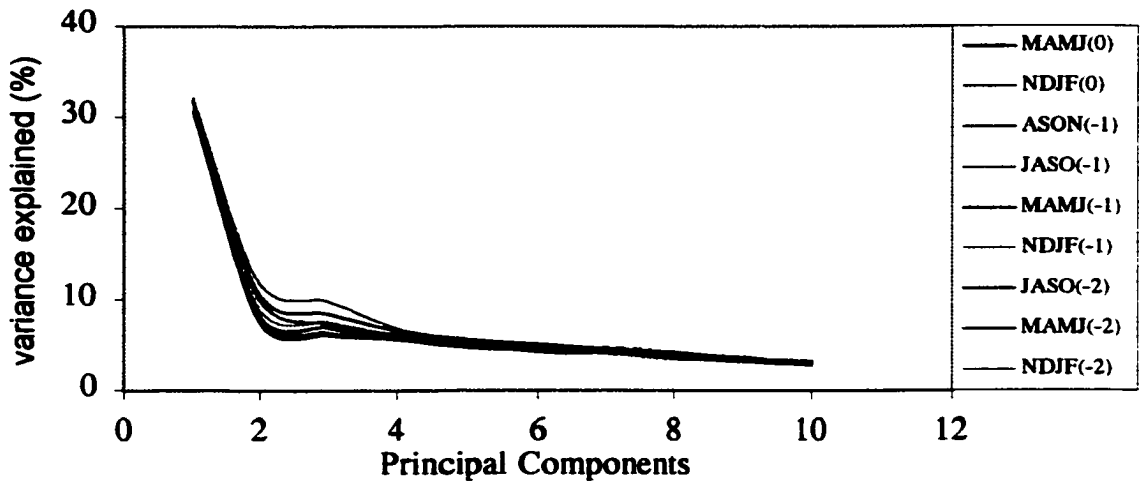

Fig. 5-4 Variance explained by each of the first 10 PCs at each lead season

Examination of the eigenvalues shows that in most of the model intermediate components have been skipped in spite of their relatively higher contribution to explaining the variance in the regression model, suggesting that the ultimate signal from the individual oceans are not included in the first few PCs. Figure 5-5 demonstrates the

Table 5-3. Assessment and validation statistics for various forecast models based on principal component regression (PCR). Values in parentheses in the second rows are for the validation phase (Category B)

LEAD-SEASON	REGRESSION EQUATIONS	ρ	R	R^2	ADJ_R^2	ADJ_RMSE	RMSE	MAE	BIAS
C_1) MAMJ(0)	$Q_{BN(0)} = -0.01 + 0.15\,PC_1 - 0.17\,PC_2 + 0.10\,PC_5 + 0.18\,PC_7 + 0.09\,PC_{10}$	0.69	0.89 (0.83)	0.80 (0.70)	0.77 (0.66)	0.50 (0.62)	0.46 (0.57)	0.36 (0.44)	-0.02 (0.01)
C_2) NDJF(0)	$Q_{BN(0)} = -0.03 + 0.15\,PC_1 - 0.13\,PC_2 + 0.18\,PC_7 - 0.29\,PC_9$	0.63	0.88 (0.83)	0.78 (0.69)	0.75 (0.66)	0.52 (0.62)	0.48 (0.57)	0.41 (0.48)	0.00 (0.01)
C_3) ASON(-1)	$Q_{BN(0)} = -0.04 + 0.16\,PC_1 - 0.12\,PC_2 - 0.11\,PC_7 - 0.30\,PC_8$	0.59	0.84 (0.79	0.72 (0.62)	0.68 (0.59)	0.58 (0.68)	0.54 (0.63)	0.46 (0.54)	0.00 (0.00)
C_4) JASO(-1)	$Q_{BN(0)} = -0.03 + 0.16PC_1 - 0.11PC_2 + 0.12PC_7 - 0.26PC_8$	0.55	0.81 (0.74)	0.65 (0.54)	0.61 (0.50)	0.65 (0.75)	0.60 (0.70)	0.50 (0.57)	-0.01 (0.01)
C_5) MAMJ(-1)	$Q_{BN(0)} = -0.04 + 0.16PC_1 - 0.09PC_2 + 0.14PC_7 - 0.27PC_8 - 0.18PC_{10}$	0.60	0.83 (0.75)	0.69 (0.56)	0.64 (0.51)	0.62 (0.75)	0.57 (0.69)	0.45 (0.53)	0.00 (0.01)
C_6) NDJF(-1)	$Q_{BN(0)} = -0.05 - 0.18\,PC_1 + 0.30\,PC_8 - 0.18\,PC_9$	0.53	0.80 (0.71)	0.64 (0.50)	0.60 (0.47)	0.65 (0.78)	0.62 (0.73)	0.49 (0.57)	0.00 (0.02)
C_7) JASO(-2)	$Q_{BN(0)} = -0.04 - 0.20\,PC_1 - 0.22\,PC_7 + 0.20\,PC_9$	0.51	0.77 (0.67)	0.59 (0.45)	0.55 (0.44)	0.69 (0.80)	0.66 (0.77)	0.50 (0.58)	0.00 (0.02)
C_8) MAMJ(-2)	$Q_{BN(0)} = -0.06 - 0.23PC_1 - 0.22PC_4 - 0.19PC_5 + 0.16PC_6$	0.60	0.81 (0.74)	0.65 (0.55)	0.61 (0.51)	0.65 (0.74)	0.61 (0.69)	0.46 (0.53)	0.00 (0.00)
C_9) NDJF(-2)	$Q_{BN(0)} = -0.08 - 0.27\,PC_1 - 0.34\,PC_5$	0.56	0.80 (0.75)	0.65 (0.57)	0.63 (0.56)	0.63 (0.71)	0.61 (0.68)	0.46 (0.50)	0.01 (0.01)

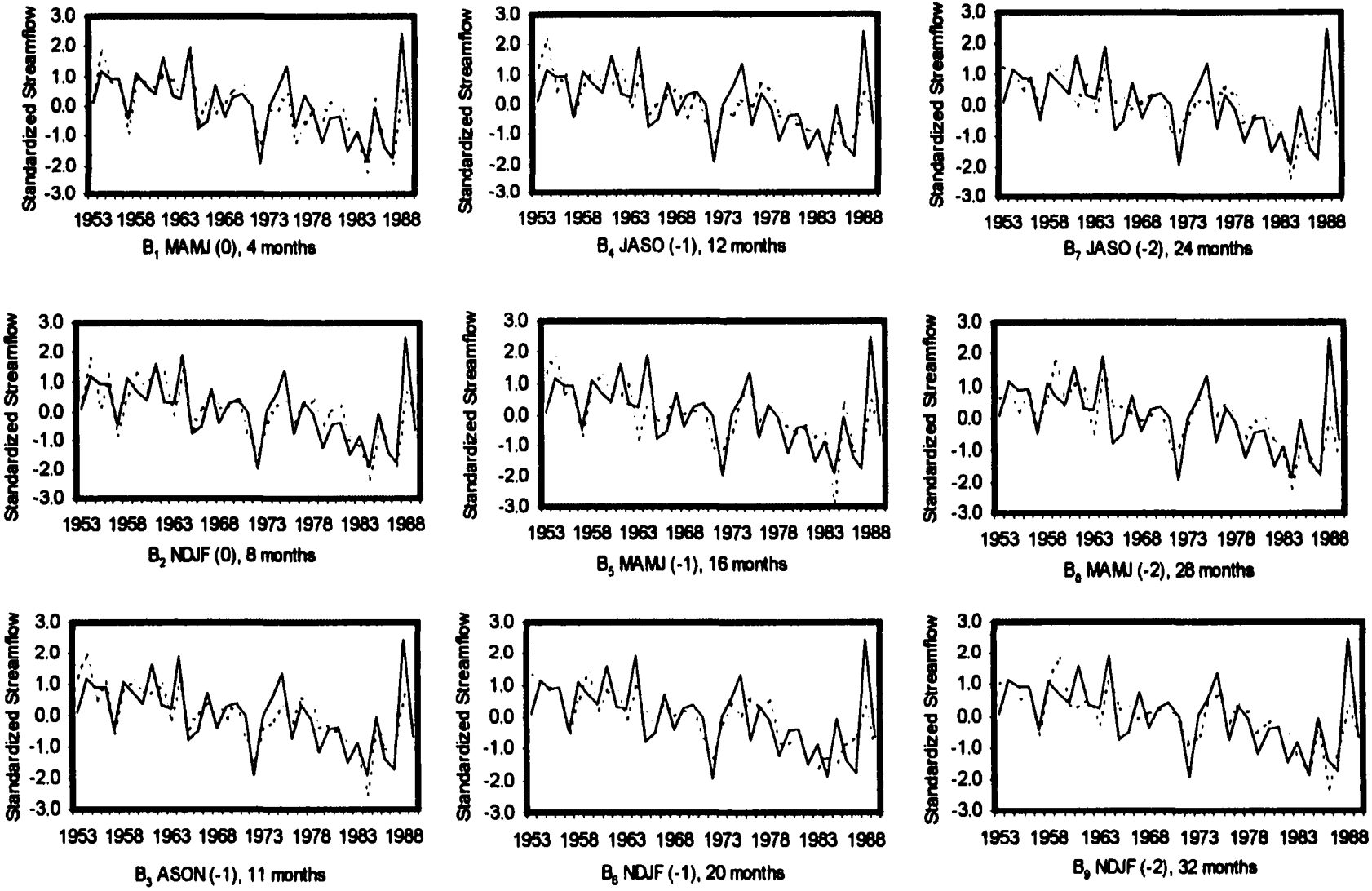

Fig. 5-5 Comparison between the observed Blue Nile River flows (solid line) and the forecasted flows (dotted line) for the models listed in Table 5-3 (category B). The forecast season and lead times were shown at the bottom of each figure

forecasted and the observed river flow at various lead seasons. These results indicate that a surprisingly strong forecast potential is available for the Blue Nile River utilizing appropriate global SSTs and the previous year's Guinea precipitation.

For comparison the variables used in the models based on Eq. 4-2 and described in Table 5-2 (category A) are used to develop forecasting models based on multiple linear regression of principal components (PCR) as in Eq. 4-6 (category C). Table 5-4 shows the resulting regression equations in terms of principal components in which nonsignificant coefficients were set equal to zero. Figure 5-2 shows a comparison between the predicted and the observed Blue Nile River flows for the five models (drawn together for comparison). Also Fig. 5-6 shows a comparison of adjusted R^2 for the two model categories. The results indicate that forecasts based on PCA outperformed those based on models in terms of the original variables. This may be attributed to the higher amount of information the PCA extracts as compared to the original variable models.

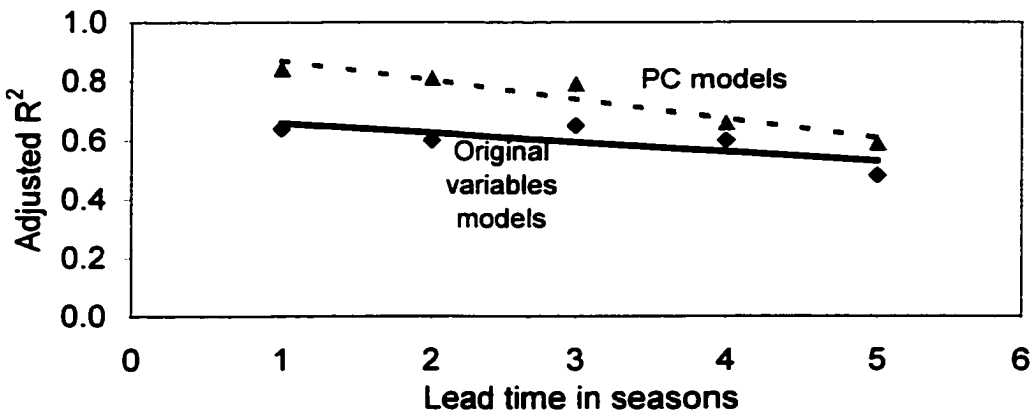

Fig. 5-6 Comparison of adjusted R^2 for forecast models of categories A and C at various lead season

Table 5-4. Assessment and validation statistics for various forecast models based on principal component regression (PCR). Values in parentheses in the second rows are for the validation phase (Category C)

LEAD-SEASON	REGRESSION EQUATION	ρ	R	R^2	ADJ_R^2	ADJ_RMSE	RMSE	MAE	BIAS
B_1) MAMJ(0)	$Q_{BN(0)} = 0.06 + 0.64PC_1 - 0.22PC_5 + 0.16PC_6$	0.76	0.94 (0.92)	0.88 (0.85)	0.87 (0.84)	0.37 (0.42)	0.35 (0.39)	0.26 (0.29)	0.00 (-0.01)
B_2) NDJF(0)	$Q_{BN(0)} = 0.05 - 0.63PC_1 - 0.34PC_5$	0.73	0.92 (0.90)	0.84 (0.82)	0.83 (0.81)	0.42 (0.46)	0.40 (0.44)	0.31 (0.34)	0.00 (0.00)
B_3) ASON(-1)	$Q_{BN(0)} = 0.03 + 0.65PC_1 + 0.33PC_4$	0.70	0.91 (0.89)	0.83 (0.80)	0.82 (0.79)	0.44 (0.48)	0.42 (0.46)	0.42 (0.37)	0.00 (0.00)
B_4) JASO(-1)	$Q_{BN(0)} = 0.02 + 0.64PC_1 + 0.22PC_2 - 0.26PC_3 + 0.22PC_4$	0.67	0.87 (0.83)	0.76 (0.69)	0.73 (0.66)	0.54 (0.62)	0.50 (0.57)	0.40 (0.46)	-0.01 (0.00)
B_5) MAMJ(-1)	$Q_{BN(0)} = -0.01 - 0.67PC_1 - 0.26PC_2 + 0.31PC_3$	0.60	0.83 (0.78)	0.69 (0.62)	0.66 (0.59)	0.60 (0.67)	0.57 (0.64)	0.45 (0.51)	0.00 (0.00)

As expected the difference in the adjusted R^2 of the original variable models (category A) and the PCA models (category C) reduces as the lead-time increases. Models in category C are also simple (parsimonious) in comparison with category A and B.

The overall measures adopted for assessment of the accuracy of the forecasts are the adjusted R^2, the mean absolute difference (MAE), the adjusted root mean square error (RMSE) and the BIAS. The values of these performance measures are shown for each model in Tables 5-2, 5-3 and 5-4. The adjusted RMSE for predicted streamflow for the 37 years used in this study was found to be in the range of 0.37 to 0.69, smaller than the standard deviation of the streamflow, which is 1.0 for standardized data. The lowest values are for the principal component analysis of the original variables (category C). In the first three category C models, the error in the predicted streamflow is smaller than half the standard deviation of the river flows. This was valid for the cross validation models as well as the calibration models. For all models the lowest adjusted R^2 value was 0.48, at MAMJ (-1) lead-time for the category A models. The absolute value of the BIAS was in the range 0.00 to 0.02. Most of the models show a perfect BIAS value of zero. The MAE values are about 50% of the standard deviation of the streamflow. Generally, these four statistics are quite comparable for the three categories. The adjusted R^2 values are significant and decrease as the lead horizon increases.

The statistics for equations based on PCA showed significant improvement in forecasting accuracy over equations developed using original variables. PCA provided better results in deveioping a forecast for the Blue Nile River flows (category C) compared to the original variable models (category A).

5.2 Contribution from Individual and Combined Oceans

This section follows a strategy similar to the one used in the previous section but with longer lead-time (MAMJ (-5) to MAMJ (0). An attempt is made to single out the contribution of each ocean basin to the ocean-atmosphere system affecting the Blue Nile River hydrology. This should give an indication of which ocean has an important influence on the variability of the Blue Nile River's flows. In order to explore the performance at longer lead times. The lead-time extends back to MAMJ (-5). 113 regions with significant correlations were identified for the three oceans, 51 for the Pacific Ocean, 33 regions in the Atlantic Ocean and 29 regions for the Indian Ocean. Principal component analysis was performed on the data at each ocean at the different lead times. The first ten principal components were used as input to the MLR model. The first five components with significant coefficients were retained and the performance criteria (adjusted R^2) at each lead-time were computed. The procedure was repeated for the combined data of the three oceans.

ENSO influences suggest that a majority of predictors come from the Pacific Ocean. As mentioned above, spatial and temporal domains of the SST predictors show that the Pacific Ocean has a larger number of significantly correlated regions compared to the Atlantic and the Indian Oceans. The data for each ocean was grouped at different lead periods, stacked and PCA was applied. Figure 5-7 shows the adjusted R^2 for each ocean and the combined oceans at each lead time. As expected the variance explained decreases as the lead-time increases. It is hypothesized that, when separate oceans carry different climatic signals significant improvement in forecast skill should be attained by combining the oceans in a single model. If forecast skill is not appreciably higher, then

the oceans probably do not contribute separate signals. The three oceans have shown higher contribution to the forecasting of the Blue Nile River flows. Surprisingly, the nearby Indian Ocean shows the lowest contribution to the Blue Nile River flows, particularly in the first 8 lead times. The Pacific Ocean contributes a higher percentage to the flow variability compared to the Indian and the Atlantic Oceans. The Atlantic Ocean contributes a higher amount to the river flow variability in the first 8 lead times compared to the Indian Ocean, at longer lead-times the Indian Ocean has a higher contribution to the flow variability. This is in agreement with the general perception that the moisture for the Ethiopian Plateau is largely from the Atlantic Ocean and has a strong correlation with the ENSO phenomenon in the Pacific Ocean. This illustrates that the sources of predictability for the July to October Blue Nile River flows using SST are not restricted to the equatorial Pacific Ocean.

For comparison and to confirm the above connection a similar procedure was repeated for the Nile River flow at the Aswan hydrological station. 81 regions with significant correlations were identified for the three oceans, 39 regions for the Pacific Ocean, 22 regions for the Atlantic Ocean and 20 regions for the Indian Ocean. Figure 5-8 shows that, the contribution from each of the oceans is lower than that for the Blue Nile River flow. As expected the variance explained decreases as the lead-time increases. As expected, the Pacific Ocean has higher contribution to the Nile River flow at Aswan compared the Atlantic and the Indian Oceans. The adjusted R^2 values are higher for combined oceans followed by the Pacific Ocean, the Atlantic and the Indian Ocean, for both the Blue Nile River and the Nile River at Aswan. However, the contributions of the oceans to the river flows are consistently lower for the Nile River at Aswan compared to

the Blue Nile River. A stronger SST signal is in the Blue Nile River flow than in the Nile River flow at Aswan. Amaraseketa et al. (1997) explained that, the White Nile River flows through the equatorial lakes and marshes in the Sudd region, is highly damped and expected to show very little association with ENSO. This may justify the lower signal in the Nile River flow at Aswan due to others tributaries contribution to the Nile River flows. The number of the strongly correlated regions are higher for the Pacific Ocean followed by the Atlantic Ocean and the relatively least correlated regions are in the Indian Ocean, for both the Blue Nile River and Nile River at Aswan.

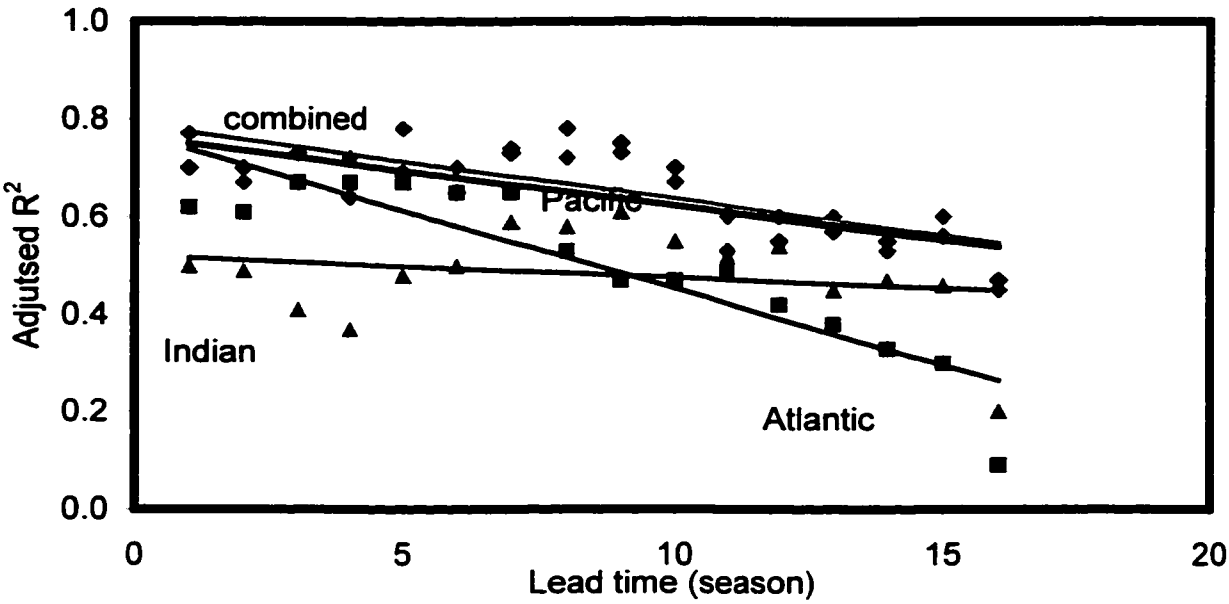

Fig. 5-7 Adjusted R^2 using PC for individual oceans and combined oceans for the lead seasons MAMJ (-5)-MAMJ (0) for the Blue Nile River

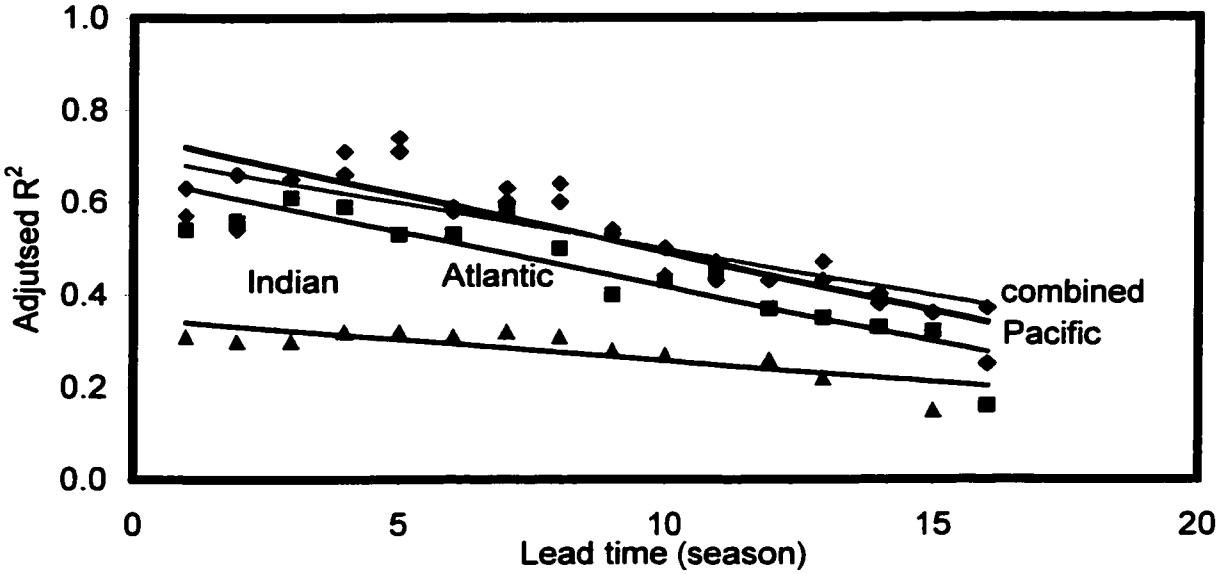

Fig. 5-8 Adjusted R^2 using PC for individual oceans and combined oceans for the lead seasons MAMJ (-5)-MAMJ (0), Nile River at Aswan

The Pacific Ocean has the highest contribution to the Blue Nile River flows variability as compared to the Atlantic and the Indian Oceans. The Pacific Ocean SST anomalies are correlated more strongly with the Blue Nile River flood well defined pools (regions) in the concomitant (JASO (0)) and subsequent (NDJF (+1)) seasons compared to the preceding seasons. SST pool size during these seasons reduces from the east equatorial Pacific Ocean to the west equatorial Pacific Ocean. The pool contains the known Niño12, Niño3, Niño34, and Niño4. In addition, the seasons JASO (0) and NDJF (+1) are defined by Rasmusson and Carpenter (1982) as transition and mature phases of the ENSO.

5.3 Forecasting the Nile River Flows and the Flows of its Tributaries

In this part of the research forecasts models were developed for the tributaries of the Nile River flows. A similar procedure as the one used in the previous sections is followed. The new locations are the Nile River at Aswan, the Atbara River and the Sobat River. The Blue Nile River flow was included for comparison and possible improvement of the forecast. Appendix B lists the predictors used at each of the four locations.

Recognizing that significant intercorrelations exist between circulation predictors, methods for reducing redundant information in the set of prediction variables have been sought. Principal component analysis (PCA) provides a promising means by which this may be achieved. Using PCA on the set of selected predictors showed that the first PC accounts for an average of 46% of the predictor set variance as well as being strongly and significantly correlated with the Nile River flows.

The idea of principal component regression models (PCR) is to regress the response variable on the PCs of predictor variables rather than the original predictor variables. The number of PCs used in the final regression model is typically much less than the number of predictor variables. Given that the primary purpose of the PCA was data reduction and intercorrelation removal, no further attempt at interpretation of the components was done. Using the principal component series, models were developed for the Nile River and its tributaries. Tables 5-5, 5-6, 5-7, and 5-8 list the algorithms and performance skill parameters for the models for various lead times for the Sobat River, the Blue Nile River, the Atbara River, and the Nile River at Aswan, respectively. As expected, predictability measured by the performance skill measures declines as the lead-time increases.

Figures 5-9, 5-10, 5-11 and 5-12 show the observed (solid) and the validated predicted flows (dashed) for the Sobat River, the Blue Nile River, the Atbara River and the Nile River at Aswan. Most of the year-to-year variability was reproduced, although there are years when the magnitude of the anomaly is underestimated or overestimated. However, the phase of the flow was well predicted. Generally, fair similarity between the observed and the predicted flow amounts are observed.

The Blue Nile River forecast improved over the forecasts in the previous sections. This may be due to the fact that the seesaw predictors were included which are more stable and have higher correlation with river flows. In addition, the models in Table 5-6 are simpler (parsimonious) than those in the previous section (Table 5-3). This may be attributed to the higher variability extracted by PC_1 with an average of 46% compared to about 32% in the previous section. In addition, by using the seesaw (the gradient between two regions oppositely correlated with the river flows), more stable predictors with higher correlations were used. It is worth noting that PC_1 predictor for the Blue Nile River shows significant and inverse correlation with the SOI (July to December) at all lead seasons. The correlation decreases as the lead-time increases and ranges from –0.60 to –0.38. Similarly, the PC_1 predictor for the Nile River flows at Aswan are significantly and inversely correlated with the SOI (July to December) at all lead seasons except for JASO (-3). The correlation decreases as the lead-time increases and ranges from –0.60 to –0.34. This shows how the ENSO phase dominates the Nile River flows, particularly in the Ethiopian Plateau Basin.

Figures 5-13 and 5-14 shows the predictability of the Nile River flows and its tributaries measured by the adjusted R^2 and agreement coefficient (ρ), respectively. The

Table 5-5 Assessment and validation statistics for various forecast models based on principal component regression (PCR). Values in parentheses in the second rows are for the validation phase, (Sobat River)

LEAD-SEASON	REGRESSION EQUATION	ρ	R	R^2	ADJ_R^2	ADJ_RMSE	RMSE	MAE	BIAS
B_1) MAMJ(0)	$Q_{SOB(0)} = 0.12 - 0.28PC_1 - 0.27PC_8$	0.65	0.89 (0.87)	0.79 (0.75)	0.78 (0.74)	0.45 (0.49)	0.43 (0.47)	0.36 (0.39)	0.00 (-0.01)
B_2) NDJF(0)	$Q_{SOB(0)} = 0.14 + 0.26PC_1 - 0.15PC_2 + 0.15PC_7 + 0.19PC_9$	0.59	0.86 (0.82)	0.74 (0.67)	0.71 (0.64)	0.52 (0.59)	0.48 (0.55)	0.37 (0.43)	0.00 (0.00)
B_3) JASO(-1)	$Q_{SOB(0)} = 0.14 - 0.25PC_1 + 0.11PC_2 - 0.21PC_5 + 0.23PC_8$	0.57	0.82 (0.77)	0.68 (0.59)	0.64 (0.55)	0.57 (0.66)	0.53 (0.61)	0.42 (0.48)	0.00 (0.00)
B_4) MAMJ(-1)	$Q_{SOB(0)} = 0.10 + 0.25PC_1$	0.40	0.69 (0.66)	0.48 (0.43)	0.47 (0.43)	0.70 (0.73)	0.68 (0.71)	0.53 (0.56)	0.00 (0.00)
B_5) NDJF(-2)	$Q_{SOB(0)} = 0.11 - 0.29PC_1 + 0.65PC_9$	0.42	0.71 (0.62)	0.50 (0.38)	0.47 (0.34)	0.70 (0.78)	0.67 (0.75)	0.53 (0.57)	0.00 (0.01)
B_6) JASO(-3)	$Q_{SOB(0)} = 0.06 + 0.39PC_1 + 0.78PC_6$	0.43	0.71 (0.66)	0.48 (0.43)	0.48 (0.42)	0.66 (0.74)	0.61 (0.71)	0.54 (0.58)	0.00 (0.01)

Table 5-6 Assessment and validation statistics for various forecast models based on principal component regression (PCR). Values in parentheses in the second rows are for the validation phase, (Blue Nile River)

LEAD-SEASON	REGRESSION EQUATION	ρ	R	R^2	ADJ_R^2	ADJ_RMSE	RMSE	MAE	BIAS
B_1) MAMJ(0)	$Q_{BN(0)} = -0.04 - 0.14PC_1 + 0.11PC_6$	0.64	0.87 (0.85)	0.76 (0.72)	0.74 (0.72)	0.52 (0.56)	0.50 (0.54)	0.38 (0.41)	0.00 (0.00)
B_2) NDJF(0)	$Q_{BN(0)} = -0.05 - 0.16PC_1 + 0.11PC_4$	0.62	0.84 (0.81)	0.71 (0.66)	0.70 (0.65)	0.57 (0.62)	0.55 (0.60)	0.41 (0.44)	0.00 (0.01)
B_3) JASO(-1)	$Q_{BN(0)} = -0.09 - 0.17PC_1 + 0.14PC_5$	0.60	0.84 (0.81)	0.70 (0.66)	0.68 (0.65)	0.58 (0.62)	0.56 (0.60)	0.42 (0.46)	0.00 (0.00)
B_4) MAMJ(-1)	$Q_{BN(0)} = -0.08 - 0.18PC_1 - 0.10PC_4 - 0.21PC_{10}$	0.61	0.84 (0.80)	0.71 (0.65)	0.68 (0.63)	0.59 (0.65)	0.55 (0.61)	0.42 (0.47)	0.00 (0.01)
B_5) NDJF(-2)	$Q_{BN(0)} = -0.11 - 0.22PC_1 - 0.28PC_{10}$	0.59	0.86 (0.83)	0.74 (0.69)	0.72 (0.68)	0.54 (0.59)	0.52 (0.57)	0.42 (0.46)	0.00 (0.00)
B_6) JASO(-3)	$Q_{BN(0)} = -0.10 - 0.26PC_1 - 0.60PC_{10}$	0.57	0.82 (0.77)	0.67 (0.60)	0.65 (0.59)	0.62 (0.68)	0.59 (0.65)	0.47 (0.51)	0.00 (0.00)

Table 5-7 Assessment and validation statistics for various forecast models based on principal component regression (PCR). Values in parentheses in the second rows are for the validation phase, (Atbara River)

LEAD-SEASON	REGRESSION EQUATION	ρ	R	R^2	ADJ_R^2	ADJ_RMSE	RMSE	MAE	BIAS
B_1) MAMJ(0)	$Q_{ATB(0)} = -0.02 - 0.24PC_1 + 0.17PC_3$	0.73	0.92 (0.91)	0.86 (0.83)	0.85 (0.82)	0.40 (0.44)	0.38 (0.42)	0.30 (0.33)	0.00 (0.01)
B_2) NDJF(0)	$Q_{ATB(0)} = -0.02 - 0.24PC_1 + 0.19PC_3$	0.71	0.92 (0.90)	0.85 (0.82)	0.84 (0.81)	0.41 (0.45)	0.39 (0.43)	0.32 (0.35)	0.00 (0.01)
B_3) JASO(-1)	$Q_{ATB(0)} = -0.02 - 0.24PC_1 + 0.19PC_4$	0.71	0.92 (0.90)	0.84 (0.81)	0.83 (0.80)	0.42 (0.46)	0.41 (0.44)	0.33 (0.36)	0.00 (0.01)
B_4) MAMJ(-1)	$Q_{ATB(0)} = -0.02 - 0.24PC_1 + 0.09PC_2 + 0.08PC_3 - 0.21PC_4 - 0.14PC_5$	0.68	0.89 (0.84)	0.79 (0.70)	0.76 (0.66)	0.50 (0.61)	0.46 (0.55)	0.38 (0.46)	0.00 (0.00)
B_5) NDJF(-2)	$Q_{ATB(0)} = -0.02 + 0.25PC_1 - 0.21PC_3 - 0.18PC_6$	0.61	0.84 (0.79)	0.71 (0.63)	0.68 (0.61)	0.57 (0.65)	0.54 (0.62)	0.44 (0.50)	0.00 (-0.01)
B_6) JASO(-3)	$Q_{ATB(0)} = 0.02 - 0.25PC_1 + 0.87PC_{10}$	0.55	0.76 (0.71)	0.59 (0.51)	0.56 (0.49)	0.68 (0.74)	0.65 (0.71)	0.48 (0.53)	0.00 (0.01)

Table 5-8 Assessment and validation statistics for various forecast models based on principal component regression (PCR). Values in parentheses in the second rows are for the validation phase, (Nile River, Aswan)

LEAD-SEASON	REGRESSION EQUATION	ρ	R	R^2	ADJ_R^2	ADJ_RMSE	RMSE	MAE	BIAS
B_1) MAMJ(0)	$Q_{ASW(0)} = -0.01 - 0.16PC_1 - 0.09PC_3 - 0.17PC_7 - 0.18PC_{10}$	0.66	0.87 (0.82)	0.76 (0.67)	0.73 (0.64)	0.54 (0.63)	0.50 (0.59)	0.35 (0.41)	0.00 (0.01)
B_2) NDJF(0)	$Q_{ASW(0)} = -0.04 - 0.18PC_1 - 0.11PC_3 + 0.14PC_4 + 0.17PC_5$	0.63	0.85 (0.79)	0.73 (0.63)	0.70 (0.60)	0.57 (0.67)	0.53 (0.62)	0.41 (0.47)	-0.01 (0.01)
B_3) JASO(-1)	$Q_{ASW(0)} = -0.06 - 0.19PC_1 + 0.10PC_3 - 0.24PC_4$	0.60	0.83 (0.76)	0.69 (0.58)	0.66 (0.55)	0.60 (0.70)	0.57 (0.67)	0.44 (0.50)	0.00 (0.01)
B_4) MAMJ(-1)	$Q_{ASW(0)} = -0.06 - 0.19PC_1 - 0.12PC_3 + 0.25PC_4$	0.61	0.83 (0.77)	0.69 (0.59)	0.67 (0.57)	0.59 (0.69)	0.56 (0.65)	0.44 (0.50)	0.00 (0.01)
B_5) NDJF(-2)	$Q_{ASW(0)} = -0.07 - 0.22PC_1 - 0.11PC_2 - 0.22PC_4$	0.55	0.82 (0.78)	0.68 (0.60)	0.65 (0.58)	0.61 (0.68)	0.58 (0.64)	0.47 (0.52)	0.00 (0.00)
B_6) JASO(-3)	$Q_{ASW(0)} = -0.06 - 0.26PC_1 + 0.65PC_7$	0.43	0.72 (0.62)	0.52 (0.39)	0.49 (0.37)	0.74 (0.84)	0.71 (0.80)	0.55 (0.62)	0.00 (0.01)

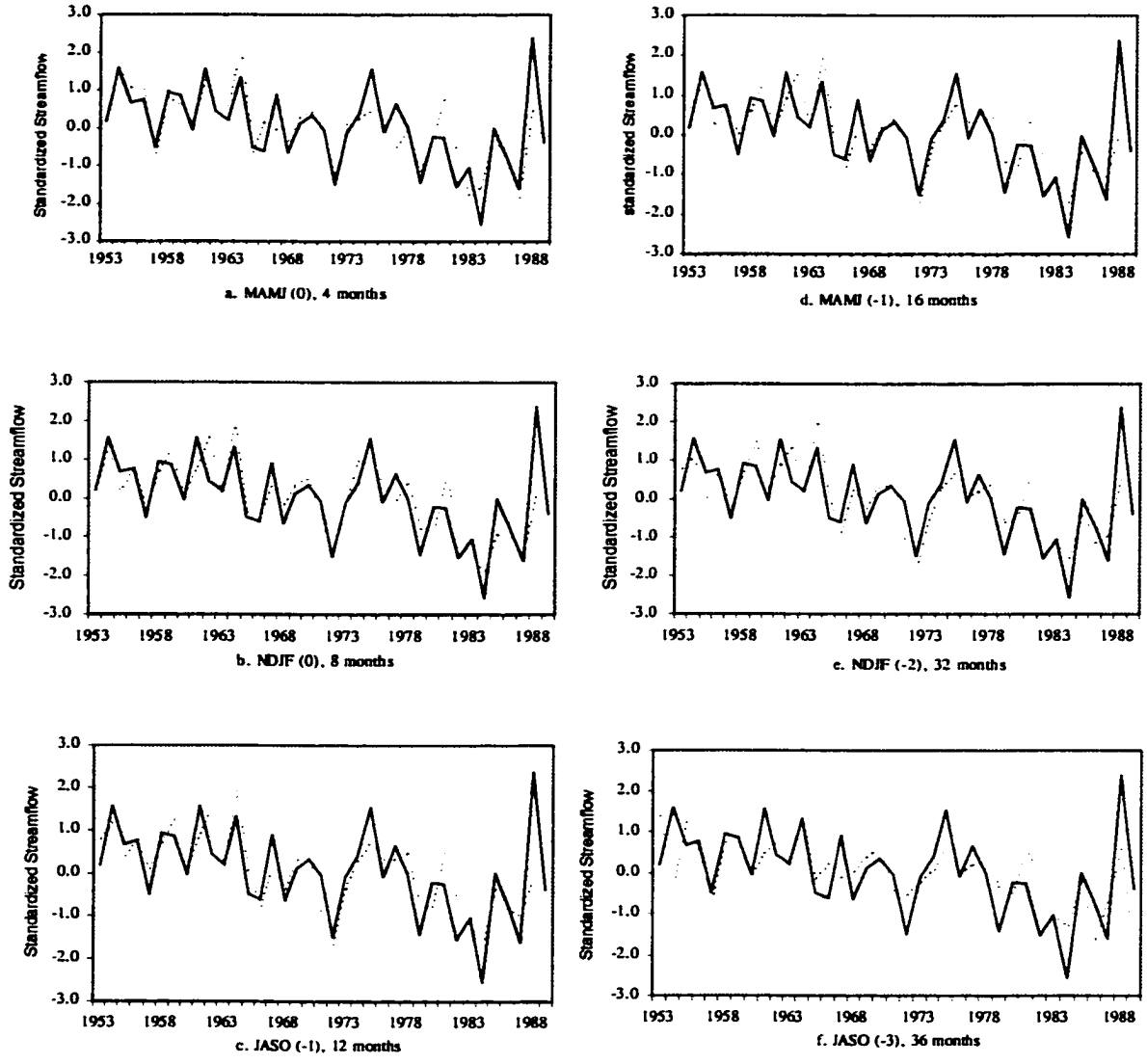

Fig. 5-9 Comparison between the observed Sobat River flows (solid line) and the validated forecasted flows (dotted line) for the models listed in Table 5-5

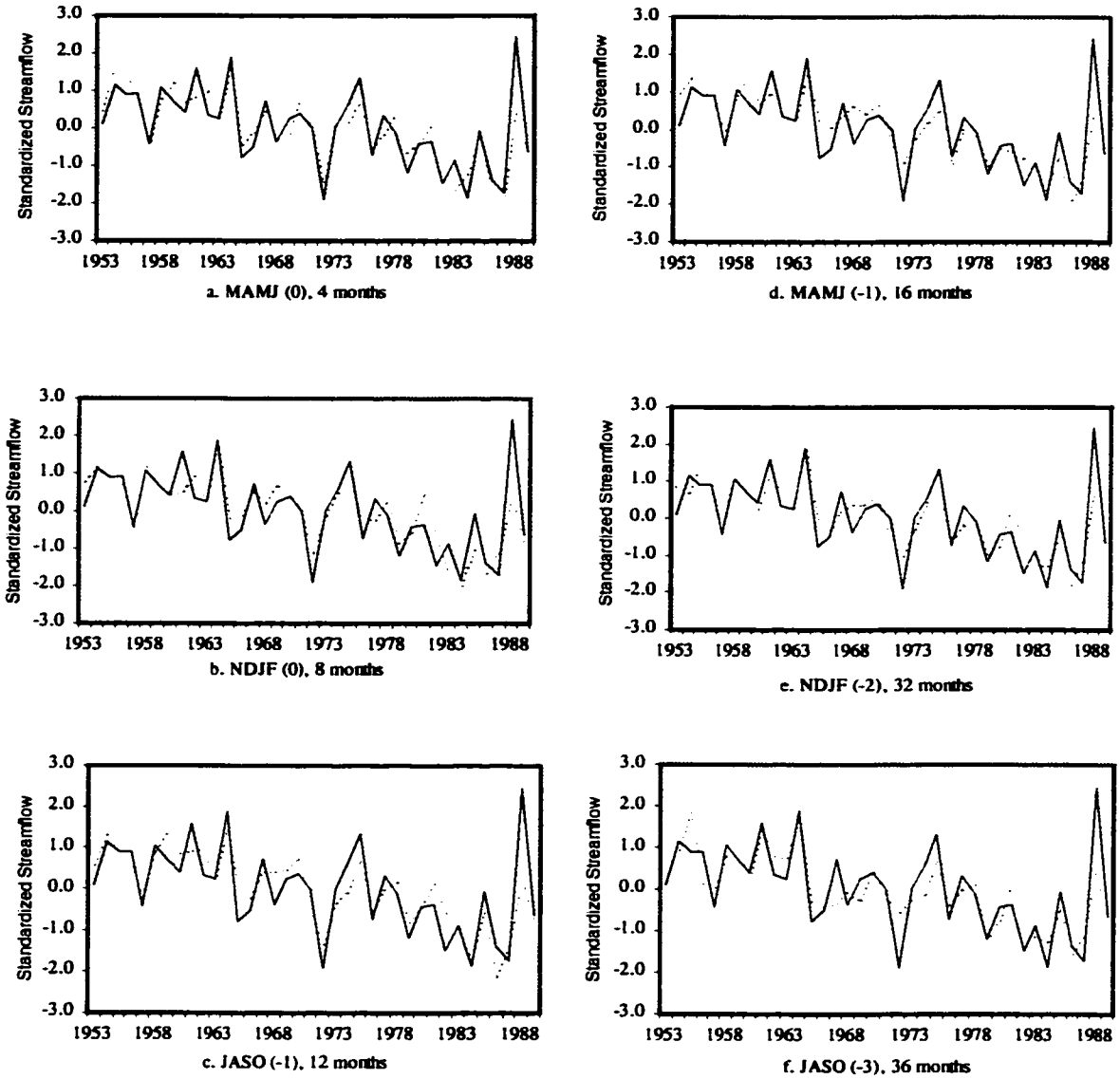

Fig. 5-10 Comparison between the observed Blue Nile River flows (solid line) and the validated forecasted flows (dotted line) for the models listed in Table 5-6

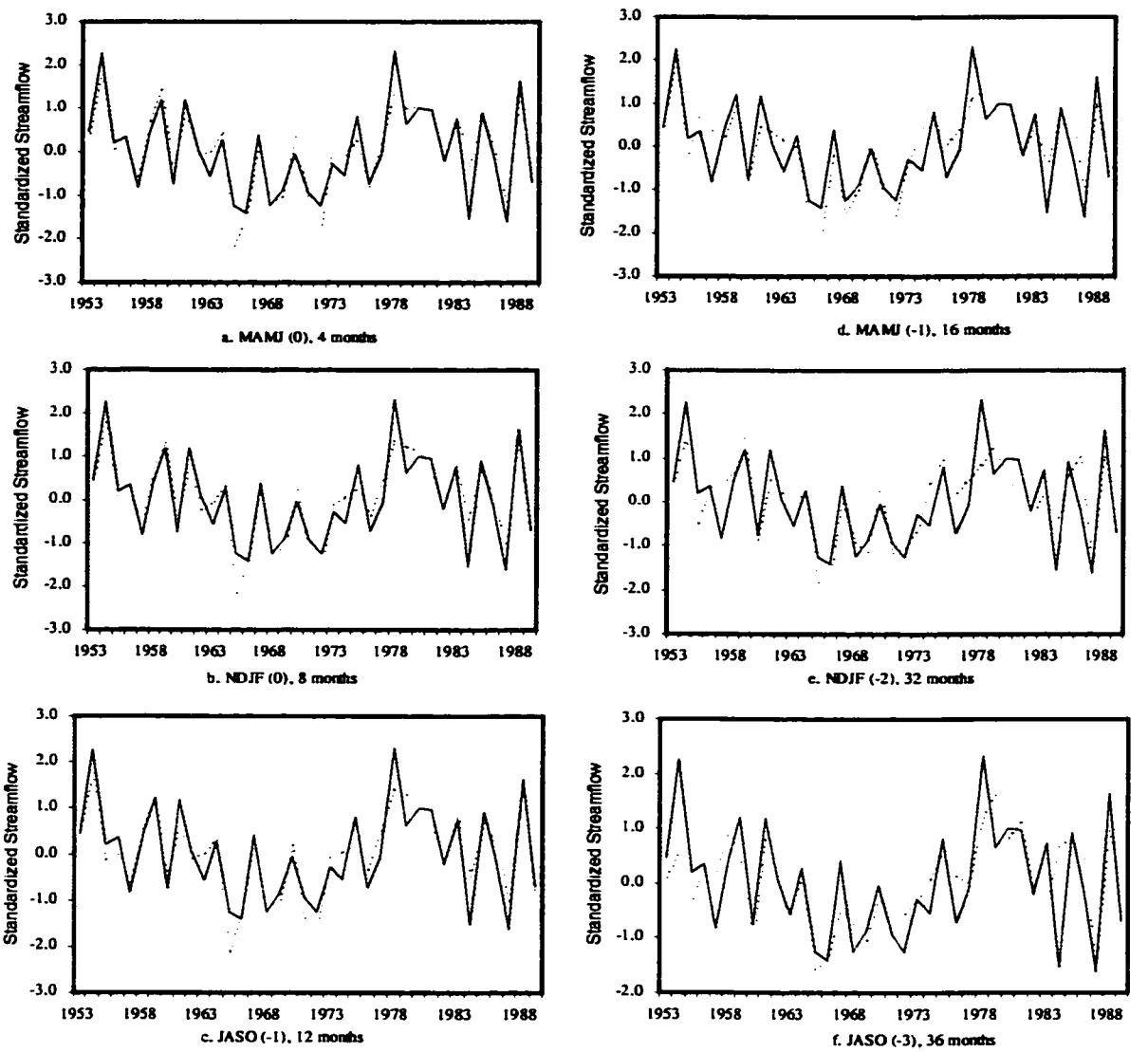

Fig. 5-11 Comparison between the observed Atbara River flows (solid line) and the validated forecasted flows (dotted line) for the models listed in Table 5-7

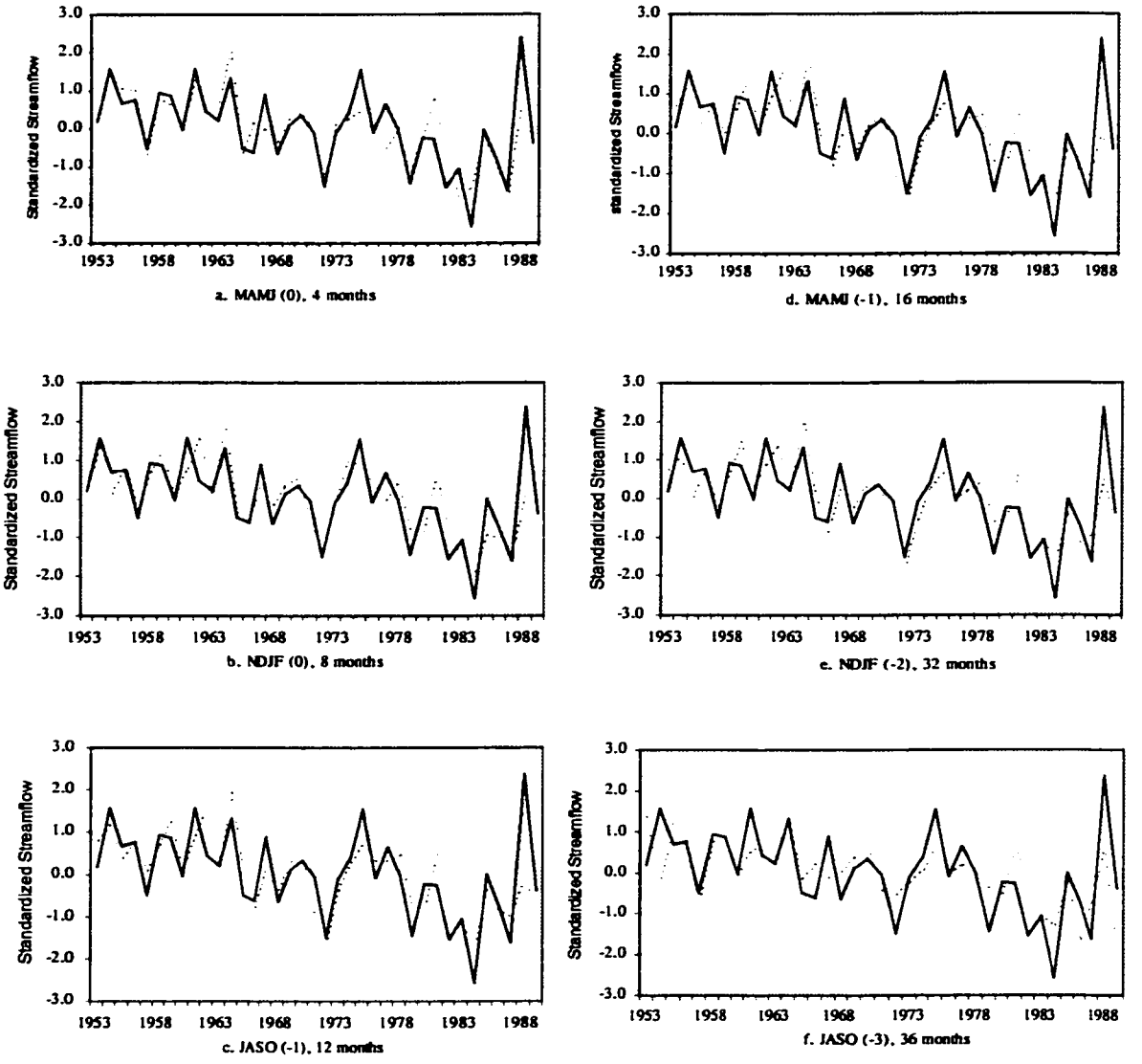

Fig. 5-12 Comparison between the observed Nile River flows at Aswan (solid line) and the validated forecasted flows (dotted line) for the models listed in Table 5-8

Atbara River show higher response to the large scale variables followed by the Blue Nile, the Nile River at Aswan and the Sobat River. However, at the first three lead seasons the Blue Nile, the Nile River at Aswan and the Sobat River show close values of the agreement coefficient, Fig. 5-14. It worth noting that the Atbara River and the Blue Nile River originate in the Ethiopian Plateau and the Sobat flows partially from the east African basin and the Ethiopian Plateau. Thus, the Sobat River flows may be highly damped by the flows from the east African basin and shows weaker association with the large-scale variables. In addition, the Atbara River is located in the northern part of the Plateau and the Blue Nile is located in the central part of the Plateau and the Sobat in the southern part of the plateau. Thus, this indicates that the association between the river flows and the large-scale variables reduced from the north to the south. It could also be concluded that the signal observed in the Nile River flows at Aswan is mainly due the large-scale variables association with the Blue Nile and Atbara River flows.

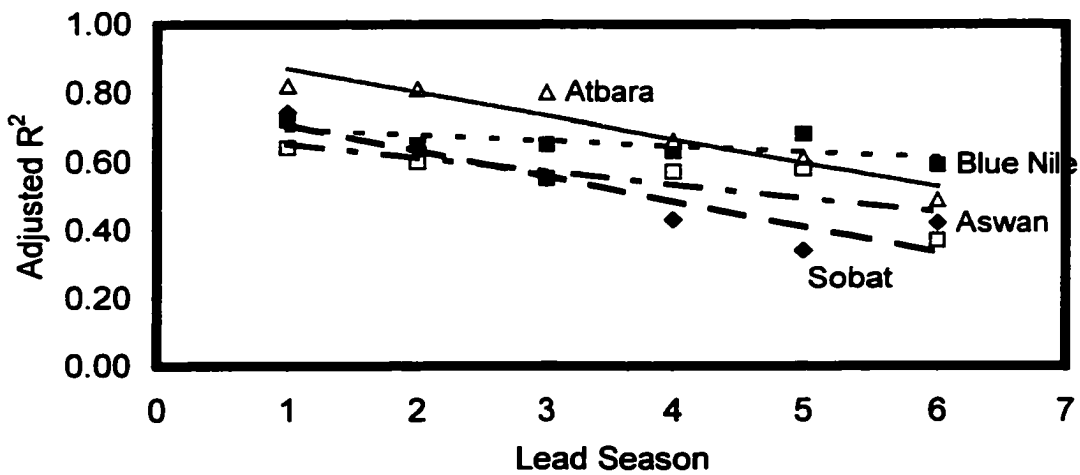

Fig. 5-13 Adjusted R^2 for the Nile River flows and its tributaries as shown in Tables 5-5 through 5-8

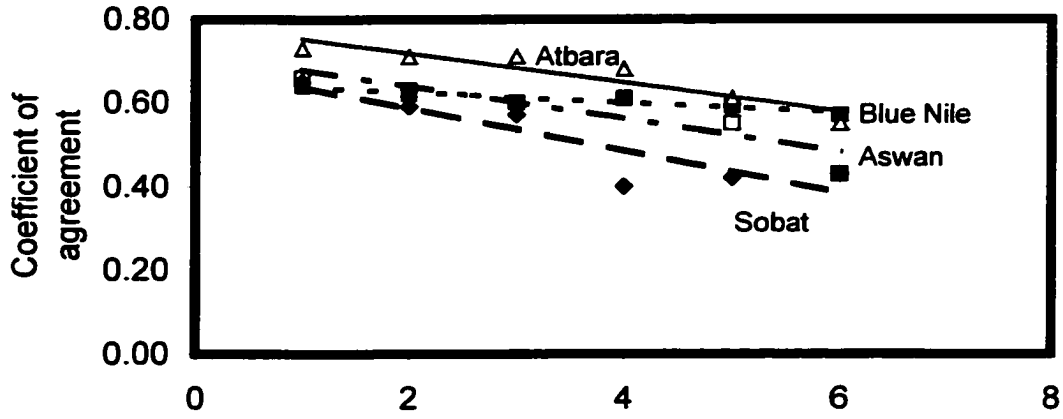

Fig. 5-14 Coefficient of agreement for the Nile River flows and its tributaries as shown in Tables 5-5 through 5-8

5.4 Ensemble Forecasts

The ensemble forecasts were adopted using the previous individual forecasts to improve the current forecast skill. The ensemble forecasts were calculated by averaging the previous forecasts which were available by the end of the forecast period. In this case, the ensemble forecasts were computed from the validated forecasts, for lead-seasons MAMJ (0), NDJF (0), JASO (-1), MAMJ (-1) and NDJF (-2). For example, the ensemble forecast for NDJF (0), calculated as the average from the individual validated forecasts of the same lead period and those at JASO (-1), MAMJ (-1), NDJF (-2) and JASO (-3) leads. Figures 5-15, 5-16, 5-17, and 5-18 show a comparison between the individual forecast and the ensemble forecast for the Blue Nile River, the Nile River at Aswan, the Atbara River and the Sobat River, respectively. The results show that the forecast skill was degraded for the Nile River at Aswan and the Atbara River. The Sobat

River shows slight improvement in the last lead times. The Blue Nile River forecasts show an improvement over the intermediate lead times.

The Blue Nile River forecasts in some lead times improved when using ensemble models as compared with the ensemble forecast of the other three locations (the Sobat River, the Atbara River and the Nile River). This method tends to improve the forecast skills in the medium lead times (NDJF (0) to MAMJ (-1)) but to slightly degrade the skills for forecasts of very short lead times (MAMJ (0)) and the longer lead times JASO (-3), Fig. 5-15. Thus, by utilizing the information already computed, one could improve the forecast for the Blue Nile River flows.

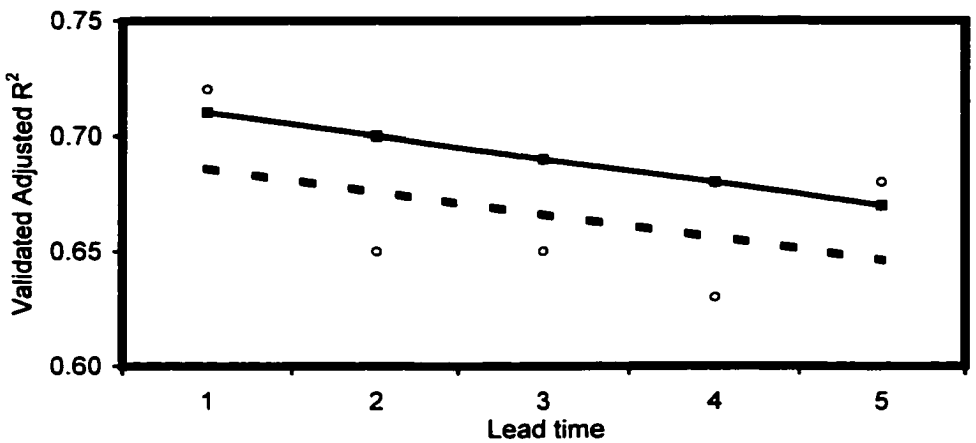

Fig. 5-15 Adjusted R^2 for the Blue Nile River flows using single season (dashed line) and ensemble model (solid line)

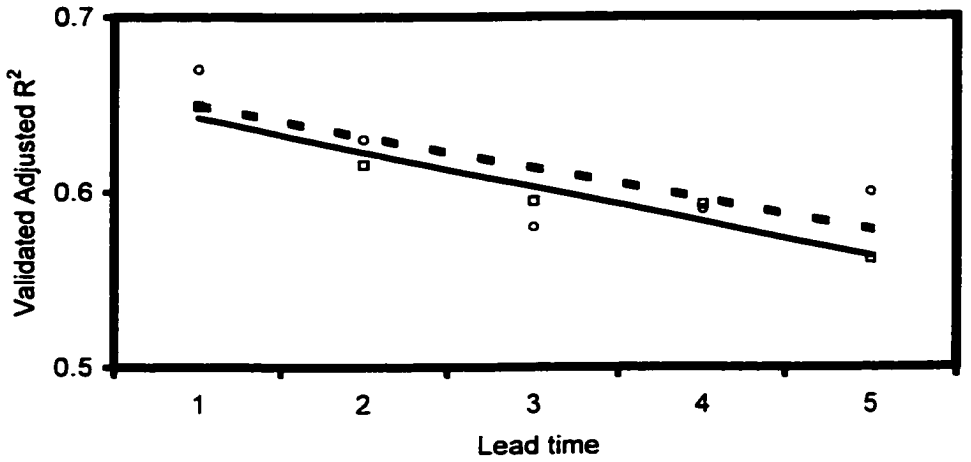

Fig. 5-16 Adjusted R^2 For the Nile River flows at Aswan using single season (dashed line) and ensemble model (solid line)

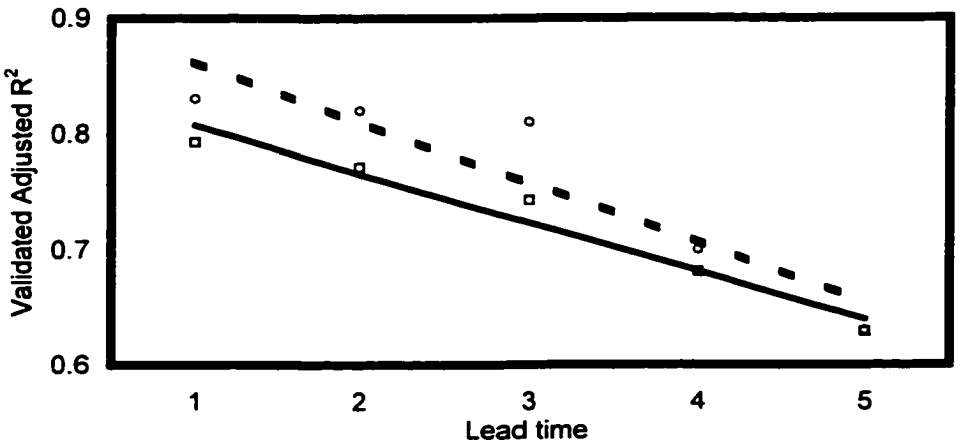

Fig. 5-17 Adjusted R^2 For the Atbara River flows using single season (dashed line) and ensemble model (solid line)

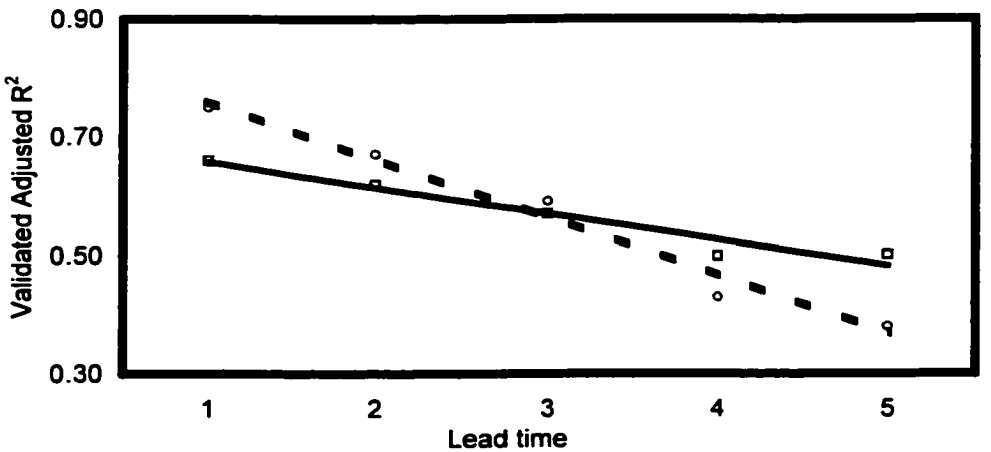

Fig. 5-18 Adjusted R^2 For the Sobat River flows using single season (dashed line) and ensemble model (solid line)

6. IDENTIFICATION OF ROBUST PREDICTORS

6.1 Selected Significant, Stable and Consistent Predictors

Irrespective of the type of forecast model used, identification of robust and statistically significant predictors for the Nile River flows continues to be of great importance. Generally, predictors have tended to fall into three categories: (1) ENSO indicator, (2) precipitation and (3) persistence. In this section the list of predictors used to this point are explored using a set of criteria to define a short list of predictors for each of the Nile River tributaries. The main purpose is to identify robust statistical relationships useful for seasonal prediction. The results discussed in the previous sections indicate that over the period 1953-1989, the flow of the Nile River and its tributaries in some seasons were significantly correlated with the large-scale variables in the preceding seasons. The results are consistent with the work carried out by Eltahir (1996) and Awadalla (1999). To the author's knowledge, no stability investigation has been carried out on the Nile River flows and the large-scale predictors. The extent of this stability has been examined in this study using the sliding-window technique. The stability of the predictor-predictand relationship was assessed through correlation coefficients on 21-, 25-, and 31-year running windows (Appendix, C). Odd number of years were chosen so that the middle point of the window could be easily identified for plotting. For example, for the 31-year window, the first value calculated for the years 1953-1983 is indexed as 1968, and the last value calculated for the 1959-1989 year

window is indexed, is 1974, Appendix C. Local statistical significance at the 5% level was obtained as, 0.36, 0.40, and 0.44 for 31-, 25- and 21-year windows, respectively. Appendix C shows the correlation of the three running windows for the Sobat River, the Blue Nile River, the Atbara River and the Nile River at Aswan, respectively. Detailed description of the predictors for the Sobat River, the Blue Nile River, the Atbara River and the Nile River are shown in Tables 6-1, 6-2, 6-3, and 6-4, respectively. When tested using the 15-year running window, the predictors in bold numbers in these tables maintain significance and stability. Some of these predictors account for over 40% of the total variance, (Tables 6-1, 6-2, 6-3, and 6-4). For example, predictor number 18 (Table 6-2) explains 47% of the Blue Nile River flows variability. So far, the author is not aware of any other single predictor which explains such a large percentage of variance of the Nile River flows using over 30 years of data.

6.2 Teleconnection Between Large-scale Variable and Upper White Nile Flows

In this part of the study, the only remaining source of the Nile River flow was tested for possible connection with the large-scale variables. No further analysis or modeling was done. The White Nile River is the tributary of the Nile River downstream of the Malakal confluence, where the Sobat River, Bahr-Gebal River and Bahr-el Gazal River join. The main sources of precipitation for the White Nile River are the eastern and central African rainfall and the Ethiopian Plateau. In this section of the study the upper White Nile River flows are defined as the flows from central African rainfall and the southern Sudan region i.e. Malakal flows (July to October) less the Sobat River flows for the season July to October. The serial correlations for the upper White Nile River for the period 1953-1989, at lags of 1, 2 and 3, are, 0.60, 0.45 and 0.19, respectively. This

Table 6-1 Locations of the stable predictors and their respective correlation coefficient with the Sobat River flows for (JASO) for various leading seasons. Bold numbering indicates stable at 15-years.

NO.	LEAD-SEASON	LOCATION	LATITUDE	LONGITUDE	CORR	LOCATION	LATITUDE	LONGITUDE	CORR	SEESAW CORR.
1	April (-3)	Ponta Delgada			-0.42					
2	July (-3)	NAO1			-0.41					
3	JASO (-3)	Pacific	35° S	145° W	-0.47	Indian	00°	50° E	0.35	-0.56
4	JASO (-3)	Indian	00°	50° E	0.35					
5	January(-2)	South Atlantic	00 →20° S	30° W→10° E	0.47					
6	NDJF (-2)	Atlantic	40° N	30° W	-0.37	Atlantic	05° N→05° S	20° W→05° E	0.51	-0.54
7	NDJF (-2)	Atlantic	40° N	30° W	-0.37	Atlantic	25° N	70° W	0.44	-0.52
8	MAMJ (-2)	Atlantic	40° N	30° W	-0.42	Atlantic	10° S	20° W	0.39	-0.53
9	MAMJ (-2)	Atlantic	10° S	20° W	0.39					
10	MAMJ (-2)	Pacific	40° S	150° E	0.41					
11	JASO (-1)	Pacific	20° N	130° W	-0.49	Pacific	40° S	140° E	0.36	-0.60
12	NDJF (0)	Indian	20° S	60° E	-0.33	Pacific	50° N	160° E	0.43	-0.48
13	MAMJ (0)	Indian	08° S→18° S	55° E→65° E	-0.38	Pacific	20° S	165° E	0.35	-0.48
14	MAMJ (0)	Pacific	10° S→20° S	100° W→90° W	-0.33	Pacific	20° S	165° E	0.35	-0.43
15	MAMJ (0)	Atlantic	00°	05° E	0.41					

Table 6-2 Locations of the stable predictors and their respective correlation coefficient with the Blue Nile River flows for (JASO) for various leading seasons. Bold numbering indicates stable at 15-years.

NO.	LEAD-SEASON	LOCATION	LATITUDE	LONGITUDE	CORR	LOCATION	LATITUDE	LONGITUDE	CORR	SEESAW CORR.
1	February (-3)	Jakarta			-0.55					
2	MAMJ (-3)	Atlantic	08° S→12° S	00° →05° E	-0.39	Pacific	20° S→30° S	170° W→145° W	0.48	-0.59
3	JASO (-3)	Indian	10° N→05° S	85° E→95° E	-0.47	Pacific	45° N→40° N	150° W→140° W	0.42	-0.52
4	NDJF (-2)	Pacific	30° S→35° S	90° W→80° W	-0.44	Pacific	50° N→35° N	160° W→140° W	0.53	-0.65
5	NDJF (-2)	Pacific	10° N→00°	148° E→155° E	-0.39	Pacific	50° N→35° N	160° W→140° W	0.53	-0.63
6	NDJF (-2)	Indian	00° →10° S	85° E→95° E	-0.36	Pacific	50° N→35° N	160° W→140° W	0.53	-0.59
7	NDJF (-2)	Atlantic	10° N→20° N	30° W→20° W	-0.44	Atlantic	40° N→30° N	70° W→60° W	0.46	-0.54
8	NDJF (-2)	Pacific	45° N→35° N	160° W→140° W	0.57					
9	MAMJ (-1)	Indian	05° N→02° S	60° E→70° E	-0.31	Pacific	20° N→10° N	110° W→100° W	0.52	-0.53
10	MAMJ (-1)	Pacific	30° S→44° S	160° W→140° W	-0.46	Pacific	20° N→10° N	110° W→100° W	0.52	-0.53
11	JASO (-1)	Pacific	00° S→35° S	140° W→100° W	-0.43	Pacific	15° N→10° N	160° E→179° E	0.35	-0.52
12	ASON (-1)	Guinea			0.63					
13	NDJF (0)	Pacific	12° S→20° S	105° W→90° W	-0.45	Indian	22° N→10° N	110° E→115° E	0.47	-0.66
14	AprMay(0)	Pacific	50° N→42° N	155° W→145° W	-0.40	Pacific	50° N→20° N	120° E→160° E	0.50	-0.58
15	NDJF (0)	Darwin			-0.50					
16	AMJ (0)	Jakarta			-0.59					
17	AMJ (0)	SOI			0.44					
18	MAMJ (0)	Pacific	02° N→05° S	130° W→90° W	-0.50	Pacific	30° N→25° N	140° E→160° E	0.34	-0.69
19	MAMJ (0)	Pacific	05° N→20° S	120° W→80° W	-0.52	Indian	10° S→20° S	110° E→125° E	0.41	-0.63
20	AMJ (0)	CTI			-0.58					
21	MayJun (0)	Global Tropics	10° N→10° S	00°→360°	-0.53					
22	MAMJ (0)	Pacific	02° N→05° S	130° W→90° W	-0.55					

Table 6-3 Locations of the stable predictors and their respective correlation coefficient with the Atbara River flows for (JASO) for various leading seasons. Bold numbering indicates stable at 15-years.

NO.	LEAD-SEASON	LOCATION	LATITUDE	LONGITUDE	CORR	LOCATION	LATITUDE	LONGITUDE	CORR	SEESAW CORR.
1	MAMJ (-3)	Atlantic	05° N→12° S	00° →05° W	-0.54	Atlantic	44° S	30° W	0.36	-0.58
2	MAMJ (-3)	Atlantic	08° S→12° S	00° →05° E	-0.49	Atlantic	44° S	30° W	0.36	-0.59
3	MAMJ (-3)	Pacific	20° N→05° N	150° E→160° E	-0.49	Indian	30° S→35° S	70° E→80° E	0.41	-0.53
4	MAMJ (-3)	Pacific	20° N→05° N	150° E→160° E	-0.49	Pacific	28° S→38° S	150° W→100° W	0.35	-0.54
5	MAMJ (-3)	Pacific	22° N→15° N	170° E→150° W	-0.49	Indian	30° S→35° S	70° E→80° E	0.41	-0.56
6	MAMJ (-3)	Pacific	22° N→15° N	170° E→150° W	-0.49	Pacific	28° S→38° S	150° W→100° W	0.35	-0.52
7	MAMJ (-3)	Atlantic	05° N→12° S	00° →05° W	-0.54					
8	MAMJ (-3)	Atlantic	08° S→12° S	00° →05° E	-0.49					
9	MAMJ (-3)	Pacific	20° N→05° N	150° E→160° E	-0.49					
10	JASO (-3)	Pacific	25° N→20° N	170° E→150° W	-0.47	Indian	35° S→40° S	60° E→90° E	0.33	-0.53
11	JASO (-3)	Pacific	20° N→10° N	130° E→170° E	-0.51	Indian	35° S→40° S	60° E→90° E	0.33	-0.48
12	JASO (-3)	Pacific	20° N→10° N	130° E→170° W	-0.51					
13	NDJF (-2)	Atlantic	20° N→10° N	30° W→20° W	-0.44	Atlantic	40° N→30° N	70° W→60° W	0.46	-0.59
14	January (-2)	Ponta Delgada			0.62					
15	MAMJ (-2)	Atlantic	25° N→15° N	25° W→15° W	-0.35	Atlantic	45° N→35° N	65° W→50° W	0.47	-0.62
16	MAMJ (-1)	Atlantic	35° S→40° S	50° W→30° W	0.56					
17	AMJ (-1)	Tahiti			-0.58					
18	JASO (-1)	Pacific	25° S→35° S	150° W→130° W	-0.64					
19	JASO (-1)	Pacific	25° S→35° S	150° W→130° W	-0.64	Indian	25° S→35° S	30° E→60° E	0.34	-0.58
20	JASO (-1)	Pacific	25° S→35° S	150° W→130° W	-0.64	Pacific	10° N	110° W	0.45	-0.63
21	JASO (-1)	Pacific	25° S→35° S	150° W→130° W	-0.64	Pacific	59° N→54° N	140° E→179° E	0.38	-0.64
22	JASO (-1)	Pacific	25° S→35° S	150° W→130° W	-0.64	Pacific	15° N→10° N	120° W→100° W	0.45	-0.64
23	MAMJ (0)	Indian	10° S→20° S	110° E→125° E	0.46					
24	April (0)	NH0090			0.45					
25	MAM-DJF (0)	Darwin			-0.50					

Table 6-4 Locations of the stable predictors and their respective correlation coefficient with the Nile River flows at Aswan for (JASO) for various leading seasons

NO.	LEAD-SEASON	LOCATION	LATITUDE	LONGITUDE	CORR	LOCATION	LATITUDE	LONGITUDE	CORR	SEESAW CORR.
1	JASO (-3)	Pacific	08° N→00°	140° E→150° E	-0.42	Pacific	45° N→32° N	120° E→140° E	0.48	0.60
2	JASO (-3)	Indian	10° N→05° S	85° E→95° E	-0.43	Pacific	45° N→35° N	120° E→140° E	0.48	-0.56
3	JASO (-3)	Pacific	20° N→05° N	130° E	-0.44	Pacific	50° N→30° N	120° E→150° E	0.45	-0.62
4	JASO (-3)	Indian	10° N→05° S	85° E→95° E	-0.43	Pacific	50° N→30° N	120° E→150° E	0.45	-0.54
5	JASO (-3)	Pacific	08° N→00°	145° E→155° E	-0.38	Pacific	50° N→30° N	120° E→150° E	0.45	-0.58
6	NDJF (-2)	Atlantic	40° N→30° N	70° W→60° W	0.57					
7	NDJF (-2)	Atlantic	20° N→10° N	30° W→20° W	-0.37	Atlantic	40° N→30° N	70° W→60° W	0.57	-0.61
8	NDJF (-2)	Indian	15° S→25° S	50° E→55° E	-0.38	Pacific	45° N→35° N	160° W→140° W	0.54	-0.61
9	NDJF (-2)	Indian	20° N→15° N	50° E→60° E	-0.38	Pacific	45° N→35° N	160° W→140° W	0.54	-0.60
10	NDJF (-2)	Indian	20° N→15° N	50° E→60° E	-0.38	Pacific	40° N→30° N	160° W→140° W	0.38	-0.51
11	NDJF (-2)	Pacific	30° S→35° S	90° W→80° W	-0.39	Pacific	45° N→35° N	160° W→140° W	0.54	-0.61
12	NDJF (-2)	Pacific	10° N→00°	148° E→155° E	-0.40	Pacific	45° N→35° N	160° W→140° W	0.54	-0.62
13	NDJF (-2)	Pacific	45° N→35° N	160° W→140° W	0.54					
14	NDJF (-2)	Indian	00° →10° S	85° E→95° E	-0.33	Pacific	50° N→35° N	160° W→140° W	0.50	-0.55
15	JASO (-2)	Pacific	10° N→00°	140° E→150° E	-0.31	Pacific	30° S→40° S	170° W→160° W	0.39	-0.54
16	MAMJ (-1)	Indian	00° →05° S	60° E→70° E	-0.35	Pacific	20° N→10° N	110° W→100° W	0.43	-0.51
17	ASON (-1)	Guinea			0.61					
18	NDJF (0)	Pacific	12° S→20° S	105° W→90° W	-0.47	Indian	22° N→10° N	110° E→115° E	0.45	-0.66
19	MAMJ (0)	Pacific	02° N→05° S	130° W→90° W	-0.52	Pacific	30° N→25° N	140° E→160° E	0.52	-0.66
20	MAMJ (0)	Pacific	05° N→20° S	120° W→80° W	-0.51	Pacific	30° N→25° N	140° E→160° E	0.52	-0.66
21	MAMJ (0)	Pacific	05° N→20° S	120° W→80° W	-0.51	Indian	10° S	110° E→125° E	0.33	-0.59
22	MayJun (0)	Global Tropics	10° N→10° S	00°→360°	-0.51					
23	AprMay (0)	Darwin			-0.47					

strong persistence may inflate the cross correlation values between the river flows and the SST shown in the correlation maps of Appendix A_5. If the sea surface temperatures in the locations of high correlations are also serially correlated, then this may add to higher inflation in the correlation coefficients. That is, one could incorrectly reject the null hypothesis, $\rho_{AB} = 0$, with a probability greater than the nominal significance level, (Ebisuzaki, 1997).

The question arises as to the significance of lagged correlations, particularly when the series are highly autocorrelated (serially correlated) as is frequently the case here. Thus, the presence of autocorrelation has to be taken into consideration. Angel (1981) adopted the equation developed by Quenouille (1952) for the cross correlation significance of two autocorrelated series, which was also used by Ananthakrishnan and Parthasarathy (1984). In this approach the number of degrees of freedom are reduced by the autocorrelation of the two series, which yields an effective number of independent observations entering into the calculation of cross correlation coefficient significance. The effective number of degrees of freedom for N pairs of values is given by:

$$N_e = \frac{N}{(1 + 2r_1 r_1' + 2r_2 r_2' + 2r_3 r_3')} \qquad [6\text{-}1]$$

where N is the number of data points in each of the two series, r_1 and r_1' are the lag-one auto-correlation of the two series, r_2 and r_2' are the lag-two autocorrelation of the two series, etc. The calculation has been terminated at lag-three because the correlation products become negligible thereafter. When the correction is made for autocorrelation, N_e becomes less than N in almost all of the cases. The significance of the

correlation has been estimated by using the effective number of independent observations so determined in $(1.96/N_e^{0.5})$ test.

The predictors for the upper White Nile River flows are defined as those statistically significant, after taking into consideration the reduction in the number of degrees of freedom due to autocorrelation, following the methodology described above. The stable and robust predictors should be at least consistent and stable over two running windows (31 years and 25 years). Table 6-5 shows a list of stable predictors which satisfy the above criteria, after taking into account the serial correlation in the predictors and the predictand time series. The stable predictors for all the Nile River tributaries outnumbered those for the upper White Nile River. In addition, the White Nile River predictors are stable over two running windows (31- and 25-year), and the other predictors for the Nile River tributaries are stable over three running windows (31-, 25-, and 20-years). Some of them are even stable for the 15-year running window as well. The relaxed criteria used for the upper White Nile River indicates weaker connection to the large scale variables in favor of the local hydroclimatic forcings.

6.3 Testing Predictability of the Stable Predictors

This section is an attempt to build a prediction algorithm to validate the predictability of the stable predictors identified in the previous section. Further analysis is concentrated on the Blue Nile River flows and the Nile River flows at Aswan, due to their importance for the Nile River basin countries, particularly Sudan and Egypt. Two lead seasons were chosen for the two sites, namely, MAMJ (0) and ASON (-1) prior to the occurrence of the Nile River flood season and seven months before the flood season (JASO), respectively. The combinations of the predictors were chosen by trial and error

Table 6-5 Locations of the stable predictors and their respective correlation coefficients with the Upper White Nile flows (JASO) for various lead seasons.

No.	LEAD SEASON	LOCATION	LATITUDE	LONGITUDE	R	LOCATION	LATITUDE	LONGITUDE	R	SEESAW CORR.
1	JASO(-3)	Atlantic	4°N	25°W	-0.33	Atlantic	42°S	25°E	0.48	-0.65
2	Dec.(-3)	Ponta Delg.			-0.49					
3	MAMJ(-2)	Pacific	28°N	170°E	-0.40	Pacific	43°S	150°W	0.51	-0.56
4	MAMJ(-2)	Pacific	43°S	150°W	0.51					
5	JASO(-2)	Pacific	40°S-44°S	140°W-160°W	0.54					
6	MAMJ(0)	Atlantic	35°N	59°W	-0.52					

from Tables 6-2 and 6-4 for the Blue Nile River and the Nile River at Aswan, respectively. The criteria for including a predictor in a model were that it be: 1) independent from its peers, 2) serially uncorrelated, and 3) it not reject the normality hypothesis. 5% significance level is specified as the level at which the retained regression coefficients were accepted as being different from zero. If the coefficients dropped below this level then the predictor was removed. The sets of predictors with better performance skill were selected. The regression coefficients were determined by using the method of least squares. Furthermore, the number of predictors would not exceed four. The four predictors were used for the shorter lead season (MAMJ (0)) and the first three in time for the longer lead season (ASON (-1)).

The predictors are designated with the $X_{(i)}$, where X is the predictor, and i stands for the index (first column of Tables 6-2 or 6-4). The subscript in the independent variable (Q), is the flow location, and the superscript is the lead season. Predictors numbered 7, 11, 17 and 23 (Table 6-4) have the best performance skill for the Nile River at Aswan, and predictors indexed 4, 7, 12, and 16 (Table 6-2) have the best performance skill for the Blue Nile River flow. Using these predictors, the following algorithms are developed for both locations and the two leading seasons.

$$Q_{ASW}^{MAMJ(0)} = -0.03 - 0.41X_{(7)} - 0.39X_{(11)} + 0.43X_{(17)} - 0.23X_{(23)} \quad [6\text{-}2]$$

$$Q_{ASW}^{ASON(-1)} = -0.04 - 0.45X_{(7)} - 0.41X_{(11)} + 0.47X_{(17)} \quad [6\text{-}3]$$

$$Q_{BN}^{MAMJ(0)} = -0.04 - 0.47X_{(4)} - 0.28X_{(7)} + 0.43X_{(12)} - 0.33X_{(16)} \quad [6\text{-}4]$$

$$Q_{BN}^{ASON(-1)} = -0.06 - 0.50X_{(4)} - 0.37X_{(7)} + 0.49X_{(12)} \quad [6\text{-}5]$$

Table 6-6 shows the performance skill for the models above. The best four stable predictors explain (validated adjusted R^2) up to 69% and 77% of the Nile River flows (Aswan) variability and the Blue Nile River flows variability, respectively, three months before the occurrence of the Nile flood peak (September). The first three stable predictors explain up to 67% and 68% of the variability at the two locations, respectively, 10 months before the flood peak. The author is not aware of any previous study that explains such a large percentage of the variance of the Nile River flows with this long lead time. A recently published study (Awadalla and Rousselle, 1999) which explained 63% of the Nile flood variability for only three months lead-time before the occurrence of the Nile flood peak. Though the four predictors were selected by trial and error from a pool of the stable predictors, they represent different regions, the Pacific Ocean, the Atlantic Ocean, the Guinea precipitation in western Africa and the Northern of Australia. It is worth noting that the Indian summer monsoon, the previous year Guinea precipitation (western Africa), and the Nile River flows have strong association which may indicate possible connection between their climatic driving forces.

Figures 6-1, 6-2, 6-3, and 6-4 show the results for 37 years of validation for the Nile River flows at Aswan and the Blue Nile River flows for the MAMJ (0) and the ASON (-1) lead seasons for the models were developed using Eqs. 6-2 through 6-5. Observed flows are given along the abscissa and predicted flows are given along the ordinate (Figs. 6-1 to 6-4). The two dashed lines represent ±10% of the observed flows. It should be noted that out of the 37 years, the forecast error is more than 10% in 5 cases for lead season MAMJ (0) and 3 cases for lead season ASON (-1) for the Nile River flows at Aswan. The forecast error is less than 10% in only 3 cases for each lead season.

Similarly, in the case of the Blue Nile River flows the forecast error is more than 10% in only 3 cases for MAMJ (0) and 6 cases for ASON (-1). The forecast error is less than 10% for only 3 cases and 4 cases for the two lead seasons, respectively.

Table 6-6 Assessment and validation statistics for various forecast models based on MLR-OLS for the models in Eqs. 6-2 to 6-5. Values in parentheses in the second rows are for validation phase

Location	Lead Season	ρ	R	R^2	Adj-R^2	Adj-RMSE	RMSE	MAE	BIAS
Nile River a	MAMJ(0)		0.89	0.79	0.78	0.50	0.46	0.37	0.00
Aswan		0.64	(0.85)	(0.72)	(0.69)	(0.58)	(0.54)	(0.44)	(0.00)
	ASON(-1)		0.87	0.76	0.74	0.53	0.50	0.39	0.00
		0.65	(0.83)	(0.69)	(0.67)	(0.60)	(0.56)	(0.43)	(0.00)
Blue Nile	MAMJ(0)		0.92	0.84	0.83	0.44	0.41	0.31	0.00
River		0.73	(0.89)	(0.79)	(0.77)	(0.51)	(0.47)	(0.36)	(0.00)
	ASON(-1)		0.87	0.76	0.74	0.53	0.50	0.38	0.00
		0.64	(0.84)	(0.70)	(0.68)	(0.60)	(0.56)	(0.43)	(0.01)

The long-term average was denoted by a vertical line shown in Figs. 6-1, 6-2, 6-3, and 6-4. Prediction of the flows for the Blue Nile River flow at lead-season MAMJ (0) and the Nile River at Aswan at lead season ASON (-1) are much better, because out of the 37 years, there are only 6 years for which the flows are outside the boundaries. It is worth noting, that out of the 6 years, the same number of years are below and above average. Similarly, prediction of above average flows for the Nile River at Aswan at MAMJ (0) and Blue Nile flows at ASON (-1), with 3 years outside the thresholds. The

models show relatively poor performance for the below average flows, for the Blue Nile River at ASON (-1) and the Nile River at Aswan at MAMJ (0). However, under these thresholds the chosen predictors perform well.

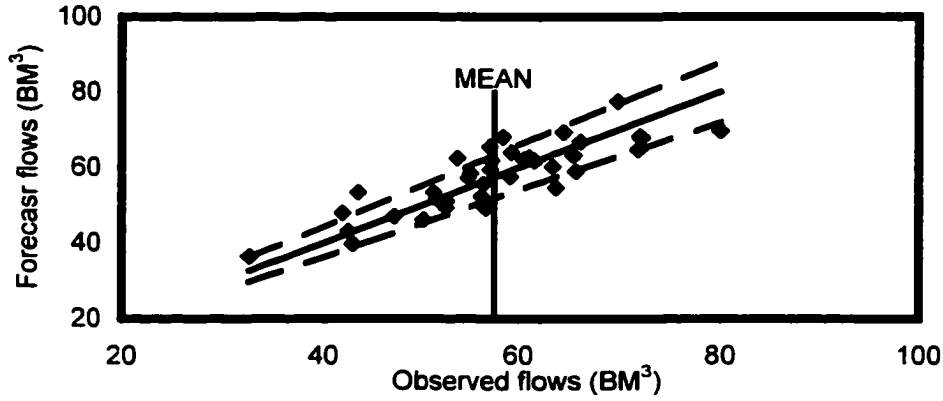

Fig. 6-1 Observed and forecasted Nile River flows at Aswan (validation) at MAMJ (0). The bar indicates the mean flows and the dashed lines represent ±10% of the solid line

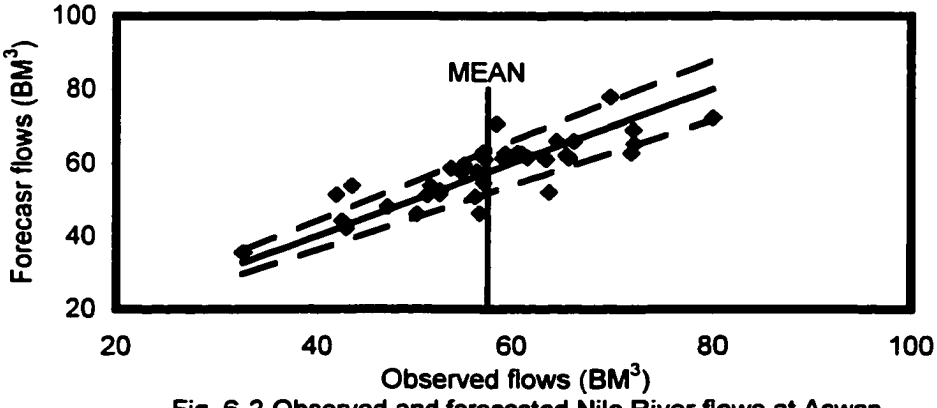

Fig. 6-2 Observed and forecasted Nile River flows at Aswan (validation) at ASON (-1). The bar indicates the mean flows and the dashed lines represent ±10% of the solid line

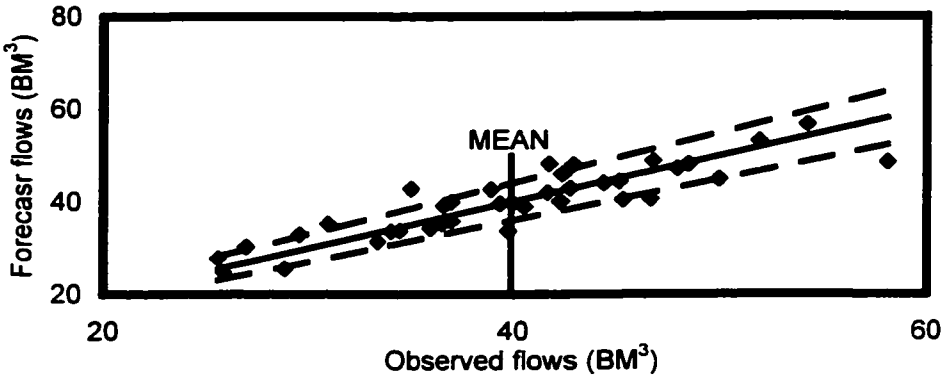

Fig. 6-3 Observed and forecasted Blue Nile River flows (validation) at MAMJ (0). The bar indicates the mean flows and the dashed lines represent ±10% of the solid line

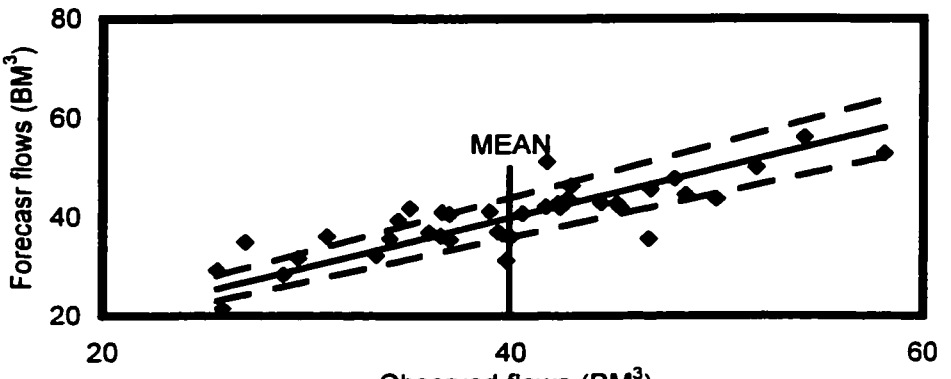

Fig. 6-4 Observed and forecasted Blue Nile River flows (validation) at ASON (-1). The bar indicates the mean flows and the dashed lines represent ±10% of the solid line

Another way of presenting the results is by means of categorical contingency analysis. The categories boundaries adopted here were similar to those used by Eltahir (1996). The normalized anomaly $(x-\bar{x})/\sigma$, (where $\bar{x}$ is the mean and σ is the standard deviation) of the predictors and the predictands have been evaluated for each of the 37 years. The years with a streamflow anomaly of less than -0.5σ were labeled as deficient

years, the years with streamflow anomaly of more than $+0.5\sigma$ were labeled as excess years and the years between the -0.5σ and $+0.5\sigma$ streamflow anomaly were labeled as normal years. There are over 10 years for each of the three categories. However, using $\pm\sigma$ as a boundary yields over 20 years as normal years and only single digits for the deficit and excess categories. This indicates that the way the boundaries are defined is reasonable. The categories are defined in such a way that the number of data points contained in every category of a specific variable are not dramatically different from each other. The new categorical variable has three possible values, which are named deficit, normal, and excess. Tables 6-7, 6-8, 6-9, and 6-10 show the observed streamflows and the validated model prediction categories.

The skill of the above models is also defined as the percentage of correct categorical forecasts, i.e. elements in the main diagonal. Tables 6-7, 6-8, 6-9, and 6-10 show the results by category for the two lead-seasons (MAMJ (0) and ASON (-1)) at the Nile River at Aswan and the Blue Nile River, respectively. The result of the correct forecast is shown in the diagonal of the tables, and the ratio with the 37 year forecast determine the skill. The results of the 26, 25, 28, and 23 diagonal cases out of the 37 cases, represents a skill of 0.70, 0.68, 0.76, and 0.62 for the two seasons (MAMJ (0), and ASON (-1)) for the Nile River flows at Aswan and the Blue Nile River flows, respectively. It is worth mentioning that these tables are based on the validation forecasts. Only the predicted value of the lead season ASON (-1) of year 1955 (deficit) differs from the observed flows (excess). However, for lead season MAMJ (0), all the extreme values (excess or deficit) are consistent with the observed values. This shows the strength of these predictors in explaining high portions of the river flows.

Table 6-7 Categorical Contingency Table for the Nile River at Aswan, MAMJ (0)

OBSERVED	PREDICTED		
	Deficit	Normal	Excess
Deficit	9	2	0
Normal	2	9	4
Excess	0	3	8

Table 6-8 Categorical contingency table of the Nile River at Aswan, ASON (-1)

OBSERVED	PREDICTED		
	Deficit	Normal	Excess
Deficit	9	2	0
Normal	2	9	4
Excess	1	3	7

Table 6-9 Categorical Contingency Table for the Blue Nile River, MAMJ (0)

OBSERVED	PREDICTED		
	Deficit	Normal	Excess
Deficit	10	1	0
Normal	3	9	3
Excess	0	2	9

Table 6-10 Categorical Contingency Table for the Blue Nile River, ASON (-1)

OBSERVED	PREDICTED		
	Deficit	Normal	Excess
Deficit	7	4	0
Normal	3	10	2
Excess	1	4	6

It is worth noting that the seasonal flows prior to the flood season (JASO) for the Nile River and tributaries have some relationship which indicate their potentiality to be used as predictors. Table 6-11 shows the correlation between the flood flows (JASO) at the Nile River and tributaries with the other two seasons, NDJF and MAMJ. The negative lag indicates that the given season is leading the flood season and therefore it could be a potential predictor. As expected, for all the Nile River tributaries the flood season is significantly correlated with the coming winter season (NDJF). For the Blue Nile River, the relationship of the flood flows with the winter season remains relatively strong for the coming two years. This is due to the fact that most of the winter flows on the Blue Nile River and other tributaries depend on the flood magnitudes. After checking the serial correlation for each season, the following seasons were found to be serially independent and strongly correlated with the flood season flows: Blue Nile River MAMJ (-1), Atbara River NDJF (-2) and MAMJ (0) for the Sobat River. However, when the MAMJ (-1) season was included as a predictor in Eqs. 6-3 and 6-4 there was no improvement in the forecast as measured by the adjusted R^2.

Table 6-11 Correlation between the July to October (JASO) flows and seasonal flows of the Nile River at Aswan (ASW) the Blue Nile River (BN), Atbara River (ATB) and the Sobat River (SOB). (Negative lags indicate that the season lead the flood season (JASO))

	November to February flows (NDJF)							March to June flows (MAMJ)						
Loca-	Lag correlation							Lag correlation						
ation	(-3)	(-2)	(-1)	(0)	(+1)	(+2)	(+3)	(-3)	(-2)	(-1)	(0)	(+1)	(+2)	(+3)
ASW	-.18	0.17	-.05	-.06	0.72	0.22	0.30	-.29	-.26	-.17	-.27	0.05	-.05	-.18
BN	0.03	0.37	0.23	0.11	0.76	0.37	0.35	-.03	-.03	0.53	0.08	-.09	0.27	-.08
ATB	-.21	0.39	0.21	0.01	0.65	0.13	0.22	-.03	-.04	0.13	-.14	-.05	-.02	-.14
SOB	0.00	0.01	0.00	0.30	0.54	0.08	0.11	-.10	0.09	-.25	0.52	0.11	-.08	-.05

6.4 Artificial Neural Networks (ANN)

Recently, neural networks have been successfully applied to many applications. The area addressed by ANN techniques includes pattern matching, optimization, data compression and function optimization (Raman and Sunilkumar, 1995). Many of the problems that engineers must deal with are exactly the types of the problems for which ANN appear to be most applicable (Garrett, 1994). Flood and Kartam (1994) presented two papers for understanding the usage and potential for application of artificial neural networks (ANN) in Civil Engineering. A neural network structure consists of processing elements (nodes), links interconnection between the elements, and information processing. A layer represents a set of parallel nodes. The interconnection between nodes is controlled by the training algorithm and the nature of the problem. The number of nodes in the input and the output layers are dictated by the dimension of input and output sets presented to the network for training. The number of hidden layers and

neurons are a quantity that must be determined empirically for each separate situation due to the complexity of the problem.

The neural network used in the present research has a three-layer structure: an input layer, a hidden layer, and an output layer. Typically, experiments are conducted with a variety of architectures in order to find one that optimizes the performance of the network. Due to the larger number of parameters and the great flexibility of ANN, the model output may fit the data very well during the training period yet produce poor forecasts during the validation period. This is a result of overfitting; overfitting occurs when an ANN fitted the training data so well that it also fitted to the noises resulting in poor forecasts over the validation period. Therefore, when experimenting with different architectures care should be taken that the number of parameters in the training data set should be greater than or equal to the number of connections (weights and biases) so that the network is not overtrained (Sahai et al., 2000). Though the data used in this study may be relatively short for data driven models, this condition is satisfied in all cases. That is why different testing periods for different network sizes were used. Thus, the configuration of the neural network is constrained to avoid the overfitting problem.

The network was trained with the Levenberg-Matgradt algorithm (MATLAB manual, 1995). In practice, the Levenberg-Matgradt algorithm often finds better optima for a variety of problems than other optimization methods (Sarle, 1999) and behaves well an ill-conditioned problems, (Awadalla and Rousselle, 1999). The network was also retrained with several starting points to avoid local minima. Training is carried out by assigning random initial weights to each of the links, and then presenting the corresponding sets of known input and output values to the network, one set at a time.

The network estimates the output values from the inputs, compares the estimates to the known output values, and then adjusts the weights in order to reduce the mean squared difference between the network output and the target output. The complete input-output sets (patterns) are usually run through the network for a number of cycles (epochs) until either the MSE is reduced to a certain level, reaches the assigned number of epochs or by the evaluation (monitoring) technique stop, whichever occurs first. The R^2, RMSE, MAE and BIAS over the validation period are used as reasonable measures for indicating the model performance skill and, in this study, were used as indices to compare the different models.

The data was partitioned into three periods: 1) 1953-1972 was used for training, 2) 1973-1977 was used for evaluation and 3) 1978-1989 was used for validation. The evaluation period was used to monitor the performance of the model during the training period for best generalization (Chapter 4). The input data to the model were the predictors used in Eqs. 6-3 and 6-5 and the output were the flows at the two locations, respectively. Figure 6-5 shows a typical configuration for the network used to forecast the Nile River flows at Aswan and the Blue Nile River flows. One hidden layer with two neurons gave a reasonable performance of the forecasted flows. The Tangent hyperbolic (Eq. 4.13) was used as an activation function in the hidden layer, and a linear activation (Eq. 4.14) was used for the output layer. The cascade correlation was found to be more stable and higher performance skills were obtained compared to the back-propagation technique. The validation performance skills for the Nile River at Aswan flows were computed to be $R^2 = 0.73$, RMSE = 0.63, MAE = 0.56, BIAS = -0.10, and for the Blue Nile River flows as $R^2 = 0.78$, RMSE = 0.59, MAE = 0.53, BIAS = -0.20. This model

will be referred to as Model I for further analysis. Table 7-6 shows these performance measures of model I along with other models. Model I was compared to MLR-OLS and MLR-LAD models at the same validation period. It is clear that for the Nile River flows at Aswan, MLR-LAD outperformed both model I and MLR-OLS in three out of the four performance measures (R^2, RMSE, MAE, and BIAS). For the same location Model I and MLR-OLS each outperformed the other in two performance measures. Assuming that the four measures are given the same weights, then MLR-LAD outperformed model I and MLR-OLS. Figures 6-6 and 6-7 show the predicted and the observed flows for the training period, the evaluation period and the validation period. The predicted flows pursue the observed flow fluctuations during the training as well as the validation period.

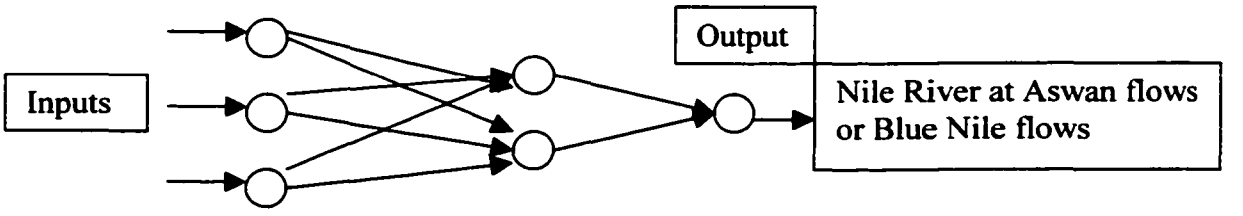

Fig. 6-5 Typical configuration of a three layer neural network (model I)

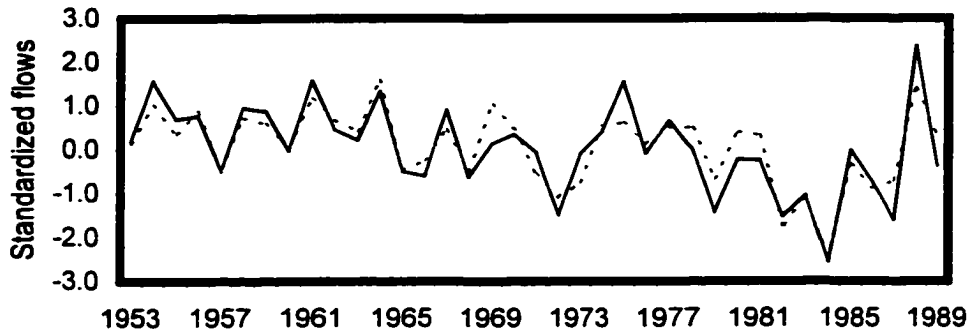

Fig 6-6 Performance of the 3 predictors models using the Nile River flows at Aswan flows as output during the training period (1953-1972), evaluation (1973-1977) and validation (1978-1989), (Model I)

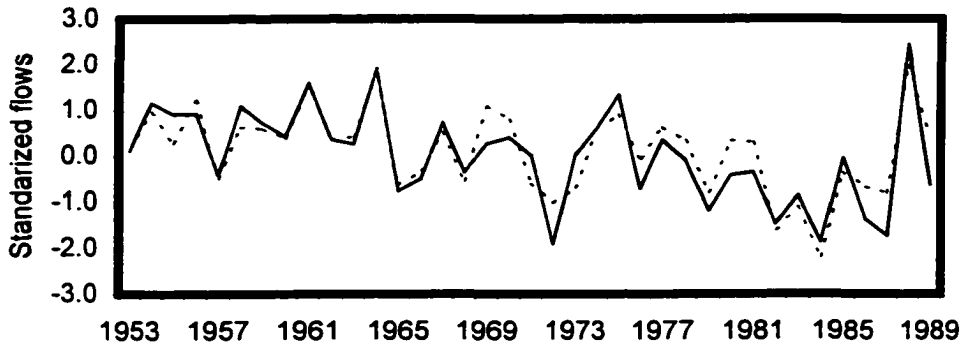

Fig. 6-7 Performance of 3 predictors ANN for Blue Nile River flows during the training (1953-1972), evaluation (1973 -1977) and validation (1978-1989), (Model I)

6.5 Multiple Linear Regression (LAD)

As a continuation of the previous analysis MLR-LAD models were evaluated for improvement and development of additional performance skill measures, e.g. measure of agreement. The output from the ordinarily least squares difference (OLS) and the least absolute difference (LAD) were compared for the Blue Nile River and the Nile River flows at Aswan. The LAD model used in this study was developed by Prof. Mielke, P. (CSU, Department of Statistics) and has been detailed in Gray et al. (1993, 1992).

The agreement coefficients (ρ) and their associated probability values (P) are given in Tables 6-12, 6-13, and 6-14, for the models developed previously by MLR-OLS (Tables 5-8 and 5-6, Eqs. 6-2 through 6-5). For comparative purposes, the corresponding values for the other performance skill measures are shown in Table 6-15, 6-16 and 6-17. The values of R^2 for the non-jackknifed MLR-LAD and MLR-OLS predictors are larger than the corresponding values of R^2 based on the cross validated (jackknifed) values. While R^2 is strictly a measure of linearity (i.e., $R^2 = 1$ implies all observed and predicted value pairs fall on a line that does not necessarily have a unit slope or pass through the origin), ρ is a measure of agreement, and $\rho = 1$ implies all observed and predicted value pairs fall on a line with unit slope that passes through the origin. Thus, the fact remains that R^2 is not a satisfactory measure of agreement, (Gray et. al., 1992).

From Tables 6-12 and 6-13, we can independently hindcast over 60% of the measure of agreement value (ρ) for the first four lead-seasons (MAMJ (0) to MAMJ (-1), for both the Nile River flows at Aswan and the Blue Nile River flows. The probability that there is no hindcast statistical skill in any of the forecast parameters is in the range 10^{-8} to 10^{-9}. In fact we can hindcast over 70% of the value of ρ for the Blue Nile River flows using the four stable predictors (4, 7, 12, and 16) at four months lead time, Table 6-14. In this case, the probability that there is no hindcast statistical skill in any of the forecast parameters is about 10^{-10}. The jackknifed LAD in some cases achieved relatively higher values of R^2 over the OLS. However, the non-jackknifed are comparable as shown in Table 5-6, 5-8, 6-6, 6-15, 6-16, and 6-17. Generally, the MLR-LAD outperforms MLR-OLS in most cases. The difference between the non-jackknifed and the

jackknifed R^2 for OLS is generally higher than the R^2 values in the LAD models. This finding may suggest that MLR-LAD is more stable and robust for such applications.

Table 6-12 Assessment and validation statistics for various forecast models based on MLR-LAD for the models in Eqs. 6-2 to 6-5. Values in parentheses in the second rows are for validation phase

Location	Lead Season	ρ	R	R^2	Adj-R^2	Adj-RMSE	RMSE	MAE	BIAS
Nile River At Aswan	MAMJ(0)	0.64	0.89	0.79	0.77	0.52	0.48	0.37	-0.04
			(0.83)	(0.68)	(0.65)	(0.62)	(0.58)	(0.49)	(-0.05)
	ASON(-1)	0.65	0.87	0.75	0.74	0.54	0.51	0.39	-0.05
			(0.84)	(0.70)	(0.69)	(0.60)	(0.57)	(0.46)	(-0.07)
Blue Nile River	MAMJ(0)	0.73	0.92	0.84	0.83	0.44	0.41	0.30	-0.05
			(0.90)	(0.80)	(0.79)	(0.49)	(0.46)	(0.36)	(-0.05)
	ASON(-1)	0.64	0.87	0.76	0.74	0.54	0.51	0.38	-0.06
			(0.85)	(0.72)	(0.70)	(0.58)	(0.55)	(0.44)	(-0.07)

Table 6-13 Assessment and validation statistics for various forecast models based on multiple linear regression (LAD) of PCA. Values in parentheses in the second rows are for the validation phase, Nile River flows Aswan

LEAD SEASON	ρ	R	R^2	ADJ-R^2	ADJ-RMSE	RMSE	MAE	BIAS
MAMJ(0)	0.66	0.86	0.75	0.72	0.56	0.52	0.34	0.00
		(0.82)	(0.68)	(0.65)	(0.62)	(0.58)	(0.42)	(-0.01)
NDJF (0)	0.63	0.83	0.70	0.67	0.60	0.56	0.39	-0.03
		(0.80)	(0.64)	(0.60)	(0.66)	(0.62)	(0.46)	(-0.06)
JASO (-1)	0.60	0.81	0.66	0.64	0.63	0.59	0.41	-0.06
		(0.78)	(0.61)	(0.59)	(0.68)	(0.64)	(0.46)	(-0.05)
MAMJ (-1)	0.61	0.81	0.66	0.64	0.63	0.60	0.41	-0.05
		(0.80)	(0.64)	(0.61)	(0.65)	(0.62)	(0.45)	(-0.05)
NDJF (-2)	0.55	0.82	0.67	0.65	0.63	0.60	0.45	-0.05
		(0.79)	(0.63)	(0.61)	(0.66)	(0.62)	(0.49)	(-0.06)
JASO (-3)	0.43	0.71	0.51	0.48	0.76	0.71	0.55	-0.06
		(0.58)	(0.34)	(0.32)	(0.86)	(0.83)	(0.67)	(-0.06)

Table 6-14 Assessment and validation statistics for various forecast models based on multiple linear regression (LAD) of PCA. Values in parentheses in the second rows are for the validation phase, Blue Nile River flows

LEAD SEASON	ρ	R	R^2	ADJ-R^2	ADJ-RMSE	RMSE	MAE	BIAS
MAMJ(0)	0.64	0.87	0.76	0.75	0.53	0.51	0.38	-0.04
		(0.86)	(0.74)	(0.73)	(0.55)	(0.53)	(0.40)	(-0.04)
NDJF (0)	0.62	0.85	0.71	0.71	0.58	0.55	0.40	-0.05
		(0.84)	(0.71)	(0.70)	(0.58)	(0.55)	(0.41)	(-0.04)
JASO (-1)	0.60	0.84	0.70	0.69	0.59	0.57	0.43	-0.09
		(0.81)	(0.66)	(0.65)	(0.63)	(0.61)	(0.48)	(-0.09)
MAMJ (-1)	0.61	0.84	0.70	0.69	0.60	0.56	0.41	-0.07
		(0.81)	(0.66)	(0.64)	(0.63)	(0.60)	(0.45)	(-0.07)
NDJF (-2)	0.59	0.86	0.74	0.73	0.57	0.55	0.42	-0.10
		(0.85)	(0.73)	(0.72)	(0.58)	(0.55)	(0.44)	(-0.10)
JASO (-3)	0.57	0.82	0.67	0.66	0.63	0.60	0.46	-0.10
		(0.81)	(0.66)	(0.65)	(0.63)	(0.60)	(0.46)	(-0.10)

Here, the predictability of the predictors used in Eqs. 6-3 and 6-5, was tested using split sample validation technique. Table 6-15 shows the performance measures for the MLR-OLS and MLR-LAD using the three predictors in Eqs. 6-3 and 6-5 for the Nile River at Aswan and Blue Nile River flows, respectively, at 11 months lead season. The difference between the performance skills computed in Table 6-15 and those of Tables 6-6 and 6-12 is that in Table 6-15 validated by the split sample technique. For further analysis, the partition of the data was carried out in the same way as in the ANN models. Two scenarios were used for validation: 1) 1973-1989 with a calibration period of 1953-1972 2) 1978-1989 with a calibration period of 1953-1977. As shown from the Table 6-18 the MLR-LAD and MLR-OLS have very similar R^2; however, the MLR-LAD outperformed the latter in all other performance skill measures. It is worth noting that the

MLR-LAD and MLR-OLS are comparable when using the drop-one jackknifing validation technique compared to the split sample technique. Figures 6-8 and 6-9 show the predicted and the observed river flows using the split sample validation technique. The models track the flow fluctuation reasonably well during the calibration period as well as during the validation period. This indicates that these predictors are stable using different validation techniques (split sampling, drop-one jackknife) and different modeling procedures (MLR, ANN) and stable under various calibration periods.

Table 6-15 Performance of different models on validation data sets for the Nile River flows at Aswan and the Blue Nile River flows using the stable predictors (7, 11, 17 and 4, 7, 12, respectively) based on MLR-LAD and MLR-OLS at ASON (-1) lead season

MODEL TYPE AND LOCATION		R^2	RMSE	MAE	BIAS
MLR-OLS for Aswan	1973-1989	0.80	0.68	0.55	-0.26
MLR-LAD for Aswan	1973-1989	0.83	0.54	0.45	-0.12
MLR-OLS for Aswan	1978-1989	0.81	0.77	0.65	-0.48
MLR-LAD for Aswan	1978-1989	0.80	0.59	0.51	-0.23
MLR-OLS for Blue Nile	1973-1989	0.74	0.64	0.53	-0.28
MLR-LAD for Blue Nile	1973-1989	0.74	0.58	0.49	-0.17
MLR-OLS for Blue Nile	1978-1989	0.79	0.67	0.56	-0.43
MLR-LAD for Blue Nile	1978-1989	0.80	0.57	0.47	-0.28

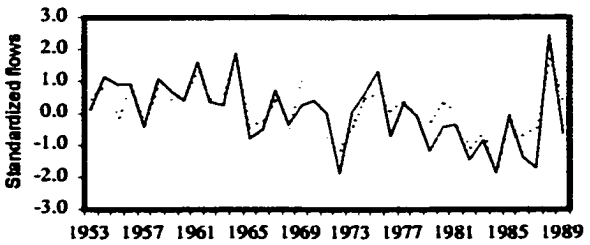

Fig. 6-8a Performance MLR-OLS of 3 predictors for the Blue Nile River flows during the Calibration (1953-1972), validation (1973-1989)

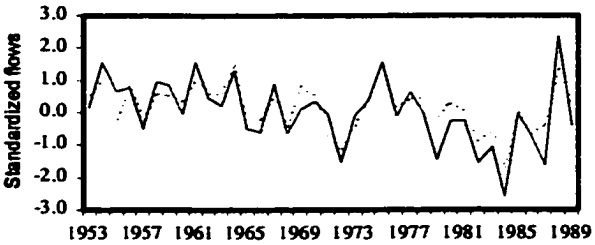

Fig. 6-8c Performance MLR-OLS of 3 predictors for Nile River flows at Aswan during the Calibration (1953-1972), validation (1973-1989)

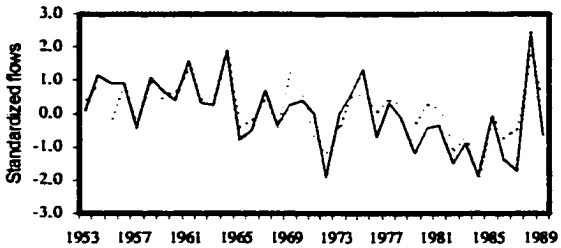

Fig. 6-8b Performance MLR-OLS of 3 predictors for the Blue Nile River flows during the Calibration (1953-1977), validation (1978-1989)

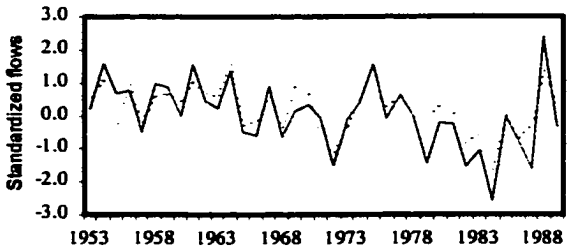

Fig. 6-8d Performance MLR-OLS of 3 predictors for Nile River flows at Aswan during the Calibration (1953-1977), validation (1978-1989)

Fig. 6-8 Comparison between the observed flows (solid line) and the forecasted flows (dotted line) based on MLR-OLS for various calibration period

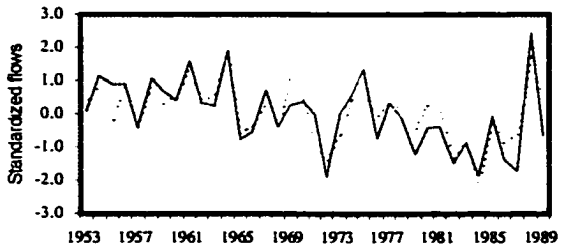

Fig. 6-9a Performance MLR-LAD of 3 predictors for the Blue Nile River flows during the Calibration (1953-1972), validation (1973-1989)

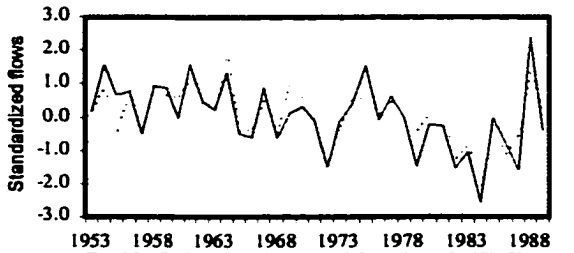

Fig. 6-9c Performance MLR-LAD of 3 predictors for Nile River flows at Aswanduring the Calibration (1953-1972), validation (1973-1989)

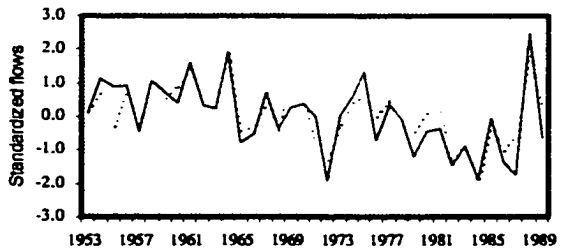

Fig. 6-9b Performance MLR-LAD of 3 predictors for the Blue Nile River flows during the Calibration (1953-1977), validation (1978-1989)

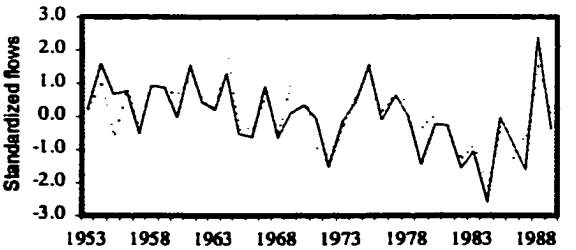

Fig. 6-9d Performance MLR-LAD of 3 predictors for Nile River flows at Aswan during the Calibration (1953-1977), validation (1978-1989)

Fig. 6-9 Comparison between the observed flows (solid line) and the forecasted flows (dotted line) based on MLR-LAD for various calibration period

6.6 Relationship between Indian Summer Monsoon and Nile River Flood Season

6.6.1 Indian Summer Monsoon, Nile River Flows and 75° E Ridge

For the long-range forecasting of the quality of the big rains in Ethiopia or summer rainfall in other parts of eastern Africa, the connection with India provides an interesting field of investigation, (Camberlin, 1997). Recent studies on prediction of Indian monsoon rainfall (e.g. Mooley et al., 1986, Shulka and Mooley, 1987) conclude that a very important parameter is the latitude position of the April 500-mb ridge axis along longitude 75° E. For the period 1953-1989, the cross-correlation between the Indian monsoon (June through September) rainfall and the Nile River flows (JASO) are, 0.70, 0.67, 0.57 and 0.15 for the Blue Nile River, the Nile River at Aswan, the Atbara River and the Sobat River, respectively. Due to this strong relationship between the Nile basin hydrology and the Indian monsoon, the April position of the 500-mb ridge at longitude 75° E was tested as a potential predictor for the Nile River flow. Shulka and Mooley (1987) described the ridge as a measure of the progression of a seasonal cycle of mid tropospheric circulation. 500-mb ridge at longitude 75° E was considered as one of the most important predictors for the Indian monsoon. This may confirm the previously stated relationship between the Indian rainfall and the Nile River flows.

The data for the Indian rainfall and the ridge are taken from Parthasarathy et. al., (1994) and Shulka and Mooley, (1987), respectively. Since the Blue Nile River is the largest contributor to the Nile River flows and has the highest correlation with the Indian precipitation it was used here. However, the ridge was not included as a predictor in forecasting models developed previously, mainly because of the limited length of record (only up to 1984). However, in this section the full available record (1939-1984) was

used. The sliding window procedure defined previously to identify the stability and the consistency of the predictors was also used here. The sliding windows (21-, 25-, 31-, and 35-year) correlation coefficient show stable and consistent relationship between the ridge and the Blue Nile River flow. Average correlation coefficients of 0.60 for each of the four sliding windows were obtained, similar to the total record (1939-1984) correlation (0.60). As indicated by by Shulka and Mooley (1987), the only limitation to this predictor is the subjectivity involved in determining the location of the 500-mb ridge along longitude 75° E. This may impose limitations on its reliability. Figure 6-10 shows how the time series of the ridge follows the fluctuations of the Blue Nile River flows. This indicates that even a regional variable of the Indian rainfall could be used as a potential predictor for the Blue Nile River flows. This relationship between the Blue Nile River basin and the Indian precipitation east of the basin and the Guinea precipitation west of the basin may be further evaluated in future studies.

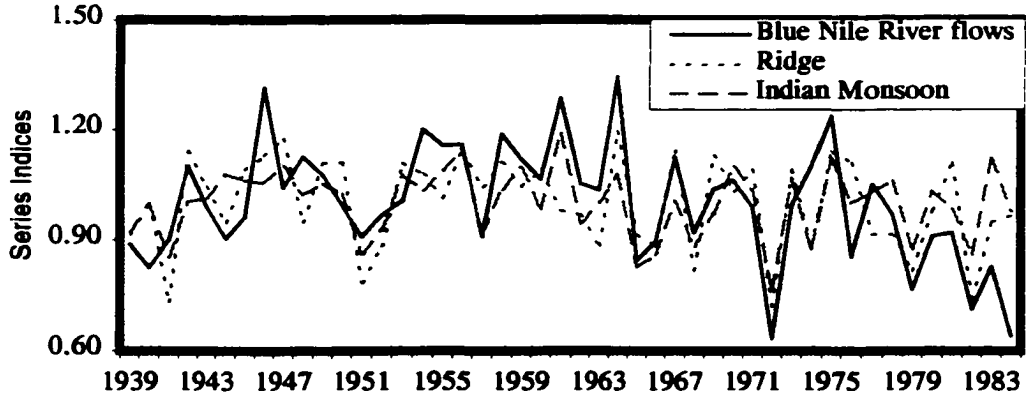

Fig. 6-10 Comparison between the Blue Nile River flows, Indian monsoon and the 500-mb ridge over the 75° E for the period 1939-1984, all series are fraction of their long term average

6.6.2 Tendency Analysis

In this study tendency denotes time series of normalized seasonal Darwin pressure difference from northern winter to spring (MAM-DJF). The purpose here is to re-examine the relationship between the southern oscillation (SO) and the Nile River using Darwin pressures for the period 1913-89. The Darwin pressure is examined because its long-term record is considered to be more reliable and homogeneous than that of others (Trenberth, 1976). Although the SOI is considered to be a better index of the SO (Chen, 1982), the Tahiti record before 1935 is less reliable, however, the extended record of Tahiti and the SOI computed will be used for comparison. The tendency analysis presented here follows Shukla and Paolino (1983) analysis for the Indian summer monsoon. The idea was to show that similar driving forces for Indian precipitation may have similar impact on the Nile River flows.

Figure 6-11 shows the data for the Blue Nile River and Darwin pressure anomalies (December-February, DJF, March-May, MAM) for the period 1913-89. For normalization, the anomalies are divided by the standard deviation. During the period 1913-1989, there were 12 major flood years, defined as years of normalized streamflow departure larger than one standard deviation [1916, 1917, 1929, 1935, 1938, 1946, 1954, 1958, 1961, 1964, 1975, and 1988] and 11 major drought years, with less than one standard deviation [1913, 1915, 1918, 1940, 1972, 1979, 1982, 1983, 1984, 1986, and 1987]. The former group of years will be referred to as the high flow years and the latter as the dry flow years. Single and double underlined years classified as La Niña and EL Niño years, respectively.

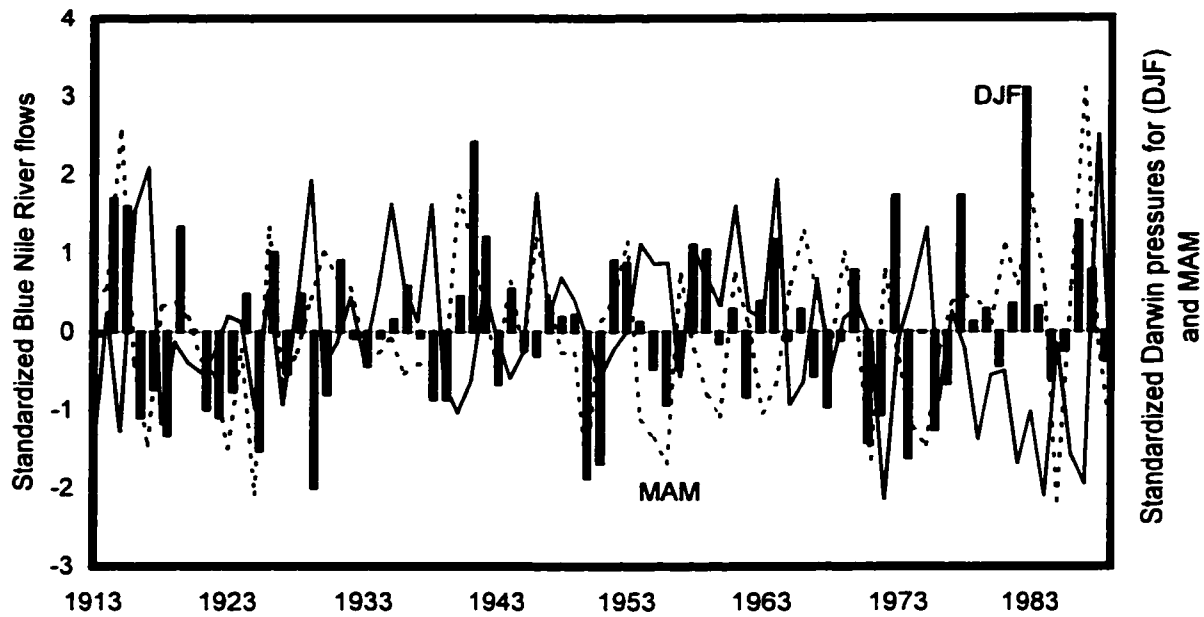

Fig. 6-11 Standardized Blue Nile River flow (JASO) and standardized Darwin pressure for December to February (DJF) and March to May (MAM), 1913-189

The normalized seasonal mean Darwin pressure anomalies averaged for the high flow years, and the dry flow years, are shown in Fig. 6-12. The central part (July-October, JASO) of Fig. 6-12 denotes the Blue Nile River flood period. One of the remarkable features of this figure is the simultaneous occurrence of high (low) Darwin pressure anomaly with low (high) Blue Nile River flow and the persistence of this pressure anomaly after the flood period. This association of pressure anomaly and the flood period, however, is not useful for the long-range forecasting of the Nile River flow, but still has forecasting potential. For the purpose of predicting the streamflow, the most useful antecedent parameter appears to be the tendency of the Darwin pressure anomaly before the flood period (July-October). The Darwin pressure anomaly decreases from DJF to MAM before the occurrence of high flows, and increases before the occurrence of

low flows (dry). The Darwin pressure tendency is defined as the MAM minus DJF pressure anomaly, which has a potential to predict the Blue Nile River flow during the flood season (July-October).

Figure 6-13 shows a scatter diagram between the normalized Darwin pressure tendency and the normalized Blue Nile River flow. Most of the severe drought years are in the lower right quadrant, and most of the high flow years are in the upper left quadrant of the scatter diagram. During the 77-year period examined in this study, there was only one occasion when the negative Darwin pressure tendency was followed by a normalized streamflow of less than –1.0 (1983). The near absence of points in the lower left corner of this scatter diagram suggests that a negative Darwin pressure tendency should be a very useful predictor for the non-occurrence of drought in the Blue Nile River. This is justified by the steep slope of the tendency line (Fig. 6-12a) before the dry period and a relatively mild slope preceding the wet years. Tables 6-12b and 6-12c, for the Tahiti and SOI show similar pattern as that of the Darwin.

Fraedrich and Muller (1992) have identified 17 El Niño years during the 77-year period examined in this study, and these years have been denoted by the rectangles in Fig. 6-13. For only 4 of the 17 El Niño events, the normalized streamflow is less than –1.0, and for 12 of the 17 events the normalized streamflow has a negative sign. During this 77-year period, there were 11 instances of normalized streamflow being less than –1.0, and 7 of these 11 cases were not associated with EL Niño. Quin et al. (1978) classified the EL Niño years by intensity (Table 6-16) and updated by Gray and Shaeaffer (1991).

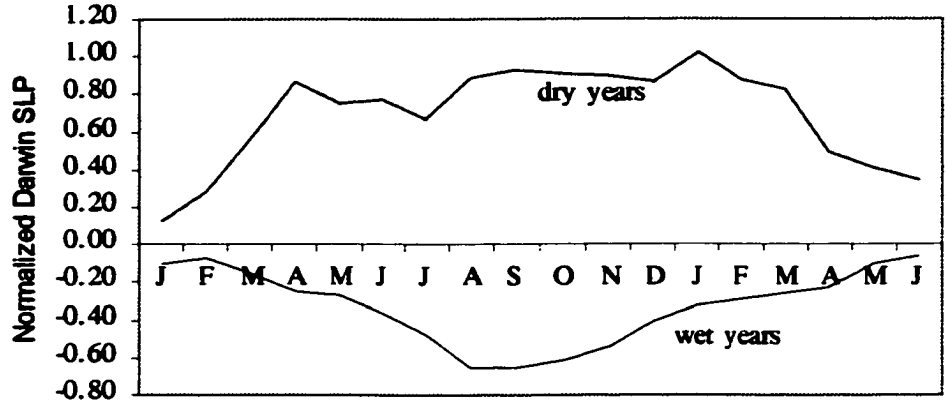

Fig. 6-12a Composite of normalized Darwin pressure anomaly (three-month running mean)

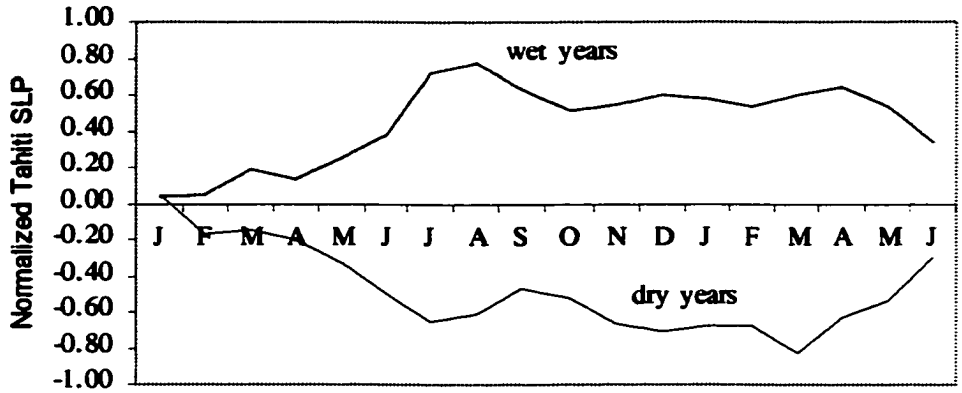

Fig. 6-12b Composite of normalized Tahiti pressure anomaly (three month running mean)

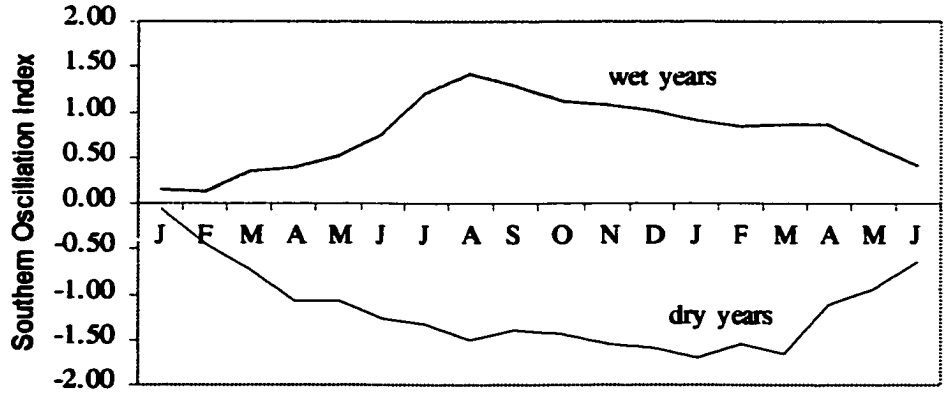

Fig. 6-12c Composite of SOI (normalized Tahiti minus normalized Darwin) (three month running mean)

Fig. 6-12 Composite anomalies and the Blue Nile River flows

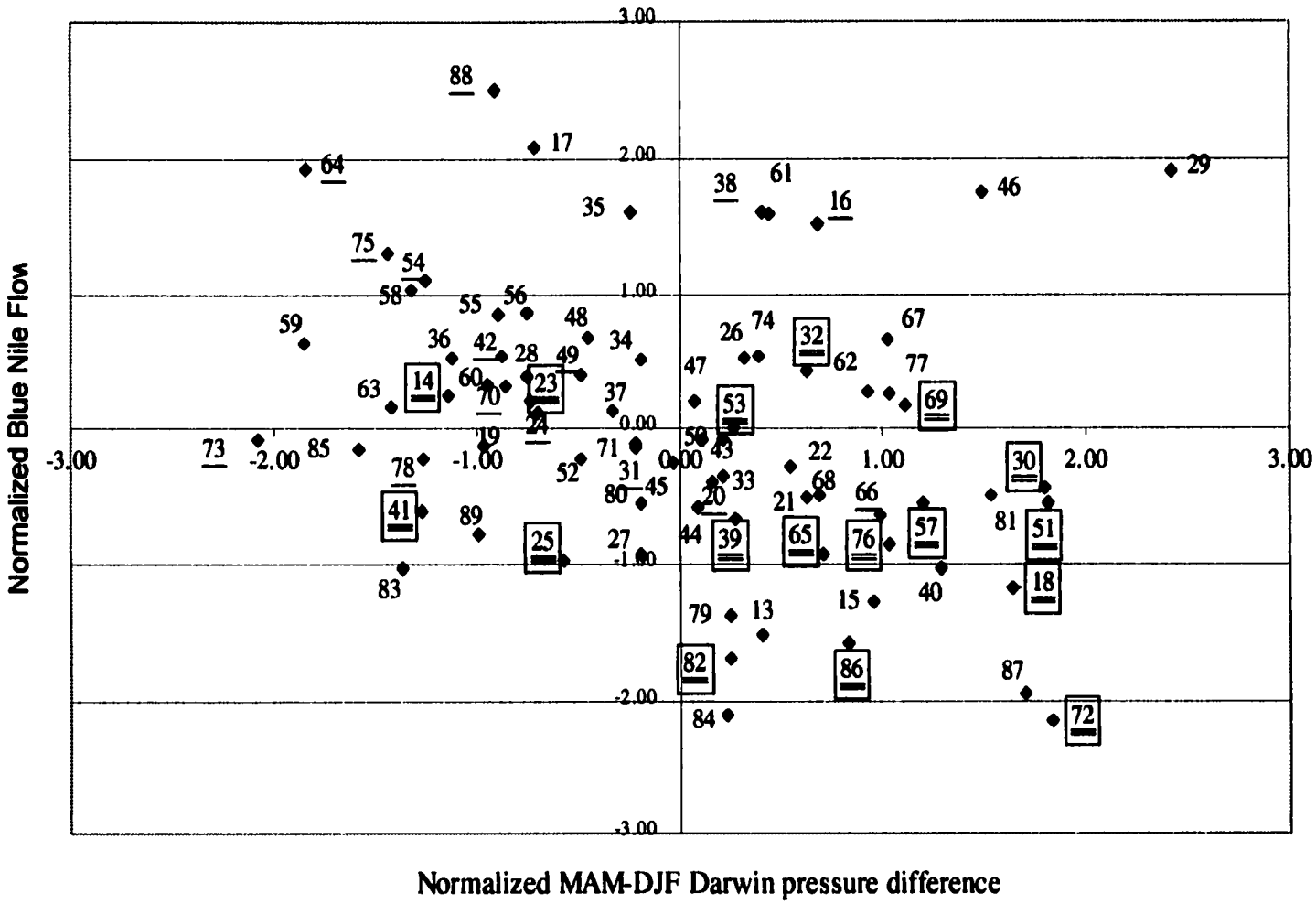

Fig 6-13 Scatter diagram between the normalized Darwin pressure trends (MAM-DJF) and normalized Blue Nile flows. The numbers denote the year (minus 1900). The El Ni±o and La Ni±a years are shown by a double underline in a box and single underline, respectively

Table 6-16 EL Niño years since 1900 by intensity as determined by Quinn et al. (1978) and updated by Gray and Shaeaffer (1991)

STRONG	MODERATE	WEAK	VERY WEAK
1983	1987	1969	1975
1982	1986	1951	1963
1972	1976	1943	1948
1957	1965	1932	1946
1941	1953	1923	
1925	1939	1917	
1918	1929		
1911	1914		
	1905		
	1902		

Fraedrich and Muller (1992) have identified 15 La Niña years during the 77-year period examined in this study, and these years have been denoted by a single underline in Fig. 6-13. For 6 of the 15 La Niña events, the normalized streamflow is greater than 1.0, and for 10 of the 15 events the normalized streamflow has a positive sign. During the 77-year period examined in this study, there were 12 instances of the normalized streamflow being greater than 1.0 and 6 of these 12 cases were not associated with La Niña. It is worth mentioning that there is no El Niño event associated with a streamflow greater than 1.0 and no single La Niña event associated with a streamflow less than –1.0. It is also worth noting that 13 of the 17 El Niño years are associated with the positive tendency in the DJF to MAM pressure, while only 4 El Niño years are associated with the negative tendency. On the other hand, 11 of the 15 La Niña years are associated with the negative tendency, while only 4 are associated with the positive tendency. The relationship between the normalized Darwin pressure tendency and the Blue Nile River flows has the

potential to predict ENSO as well. Thus, the similarity between analysis presented for the Blue Nile River flows and that presented by Shukla and Paolino (1983) for the Indian summer monsoon indicates the strength of the relationship between these two regions.

6.7 Relationship between Indian Precipitation, Guinea precipitation, Pacific SST and the Nile River Flows

The Nile River flows during the flood season (July to October) are strongly correlated with the Indian summer monsoon (June to September) in the same year. The Indian summer monsoon for the period 1953-1989 is associated with the Nile River flows at Aswan, the Blue Nile river flows, the Atbara river flows and the Sobat River flows with a linear correlation coefficient of 0.67, 0.70, 0.57 and 0.15, respectively. These four Nile River tributaries have correlation with the previous year's (August to November) precipitation over Guinea (Western Africa) of, 0.63, 0.61, 0.26 and 0.29, respectively. Indian summer monsoon precipitation has a correlation of 0.37 with the previous year's Guinea precipitation. The linear associations between the three regions suggest the interconnection between their climatic driving forces.

In this section the predictability of the Nile River flows using the Indian precipitation, Guinea precipitation, and the Pacific Ocean SSTs is tested. A neural network is used to test the prediction skill of these predictors. For comparison MLR models were also developed. October of year (-3) for the Indian precipitation has a relatively consistent correlation with the JASO season of the Nile River flows. October (-3) Indian precipitation, the ASON (-1) Guinea precipitation and predictor number 4 (in the Pacific Ocean) from the Blue Nile River flows stable predictors (Table 6-2) are used

as predictors for the Nile River flows. The Blue Nile River flows and the Nile River flows at Aswan are used as predictands.

A three layer neural network with three inputs, two hidden nodes of a single hidden layer, and one output node was developed to predict the Blue Nile River flows and the Nile River flows at Aswan. The data was partitioned into three subsets: 1) 1953-1972 for training, 2) 1973-1977 for evaluation, and 3) 1978-1989 for validation. For comparison the MLR-OLS and MLR-LAD models were developed. Equations 6-6 and 6-7 were formulated for the calibration period 1953-1972. Table 6-17 summarizes the performance skill measures for the ANN and MLR models. It is clear that the ANN outperformed the MLR-LAD and MLR-OLS. This indicates the nonlinear relationship between the predictors and the predictands. MLR-LAD outperforms MLR-OLS in three performance measures (RMSE, MAE, and BIAS) with marginal difference in the fourth measure (R). Figure 6-14 shows the performance of the models during the training, the evaluation and the validation stage. The forecasted flows track the observed flows during

$$Q_{ASW}^{ASON(-1)} = 0.15 - 0.17 Pacific_{SST} + 0.28 Indian_{p} + 0.32 Guinea_{p} \quad [6\text{-}6]$$

$$Q_{BN}^{ASON(-1)} = 0.13 - 0.29 Pacific_{SST} + 0.24 Indian_{p} + 0.43 Guinea_{p} \quad [6\text{-}7]$$

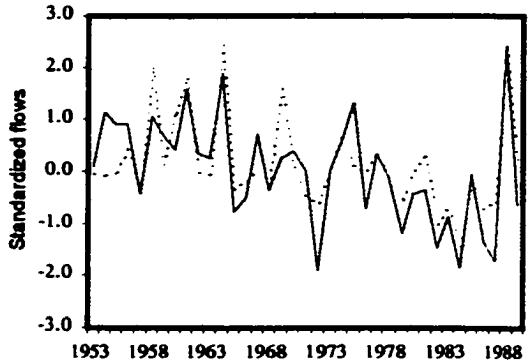

Fig. 6-14a Time series for standardized Blue Nile flows (solid line) and predicted flows, training (1953-1972), evaluation (1973-1977) and validation (1978-1989), using ANN

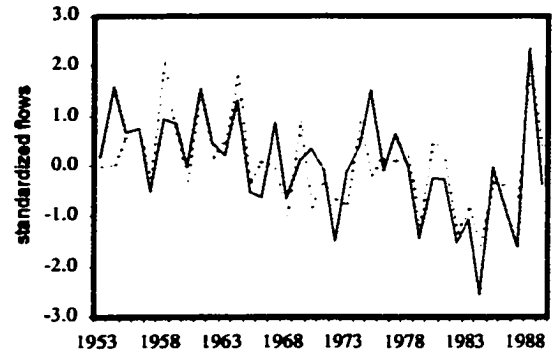

Fig. 6-14b Time series for standardized Aswan flows (solid line) and predicted flows, training (1953-1972), evaluation (1973-1977) and validation (1978-1989), using ANN

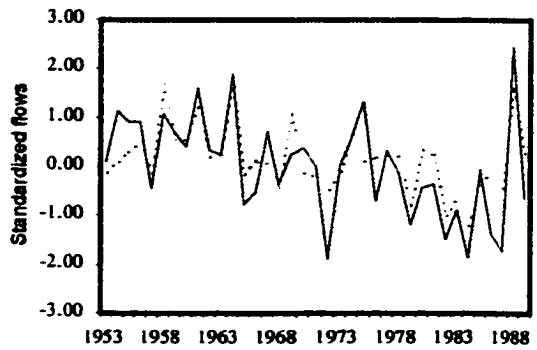

Fig. 6-14c Time series for standardized Blue Nile flows (solid line) and predicted flows, using MLR-OLS model (1953-1972), and validation (1973-1989)

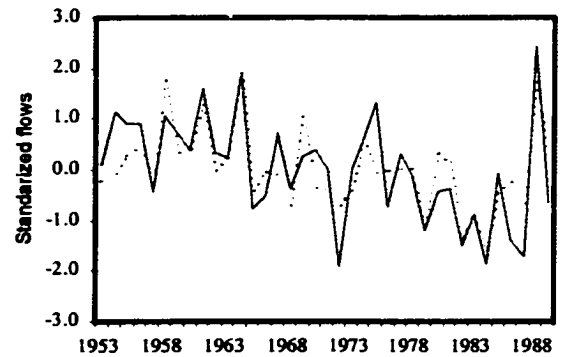

Fig. 6-14d Time series for standardized Blue Nile flows (solid line) and predicted flows, using MLR-LAD model (1953-1972), and validation (1973-1989)

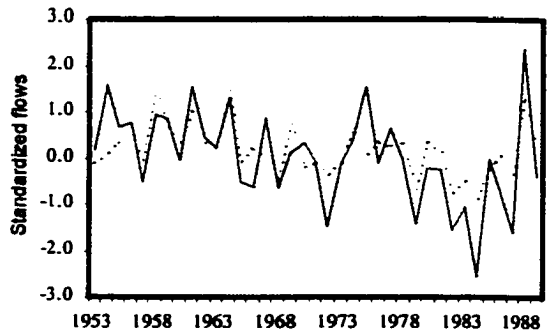

Fig. 6-14e Time series for standardized Aswan flows (solid line) and predicted flows, using MLR-OLS model (1953-1972) validation (1973-1989)

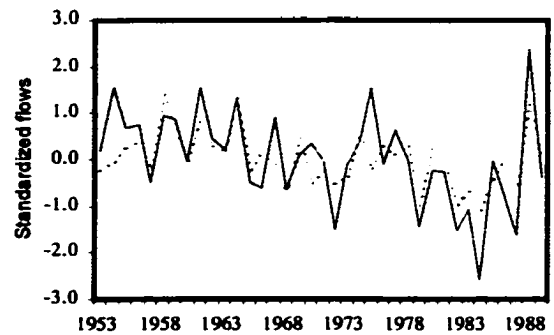

Fig. 6-14f Time series for standardized Aswan flows (solid line) and predicted flows, using MLR-LAD model (1953-1972) validation (1973-1989)

Fig. 6-14 Comparison between the observed flows (solid line) and the forecasted flows (dotted line) based on an ANN, MLR-OLS and MLR-LAD

Table 6-17 Models performance skills for the validation period (1978-1989) for the Nile River at Aswan and Blue Nile River

LOCATION, MODEL TYPE	R	R^2	RMSE	MAE	BIAS
Nile river at Aswan (NN)	0.94	0.89	0.56	0.48	-0.37
Blue Nile river (NN)	0.96	0.92	0.56	0.47	-0.44
Nile river at Aswan (MLR-OLS)	0.93	0.86	0.85	0.76	-0.54
Blue Nile river (MLR-OLS)	0.88	0.78	0.74	0.66	-0.48
Nile river at Aswan (MLR-LAD)	0.91	0.82	0.75	0.65	-0.38
Blue Nile river (MLR-LAD)	0.87	0.77	0.63	0.51	-0.32

7. MULTISITE ANALYSIS

7.1 Canonical Correlation Analysis

7.1.1 General Description

This part of the research analyzes the Nile River flows using canonical correlation analysis (CCA), with the purpose of improving the forecast performance. Canonical correlation Analysis (CCA) is a multivariate statistical methodology to determine linear combinations of two data sets (the predictor data and the predictand data set), i.e. multicomponent predictors are linearly related to multicomponent predictands such that the sum of the squared errors is minimized. The technique is a generalization of the multiple regression analysis that allows one field to be regressed on another field and depicts the major patterns of covariance between the fields analyzed (Graham et al., 1987b). The CCA technique is considered as an extension of multivariate regression and correlation analysis, and closely related to MLR and PCA. However, CCA differs from MLR in that CCA allows multiple dependent variables; MLR allows multiple independent variables but only a single dependent variable. Barnett and Preisendorfer (1987) characterized CCA to be at the top of the regression modeling hierarchy.

The goal of CCA is to calculate two new paired sets of variables, Z and W, that are linear combinations of X (predictors) and Y (predictands). Corresponding Z's and W's have the largest correlation possible and the Z's are orthogonal as are the W's. The square of the canonical correlations is often called the eigenvalues. The predictor and the

predictand data sets are first standardized to ensure that all the variables have equal opportunity to participate in the prediction process, regardless of their original variance. The predictands considered are the July to October flows for the Sobat River, the Blue Nile River, the Atbara River, and the Nile River at Aswan. The predictors were selected from a pool of stable predictors shown in Tables 6-1, 6-2, 6-3, and 6-4, at the four locations, respectively. The predictors were selected for each flow location to produce the maximum R^2 using MLR and to be serially uncorrelated. Also each of the predictors is not significantly correlated with its peers at that particular location.

To control for artificial skill produced by the overfitting of random data variability in the relatively short period of record, cross-validation (Michaelsen, 1987) is used in evaluating forecast skill. Further details about the forecast skill measures are presented in section 4.7. The drop-one Jackknifing procedure was used: that is each of the 37 years is held out in turn, and CCA is used to develop a prediction model from the remaining 36 years. The predictor data for the withheld year are then projected onto the prediction CCA loading pattern, and predictand values are generated and verified against observed data for the withheld year. For comparison, performance skills of the multiple linear regression (MLR) and principal component regression (PCR) models using both ordinary least squared (OLS) and least absolute difference (LAD) techniques were developed. The lead time, or amount of time between the end of the latest predictor season and the end of the 4-month predictand season, is varied from 4 to 32 months. The prediction skill results are evaluated by the performance measures presented in section 4.7. In addition, links with other large scale oceanic and atmospheric processes leading to the skillful forecasts is sought by examining the leading canonical component time

series (CCTS) predictor mode and the sea surface temperature (SST). Correlation maps between the SST and the leading canonical component time series were presented to identify the locations of the oceanic forces that contribute to the Nile River flows predictability. Furthermore, similar to empirical orthogonal function (EOF) patterns, in the CCA the canonical loading patterns of the predictors were obtained. When the loading patterns are normalized, the relative importance of each of the predictor data fields can be determined.

7.1.2 Forecasting River Flows at Lead Season MAMJ (0), 4 Months

At this lead season the predictors were selected from a pool of stable predictors presented earlier in Tables 6-1, 6-2, 6-3, and 6-4 for each of the four predictands (the Sobat River, the Blue Nile River, the Atbara River and the Nile River at Aswan, respectively). Predictors numbered 4, 7, 12, and 16 (Table 6-2) were selected for the Blue Nile River, predictors 7, 11,17 and 23 (Table 6-4) were selected for the Nile River flows at Aswan, predictors 11, 13, and 19 (Table 6-3) were selected for Atbara River flows, and predictors 2, 7, and 11 (Table 6-1) were selected for the Sobat River. However, due to the similarity between some of these predictors only nine predictors were included in multivariate models (CCA). Eight of these predictors are listed in Table 7-3 and the ninth predictor is predictor number 16 of Table 6-2. Univariate MLR forecast models and PCA models for the Nile River flows at Aswan and the Blue Nile River flows were used as a control against which the skill of the multivariate model is assessed. The first four principal components (PCs) were used to develop the principal component regression models. The first four PCs explain about 68% of the variability of the predictors and have significant regression coefficients with the Nile River flows at Aswan

and the Blue Nile River flows. The performance skill measures of the principal component regression models (PCR) and those for the MLR models are presented in Table 7-1. In this case the PCR models were comparable with the MLR models, this may be attributed to the lower degree of multicollinearity between the predictors. The CCA model shows better performance over the MLR models and the PCR models for the Nile River flows at Aswan and the Blue Nile River flows. The performance skills degraded in the CCA model for the Atbara River and the Sobat River. However, the cross correlation coefficients between the predicted flows of the four locations are preserved as shown in Table 7-2.

The first CCTS predictor mode was significantly correlated with the river flows. The correlation between the first and the second CCTS predictor mode and those of the predictands are 0.95 (R^2 = 0.82) and 0.85 (R^2 = 0.72), respectively. The correlation between the first CCA predictor mode and the Blue Nile River flows and the Nile River flows at Aswan were –0.92 (R^2 = 0.84) and –0.90 (R^2 = 0.82), respectively. The leading CCST predictor mode is shown in Fig. 7-3. The pattern is similar to that of the cross-validated Blue Nile River flows and the Nile River flows at Aswan (not shown). Figure 7-1 shows the correlation maps between the first mode predictor time series and the SST for the season JASO. The first CCA mode exhibits areas of importance at the three oceans over mainly the Pacific Ocean, the southern Atlantic Ocean and the southern Indian Ocean. The canonical component time series associated with the mode 1 predictors scenario, shown in Fig. 7-3, further confirms that ENSO is being described by

Table 7.1 Performance skill of the univariate and multivariate models at 4 months lead season

LOCATION	METHOD	R	R^2	RMSE	MAE	BIAS
Nile River	MLR-OLS	0.85	0.72	0.54	0.44	0.00
at Aswan	MLR-LAD	0.83	0.68	0.58	0.49	-0.05
	PCA-OLS	0.84	0.71	0.55	0.44	-0.03
	PCA-LAD	0.85	0.72	0.54	0.44	-0.03
	CCA	0.91	0.82	0.42	0.33	0.00
Blue Nile	MLR-OLS	0.89	0.79	0.47	0.36	0.00
River	MLR-LAD	0.90	0.80	0.46	0.36	-0.05
	PCA-OLS	0.88	0.77	0.49	0.38	-0.04
	PCA-LAD	0.87	0.76	0.50	0.39	-0.02
	CCA	0.91	0.83	0.40	0.30	0.00
Atbara	MLR-OLS	0.81	0.66	0.59	0.43	0.00
River	MLR-LAD	0.83	0.69	0.55	0.42	-0.02
	PCA-OLS	0.83	0.68	0.57	0.43	-0.02
	PCA-LAD	0.83	0.69	0.55	0.43	-0.04
	CCA	0.78	0.61	0.62	0.51	0.00
Sobat	MLR-OLS	0.73	0.53	0.69	0.55	-0.01
.River	MLR-LAD	0.67	0.45	0.75	0.63	0.05
	PCA-OLS	0.78	0.60	0.62	0.45	0.08
	PCA-LAD	0.81	0.66	0.59	0.43	0.09
	CCA	0.79	0.62	0.61	0.52	0.00

this mode. The "W" and "C" symbols denote warm and cold ENSO years as identified by Fraedrich and Muller (1992). Furthermore, the correlation between the southern oscillation index (defined as the difference between the standardized sea level pressure at

Tahiti and Darwin) for JASO season and the first CCST predictor mode was –0.56 and had no correlation with the second CCTS mode. In addition, the second CCST predictor mode exhibits very weak correlations with the SST (Fig. 7-2) and does not exhibit any ENSO-like features. As previously indicated the Pacific Ocean plays an important role in the Nile River flows predictability. The positive center over the equatorial Pacific is consistent with these findings. To investigate the relative importance of the predictors, the canonical loading patterns of the predictors are normalized. The first normalized canonical loading pattern associated mainly with predictor number 8 (i.e. the Guinea precipitation), then predictors 3 and 4 of Table 7-3. It is worth noting that, these three predictors represent the Western African region, the Pacific Ocean and the Atlantic Ocean. The latter predictor in its north-south gradient resembles the North Atlantic Oscillation. For this lead season most of the predictability of the region provided by the equatorial Pacific Ocean.

Table 7-2 Correlation matrix of Nile River flows at four locations observed (upper right section) and CCA forecasted (lower left section), MAMJ (0), 4-month lead season

	BLUE NILE RIVER	NILE RIVER AT (ASWAN)	ATBARA RIVER	SOBAT RIVER
Blue Nile River	1.00	0.96	0.54	0.25
Nile River at Aswan	0.99	1.00	0.59	0.22
Atbara River	0.61	0.64	1.00	-0.12
Sobat River	0.34	0.37	0.00	1.00

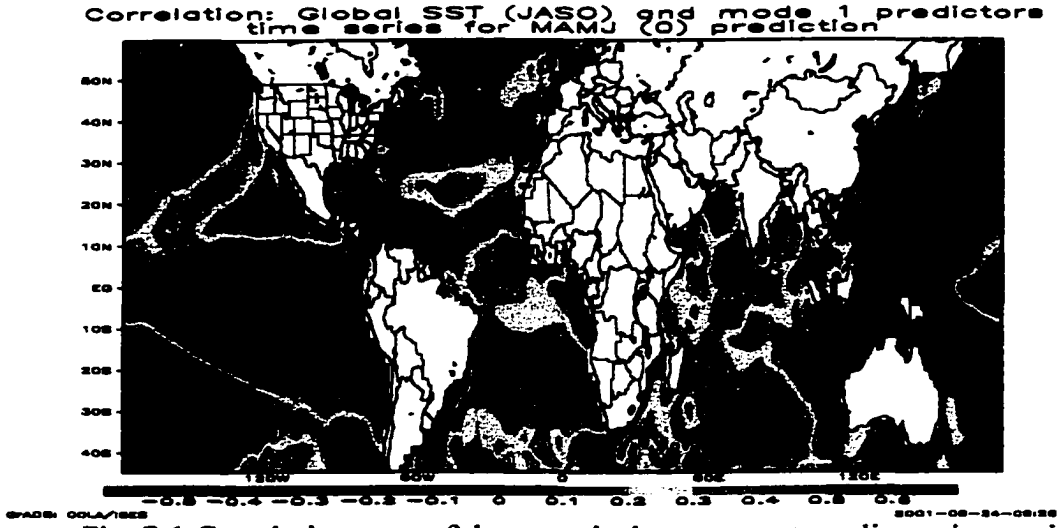

Fig. 7-1 Correlation map of the canonical component predictor time series for mode 1 for the prediction of MAMJ (0) and SST for JASO season

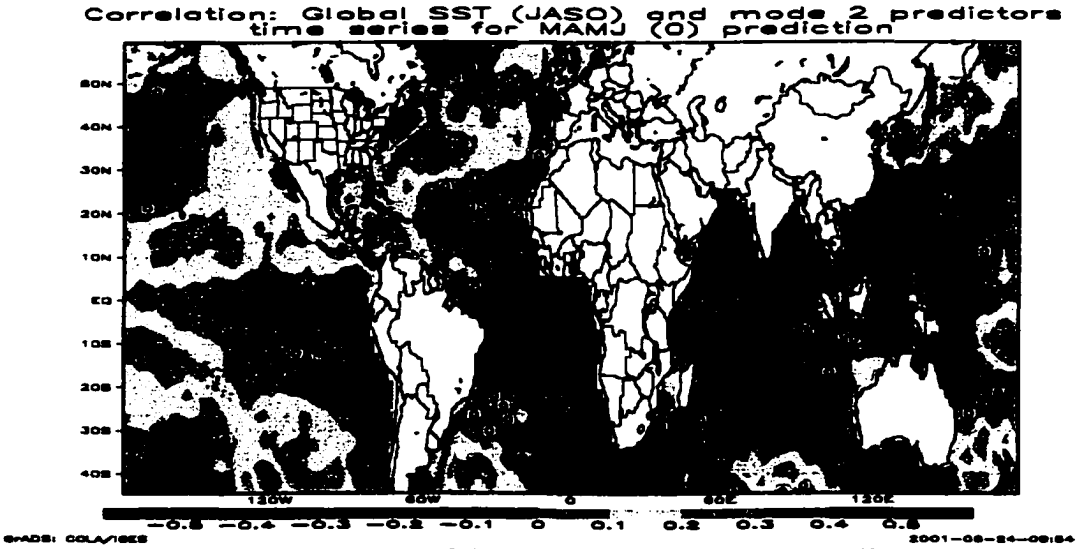

Fig. 7-2 Correlation map of the canonical component predictor time series for mode 2 for the prediction of MAMJ (0) and SST for JASO season

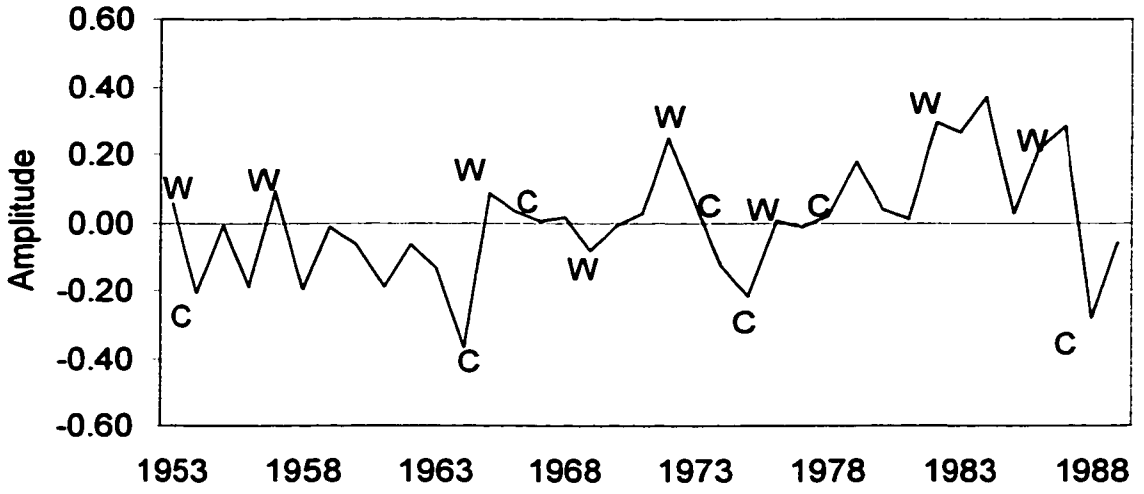

Fig. 7-3 The canonical component predictor time series for mode 1 for the prediction of MAMJ (0). Symbols along the curve denote warm and cold ENSO events

7.1.3 Forecasting River Flows at Lead Season ASON (-1), 11 Months

The predictors were selected from a pool of stable predictors shown in Tables 6-1, 6-2, 6-3, and 6-4 for the four Nile River flows locations. Up to three predictors were selected from each of the location flows using the same criteria mentioned previously. The predictors numbered 4, 7, and 12 (Table 6-2) were selected for the Blue Nile River, predictors numbers 7, 11, and 17 (Table 6-4) were selected for the Nile River flows at Aswan, predictors numbers 11, 13, and 19 (Table 6-3) were selected for Atbara River flows, and predictors numbers 2, 7, and 11 (Table 6-1) were selected for the Sobat River. However, due to the similarity between some of these predictors only eight predictors were included in the multivariate models (CCA) as listed in Table 7.3. Univariate MLR forecast models and PCA models were developed as a control against which the skill of the multivariate model is assessed. In this case the PCR model was developed using the

second (PC_2), third (PC_3), and fifth principal component (PC_5) as predictors and the MLR using the original predictors defined above.

Table 7.3 Predictors locations used in the multivariate model

NO.	LEAD-SEASON	LOCAT	LATIT.	LONG.	LOCAT.	LATIT.	LONG.
1	July (-3)	NAO1					
2	JASO (-3)	Pacific	20°N→10°N	130°E→170°E	Indian	35° S→40° S	60°E→90° E
3	NDJF (-2)	Pacific	30° S→35° S	90° W→80° W	Pacific	50° N→35° N	160°W→140°W
4	NDJF (-2)	Atlantic	10°N→20°N	30° W→20° W	Atlantic	40° N→30° N	70°W→60°W
5	NDJF (-2)	Atlantic	40° N	30° W	Atlantic	25° N	70° W
6	JASO (-1)	Pacific	20° N	130° W	Pacific	40° S	140° E
7	JASO (-1)	Pacific	25°S→35° S	150°W→130°W	Indian	25° S→35° S	30°E→60° E
8	ASON(-1)	Guinea					

Table 7-4 lists the cross validation performance skills forecast measures for the MLR and PCR models, for both the ordinary least square and the least absolute difference (LAD) and the CCA models. The CCA predictions appear to have smaller errors values and higher correlation coefficients than the corresponding values computed from the MLR and PCR models. It is clear from Table 7-4 that the multivariate models (CCA) outperform the univariate models in all the performance measures. The CCA models explain the river flow variability with MAE less than 50% of the standard deviation and zero BIAS values. However, the MLR and PCR models showed a

marginal difference between their performance measures. The CCA forecasted flows and the observed flows (not shown) show similar fluctuation behaviors. Forecasts for most of

Table 7-4 Performance skill of the univariate and multivariate models at 11 months lead season

LOCATION	METHOD	R	R^2	RMSE	MAE	BIAS
Nile River	MLR-OLS	0.83	0.69	0.56	0.43	0.00
at Aswan	MLR-LAD	0.84	0.70	0.57	0.46	-0.07
	PCA-OLS	0.82	0.67	0.58	0.48	-0.03
	PCA-LAD	0.82	0.67	0.59	0.50	-0.04
	CCA	0.87	0.77	0.48	0.39	0.00
Blue Nile	MLR-OLS	0.84	0.70	0.56	0.43	0.01
River	MLR-LAD	0.85	0.72	0.55	0.44	-0.07
	PCA-OLS	0.83	0.69	0.58	0.46	-0.03
	PCA-LAD	0.84	0.71	0.56	0.46	-0.02
	CCA	0.89	0.78	0.46	0.35	0.00
Atbara	MLR-OLS	0.76	0.58	0.65	0.53	0.00
River	MLR-LAD	0.77	0.60	0.63	0.50	-0.04
	PCA-OLS	0.76	0.57	0.66	0.48	-0.03
	PCA-LAD	0.78	0.60	0.64	0.47	-0.04
	CCA	0.84	0.71	0.53	0.42	0.00
Sobat	MLR-OLS	0.75	0.56	0.66	0.52	-0.01
River	MLR-LAD	0.72	0.52	0.70	0.60	0.07
	PCA-OLS	0.80	0.64	0.59	0.49	-0.03
	PCA-LAD	0.82	0.67	0.58	0.43	0.06
	CCA	0.86	0.74	0.50	0.42	0.00

the years are close to the obrved flow, in the case of Aswan flows, the forecasts for 1964 was overestimated and that of 1955 was underestimated, while the Blue Nile River flows forecasts show reasonable forecast for 1964 flows and underestimated the 1955 flows. In addition, Table 7-5 shows that the cross correlation coefficients for the predicted flows between the four locations are reserved.

The correlation between the first and the second CCA mode of the predictors and the predictands are 0.92 (R^2 = 0.84) and 0.87 (R^2 = 0.75), respectively. The correlation between the first CCA predictor mode and the Blue Nile River flows and the Nile River flows at Aswan are 0.78 (R^2 = 0.61) and 0.76 (R^2 = 0.58), respectively. Thus, the leading canonical mode explains a high proportion of the variability of the Blue Nile River flows and the Nile River flows at Aswan. Time series of the first canonical variate of the predictors and the river flows (not shown) reveals similar fluctuations for both series. This indicates that the first canonical variate carries the most predictive information for the Nile River flows.

Table 7-5 Correlation matrix of Nile River flows at four locations observed (upper right section) and CCA forecasted (lower left section), ASON (-1), 11-month lead season

	BLUE NILE RIVER	NILE RIVER AT (ASWAN)	ATBARA RIVER	SOBAT RIVER
Blue Nile River	1.00	0.96	0.54	0.25
Nile River at Aswan	0.99	1.00	0.59	0.22
Atbara River	0.56	0.61	1.00	-0.12
Sobat River	0.31	0.32	-0.12	1.00

Figure 7-4 shows the correlation maps between the first CCTS predictor mode and the SST for the JASO season. Areas of significance are found over the Pacific Ocean, the southern Atlantic and the southern Indian Ocean. However, the correlation regions for the southern Atlantic Ocean and the southern Indian Ocean have smaller association regions compared to those of the Pacific Ocean. The southern Indian Ocean shows stronger association in comparison with the southern Atlantic Ocean. Figure 7-4 exhibits an ENSO-like region in the Pacific Ocean. The canonical component time series associated with the mode 1 predictors scenario, shown in Fig. 7-6, further confirms that ENSO is being described by this mode. However, the warm and cold years were not well defined as is the case in the previous lead season forecasts. Furthermore, the correlation between the southern oscillation index (defined as standardized sea level pressure at Tahiti and Darwin) for the JASO season and the first CCA mode was 0.48 and the correlation with the second CCTS mode was very weak. Figure 7-5 further indicates a weaker association between the second CCTS mode and the SSTs. However, the correlation may exhibit a spatial ENSO-like region. In addition, relatively strongly association was found in the North Atlantic Ocean.

As previously indicated the Pacific Ocean plays an important role in the Nile River flows predictability. The negative center over the equatorial Pacific is consistent with the ENSO regions. To define the importance of each of the predictors in the forecasting skill, the first normalized canonical loading pattern was computed. It was found that the first normalized canonical loading pattern computed was associated mainly with predictor number 8 (the Guinea precipitation), then predictors numbers 6, 4, and 3 (Table 7-3). It is particularly noteworthy that the four predictors are from the Western

African region, the Pacific Ocean, and the Atlantic Ocean. As stated earlier in this study and in other research findings (e.g. Eltahir 1996, Awadalla, 2000, and Seleshi (1991)), these three regions influence the Nile hydrology. Both the Western African precipitation and the Atlantic Ocean contribute moisture to the Nile basin.

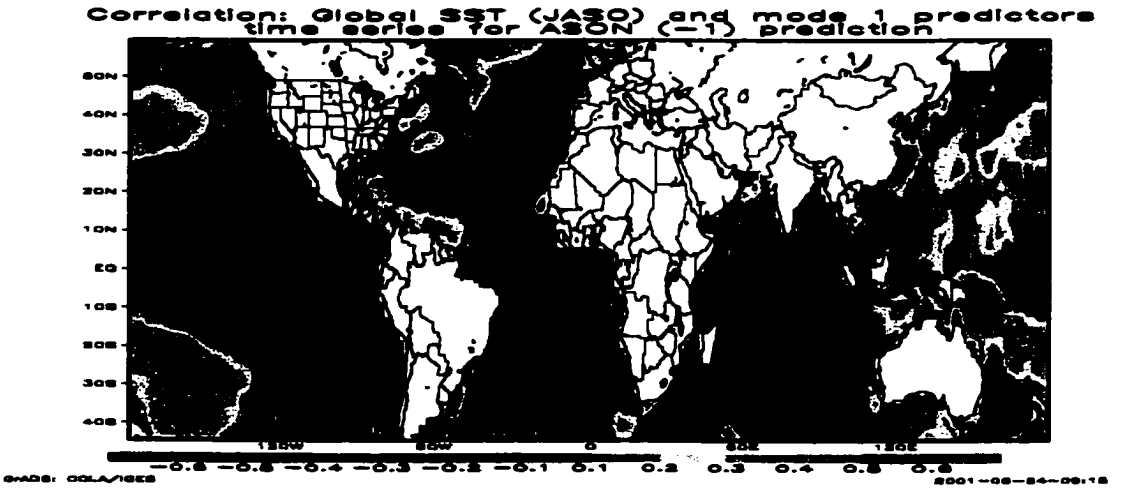

Fig. 7-4 Correlation map between the canonical component predictor time series for mode 1 for the prediction of ASON (-1) and the SST for JASO season

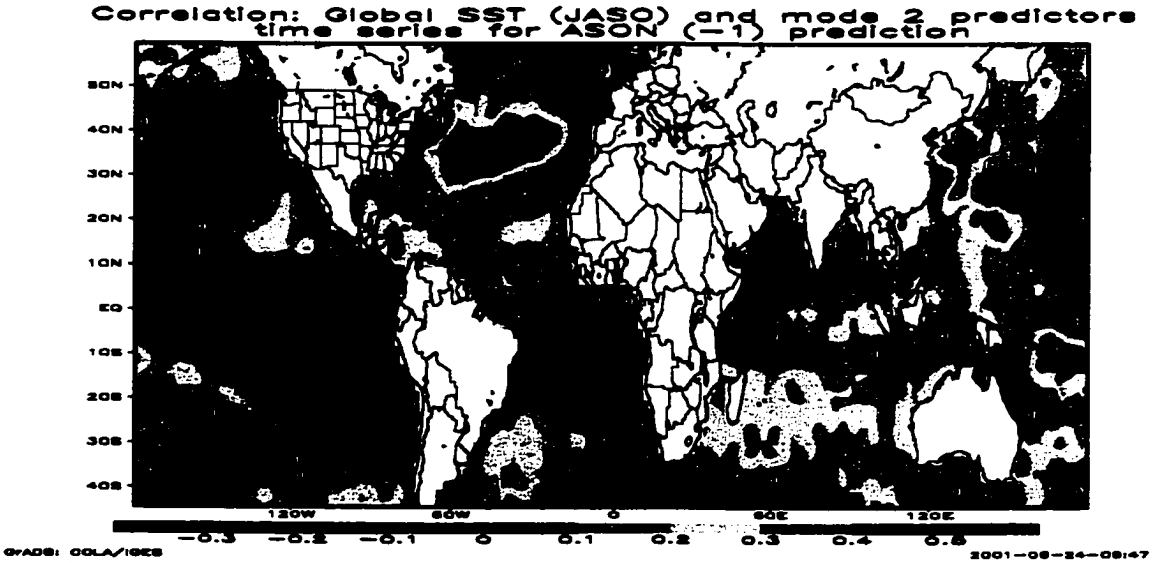

Fig. 7-5 Correlation map between the canonical component predictor time series for mode 2 for the prediction of ASON (-1) and the SST for JASO season

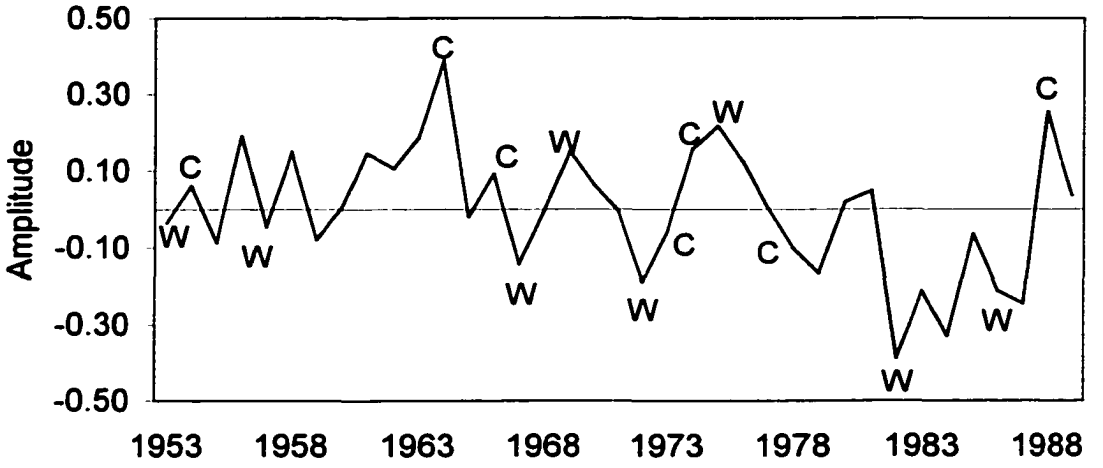

Fig. 7-6 The canonical component predictor time series for mode 1 for the prediction of ASON (-1). Symbols along the curve denote warm and cold ENSO events

7.1.4 Forecasting River Flows at Lead Season NDJF (-2), 32 Months

Here the potential of predictability at a longer forecasting lead time (over two years in advance) was considered. The predictors were selected from a pool of stable predictors shown in Tables 6-1, 6-2, 6-3, and 6-4, at the four locations. Predictors were selected from each of the location flows using the selection criteria mentioned earlier. The predictors numbered 1, 2, and 7 (Table 6-2) were selected for the Blue Nile River, predictors numbers 7, 10, and 11 (Table 6-4) were selected for the Nile River flows at Aswan, predictors numbers 8, 12, and 14 (Table 6-3) were selected for Atbara River flows, and predictors numbers 1 and 7 (Table 6-1) were selected for the Sobat River. Table 7-6 lists the predictors used in the multivariate CCA models. As indicated earlier, univariate MLR and PCR forecast models were developed as well, and their performance measures were listed as a control against which the skill of the multivariate model is

assessed. The PCR models were developed using first (PC_1) and the fourth principal component (PC_4) as independent variables.

Table 7-7 lists the performance measures of the models. The performance of the CCA appears to be better than that of the MLR and PCR models. It is clear that the PCR models outperformed the MLR models. These results, therefore, seem to be important in forecasting of the Nile River flows at this very long lead time. This also indicates the stability of these predictors and their connection with large scale phenomena such as the ENSO and the NAO. In addition, the cross correlation between the forecasted flows shown in Table 7-8 reasonably agrees with the observed cross correlation coefficients. The correlation between the first and the second CCTS mode of the predictors are 0.92 (R^2 = 0.85) and 0.82 (R^2 = 0.67), respectively. The correlation between the first CCTS predictor mode and the Blue Nile River flows and the Nile River flows at Aswan are –0.85 (R^2 = 0.72) and –0.84 (R^2 = 0.70), respectively. Thus, the first CCTS predictor mode offers a lot of information about the variability of the Nile River flows and has a strong contribution to the forecast skill.

Figure 7-7 shows the correlation maps between the first mode predictors time series and the SST for the season JASO. The first CCTS predictor mode exhibits areas of importance at the three oceans over mainly the Pacific Ocean and with lesser magnitude over the southern Atlantic Ocean. Surprisingly, the nearby Indian Ocean shows weak correlations at this long lead time. The canonical component time series associated with the mode 1 predictors scenario, shown in Fig. 7-9, further confirms that ENSO is being described by this mode. The "W" and "C" symbols denote warm and cold ENSO years as identified by Fraedrich and Muller (1992). Furthermore, the correlation between the

southern oscillation index (defined as standardized sea level pressure at Tahiti and Darwin) for JASO season and the first CCA mode was -0.45 and had no correlation with the second CCTS predictor mode. Figure 7-8 indicates a weaker association between the SSTs and the second CCTS predictor mode and does not exhibit any ENSO-like features. As previously indicated the Pacific Ocean plays an important role in the Nile River flows' predictability. The positive center over the equatorial Pacific (Fig. 7-7) is consistent with the ENSO regions. The importance of the predictors from the first CCTS predictor mode using the first normalized canonical loading pattern associated mainly with predictors number 4, 7, 2 and 3 of Table 7-6. As for the previous lead seasons, the predictors were found to represent the Pacific Ocean, the Atlantic and the northern Australian region.

Table 7.6 Predictors locations used in the multivariate model at NDJF (-2) lead season

NO.	LEAD-SEASON	LOCAT	LATIT.	LONG.	LOCAT	LATIT.	LONG.
1	NDJF (-2)	Indian	20° N→15° N	50° E→60° E	Pacific	40° N→30° N	160° W→140° W
2	NDJF (-2)	Pacific	30° S→35° S	90° W→80° W	Pacific	45° N→35° N	160° W→140° W
3	February (-3)	Jakarta					
4	MAMJ (-3)	Atlantic	08° S→12° S	00° →05° E	Pacific	20° S→30° S	170° W→145° W
5	NDJF (-2)	Atlantic	20° N→10° N	30° W→20° W	Atlantic	40° N→30° N	70° W→60° W
6	JASO (-3)	Pacific	20° N→10° N	130° E→170° W			
7	January (-2)	Ponta Delgada					
8	April (-3)	Ponta Delgada					
9	NDJF (-2)	Atlantic	40° N	30° W	Atlantic	25° N	70° W

Table 7-7 Performance skill of the univariate and multivariate models at 32 months lead season

LOCATION	METHOD	R	R^2	RMSE	MAE	BIAS
Nile River	MLR-OLS	0.74	0.55	0.69	0.54	-0.01
at Aswan	MLR-LAD	0.78	0.61	0.64	0.48	-0.07
	PCA-OLS	0.83	0.69	0.56	0.42	0.02
	PCA-LAD	0.84	0.70	0.56	0.43	0.00
	CCA	0.87	0.75	0.49	0.38	0.00
Blue Nile	MLR-OLS	0.71	0.50	0.73	0.58	0.01
River	MLR-LAD	0.75	0.56	0.69	0.52	-0.05
	PCA-OLS	0.84	0.70	0.56	0.44	0.00
	PCA-LAD	0.84	0.71	0.56	0.43	0.01
	CCA	0.88	0.78	0.47	0.38	0.00
Atbara	MLR-OLS	0.76	0.57	0.66	0.51	0.01
River	MLR-LAD	0.77	0.60	0.63	0.48	0.00
	PCA-OLS	0.77	0.59	0.64	0.52	0.00
	PCA-LAD	0.77	0.60	0.64	0.50	0.03
	CCA	0.85	0.72	0.52	0.42	0.00
Sobat	MLR-OLS	0.58	0.34	0.81	0.65	0.01
River	MLR-LAD	0.61	0.37	0.78	0.63	0.02
	PCA-OLS	0.57	0.33	0.82	0.65	0.00
	PCA-LAD	0.53	0.28	0.87	0.71	0.02
	CCA	0.71	0.50	0.70	0.54	0.00

Table 7-8 Correlation matrix of Nile River flows at four locations observed (upper right section) and CCA forecasted (lower left section), NDJF (-2), 32-month lead season

	BLUE NILE RIVER	NILE RIVER AT (ASWAN)	ATBARA RIVER	SOBAT RIVER
Blue Nile River	1.00	0.96	0.54	0.25
Nile River at Aswan	0.99	1.00	0.59	0.22
Atbara River	0.73	0.77	1.00	-0.12
Sobat River	0.14	0.19	0.00	1.00

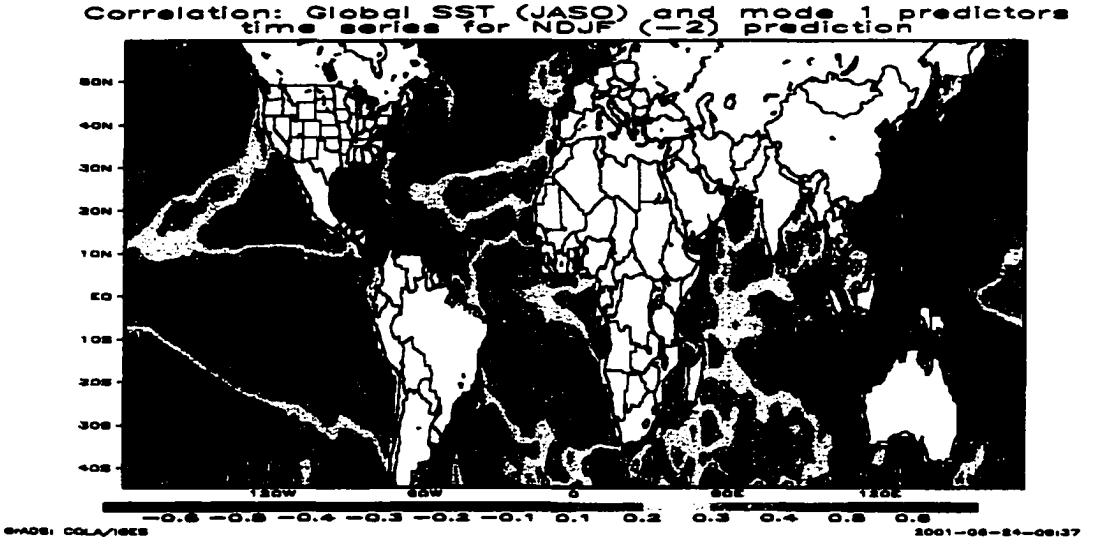

Fig. 7-7 Correlation map between the canonical component predictor time series for mode 1 for the prediction of NDJF (-2) and the SST for season JASO

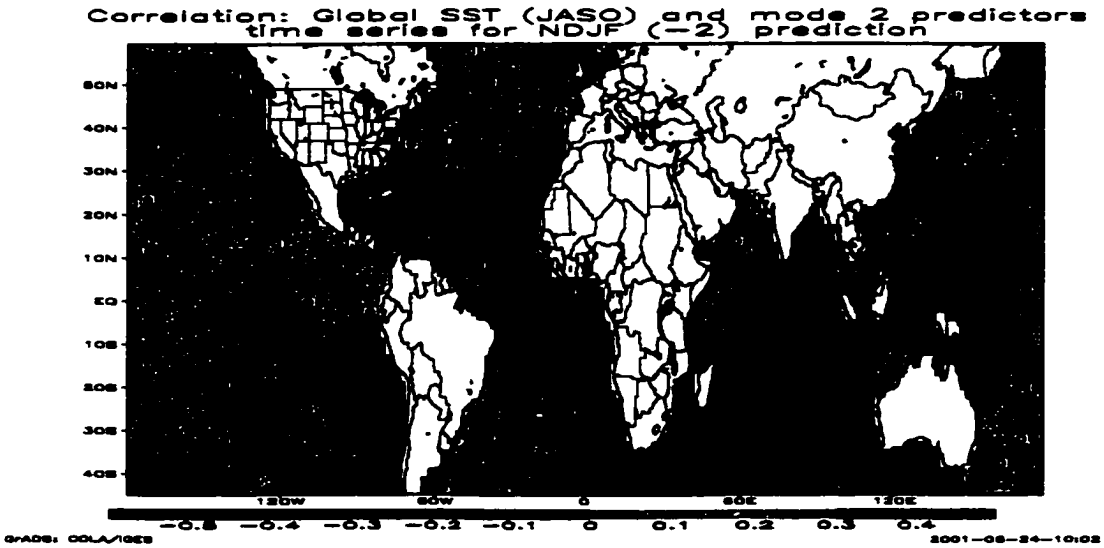

Fig. 7-8 Correlation map between the canonical component predictor time series for mode 2 for the prediction of NDJF (-2) and the SST for JASO season

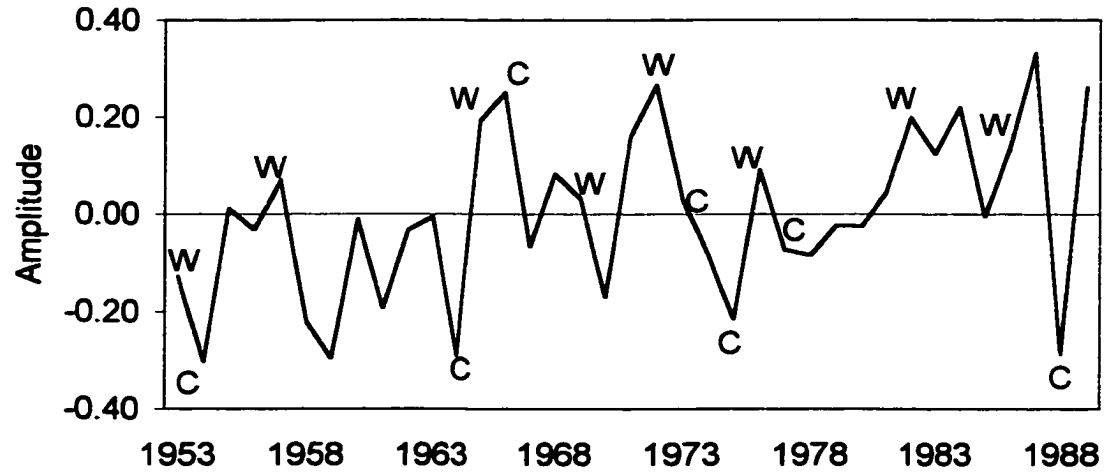

Fig. 7-9 The canonical component predictor time series for mode 1 for the prediction of NDJF (-2). Symbols along the curve denote warm and cold ENSO events

7.1.5 Remarks

The CCA models developed show useful predictive skills for the Nile River's flows. Using the multivariate statistical technique of CCA, reliable prediction skills for the Nile River flows were found for a lead time of up to 32 months. The MLR and the PCR show comparative performance in the first two lead seasons (MAMJ (0) and ASON (-1)) however, the PCR models outperformed the MLR in the longer lead season, NDJF (-2). The improvement of the PCR models over the MLR models depends on the degree of interdependence between the original variables. The CCA models performed comparatively better than the PCR and MLR models probably because the CCA technique can extract the dominant modes of co-variability between the predictor and the predictand data.

The correlation maps of the SST and the first canonical component time series of the predictor mode exhibit features that are associated with ENSO for the 3 lead seasons. However, the areas of correlation get smaller as the lead time increases. Higher–order modes were not clearly related to physical mechanisms such as ENSO and probably were not contributing significantly to the predictability of the Nile River flows. However, at lead season ASON (-1) the second CCTS predictor mode exhibits an ENSO-like correlation region but with smaller correlation magnitudes. The Indian Ocean becomes less important with increasing lead-time within the predictor field, and the significant region is restricted mainly to the southern Indian Ocean. The Atlantic Ocean behaves similarly to the Indian Ocean. However, the Pacific Ocean maintains relatively strong association with the first mode, but with reduced correlation areas. This is also confirmed with the reduction of the correlation coefficients of the first predictor mode

and the SOI. This is in agreement with the previous findings presented in this research that the Pacific Ocean seems to carry a significant climatological signal (over all lead seasons) that can influence the predictability of the Nile River flows.

7.2 Artificial Neural Networks

As a continuation of the previous analysis, nonlinearity in a multivariate approach was considered, with the hope that by examining nonlinear models possible improvements in forecasting performance skills would be attained. During this part of the research, an attempt was made to explore the potential of using ANN techniques for long-range forecasts of the Nile River flows. Recently, this technique has drawn considerable attention as it can handle complex and nonlinear problems better than conventional statistical techniques and has been successfully applied to a variety of problems. Awadalla and Rosseille (1999) used ANN and transfer function models successfully to predict the Nile River flows. They concluded that both the transfer function model and the ANN have comparable performances.

In this part of the study two scenarios of ANN models have been developed. Model I was developed for the Nile River flows at Aswan and Blue Nile River flows using their respective predictors that were discussed earlier. Model II uses three predictors (the Blue Nile River predictors in Eq. 6-5) as input and the combined Blue Nile River and the Nile River flows at Aswan as predictands. By combining the predictors for the four locations and using the combined Blue Nile River and the Nile River flows at Aswan as predictands model III was developed. The predictors from the four locations were selected from Tables 6-1 through 6-4 as follows: predictors number 2,

7, and 11 for the Sobat River; predictors number 4, 7, 12, for the Blue Nile River; predictors number 11, 13, and 19 for the Atbara River; and predictors number 7, 11, and 17 for the Nile River at Aswan. It is worth noting that in Model III the 12 combined predictors were reduced to 8 predictors (Table 7-3) due to interdependence between the predictors and similarity in some cases.

Figures 7-10 and 7-11 show the network configurations used for model II and III, respectively. In case of model II, the data was partitioned into three periods: 1) period 1953-1972 was applied for training; 2) period 1973-1977 was applied for evaluation; and 3) period 1978-1989 was applied for validation. The evaluation period was used to monitor the performance of the model during the training period for best generalization (Chapter 4 and section 6-4). To meet the criteria (mentioned before) that the number of parameters in the training data set should be greater than or equal to the number of connections (weights and biases), the data for model III were partitioned differently. In case of model III, the data was partitioned in three periods: 1) period 1953-1977 was applied for training; 2) period 1978-1982 was applied for evaluation; and 3) period 1983-1989 was applied for validation. Both networks were trained by the cascade correlation technique with the Levenberg-Matgradt algorithm. One hidden layer with one neuron

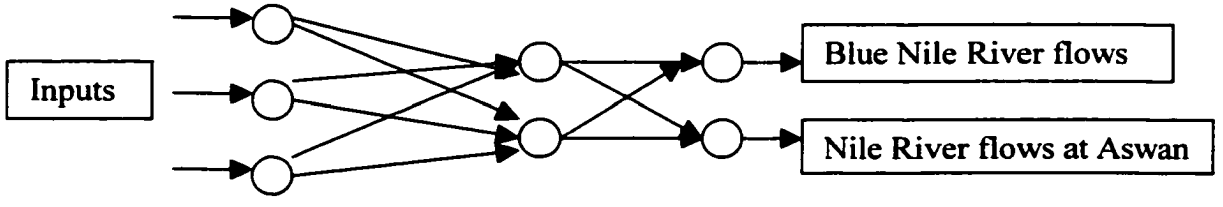

Fig. 7-10 Typical Configuration of a three layer neural network (Model II)

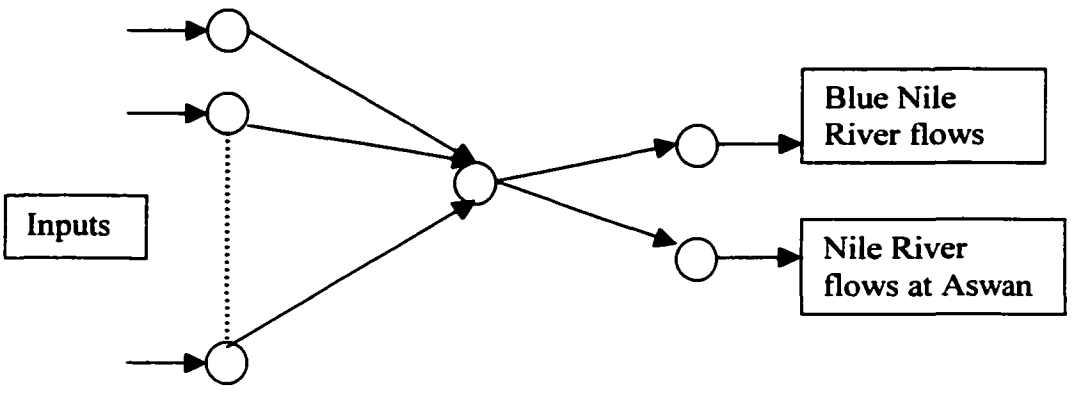

Fig. 7-11 Typical Configuration of a three layer neural network (Model III)

gave a reasonable performance of the forecasted flows. The tangent hyperbolic function was used as the activation function in the hidden layer, and a linear activation was used for the output layer.

To compare the performance of the ANN models with the MLR models a split sample validation technique was used for both methods. The models were developed on a subset of the data and then independently validated on different subset of the data that was not used in the formation of the model. The data for the MLR models were partitioned in the same way as for the ANN models. The MLR models were developed on the first 20 years (1953-1972) and the first 25 years (1953-1977) and then validated on the remaining data set. However, in the case of the ANN models a 5 years data set was used for model evaluation (early stopping) but was not included in the validation. Consequently, the models were compared for two validation periods: 1) the last 12 years (1977-1989); and 2) the last 7 years (1983-1989). Table 7-9 shows the performance skill measures for all the models at the various validation periods. The results of Model II

outperform the MLR models. The MLR-LAD improved the performance forecasts skills in three measures (RMSE, MAE, and BIAS) over the MLR-OLS, however, similar results noticed in the fourth measure R^2. Model III improved the forecast skill measures over MLR models and over model I. Generally, the results indicate that the multsite models show improved forecasting measures compared to the single site and the MLR-LAD compared to the MLR-OLS.

Table 7-9 Performance of different models on validation data sets for the Nile River flows at Aswan and the Blue Nile River flows using the stable predictors (7, 11, 17 and 4, 7, 12, respectively) ASON (-1) lead season

MODEL TYPE AND LOCATION		R^2	RMSE	MAE	BIAS
MLR-OLS for Aswan	1978-1989	0.83	0.75	0.63	-0.46
MLR-LAD for Aswan	1978-1989	(0.83)	(0.58)	(0.51)	(-0.25)
MLR-OLS for Aswan	1983-1989	0.88	0.77	0.63	-0.33
MLR-LAD for Aswan	1983-1989	(0.86)	(0.60)	(0.53)	(-0.05)
MLR-OLS for Blue N.	1978-1989	0.78	0.68	0.57	-0.44
MLR-LAD for Blue N.	1978-1989	(0.78)	(0.60)	(0.50)	(-0.32)
MLR-OLS for Blue N.	1983-1989	0.81	0.71	0.55	-0.33
MLR-LAD for Blue N.	1983-1989	(0.82)	(0.62)	(0.50)	(-0.17)
ANN (Blue N) Model I	1978-1989	0.78	0.59	0.53	-0.20
ANN (Aswan) Model I	1978-1989	0.73	0.63	0.56	-0.10
ANN (Blue N) Model II	1978-1989	0.84	0.55	0.47	-0.25
ANN (Aswan) Model II	1978-1989	0.83	0.55	0.45	-0.19
ANN (Blue N) Model III	1983-1989	0.87	0.53	0.40	-0.19
ANN (Aswan) Model III	1983-1989	0.90	0.58	0.49	-0.35

Figures 7-12 and 7-13 show the predicted and the observed flows for the training period, the evaluation period, and the validation period for model II at the Blue Nile River and the Nile River at Aswan, respectively. Figures 7-14 and 7-15 show the predicted and the observed flows for the training period, the evaluation period, and the validation period for model III for the Blue Nile River flows and the Nile River flows at Aswan, respectively. The predicted flows pursue the observed flow fluctuations during the training as well as during the validation period.

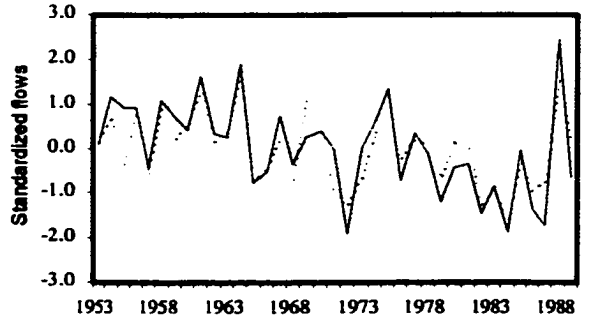

Fig. 7-12 Performance of 3 predictors and combined Blue Nile River and Nile River flows at Aswan as output, training (1953-1972), evaluation (1973-1977) and validation (1978-1989). Blue Nile, Model II

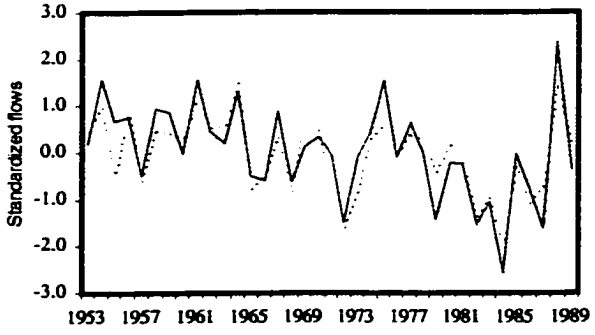

Fig. 7-13 Performance of the 3 predictors and combined Blue Nile River and Nile River flows at Aswan as output, training (1953-1972), evaluation (1973-1977) and validation (1978-1989). Aswan, Model II

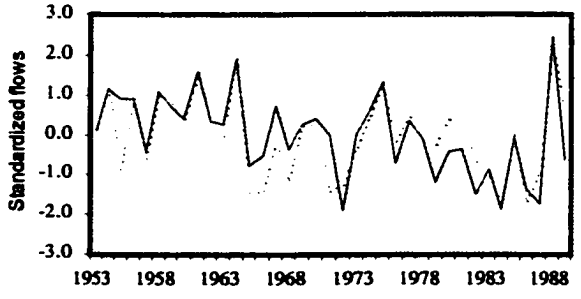

Fig. 7-14 Performance of 8 predictors and combined Blue Nile River and Nile River flows at Aswanas output, training (1953-1977), evaluation (1978-1982) and validation (1983-1989). Blue Nile, Model III

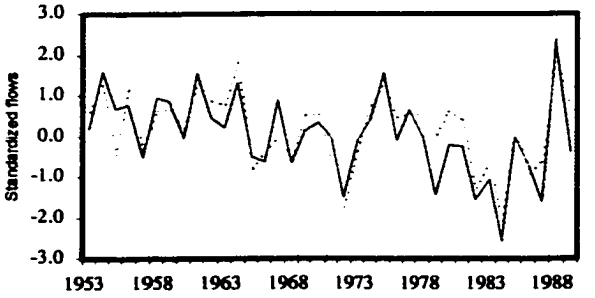

Fig. 7-15 Performance of the 8 predictors and combined Blue Nile River and Nile River flows at Aswan as output, training (1953-1977), evaluation (1978-1982) and validation (1983-1989). Aswan, Model III

8. DISCUSSION

Correlation analysis was used to establish the connection between the Nile River flows and leading climatic indicators. Additionally, connections between historical large scale variables, such as gridded seasonal SST data from the Oceans and the Nile River flows were explored in an effort to establish a basis for quantitative hydrological flow prediction. Sets of statistical models were developed to forecast the flows of the Nile River and its tributaries for various lead seasons based on the large scale variables, such as SST in the three oceans and the previous year Guinea precipitation in western Africa. More predictors for the Nile River flood flows have been identified to use on a long-time scale other than those previously used.

In this study, three types of models were developed to predict the July to October flows of the Nile River. The first model is a multiple linear regression model (MLR) and principal component regression (PCR) based on least squares technique (OLS) and least absolute difference technique (LAD), the second is an artificial neural network model (ANN), and the third is canonical correlation analysis (CCA) i.e. linear, nonlinear, and linear, respectively. The models have been tested on a validation data set not used for the parameter estimation. Two techniques for validation were used: the drop-one jackknife and the split sample technique. Principal component analysis (PCA) was used to make sure that any intercorrelation among the original variables was removed and to reduce their dimensionality. The overall measures adopted for assessment of the accuracy of the

forecasts were the coefficient of agreement (ρ), the correlation coefficient (R), R^2, adjusted R^2, the mean absolute difference (MAE), the root mean square error (RMSE), the adjusted RMSE and the BIAS. The adjusted RMSE and MAE for all the models were smaller than the standard deviation of the river flows, which is 1.0 for standardized data. This was valid for the calibration models as well as the cross validation models. The split sample validation technique showed relatively higher values of the BIAS compared to the drop-one jackknife technique. The absolute value of the BIAS was in the range of 0.00 to 0.02 based on the latter technique. Generally, the statistics for equations based on PCA showed improvement in the forecasting accuracy over the equations developed using original variables. This is due to the fact that more information is extracted by the principal component (PC) variables.

Assuming equal weights for the performance measures, an ANN has the best performance compared to MLR when the Indian precipitation was included as one of the predictors, also better than the ANN using the three stable predictors mentioned above. Based on the split sample technique, MLR-OLS and MLR-LAD have marginal differences over R^2 values. Still, MLR-LAD generally outperforms MLR-OLS in the remaining three performance measures (RMSE, MAE, and BIAS). On the other hand, based on the drop-one jackknife technique, the performance measures values for MLR-OLS and MLR-LAD were generally comparable. However, in most cases MLR-LAD performance skills were relatively better than the MLR-OLS. The differences between the non-jackknifed and the jackknifed performance measures for MLR-OLS are generally higher than the values in the MLR-LAD models. This finding may suggest that the MLR-LAD is more stable and robust for such applications. The ANN (Model III)

improved the forecast skill measures over MLR models, and MLR-LAD show better results compared to MLR-OLS for the same validation period. The results of MLR models are comparable with the model I results. The ANN (Model III) showed better performance over model I. Generally, the results indicate that multsite models using ANN show improvement in the forecasting measures compared to a single site, and the MLR-LAD shows improved results compared to the MLR-OLS. Generally, multivariate CCA models outperformed the univariate models over all lead seasons. Also, CCA preserved the cross-correlation between the river flows for the four locations.

The results obtained for MLR and the ANN indicate that a linear relationship dominates the association between SST predictors and the Nile River flows, which confirms recent results from Awadalla (2000). ANN models outperformed MLR models when using Indian precipitation of October of year (-3) with the Pacific SST and Guinea previous year precipitation. This indicates that the performance of the model depends on the combination of the predictors used. However, success has been achieved in training the networks to learn the flows for each of the locations and making reasonable flow predictions.

Generally, in the various forecast models, the year-to-year variability was reproduced. Although there are years when the magnitude of the anomaly is underestimated or overestimated, the phase of the flow was frequently well predicted. The predicted flows follow the fluctuations of the streamflows up and down, but did not match exactly the actual observed values. However, fair similarity between the observed and the predicted flow amounts are noticed. As demonstrated, the performance remains high even with a relatively shorter calibration period or a longer period. Comparing the

different models (MLR, PCR, ANN, and CCA) and the different validation techniques (split sampling and jackknife drop-one) indicates that the predictors used are quite stable and robust for the Nile River flows.

The Pacific Ocean SSTs have a higher contribution to the Nile River flows at Aswan and the Blue Nile River flows variability as compared to the Atlantic and the Indian Oceans. The Pacific Ocean SST anomalies are correlated more strongly with the Blue Nile River flood and have well defined correlation pools (regions) in the concomitant, JASO (0), and the subsequent, NDJF (+1) seasons, compared to the preceding seasons. The SST correlation region size during these seasons reduces from the east equatorial Pacific to the west equatorial Pacific. This covers the known Niño12, Niño3, Niño34, and Niño4 regions and researchers describe these seasons as the transition and the maturity stages for ENSO, respectively. This is also consistent with the previous studies associating the ENSO index with the Nile River flows. In addition, the strongest connections between the Blue Nile River flows and SST in the eastern and the central Pacific Ocean during the concomitant and the subsequent seasons may indicate an active role of the Blue Nile River basin hydrology in the large-scale ENSO phenomena. It was also found that at each ENSO stage significant correlation region between the SST and the Blue Nile River flows are consistent with ENSO development, which suggests that the evolution of ENSO signal is clearly an important component in the large-scale interaction between SST and the Blue Nile River flows. In addition, the first principal component for the Blue Nile river predictors has a significant and inverse correlation with the SOI (July to December) at all lead seasons. The correlation decreases as the lead-time increases and ranges from –0.60 to –0.38. Similarly, the first principal

component for the Nile River flows at Aswan predictors are significantly and inversely correlated with the SOI (July to December) at all lead seasons except for JASO (-3). The correlation decreases as the lead-time increases and ranges from –0.60 to –0.34. This shows how the ENSO phase dominates the Nile River flows.

Some of the highly correlated regions in the oceans, at times appear to be associated with well defined developments in the oceanic-atmospheric system such as, North Pacific Pattern SST region (30° N°-65, 100° E-140° W), Niño3 (5° N°-5° S, 150° W-90° W), and cyclone sources regions. Sea surface temperature in the Caribbean Sea shows a positive correlation of about 0.5 with the Blue Nile River flow for lead season JASO (-1). This region extends west to the east Pacific Ocean with the same correlation magnitude. The whole region was defined by Elsner and Kara (1999) as a tropical cyclone source. This suggests that it may be worth considering other climatic variables as driving forces in the Nile River hydrology.

El Niño southern oscillation (ENSO) influences suggest that a majority of predictors come from the east-west seesaw in the Pacific-Indian Oceans, and NAO influences suggest that a majority of the predictors come from the north-south seesaw in the Atlantic Ocean. The stable predictors of the Nile River flow are related to these two large scale phenomenon. As might be expected, the correlations are strongest in the Indian-Pacific seesaw, the regions closest to the anomalous warm waters in the equatorial eastern Pacific associated with El Niño. This supports the findings of the other studies which associated the ENSO with the Nile River's flows. It is particularly noteworthy that most predictors in the season prior to the Nile River flood season (JASO) for the Nile River flows at Aswan and Blue Nile River flows are significantly correlated with the July

to December (JASOND) SOI. This suggests that the atmopsheric changes taking place over the Blue Nile River basin in the seasons immediately preceding the high flows have considerable influence in determining the performance of the following season.

Measured by the adjusted R^2 and agreement coefficient (ρ), the Atbara River shows higher response (predictability) to the large scale variables followed by the Blue Nile River, the Nile River at Aswan and the Sobat River. However, at the first three lead seasons the Blue Nile River, the Nile River at Aswan and the Sobat River show close values of the agreement coefficient. It worth noting that the Atbara River and the Blue Nile River originate in the Ethiopian Plateau and the Sobat River flows partially from the east African basin and the Ethiopian Plateau. Thus, the Sobat River flows may be highly damped by the flows from the east African basin and shows weaker association with the large-scale variables. In addition, the Atbara River is located in the northern part of the Plateau and the Blue Nile River is located in the central part of the Plateau and the Sobat River in the southern part of the plateau. Thus, this indicates that the association between the river flows and the large-scale variables reduced from the north to the south. It could also be concluded that the signal observed in the Nile River flows at Aswan is mainly due the large-scale variables association with the Blue Nile River and the Atbara River flows. The difference in response to large-scale signals is one that requires further research.

A crucial step in developing empirical formulae for long-range forecasting requires the selection of appropriate predictors. This has been guided by an objective search among a large number of predictors. The stability and consistency of the predictor-predictand relationship has been examined by evaluating the 21-, 25-, and 31-year sliding window correlation coefficients. In addition, the selected predictors were also tested for

a significant correlation over the 15-year running window, and those that remained significant were identified. Stable predictors were identified for the Nile River and each of its tributaries. At different lead seasons, there are 15 predictors for the Sobat River flows, 22 for the Blue Nile River flows, 25 for the Atbara River flows and 23 for the Nile River at Aswan. This indicates that there are different driving forces between the Blue Nile River, the Atbara River and the Sobat River flows even though the Blue Nile River and the Atbara River basins are within the Ethiopian Plateau and much of the Sobat River flows originate from the Ethiopian Plateau.

The predictability of the selected stable predictors was tested for the most important sites: the Nile River flows at Aswan and the Blue Nile River flows. In MAMJ (0), the best four stable predictors explain (validated adjusted R^2) 69% of the variability of the Nile River flows at Aswan and 77% of the variability of the Blue Nile River flows. The first (in time) three stable predictors explain 67% and 68% of the variability at the two sites during ASON (-1), respectively. These predictors show a stable predictability under different methods (MLR, ANN), using different validation techniques (split sampling and drop-one jackknife) and for different calibration periods (1953-1972, 1953-1977). Though the predictors were selected by trial and error from a pool of the stable predictors, they were found to represent different driving forces: the Pacific Ocean, the Atlantic Ocean, the Guinea precipitation in western Africa and the SST of Northern Australia. It is worth noting that, Indian summer monsoon, Guinea precipitation in western Africa and the Nile River flows have strong association which may indicate possible connection between their climatic driving forces. The neural network method using the precipitation of October of the year (-3), Guinea precipitation and the Pacific

Ocean's SSTs outperformed MLR models and the results shown above. However, the split sample technique was used which resulted in a shorter validation period. In addition, the BIAS was very high compared to the drop-one jackknife technique.

The seesaw emerged as a more stable predictor having higher correlations with the river flows compared to the single site predictors. The seesaw is defined as the SST difference between two regions oppositely correlated with river flows i.e. one region has a positive correlation and the other has a negative correlation (referred to as dipole). The various forecast models for the Blue Nile River flow, including the more stable predictors and the seesaw technique, improved over the forecasts using only the single region predictors. This is because the seesaw predictors are generally more stable and have a higher correlation with river flows compared to the single site predictors. This is also attributed to the higher variability extracted by PC_1 with an average of 46% compared to about 32% without including the seesaw predictors. In addition, the models using the seesaw predictors are simpler (parsimonious) compared to the ones using the single region. When including the seesaw predictors, the number of PCs used in the final regression models was typically less than the number of PCs in the single region predictors. It was also noticed that the stable seesaw predictors in some cases outnumbered the stable single site predictors. Except for the Sobat River flow, the longer lead-time stable predictors are mostly seesaw variables. It might be argued that SST gradient is a measure of intensity and is better suited for examining the connection between large-scale forcing and the Nile River hydrology than one station SST. The degree to which these oscillations (seesaw) interact, is not well understood, however, the

overall relationship between the seesaw indices and the hydrological variables is very consistent and physically reasonable.

Further consideration for the Nile River flows from the African lakes, the upper White Nile River flows (defined as difference between Malakal flows on the White Nile and Doleib flows on the Sobat River) was tested for connection with large-scale variables. Amarasekera et al. (1997) stated that a strong ENSO signal is expected in annual Blue Nile and Atbara River discharges, but the White Nile River is highly damped by flows from equatorial lakes and marshes in the Sudd region and shows very little association with ENSO. The running window criteria adopted to select the stable predictors for the other Nile tributaries was relaxed for the upper White Nile River flow. Instead a predictor was considered to be stable if its correlation with river flows is significant over 25- and 31-year running windows. This confirmed the weaker connection between the large-scale variables and the upper White Nile River flows compared to the other Nile River tributaries. Tributaries originating from the Ethiopian Plateau have more stable predictors compared to the upper White Nile River and the Sobat River though about 50% of the Sobat River flows are from the Ethiopian Plateau. Despite this relaxed criteria, only six predictors were identified. It was also noticed that about 50% of the Sobat River and the upper White Nile River predictors were from the Atlantic Ocean while the other tributaries are dominated by the Pacific-Indian Oceans predictors.

The previous August to November rainfall over Guinea is strongly and positively related with the Blue Nile River flow ($r = 0.63$) for the period 1953-1989. This association appears to be one of the strongest of any of the individual predictors. This

indicates that the Guinea rainfall is a potential predictor for the Nile River flow with a lead-time of 11 months. The significant positive correlation of the Nile River flows and Guinea's previous year precipitation can be interpreted as contributing to moist air in the Ethiopian Plateau through evapotranspiration processes from that region and thus is associated positively with the river flows anomalies. Seleshi (1991) attributed the cause of Ethiopian rainfall to the flow of moist air from high pressures systems over the Gulf of Guinea towards the low pressure center in Arabia. Gray et al. (1993) and Elsner and Schmertmann (1993) reported the strong association between hurricanes over the Atlantic basin and the previous year western Africa rainfall. Gray et al. (1992) attributed this to feedback on the monsoon circulation from one year to the next. This may be the same cause for the strong connection between the Nile River flow and the previous year's Guinea precipitation, and the feedback may contribute to the moisture of the Blue Nile River basin as mentioned above. This also confirms the Nile River flows predictive signals in the Atlantic Ocean.

The Nile flows during the flood season (July to October) are strongly correlated with the Indian summer monsoon (June to September) in the same year. The Indian summer monsoon for the period 1953-1989 is associated with the Nile River flows at Aswan, Blue Nile River flows, Atbara River flows and the Sobat River flows by a linear correlation coefficient of 0.67, 0.70, 0.57 and 0.15, respectively. These four Nile River tributaries have correlations with the previous year's (August to November) precipitation over Guinea (Western Africa) of, 0.63, 0.61, 0.26 and 0.29, respectively. The Indian summer monsoon precipitation has a correlation of 0.37 with the previous year's Guinea

precipitation. The linear associations between the three regions suggest the interconnection between their climatic driving forces.

It's clear from this analysis that the hydro-climatic connections between the large-scale variables and the Nile River flows are strong. The gradients are emerging as better predictors, especially at larger lead-times. The question of why there exists strong long-lead correlation has yet to be answered. Whatever the answer to this question might be, the strong correlations presented in this dissertation are evidence of physical teleconnections that appear to drive Nile basin hydrology.

9. CONCLUSIONS

The main objective of this research was to investigate connections between the Nile River flows and its tributaries with atmospheric-oceanic variables and to develop long-range forecasting models. Correlation analysis was used to establish the connection between the Nile River flows and leading climatic indicators. Additionally, connections between historical gridded seasonally SST data from the Oceans and the Nile River flows are explored to establish a basis for quantitative contribution of the Oceans in the Nile River flows variability. Statistical models based on multiple linear regression (MLR), principal component analysis (PCA), neural networks (NN) and canonical correlation analysis (CCA) were developed to forecast the Nile River flows and its tributaries. The models based on PCA showed better improvement in forecasting accuracy over models developed in terms of the original variables and the multivariate models improve the forecasting skills over the univariate models.

Guided by an objective search, more stable predictors for the Nile River flows have been identified to operate on a long-time scale, other than those previously used. The main conclusion we can draw is the existence of a long-range potential predictability of the Nile River flows based on large scale variables. This predictability is shown to be highest in the preceding season and decrease as the lead-time increases. The strong correlations presented in this research are evidence of physical teleconnections that appear to drive the hydrology of the Nile River as well as other of the Ethiopian Plateau

climate. In addition, the strongest connections between the Blue Nile River flows and SST in the eastern and the central Pacific Ocean with latter seasons (JASO(0), NDJF(+1)) may indicate an active role of the Blue Nile River hydrology in the large-scale phenomena such as ENSO. It was also found that at each ENSO stage significant correlation region between the SST and the Blue Nile River flows are consistent with ENSO development, which suggests that the evolution of the ENSO signal is clearly an important component in the large-scale interaction between SST and the Blue Nile River flows.

During the course of this research the following specific conclusions were reached:

1) The existence of a long-range potential predictability of the Nile River flows based on large scale variables such as SST and Guinea precipitation in western Africa. This predictability is shown to be highest in the preceding season and decrease as the lead-time increases.
2) It was found that SST variability associated with the Nile River flows, as selected by correlation analysis linked the eastern Pacific Ocean with the western Pacific Ocean and the Indian Ocean, and the North Atlantic Ocean with the South Atlantic in an interbasin mode.
3) The research developed stable predictors for the flows of the Nile River and its tributaries.
4) The validated forecasting procedure using the stable predictors was capable of explaining up to about 67% of the Nile River flows variability, 10 months before the occurrence of peak flood in September.

5) The seesaw emerged as a more stable predictor having higher correlation with the river flows compared to the single site predictors.

6) The Nile rivers from the Ethiopian Plateau have stronger connections with the large-scale variables. In addition their predictors outnumbered those for rivers partially (the Sobat River) or totally (the upper White Nile River) originating from the central African basin.

7) From step (6), the Blue Nile River and Atbara River are mainly responsible for the large-scale variables signal observed in the aggregated flows at Aswan.

8) The forecasting models are proven to be stable under different validation procedures (Jackknife drop-one and split sampling procedure), different sample sizes and under different methods (MLR-OLS, MLR-LAD, PCR, CCA and ANN).

9) The research has demonstrated that the Pacific Ocean shows the highest contribution to the Nile river flows variability followed by the Atlantic Ocean and then the Indian Ocean.

10) The results from the ANN and the MLR models demonstrate that linear association dominates the relationship between the Nile River flows and the selected predictors.

11) The CCA multivariate approach improved the performance measures over the univariate models.

12) The ANN multisite approach (model III) improved the performance measures over the single site models.

13) The statistics for equations based on PCA showed improvement in forecasting performance over equations developed using original variables.

14) Indian summer monsoon, Guinea precipitation in western Africa and the Nile River flows have a strong association which may indicate an association with their climatic forcings.

15) MLR-LAD and MLR-OLS have more comparable results when using drop-one jackknife validation technique than the split sample validation technique. Generally, MLR-LAD outperformed MLR-OLS when using the latter validation technique. In addition, the difference between the non-jackknifed and the jackknifed performance measures for the MLR-OLS are generally higher than their corresponding values in the MLR-LAD models. This may suggest that MLR-LAD is more stable and robust for such applications. However, MLR-LAD has relatively higher BIAS values compared to MLR-OLS in drop-one validation technique and lower in the split sample technique.

16) Atbara River flows show higher response to large scale variables measured by the adjusted R^2 and the coefficient of agreement (ρ) followed by the Blue Nile River, Nile River at Aswan and the Sobat River.

17) It was found that the Blue Nile River flows were associated with the ENSO development in the eastern Pacific Ocean at its various stages and regions as defined by Rasmusson and carpenter (1982).

10. RECOMMENDATIONS FOR FUTURE RESEARCH

In light of the results reached during the course of this research, the following recommendations for future work are made:

1) To investigate the connection that may exist between the selected stable Nile River predictors and the large scale climatic phenomenon such as ENSO and NAO, and to investigate the capability (potentiality) of using these relationships (if they exist) to further forecast these large scale variables.
2) With the availability of the stable predictors for the Nile River flows, a further study should be conducted to investigate their potential predictability for other hydroclimatic variables, particularly the large river flows such as: the Amazon, the Niger, the Mississippi, the Congo and the Parana.
3) Further study on the climatic forcing connections between Nile basin hydrology, the Indian monsoon and the Guinea precipitation in western Africa.
4) For operational purposes, this study should be extended for monthly forecast of the Nile River flows. The first attempt could be to forecast the flood season on a monthly basis (July, August, September, and October) using the stable predictors established in this study.
5) A study to extend the methodology developed during this research for the oceans SSTs contribution to the Nile River flows variability further to the combined two oceans contribution (Pacific and Atlantic, Pacific and Indian, and Indian and

Atlantic). In addition, this methodology could be investigated on other Nile River tributaries, and other hydroclimatic variables, and other large rivers such as those listed in step 2.

6) Further investigation in the response strength at the different locations.

11. BIBLIOGRAPHY

Abrahart, R. J., and L. See, Comparing neural network and autoregressive moving average techniques for the provision of continuous river flow forecasts intwo contrasting catchments, *Hyrol. Process*, 14, 2157-2172, 2000.

Allan, R. J., N. Nicholls, P. D. Jones, and I. J. Butterworth, A further extension of the Tahiti-Darwin SOI, early ENSO events and Darwin pressure, *J. Climate*, 4, 743-749, 1991.

Alley, W. M., The Palmer Drought Severity Index as a measure of hydrologic drought, *Water Resour. B.*, 21(1), 105-114, 1985.

Amarasekera, K. N., Lee, R. F., Williams, E. R., and E. A. B. Eltahir, ENSO and the natural variability in the tropical rivers, J. of Hydro., 200, 24-39, 1997.

Ananthakrishnan, R., and B. Parthasarathy, Indian rainfall in Europian to the sunspot cycle: 1871-1978, *J. of Climatol.*, 4, 149-169, 1984.

Angel, J. K., Comparison of variations in atmospheric quantities with seas surface temperature variations in the Equatorial Eastern Pacific, *Mon. Wea. Rev.*, 109, 230-243, 1981.

Astaf'eva, N. M., Analysis of a long-term structure of the southern oscillation index and EL Niño events, *Izvestiya Atm. Oceanic phy.*, 33(6), 788-796, 1997.

Attia, B. B., and A. B. Abulhoda, The ENSO phenomenon and its impact on the Nile's hydrology, Climatic fluctuations and water management, (ed.), Abu Zeid, M. A., and A. K. Biswas, 71-79, 1992.

Awadalla, A. G., and J. Rousselle, Improving forecasts of Nile flood using SST inputs in TFN model, *J. Hyrol. Eng.*, ASCE. 5(4), 371-379, 2000.

Awadalla, A. G., and J. Rousselle, Forecasting the Nile flood using seas surface temperatures as inputs: A comparison between Transfer Function with noise and Neural Network , Proc. of the 19th annual AGU, Hydrology Days, 23-36, 1999.

Awadalla, A. G., and J. Rousselle, Hydo-climatologie globale pour prevision des crues du Nil au moyen de fonctions de transfert avec bruit et de reseaux de neurons artificiels, These de Doctrat, Ecole polytechnique de Montreal, 1999.

Awwad, H. M., and J. B. Valdes, Adaptive parameter estimation for multisite hydrologic forecasting, *J. Hydr. Eng.*, ASCE. 118(9), 1201-1221, 1192.

Baeriswy, P. A., and M. Rebetez, Regionalization of precipitation in Switzerland by means of principal component analysis, *Theor. Appl. Climatol.*, 58, 31-41, 1997.

Bhalme, H. N., Moolet, S. K., and BH. V. Ramana Murty, Forecasting of monsoon performance over India, J. of Climatol., 6, 347-354, 1986.

Barnet, T. P., Prediction of the EL Niño of 1982-83, *Mon. Wea. Rev.*, 112, 1403-1407, 1984.

Barnett, T. P, and R. Preisendorfer, Origins and levels of monthly and seasonal forecast skill for United States surface air temperatures determined by canonical correlation analysis, *Amer. Met. Soc.*, 115, 1825-1850, 1987.

Barnston, A. B., linear statistical short-term climate predictive skill in the Northern Hemisphere, *J. Climate*, 7, 1513-1564, 1994.

Barnston , A. G., and C. F. Ropelewski, Prediction of ENSO Episodes using Canonical Coreelation Analysis, *J. Climate*, 5, 1316-1345, 1992.

Basher, R. E., and C. S. Thompson, Relationship of air temperatures in New Zealand to regional anomalies in sea-surface temperature and atmospheric circulation, *Int. J. Climatolog.*, 16, 405-425, 1996.

Bender, M. and S. Simonovic, Time-Series modeling for long-range streamflow forecasting, *J. Water Resour. Plng. and Mgmt.*, ASCE, 120(6), 857-870, 1994.

Bergman, M. J., and J. W. Delleur, Kalman filter estimation and prediction of daily stream flows: I. Review, Algorithm, and simulation experiments, *Water Resour. B.*, 21(5), 815-825, 1985.

Bergman, M. J., and J. W. Delleur, Kalman filter estimation and prediction of daily stream flows: II. Application to the Potomac river, *Water Resour. B.*, 21(5), 827-832, 1985.

Berri, G. J., and E. A. Flamenco, Seasonal volume of the Diamante River, Argentina, based on El Niño observations and predictions, *Water Resour. Res.*, 35(12), 3803-3810, 1999.

Bunkers, M. J., J. R. Miller JR., and A. T. DeGaetano, An examination of EL Niño-La Niña-Related precipitation and temperature anomalies across the Northern plains, *J. Climate*, 9, 147-160, 1996.

Burn, D. H., and E. A. McBean, River flow forecasting model for Sturgeon river, *J. Hydr. Eng.*, ASCE, 111(2), 316-333, 1985.

Camberlin, P., Rainfall anomalies in the source region of the Nile and their connection with Indian summer monsoon, *J. Climate*, 10, 1380-1392, 1997.

Campolo, M., Andreussi, P., and A. Soldati, River flood forecasting with a neural network model, *Water Resour. Res.*, 35(4), 1191-1197, 1999.

Casey, T., Optimal linear combination of seasonal forecasts, *Aust. Met. Mag.*, 44, 219-224, 1995.

Chakraborty, K., Mehrotra, K., Mohan, C. K., and S. Ranka, Forecasting the behavior of multivariate time series using neural networks, *Neural Networks*, 5, 961-970, 1992.

Chang, W. Y. B., ENSO: Extreme climate events and their impacts on Asian deltas, *J. Am. Water Resour. Ass.*, 33(3), 605-614,1997.

Chen, L., R. Wu, The role of the Asian/Australian Monsoons and the Southern/Northern Oscillation in the ENSO cycle, *Theor. App. Climatol.*, 65, 37-47, 2000.

Chen, W. Y., Assessment of southern oscillation sea-level pressure indices, *Mon. Wea Rev.*, 110, 800-807, 1982.

Chiew, F. H. S., and T. A. McMahon, Detection of trend or change in annual flow of Australian rivers, *Int. J. Climatog.*, 13, 643-653, 1993.

Chiew, F. H. S., T. C. Piechota, J. A. Dracup, and T. A. McMahon, EL Niño/Southern oscillation and Australian rainfall, streamflow and drought: links and potential for forecasting, *J. Hydro.*, 204, 138-149, 1998.

Chu, P., and Y. He, Long-range prediction of Hawaiian winter rainfall using canonical correlation analysis, *Int. J. Climatol.*, 14, 659-669, 1994.

Chu, P., Spectral estimation from time series models with relevence to the southern oscillation, *J. Climate*, 2, 86-90, 1989.

Conway, D., A water balance model of the Upper Blue Nile in Ethiopia, *Hydro. Sci. J.*, 42(2), 265-286, 1997.

Conway, D., and M. Hulme, Recent fluctuations in precipitation and runoff over the Nile sub-basins and their impact on main Nile discharge, *Clim. Change*, 25, 127-151, 1993.

Davey, M. K., D. L. T. Anderson, and S. Lawrence, A simulation of variability of ENSO forecast skill, *J. Climate*, 9, 240-246, 1996.

Davis, D. T., and J. N. Hwang, Solving inverse problems by Bayesian neural network iterative inversion with ground truth incorporation, *IEEE trans. On signal processing*, 45(11), 2749-2757, 1997.

Diaz, A. F., C. D. studzinski, and C. R. Mechoso, Relationships between precipitation anomalies in Uruguay and Southern Brazil and Sea Surface Temperature in the Pacific and Atlantic Oceans, *J. Climate*, 11, 251-271, 1998.

Diaz, H. F., and V. Markgraf (ed.), EL Niño historical and paleoclimatic aspects of the southern oscillation, Cambridge University Press, 1992.

Dracup, J. A., and E. Kahya, The relationships between U.S. streamflow and La Niña events, *Water Resour. Res.* 30(7), 2133-2141, 1994.

Dugam, S. S., S. B. Kakade, and R. K. Verma, Interannual and long-term varaibility in the North Atlantic Oscillation and Indian summer mosoon rainfall, *Theor. Appl. Climatol.*, 58, 21-29, 1997.

Ebisuzaki, W., A method to estimate the statistical significance of a correlation when the data are serially correlated, *Amer. Met. Soc.*, 10, 2147-2153, 1997.

Efimov, V. V., Prusov, A. V., and M. V. Shokurov, Spatiotemporal pattern of decadal variability in sea surface temperature, wind speed, and sea level pressure in the North Atlantic, Atmo. Oceanic phys., 35(1), 97-109, 1999.

Elsner, J. B., and C. P., Schmertmann, Improving extended-range seasonal predictions of intense Atlantic hurricane activity, Amer. Meteor. Soc., 8, 345-351, 1993.

Eltahir, E. A., EL Niño and the natural variability in the flow of the Nile River, *Water Resour. Res.*, 32(1), 131-137, 1996.

Entekhabi, D., I. Rodriguez-Iturbe, and R. L. Bras, Variability in Large-Scale water balance with land-surface-atmosphere interactions, *J. Climate*, 5, 798-813.

Fraedrich, K., Jiang, J., Gerstengarbe, F. W., and P. C. Werner, Multiscale detection of abrupt climate changes: Application to river Nile flood levels, *Int. J. Climat.*, 17, 1301-1315, 1997.

Fraedrich K., and K. Muller, Climate anomalies in Europe associated with ENSO extremes, *Int. J. of Climatol.*, 1, 25-31, 1992.

Firor, S. E., B. A. Finney, R. Willis, and J. A. Dracup, Disaggregation modeling process for climatic time series, *J. Water Resour. Plng. and Mgmt.*, ASCE, 122(3), 205-212, 1996.

Flood, I., and N. Kartam, Neural networks in Civil Engineering I: Principles and Understanding, *J. Comp. In Civil Eng.*, 8(2), 131-148, 1994.

Flood, I., and N. Kartam, Neural networks in Civil Engineering II: Principles and Understanding, *J. Comp. In Civil Eng.*, 8(2), 149-162, 1994.

Fraedrich, K., and K. Muller, Climate anomalies in Europe associated with ENSO extremes, *Int. J. Climatol.*, 12, 25-31, 1992.

French, M. N., Krajewski, W. F., and R. R. Cuykendall, Rainfall forecasting in space and time using a neural network, *J. Hydro.*, 137, 1-13, 1992.

Findell, K. L., and E. A. B. Eltahir, An analysis of the soil moisture-rainfall feedback based on direct observations from Illinois, *Water Resour. Res.*, 33(4), 725-735, 1997.

Gan, K. C., McMahon, T. A., and B. L. Finlayson, Analysis of periodicity in streamflow and rainfall data by Colwell's indices, *J. Hydro.*, 123, 105-118, 1991.

Gangopadhyay, S., Gautam, T. R., and A. D. Gupta, Subsurface characterization using artificial neural network and GIS, *J. Comp. In Civil Eng.*, 13(3), 153-161, 1999.

Garen, D. C., Improved techniques in regression-based streamflow volume forecasting, *J. Water Resour. Plng. and Mgmt.*, ASCE, 118(6), 654-670, 1992.

Garnett, E. R., M. L. Khandekar, and J. C. Babb, On the utility of ENSO and PNA indices for long-lead forecasting of summer weather over the crop-growing region of the Candian Parairies, J. *Appl. Meteor.*, 60, 37-45, 1998.

Georgakakos, A. P., and D. H., Marks, A new method for the control of the River Nile, *Water, Resour. Devlop.*, 3(2), 133-141, 1987.

Glahn, H. R., Canonical correlation and its relationship to discriminant analysis and multiple regression, *J. Atm. Sci.*, 25, 23-31, 1968.

Goel, N. K., S. M. Seth, and S. Chandra. Multivariate modeling of flood flows, *J. Hydr. Eng.*, 124(2), 146-155, 1998.

Goh, A. T. C., Modeling soil correlations using neural networks, J. Comp. In Civil Eng., 9(4), 275-274, 1995.

Gordon, N. D., The southern oscillation and New Zealand weather, *Mon. Wea. Rev.*, 114, 371-387, 1986.

Graham, N. E., Michaelsen, J., and T. P. Barnett, An investigation of the El Nino-Southern oscillation cycle with statistical models: 1. Predictor field characteristics, *J. Geophy. Res.*, 92(c13), 14251-14270, 1987a.

Graham, N. E., Michaelsen, J., and T. P. Barnett, An investigation of the El Nino-Southern oscillation cycle with statistical models: 2. Model results, *J. Geophy. Res.*, 92(c13), 14271-14289, 1987b.

Gray, W. M., Landsea, C. W., African rainfall as precursor of hurricane-related destruction on the U.S. East Coast, *Amer. Meteor. Soc.*, 73, 9, 1352-1364, 1992a.

Gray, W. M., J. D. Sheaffer, EL Niño and QBO influences on tropical cyclone activity, In Glantz, M., Katz, R., and Nicholls, N. (eds.), *Teleconnections linking world wide climate anomalies, Cambridge University Press, Cambridge*, 257-287, 1991.

Gray, W. M., Landsea, C. W., Mielke, P. W. Jr., and K. J. Berry, Predicting Atlantic Basin seasonal tropical cyclonic activity by 1 August, *Weather and Forecasting*, 8, 73-86, 1993.

Gray, W. M., Landsea, C. W., Mielke, P. W. Jr., and K. J. Berry, Predicting Atlantic Basin seasonal tropical cyclonic activity by 1 June, *Amer. Meteor. Soc.*, 9, 103-115, 1994.

Gray, W. M., Landsea, C. W., Mielke, P. W. Jr., and K. J. Berry, Predicting Atlantic seasonal hurricane activity 6-11 months in advance, *Weather and Forecasting*, 7, 440-455, 1992b.

Gray, W. M., Landsea, C. W., Mielke, P. W. Jr., Berry, K. J., and J. A. Knaff, Predicting ENSO 9-14 months in advance, Colorado State University, Fort Collins, 1994.

Gray, W. M., Landsea, C. W., Mielke, P. W. Jr., and K. J. Berry, Predicting Atlantic Basin seasonal tropical cyclonic activity by 1 June, *Weather and Forecasting*, 9, 103-115, 1994.

Gray, W. M., W. L., Christopher, P. W. Mielke, and K. J. Berry, Predicting Atlantic basin seasonal tropical cyclone activity by 1 June, *Weather Forecasting*, 9, 103-115, 1994.

Gray, W. M., W. L., Christopher, P. W. Mielke, and K. J. Berry, Predicting Atlantic seasonal hurricane activity 6-11 months in advance, *Weather and Forecasting*, 7, 440-455, 1992.

Griffies, S. M., and K. Bryan, Predictability of North Atlantic multidecadal climate variability, *Science*, 275, 181-184, 1997.

Grijsen, J. G., C. J. M. Vermeulen, M. E. M. Nur, and Y. A. Mohamed, An information system for flood early warning, 3rd Int. Conf. On floods and flood management, 1992.

Guetter, A. K., K. P. Georgakakos, Are the EL Niño and La Niña predictors of the Iowa River seasonal flow? J. *Appl. Meteor.*, 35, 690-705, 1996.

Hamed, K. H., and A. R. Rao, A modified Mann-Kendall trend test for autocorrelated data, *J. Hydro.*, 204, 182-196, 1998.

Hamlet, A. F., and D. P. Lettenmaier, Columbia river streamflow forecasting based on ENSO and PDO climate signals, *Water Resour. Plann. Mgt*, 125, 6, 333-341, 1999.

Hansen, J., and S. Lebedeff, Global trends of measured surface air temperature, J. Geophs. Res., 92(D11), 13345-13372, 1987.

Hastenrath, S., Diagnostics and prediction of anomalies river discharge in Nothern South America, *J. Climate*, 3, 1080-1060, 1990.

Hastenrath, S., Recent advances in tropical climate prediction, *J. Climate*, 8, 1519-1532, 1995.

Hsieh, W. W., and B. Tang, Applying neural network models to prediction and data analysis in meteorology and oceanography, *Bull. Amer. Met. Soc.*, 1855-1870, 1998.

Hsu, K., H. V., Gupta, and S. Sorooshian, Artificial neural network modeling of the rainfall-runoff process, *Water Resour. Res.*, 31(10), 2517-2530, 1995.

Inoue, M, and J. J. O'Brien, Predictability of the decay of the 1982/83 EL Niño, *Mon. Wea. Rev.*, 114, 967-972, 1986.

Jain, S. K., Das, A., and D. K., Srivastava, Application of ANN for reservoir inflow prediction and operation, Water Resour. Res., 125(5), 263-271, 1999.

Jones, P. D., Raper S. C. B., Bradley R. S., Diaz H. F., Kelly P. M., and T. M. L. Wigley, Northern hemisphere surface air temperature variations: 1851-1984, *Journal of Climate and Appl. Met.*, 25, 161-179.1986a.

Jones, P. D., Raper S. C. B., and T. M. L. Wigley, Southern hemisphere surface air temperature variations: 1851-1984, *Journal of Climate and Appl. Met.*, 25, 1213-1230.1986b.

Jones, P. D., Wigley T. M. L., and P. M. Kelly, Variations in surface air temperatures: Part I. Northern Hemisphere, 1881-1980, *Mon. Wea. Rev.*, 110(2), 59-70,1982.

Jury, M. R., and B. Pathack, A study of climate and weather variability over the Tropical Southwest Indian Ocean, *Met. Atmos. Phys.*, 47, 37-48, 1991.

Jury, M. R., Long-range forecasting of South African summer rainfall using ENSO teleconnections, *Fifth Conference on Southern hemisphere meteorology and Oceanography, American Meteorology Society*, Pretoria, South, Africa, p103, 1997.

Kahya, E., and J. A. Dracup, U.S. Streamflow patterns in relation to the EL Niño/Southern Oscillation, *Watre Resour. Res.*, 29(8), 2491-2503, 1993.

Karunanithi, N, Grenney, W. J., Whitley, D., and K. Bovee, Neural Network for river flow prediction, *J. Comp. In Civil Eng.*, 8(2), 201-220, 1994.

Kawamura, A., A. I. McKerchar. R. H. Spigel, and K. Jinno, Chaotic characteristics of the southern oscillation index time series, *J. Hydro.*,204, 168-181, 1998.

Kiladas, G. N., and Diaz, H. F., An analysis of the 1877-78 ENSO Episode and comparison with 1982-83, *Mon. Wea. Rev.*, 114, 10635-1047, 1986.

Kiladas, G. N., and Diaz, H. F., Global climatic anomalies associated with extremes in the Southern Oscillation, *J. Climate*, 2, 1069-1090, 1989.

Kite, G. W., Analysis of lake Victoria levels, *Hydro. Sci. J.*, 27(2), 99-110.

Kite, G. W., Recent changes in level of lake Victoria, *Hydro. Sci. J.*, 26(3), 233-243.

Klooper, E., Landman, W. A., and J. V. Heerden, The predictability of seasonal maximum temperature in South Africa, *Int. J. Climatol.*, 18, 741-758, 1998.

Krzysztofowicz, R., Bayesian models of forecasted time series, *Water Resour. Res.*, B., 21(5), 805-814, 1985.

Kuhnel, I., McMahan, T. A., Finlayson, B. L., Haines, A., Whetton, P. H., and T. T. Gibson, Climatic influences on streamflow variability: A comparison between southeastern Australia and southeastern United States of America, *Water Resour. Res.*, 26(10), 2483-2496, 1990.

Kuligowski, R. J., and A. P. Barros, Using artificial neural networks to estimate missing rainfall data, *J. Amer. Water Resour. Assoc.*, 34(6), 1437-1447, 1998.

Kundzewicz, Z. W., and Somlyody, L., Climatic change impact on water resources in a systems perspective, *Water Resour. Mngt.*, 11, 407-435, 1997.
Kung, E. C., and T. A. Sharif, Regression forecasting of the onset of the Indian summer monsoon with antecedent upper air conditions, *J. App. Met.*, 19, 370-380, 1980.

Landman, W. A., Study of the predictability of the Equatorial Indian Ocean Sea-Surface temperatures, *Fifth International Conference on Southern Hemisphere, Amer. Meteor. Society*, P140, 1997.

Lana. X., and A. Burgueno, Spatial and temporal characterization of annual extreme droughts in Catalonia (Northeast Spain), *Int. J. Climatolog.*, 18. 93-110, 1998.

Landsea, W. C., Gray, W. M., Mielke, P. W., and K. J. berry, Forecasting seasonal Sahelian rainfall by 1 December of the previous year, 1992.

Landsea, W. C., Gray, W. M., Mielke, P. W., and K. J. berry, Long-Term variations of Western Sahelian monsoon rainfall and intense U.S. landfalling hurricanes, *Amer. Meteor. Soc.*, 5, 1528-1534, 1992.

Latif, M., Dommenget, D., Dima, M., and A. Grotzner, The role of Indian Sea surface temperature in forcing East African rainfall anomalies during December-January 1997/98, *Amer. Meteor. Soc.*, 12, 3497-3504, 1999.

Lins, H. F., Interannual streamflow variability in the United States based on principal components, *Water Resour. Res.*, 21(5), 691-701.

Lins, H. F., Streamflow variability in the United States: 1931-78, *J. Clim. And Appl. Meteorol.*, 24, 464-471, 1985.

Lohani, V. K., and G. V. Loganathan, An early warning system for drought management using the Palmer Drought Index, *J. Amr. Water Resour. Assoc.*, 33(6), 1375-1386, (1997).

Maier, H. R., and G. C. Dandy, The use of artificial neural networks for the prediction of water quality parameters, Water Res.our. Res., 33(4), 1013-1022, 1996.

Malmgren, B. A., and A. Winter, Climate zonation in Puerto Rico based on principal components analysis and an artificial neural network, *Amer. Met. Soc.*, 977-985, 1999.
Marengo, J. A., Variations and change in south American streamflow, *Clim. Change*, 31, 99-117, 1995.

Marengo, J. A., and J. Tomasella, trends in streamflow and rainfall in tropical South America: Amazonia, eastern Brazil, and northwestern Peru, *J. Geoghy. Res.*, 103(D2), 1775-1783, 1998.

Marsden, M. A., and R. T. Davis, Regression on Principal Components as a tool in water supply forecasting, *Proceedings of the Western Snow Conference*, Lake Tahoe, Nevada, 33-40, 1968.

McBride, J. L., and N. Nicholls, Seasonal relationships between Australian rainfall and the southern oscillation, *Mon. Wea. Rev.*, 111, 1998-2004, 1983.

McKerchar, A. I., C. P. Pearson, Forecasts of seasonal river flows using southern oscillation index, *J. Hyrol.* (NZ), 32(2), 16-29, 1994.

McKerchar, A. I., C. P. Pearson, and M. E. Moss, Prediction of summer inflows to lakes in the Southern Alpes, New Zealand, using the spring Southern Oscillation Index, *J. Hyrol.*, 184, 175-187, 1996.

Mechoso, C., and G. P. Iribarren, Streamflow in southeastern South America and the southern oscillation, *J. Clim.*, 5, 1535-1539, 1992.

Michaelsen, J., Cross-Validation in statistical climate forecast models, *J. Clim. App. Meteor.*, 26, 1589-1600, 1987.

Mielke, P. W., Berry, K. J., Landsea, C. W., and W. M. Gray, Artificial skill and validation in meteorological shrinkage, *Weather and Forecasting*, 11, 153-169, 1996.

Mielke, P. W., Berry, K. J., Landsea, C. W., and W. M. Gray, A single-sample estimate of shrinkage in meteorological forecasting, *Weather and Forecasting*, 12, 847-858, 1997.

Minns, A. W., and M. J. Hall, Artificial neural networks as rainfall-runoff models, *Hyro. Sci. J.*, 41(3), 399-417, 1996.

Mitchell, T. P., and J. M. Wallace, ENSO seasonality: 1950-78 versus 1979-92, *J. Climate*, 9, 3149-3161, 1996.

Mooley, D. A., Parthasarathy, B., G. B. Pant, Relationship between Indian summer monsoon rainfall and location of the ridge at the 500-mb level along 75° E, Amer. Met. Soc., 633-640, 1986.

Moss, M. E., C. R. Pearson, and A. I. McKerchar, The southern oscillation index as a predictor of the probability of low streamflows in New Zealand, *Water Resour. Res.*, 30(10), 2717-2723, 1994.
Mesa, O. J., and G. Poveda, The Hurst: The scale of fluctuation approach, *Water Resour. Res.*, 29(12), 3995-4002, 1993.

Nakayama, M., and M. H. Glantz, Liking ENSO and the Mekong hydrologic regime, Econom. and Soc. Comm. For Asia and the Pacific, *Water Resour. J.*, UN, 93-99.

Nam, Le H., Phien, H. N., and A. D. Gupta, Filtering and forecasting of monthly streamflows by backpropagation neural networks with an error updating method, *Water Research*, 29-39, 1998.

Navarra, A., Teleconnection patterns, Analysis of climate variability, edited by: Storch, H. V., and Navarra, A., Springer, 217-229, 1999.

Navone, HD, and HA Ceccato, Predicting Indian monsoon rainfall: a neural network approach, *Clim. Dyn.*, 10, 305-312, 1994.

Ngan, P., and S. O. Russell, Example of flow forecasting with Kalman Filter, *J. Hydr. Eng.*, ASCE,112(9), 818-832, 1986.

Nicholls, N., All-India summer monsoon rainfall and sea surface temperatures around Nothern Australia and Indonesia, *J. Climate*, 8, 1463-1467, 1995.

Nicholls, N., The use of Canonical correlation to study teleconnections, *Mon. Weather Rev.*, 115, 393-399, 1987.

Nicholls, N., and A. kariko, East Australian rainfall events: Interannual variations, Trends, and relationship with the southern ascillation, *J. Climate*, 6, 1141-11521467, 1993.

Pant, G. B., and K. R. Kumar, Climates of South Asia, *John Wiley and Sons Ltd, England*, 1997.

Pan, Y. H., and A. H. Oort, Correlation between sea surface temperature anomalies in the eastern equatorial Pacific and the world ocean, *Clim. Dyn.* 4, 191-205,1990.

Parthasarthy, B., Munot A. A., and D. R. Kothawale, All-India monthly and seasonal rainfall series: 1871-1993, *Theor. Appl. Climatol*, 49, 217-224, 1994.

Parthasarthy, B., Munot A. A., and D. R. Kothawale, Droughts/Floods in the summer monsoon season over different meteorological subdivisions of India for the period: 1871-1984, *J. Climatol*, 7, 57-70, 1987.

Pelletier, J. D., and D. L. Turcotte, Long-range persistence in climatological and hydrological time series: analysis, modeling and application to drought hazard assessment, *J. Hydro.*, 203, 198-208.

Philander, S. G., EL Niño, La Niña, and the southern oscillation, Academic Press INC., 1990.

Picaut, J., Masia, F., and Y. du Penhoat, An advective-reflective conceptual model for the oscillatory nature of the ENSO.

Piechota, T. C., Chiew, F. H. S., Dracup J. A., and T. A. McMahon, Seasonal streamflow forecasting in Eastern Australia and the EL Niño-Southern Oscillation, *Water Resour. Res.*, 34(11), 3035-3044, 1998.

Piechota, T. C., and J. A. Dracup, Drought and regional hydrologic variation in the United States: Associations with the EL Niño-Southern Oscillation, *Water Resour. Res.*, 32(5), 1359-1373, 1996.

Piechota, T. C., and J. A. Dracup, Long-Range streamflow forecasting using EL Niño-Southern Oscillation Indiactors, *Hydro. Engg.*, 4(2), 144-151, 1997.

Piechota, T. C., Long-Range seasonal streamflow forecasting and the EL Niño-Southern Oscillation, PhD Dissertation, University of California, LA, 1997.

Piper, B. S., Plinston, D. T., and J. V., Sutcliffe, The water balance of lake Victoria, Hydro. Sci. J., 31(1), 25-36, 1986.

Pisciottano, G., A. Diaz, G. Cazes, and C. Mechoso, EL Niño-Southern Oscillation impact on rainfall in Uruguay, *J. Climate*, 7, 1286-1302.

Prasad K. D., and S. V. Singh, Forecasting the spatial variability of the Indian monsoon rainfall using canonical correlation analysis, *Int. J. Climatol.*, 16, 1379-1390, 1996.

Quin, W. H., A study of Southern Oscillation-related climatic activity for A.D. 622-1900 incorporating Nile River flood data, *In Diaz, H. F., and Markgraf, V. (eds), EL Niño Historical and Paleoclimatic Aspects of the Southern Oscillation*, 119-149, 1992.

Quin, W. H., and V. T. Neal, EL Niño occurrences over the past four and a half centuries, J. Geoph. R., 92, 14449-144461, 1987.

Raman, H., and N. Sunilkumar, Multivariate modeling of water resources time series using artificial neural networks, Hydro. Sci. J., 40(2), 145-163, 1995.

Raman, H., and V. Chandramouli, Deriving a general operating policy for reservoirs using neutral network, *J. Water Resour. Plng. and Mgmt.*, 122(5), 342-347, 1996.

Rasmusson, E. M. and T. H. Carpenter, The relationship between eastern equatorial Pacific sea surface temperatures and rainfall over India and Sri Lanka, *Mon. Weather Rev.*, 111, 517-528, 1983.

Rasmusson, E. M., T. H., Carpenter, Variations in tropical sea surface temperature and surface wind fields associated with the Southern Oscillation/ El Niño, *Mon. Wea. Rev.*, 110, 354-384, 1982.

Redmond, K. T., and R. W. Koch, Surface climate and streamflow variability in the western United States and their relationship to large-scale circulation indices, *Water Resour. Res*, 27(9), 2381-2399, 1991.

Rogers, J. C., The association between the North Atlantic oscillation and the southern oscillation in the Northern Hemisphere, *Mon. Wea. Rev.*, 112, 1999-2015, 1984.

Ropelewski, C. F., and M. S. Halpert, Global and regional scale precipitation patterns associated with the EL Niño/Southern Oscillation, *Mon. Weather Rev.*, 115, 1606-1626, 1987.

Ropelewski, C. F., and M. S. Halpert, Global and regional scale precipitation patterns associated with the EL Niño/Southern Oscillation, *Mon. Weather Rev.*, 115, 1606-1626, 1987.

Ropelewski, C. F., and M. S. Halpert, Quantifying southern oscillation-precipitation relationships, *J. Climate*, 9, 1043-1059, 1996.

Ropelewski, C. F., and M. S. Halpert, North American precipitation and temperature patterns associated with the EL Niño/Southern Oscillation (ENSO), *Mon. Weather Rev.*, 114, 2352-2362, 1986.

Ropelewski, C. F., and M. S. Halpert, Precipitation patterns associated with the high index phase of the southen oscillation, *J. Climate*, 2, 268-284, 1989.

Saad, M., Bigras, A. T., and R. Duquette, Learning disaggregation technique for the operation of long-term hydroelectric power systems, *Water Resour. Res.*, 30(11), 3195-3202, 1994.

Said, R., The Nile river, geology, hydrology, and utilization, Pergamon press, 1993.

Salas, J. D., D. C. B., and V. Yevjevich, On the Hurst phenomenon. *In modeling hydrologic processes*, ed. H. J. More-Seytoux, 116-124, 1979a.

Salas, J. D., D. C. B., V. Yevjevich, and G. G. S. Pegram, Hurst phenomenon as a pre-asymptotic behavior, *J. Hydro.*, 44, 1-15, 1979b.

Salas, J. D., J. W. Delleur, V. Yevevich, and W. L. Lane, Applied modeling of hydrologic time series, *Water Resources Publications*, Littleton, Co., USA, 1980.

Seleshi, Y., Statistical analysis of the Ethiopian droughts in the XX^{th} century based on monthly and yearly precipitation totals, *MS thesis, Vrije Universiteit, Belgium*, 1991.

Selten, F. M., R. J. Haarsma, and J. D. Opsteegh, On the mechanism of North Atlantic Decadal variability, J. Clim., 12(7), 1956-1973, 1999.

Sene, K. J., Theoretical estimates for the influence of lake Victoria on flows in the upper White Nile, *Hydro. Sci. J.*, 45(1), 125-145, 2000.

Shamseldin, A. Y., Application of a neural network technique to rainfall-runoff modeling, J. Hydro., 199, 272-294, 1997.

Shigidi, A. M. T., Solving the inverse problem in groundwater flow by iterative inversion of a neural network, *Ph.D. dissertation*, Colorado State University, Fort Collins, Colorado, 2000.

Shukla, J., and D. A. Mooley, Emeprical prediction of the summer monsoon rainfall over India, *Amer. Met. Soc.*, 115, 695-703, 1987.

Shukla, J., and D. A. Paolino, The southern oscillation and long-range forecasting of the summer monsoon rainfall over India, *Mon. Wea. Rev.*, 111, 1830-1837, 1983.

Simpson, H. J., M. A. Cane, A. L. Herczeg, S. E. Zebiak, and J. H. Simpson, Annual river discharge in Southern Australia related to EL Niño-Southern Oscillation forecasts of sea surface temperature, *Water Resour. Res.*, 29, 3671-3680, 1993a.

Simpson, H. J., Cane, M. A., Lin, S. K., and S. E. Zebiak, Forecasting annual discharge of river Murray, Australia, from a geophysical model of ENSO, *J. Clim.*, 6, 386-390, 1993b.

Simpson, H. J., Cane, M. A., Herczeg, A. L., Zebiak, S. E., and J. H. Simpson, Annual river discharge in southeastern Australia related to EL Niño-Southern Oscillation forecasts of sea surface temperatures, *Water Resour. Res.*, 29(11), 3671-3680, 1993b.

SNNS4.1 User Manual, University of Stuttgart, Institute for Parallel and distributed high performance systems (IPVR), report No. 6/95, 1995.

Solow, A. and N. Nicholis, The relationship between the southern oscillation and tropical cyclone frequency in the Australian region, *J. Climate*, 3, 1097-1101, 1990.

Soule, P. T., Spatial patterns of drought frequency and duration in the contiguous USA based on multiple drought event definitions, 12, 11-24, 1992.

Smith, J., R. N., Eli, Neural-Network models of rainfall-runoff process, *J. Water Resour. Plng. and Mgmt.*, 121(6), 499-508, 1995.

Smith, R. A., and O. J. Mesa, EL Niño effect on Colombian hydrology practices, *Water resour. Eng.*, Proc. San Antonio, TX, ASCE, ed. Espry, W. H., and P. G. Combs, Vol. 1, 1995.

Sun, H., and D. Furbish, Annual precipitation and river discharges in Florida in response to EL Niño- and La Niña-sea surface temperature, *J. Hydro.*, 74-87, 1997.

Sureerattanan, S., and H. N., Phien, Back-Propagation networks for daily streamflow forecasting, Water Research, 1-7, 1997.

Tanco, R. A., and G. J. Berri, CLIMBLAB2000, deverloped at the International Research Institute for Climate Prediction, Applications and Training Pilot Project, 1999.

Tangang, F. T., Tang B., Mohanan, A. H., and W. W. Hsieh, Forecasting ENSO events: A neural network-extended EOF approach, *J. Climate*, 11(1), 29-41, 1998.

Thompstone, R. M., K. H. Hipel, and A. I. McLeod, Forecasting quarter-monthly riverflow, *Water Resour. B.*, 21(5), 731-741, 1985.

Tokar. A. S., and P. A., Johnson, Rainfall-Runoff modeling using artificial neural networks, *J. Hydro. Engg.*, ASCE, 4(3), 232-239, 1999.

Trenberth, K. E., Signal versus noise in the southern oscillation, *Mon. Wea. Rev.*, 112, 326-332, 1984.

Vinnikov, K. Y., Groisman, P. Y., and K. M. Lugina, Emperical data on contemporary Global climate changes (temperature and precipitation), *J. Climate*, 3, 662-677, 1990.

Vogel, R. M., and I. Wilson, Probability distribution of annual maximum, mean and minimum streamflows in the United States, *J. Hydro. Engg.*, ASCE, 1(2), 69-87, 1996.

Wang, B., interdecadal changes in EL Niño in the last four decades, J. climate, 8, 1995.

Wang, G., and E. A. B. Eltahir, Use of ENSO information in Medium and Long-Range forecasting of the Nile floods, *Amer. Met. Soc.*, 12, 1726-737, 1999.

Waylen, P. R., and C. N. Caviedes, EL Niño and annual floods on the North Peruvian Littoral, *J. Hydrol.*, 89, 141-156, 1986.

Wood, E. F., An aplication of Kalman filtering to river flow forecasting, *Princeton University*, Princeton, New Jersey, U.S.A., 385-407, 1978.

Wood, E. F., Filtering of partitioned large scale hydrological systems, *Hydro. Sc. B.*, 26(1), 33-46, 1981.

Wortman, R. T., Statistical forecast model for Libby Basin, Montana, *Proceedings of the Western Snow Conference*, Fort Collins, Co., 100-107, 1989.

Wright, P. B., Homogenized long-period southern oscillation indices, *Int. J. Climatol.*, 9, 33-54, 1989.

Wright, P. B., Relationships between indices of the southern oscillation, *Mon. Wea. Rev.*, 112, 1913-1919, 1984.

Yu, Z., Predictive skill of seasonal to annual rainfall variations in the U.S. affiliated Pacific Islands: Canonical correlation analysis and multivariate principal component regression approaches, *J. Climate*, 10, 2586-2599, 1997.

Zealand, C. M., Burn, D. H., and S. P., Simonovic, Short term streamflow forecasting using artificial neural networks, J. Hydro., 214, 32-48, 1999.

Zhang, Y., J. M. Wallace, and D. Battisti, ENSO-like interdecadal variability: 1900-93, *J. Climate*, 10, 1004-1020, 1997.

Zhang, Y. E., P. E., Trimble, and P. Trimble, Forecasting water availability by applying neural networks with global and solar indices, *Proceedings of the sixteenth annual Amercian Geophysical Union*, 1996.

APPENDIX A

CORRELATION MAPS

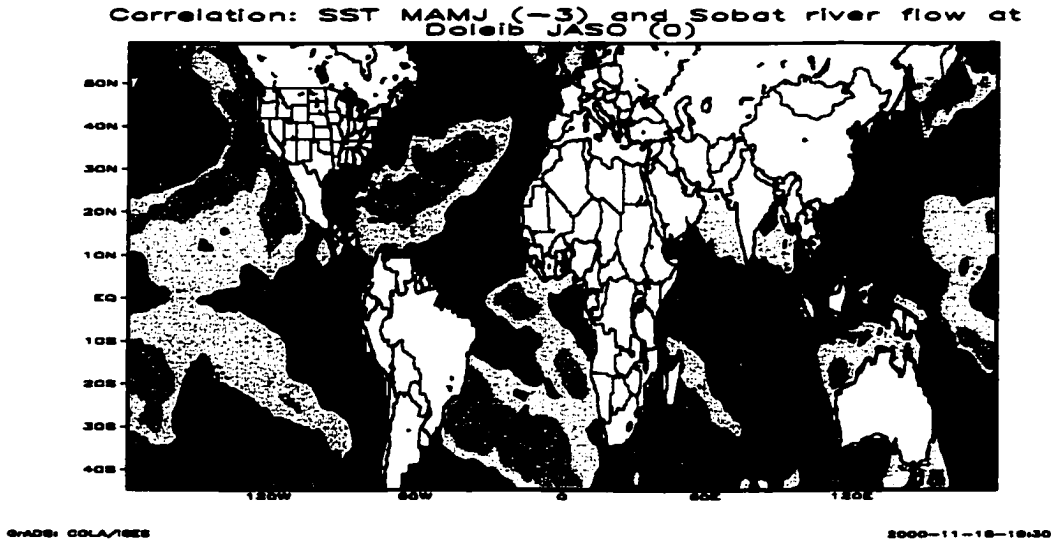

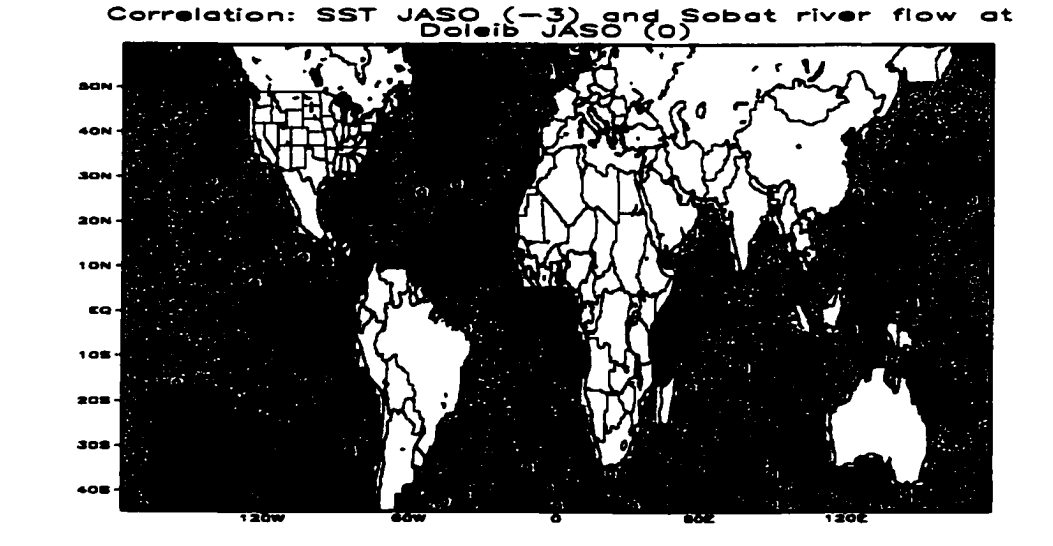

Fig. A_1 Correlation maps for the Sobat River flows (July to October) and the SST at various lead seasons shown at the top of each graphs

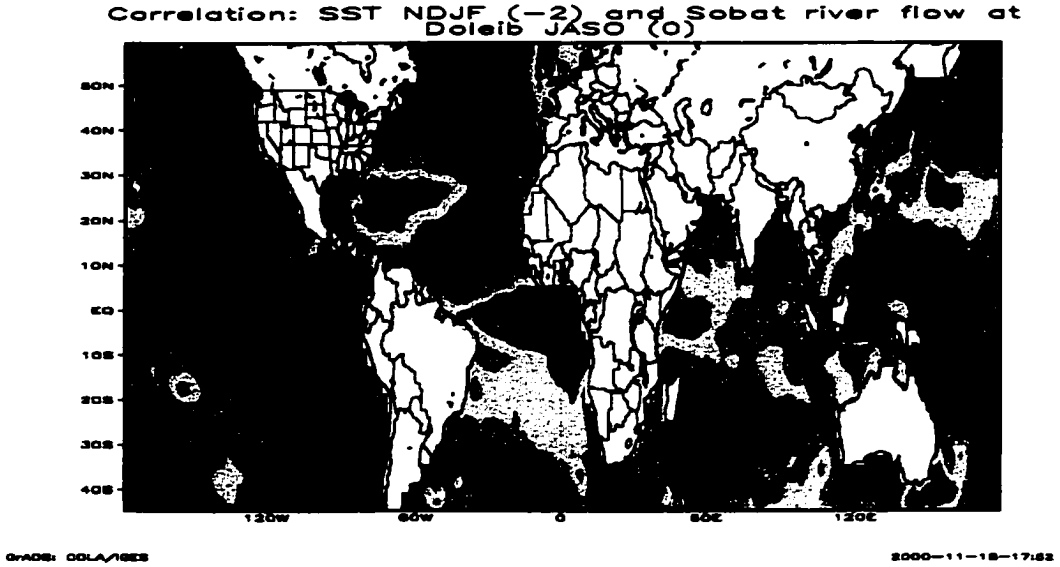

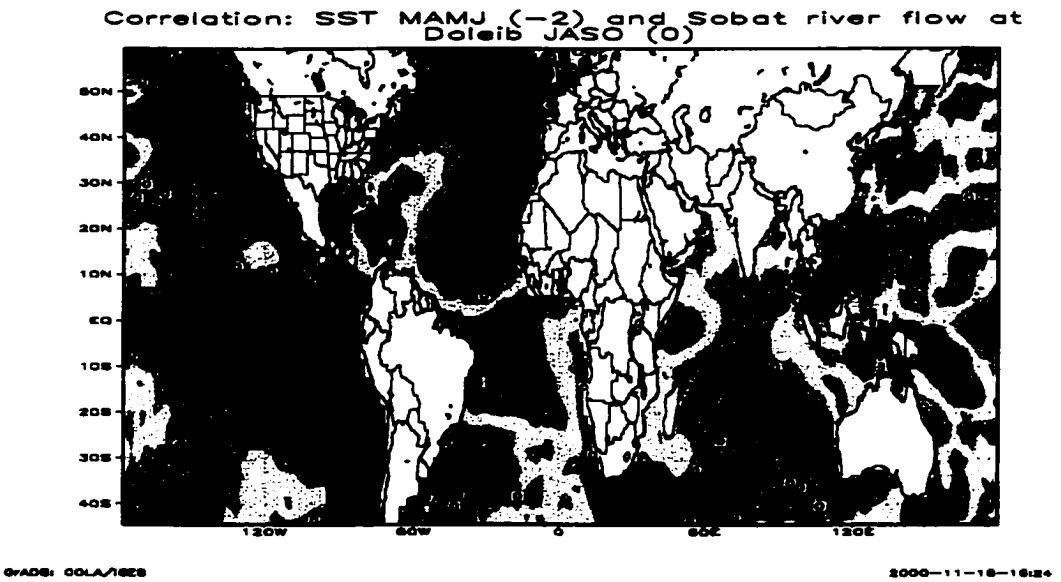

Fig. A_1 Cont.

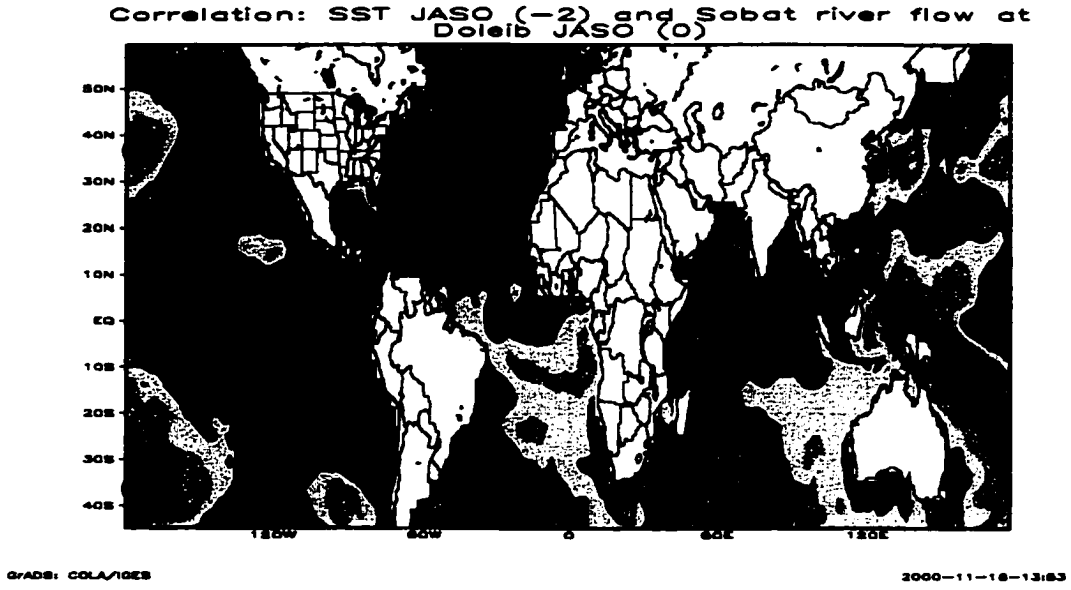

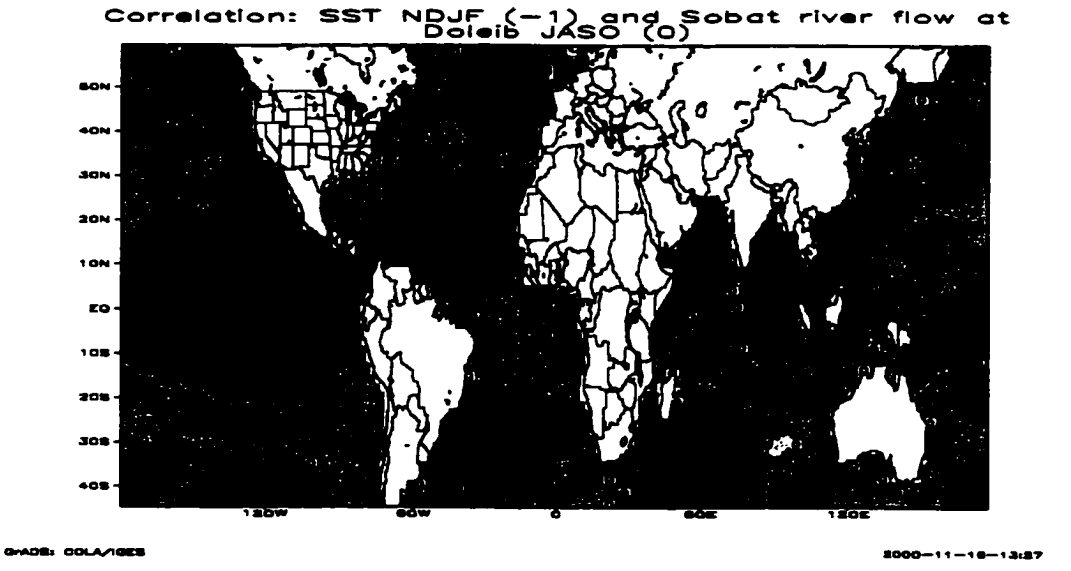

Fig. A_1 Cont.

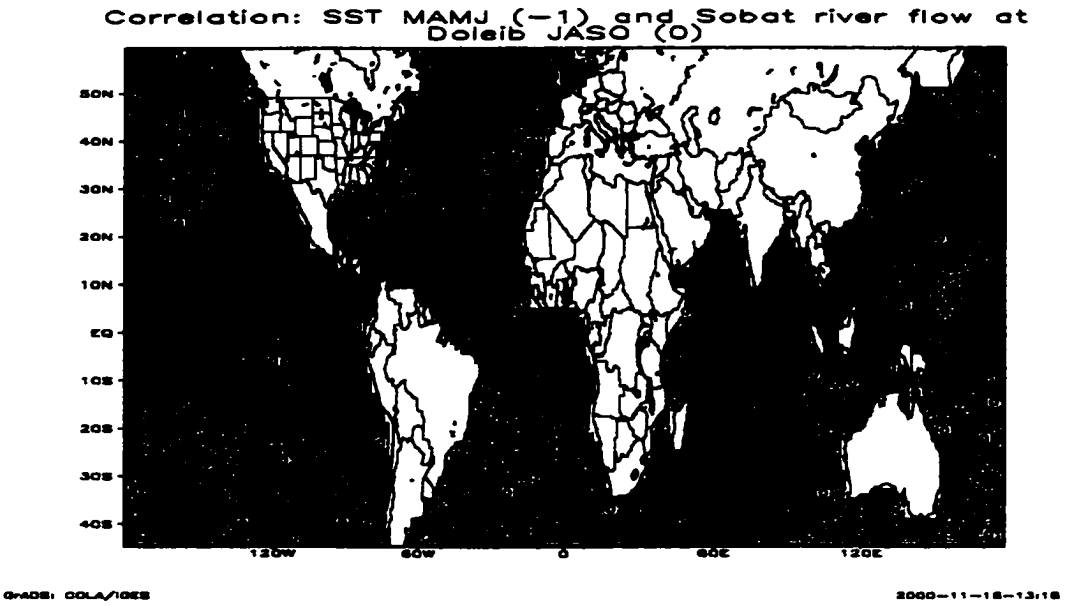

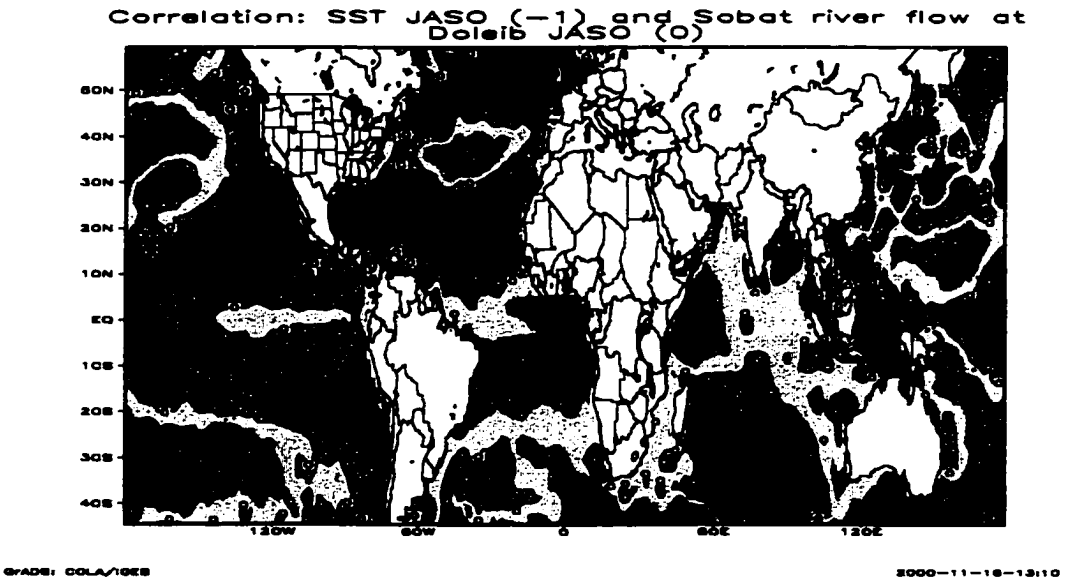

Fig. A_1 Cont.

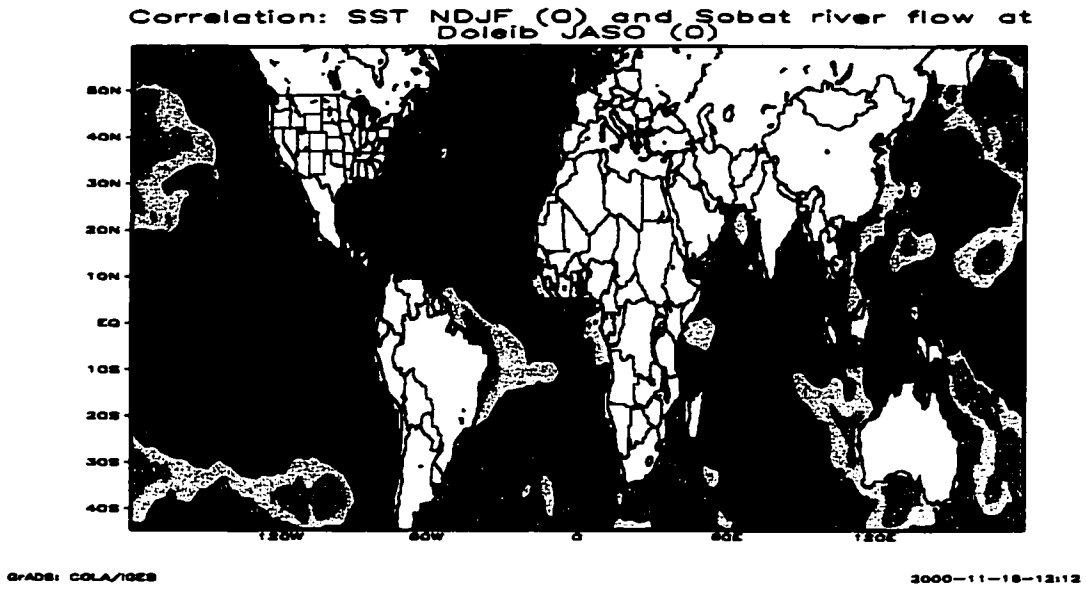

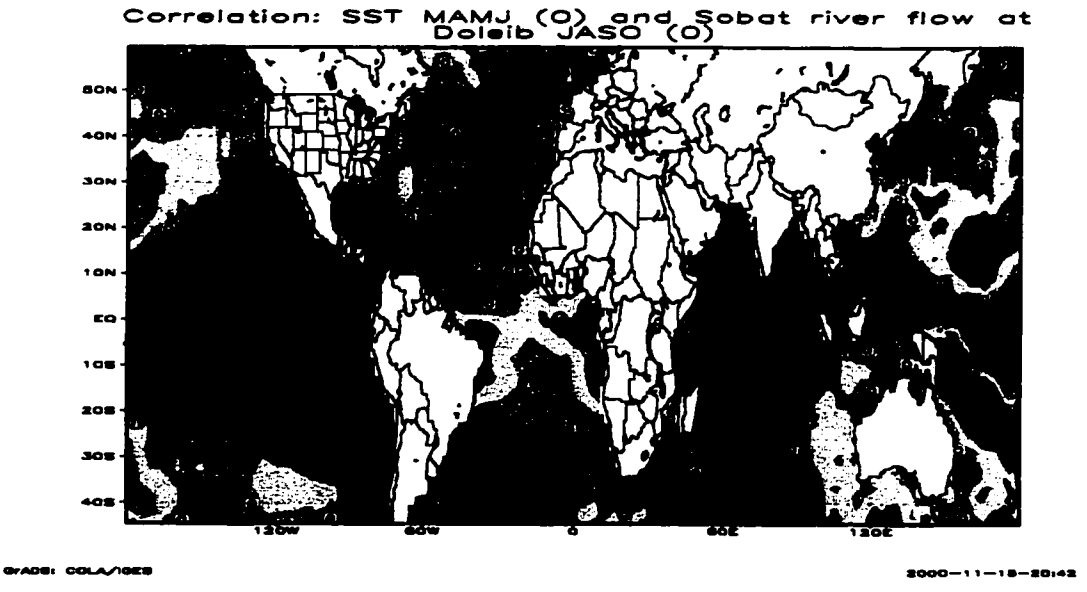

Fig. A_1 Cont.

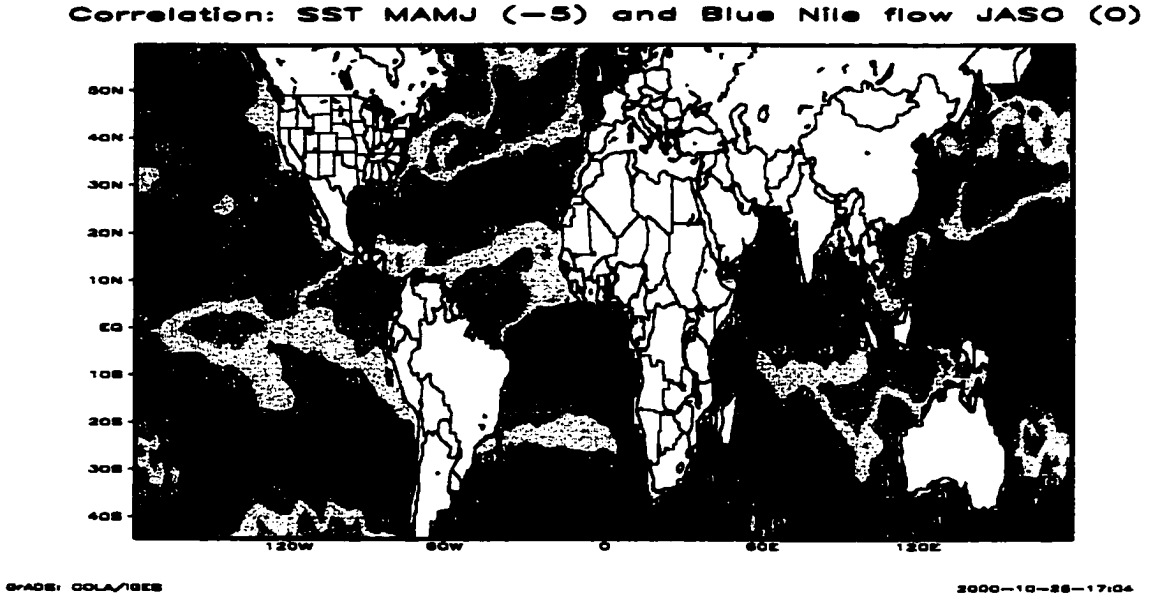

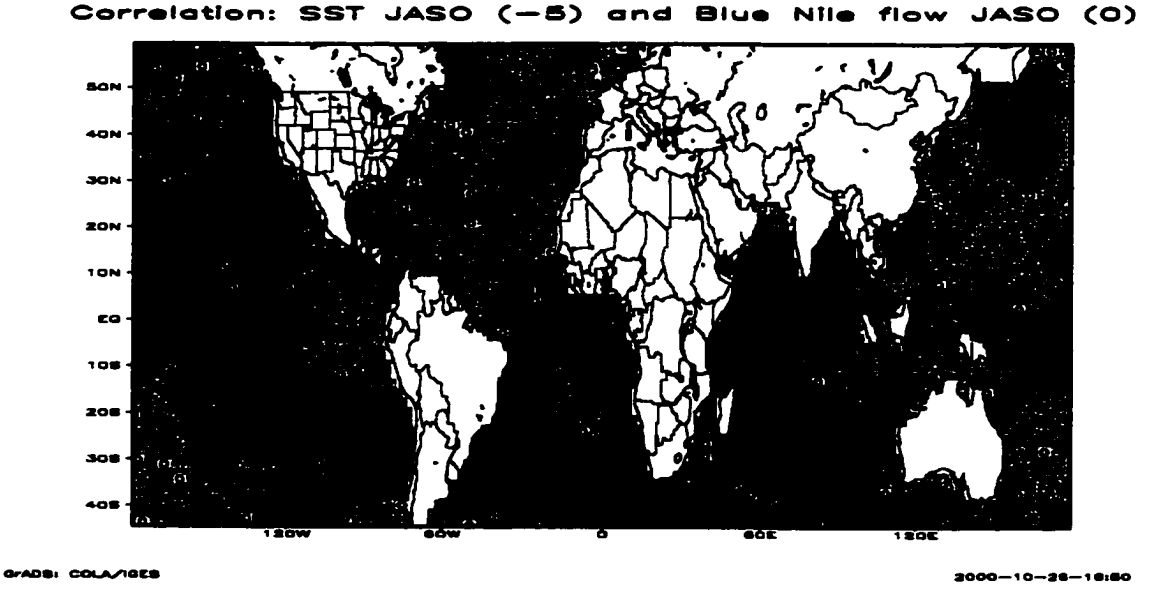

Fig. A_2 Correlation maps for the Blue Nile River flows (July to October) and the SST at various lead seasons shown at the top of each graphs

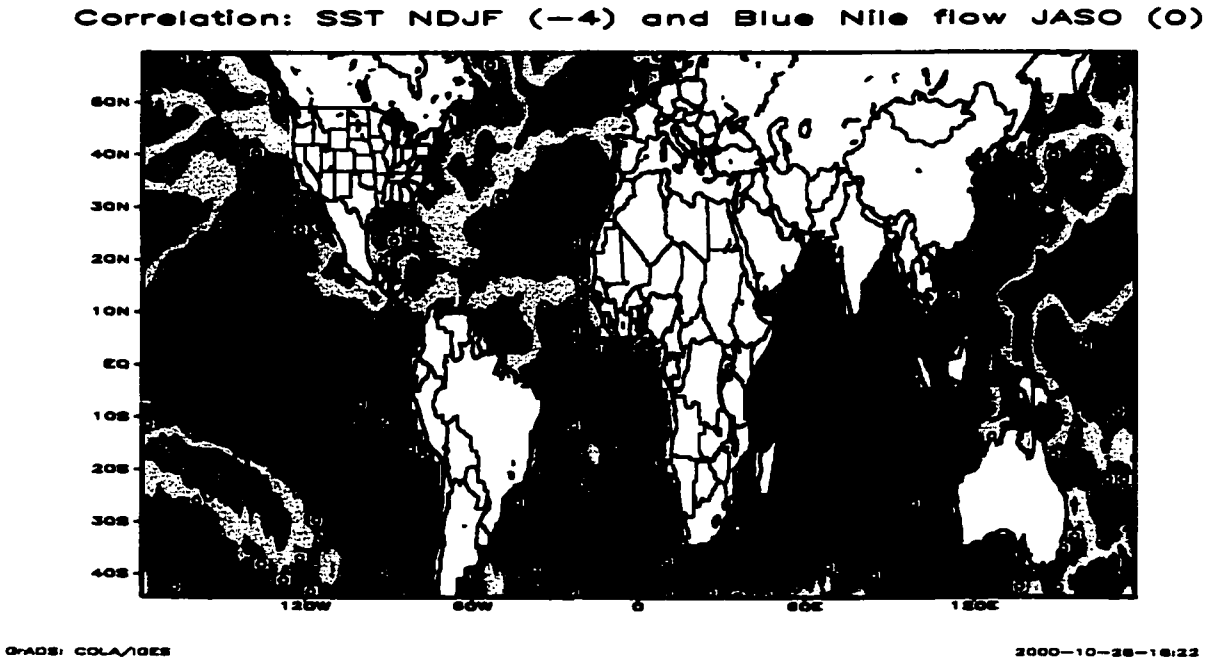

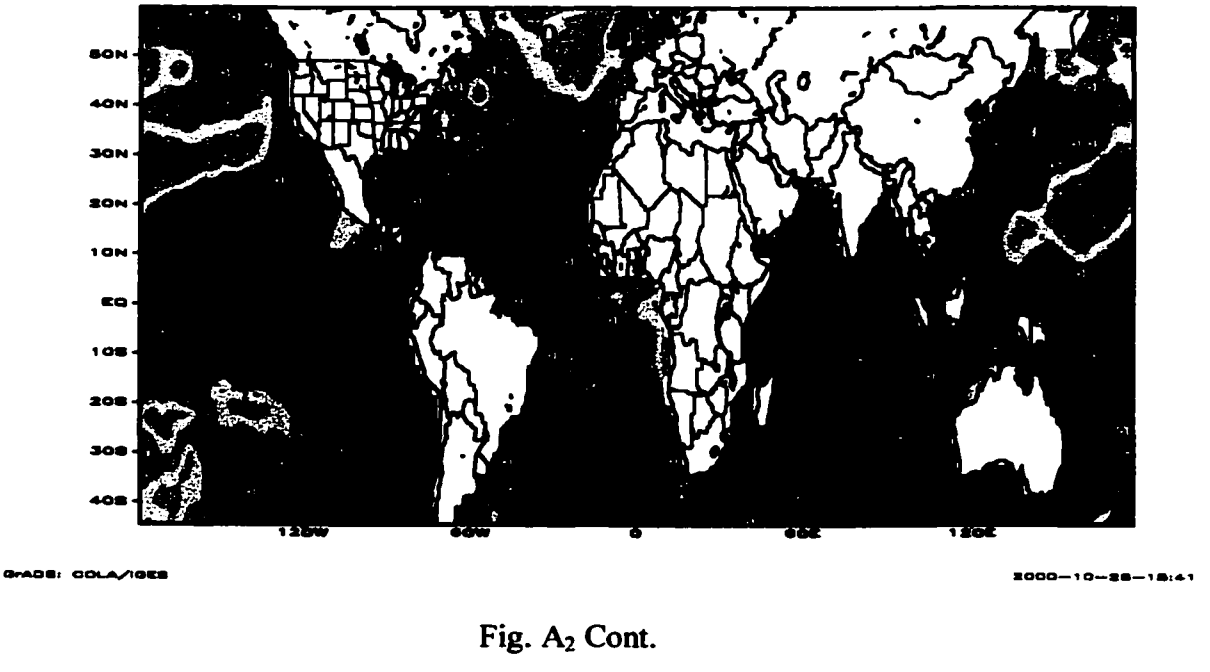

Fig. A_2 Cont.

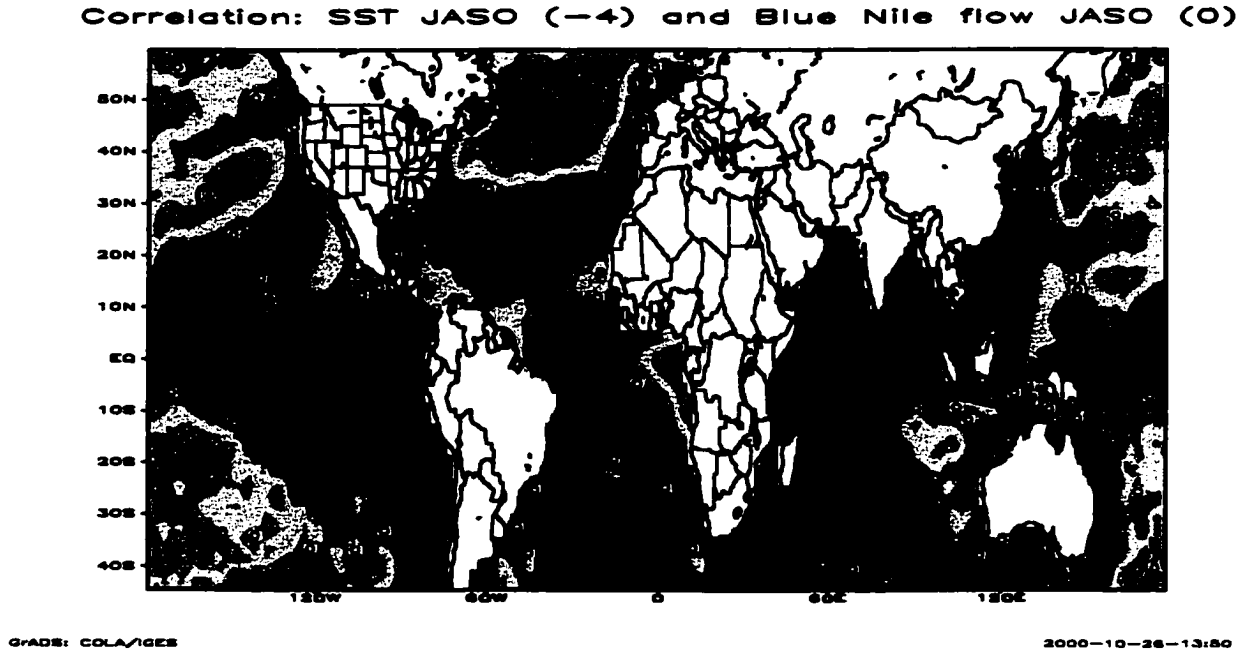

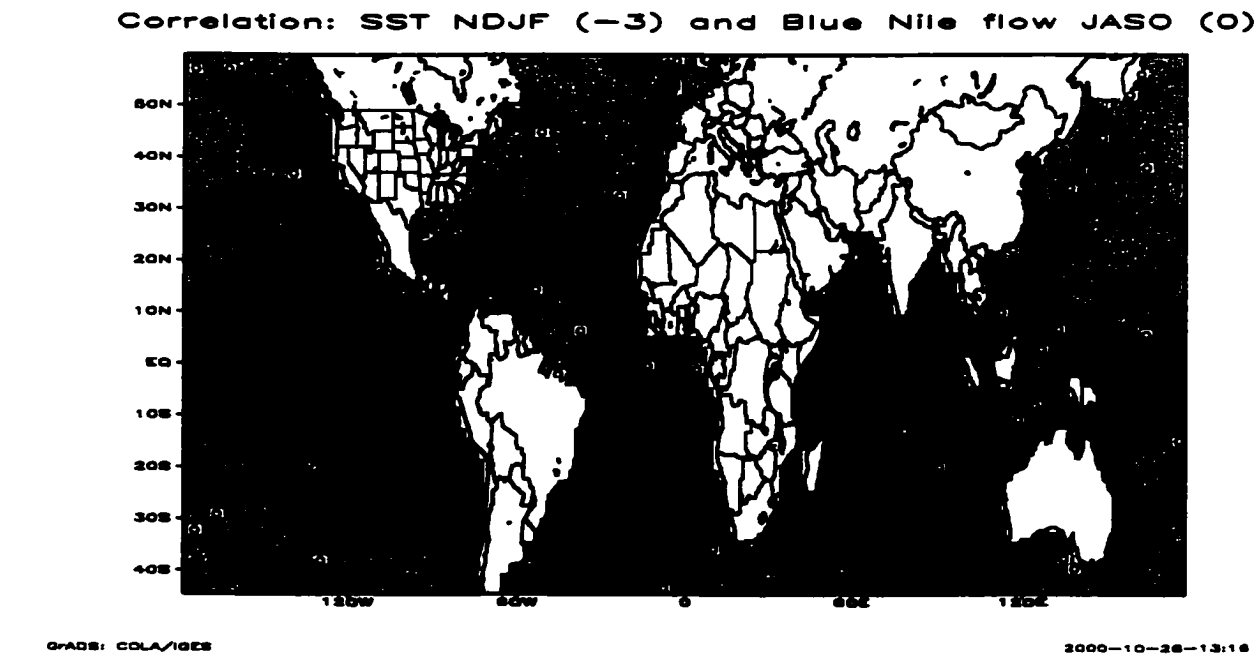

Fig. A_2 Cont.

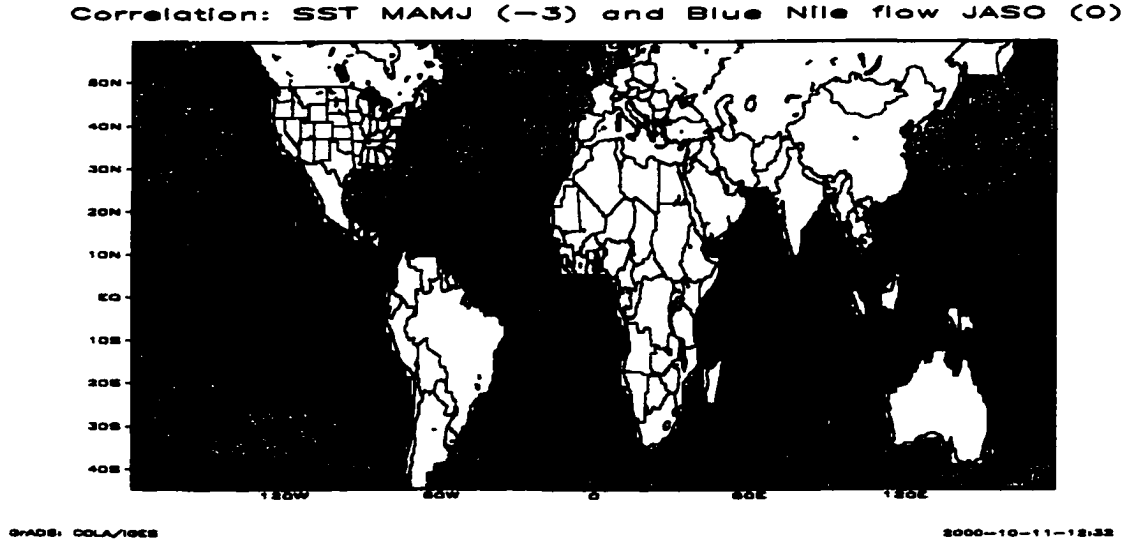

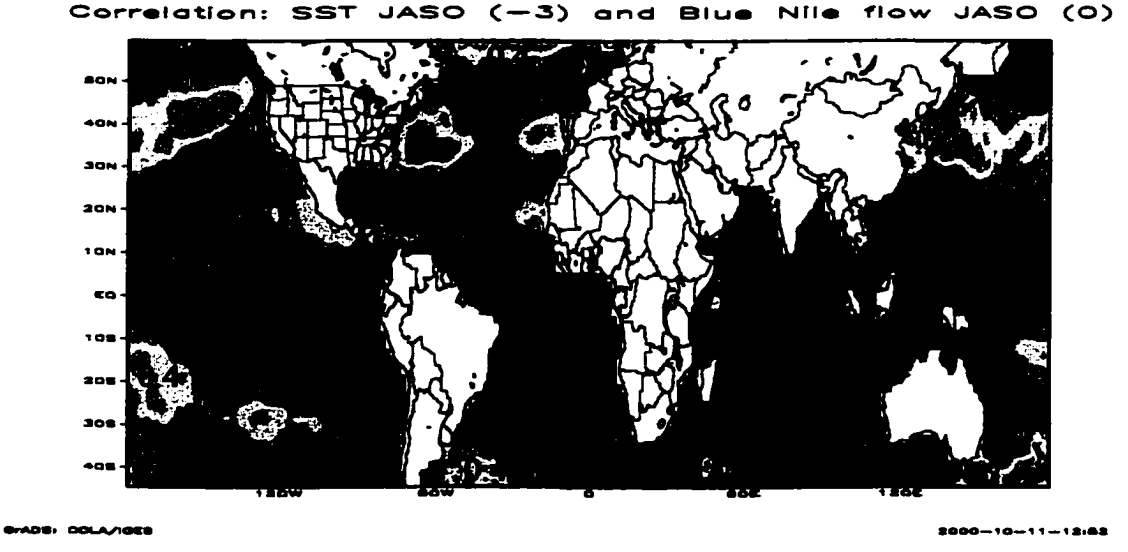

Fig. A_2 Cont.

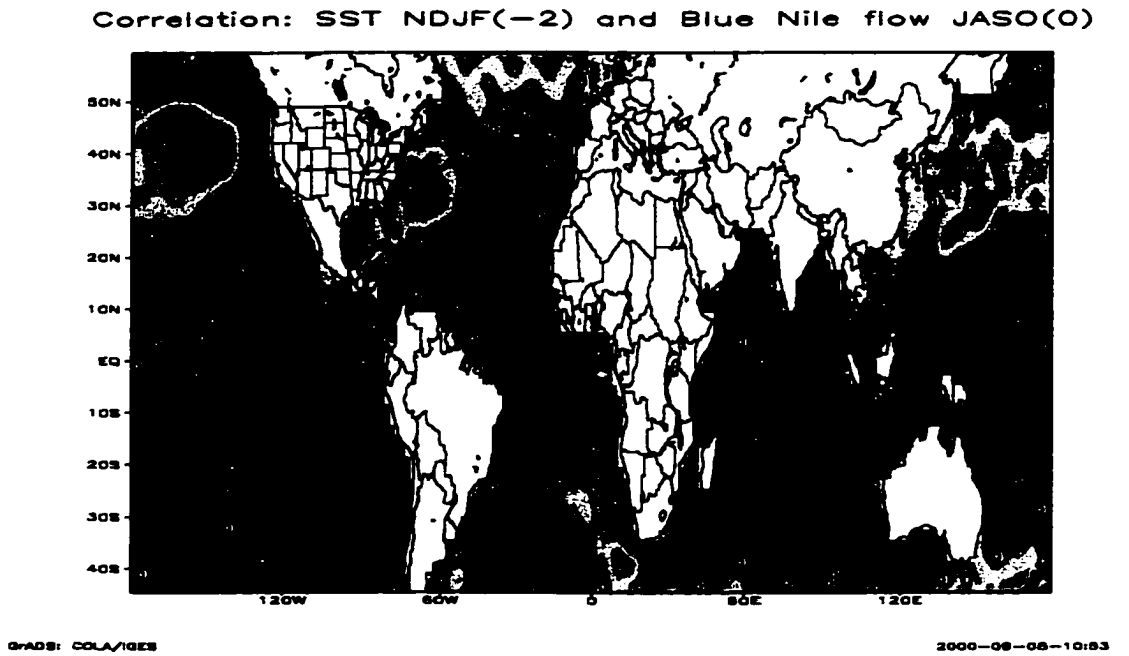

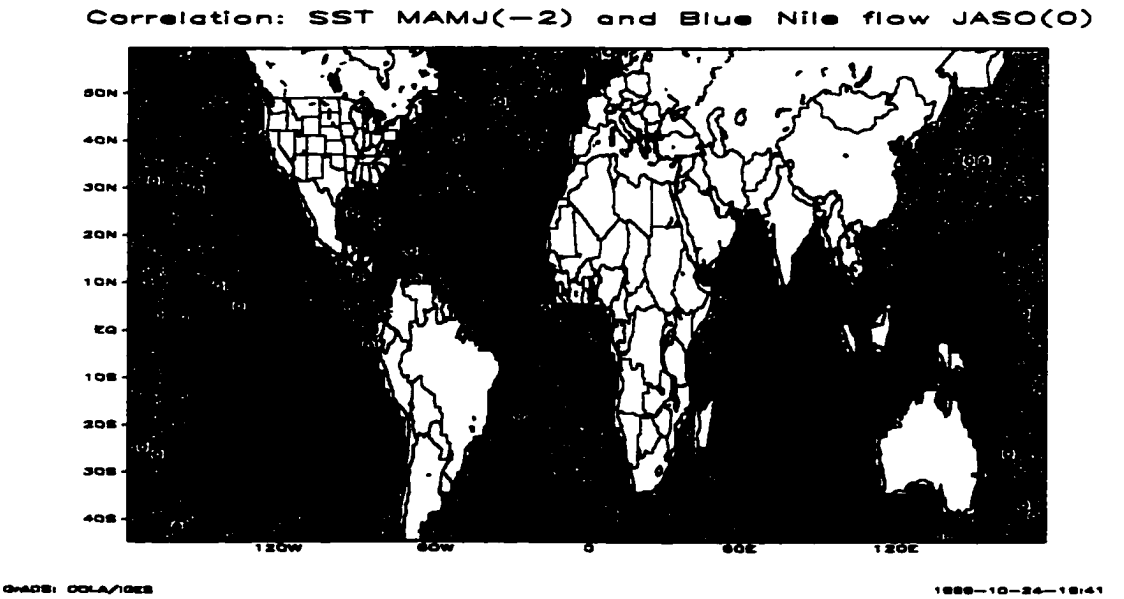

Fig. A_2 Cont.

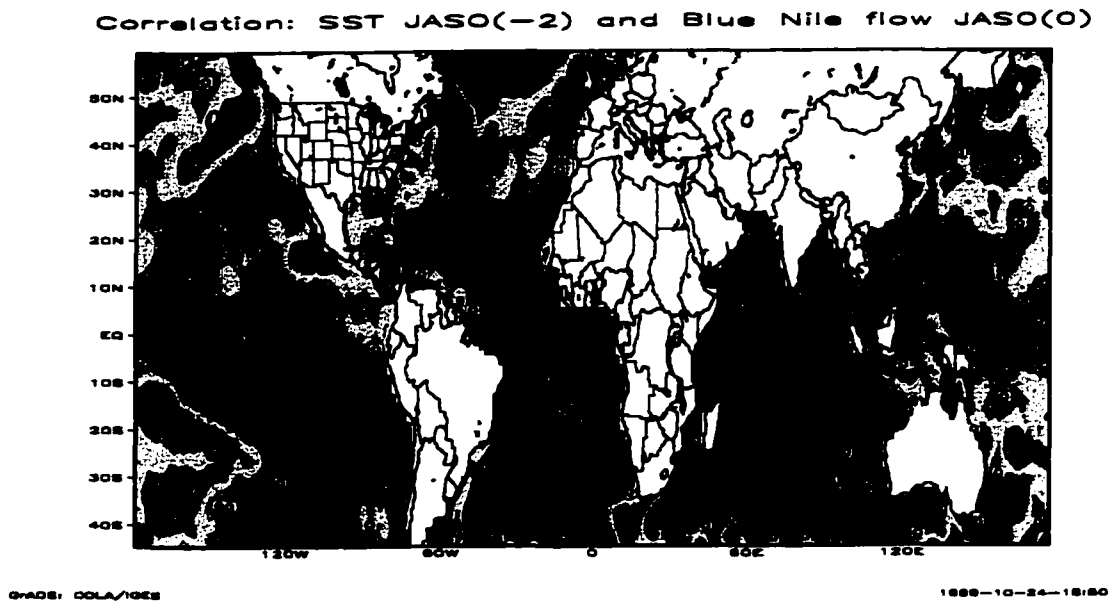

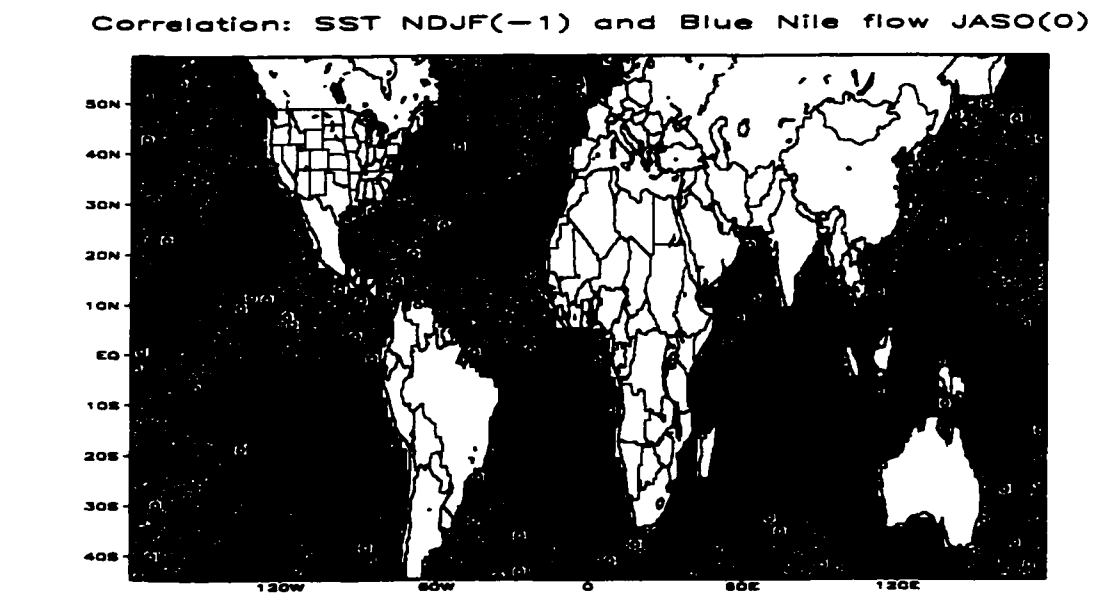

Fig. A_2 Cont

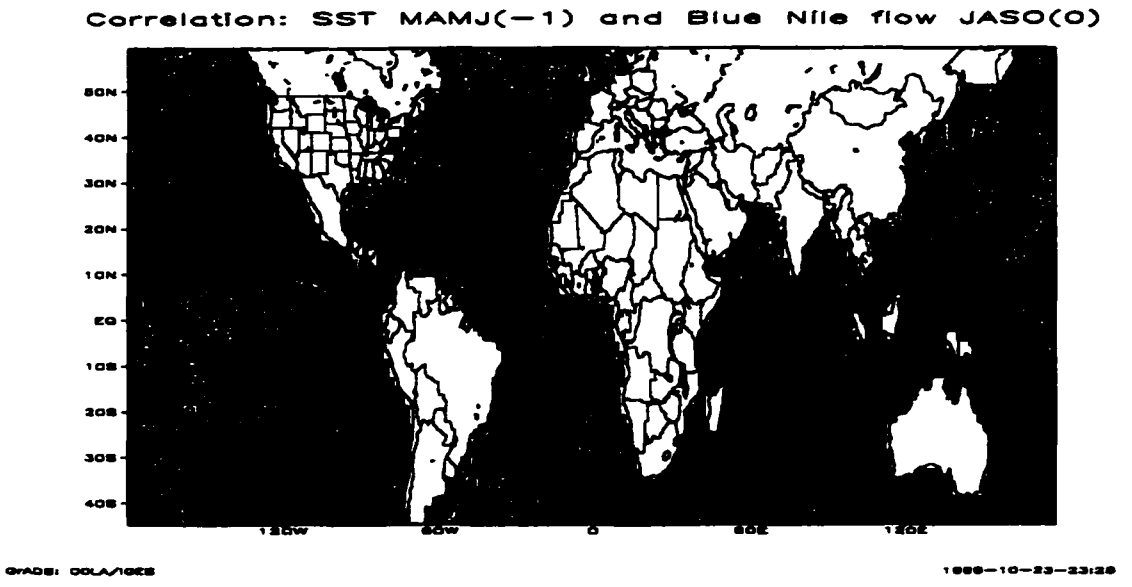

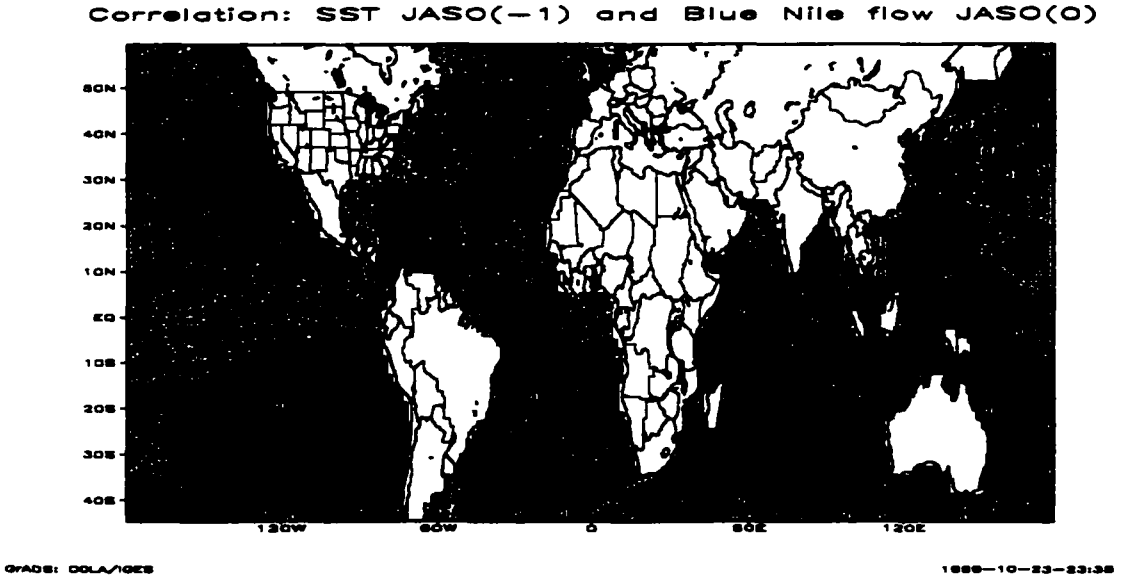

Fig. A_2 Cont.

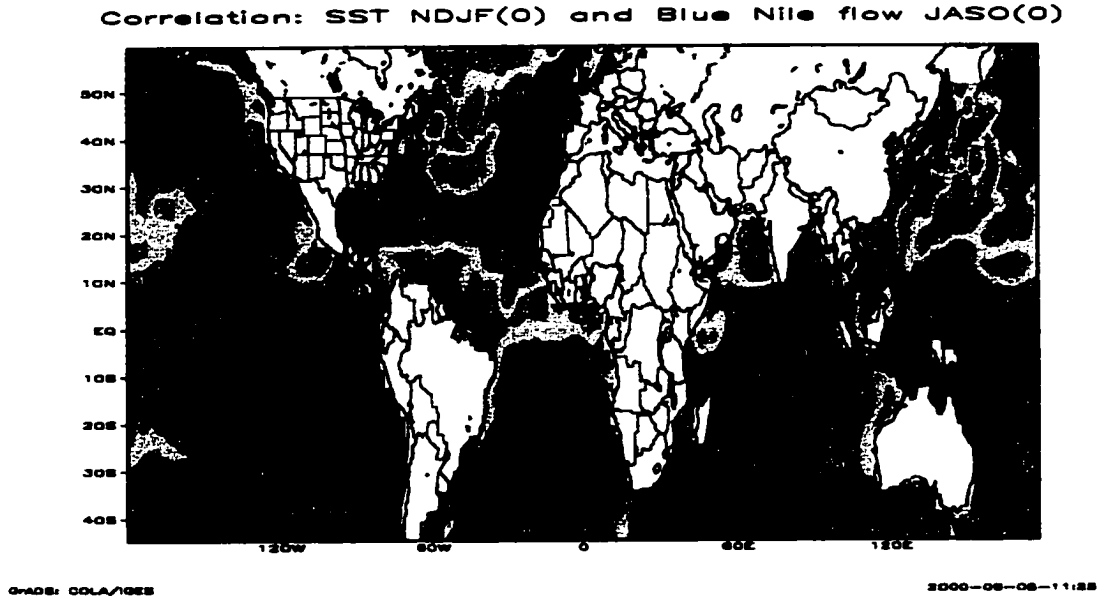

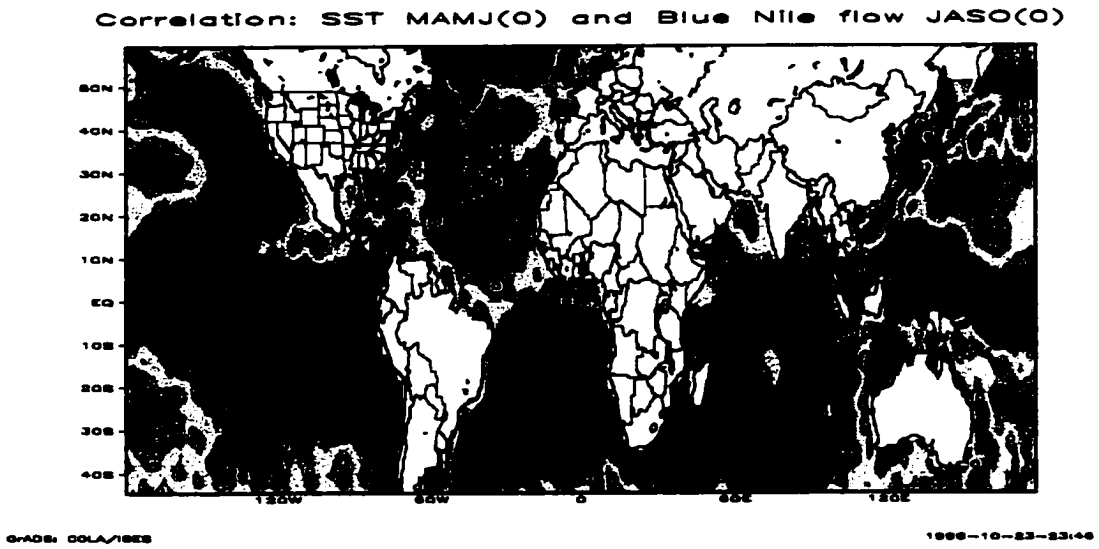

Fig. A_2 Cont.

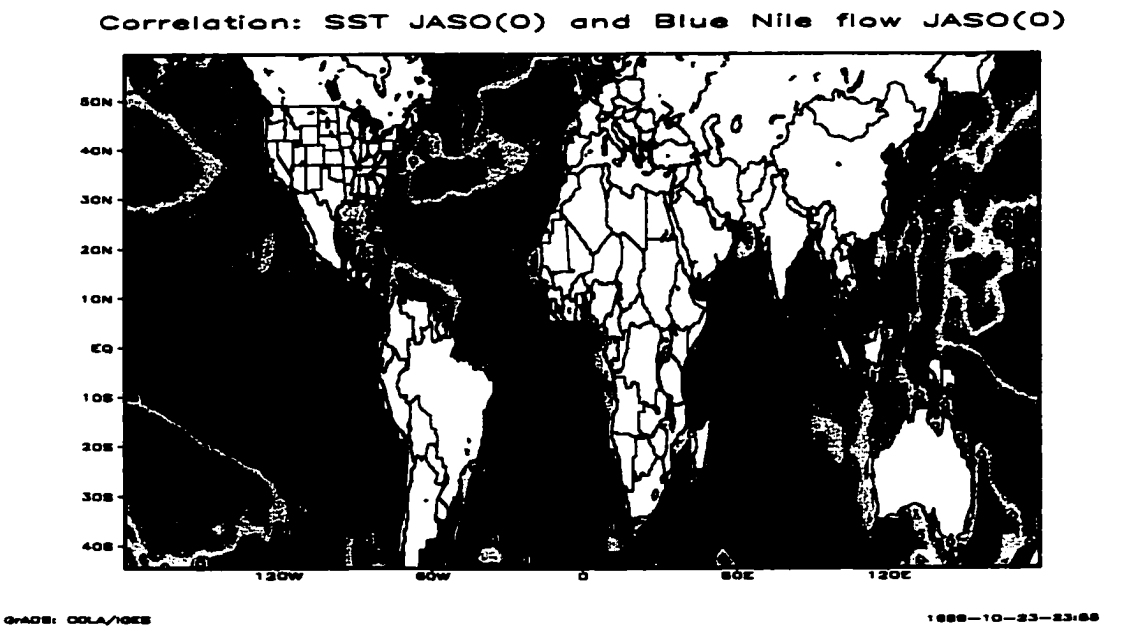

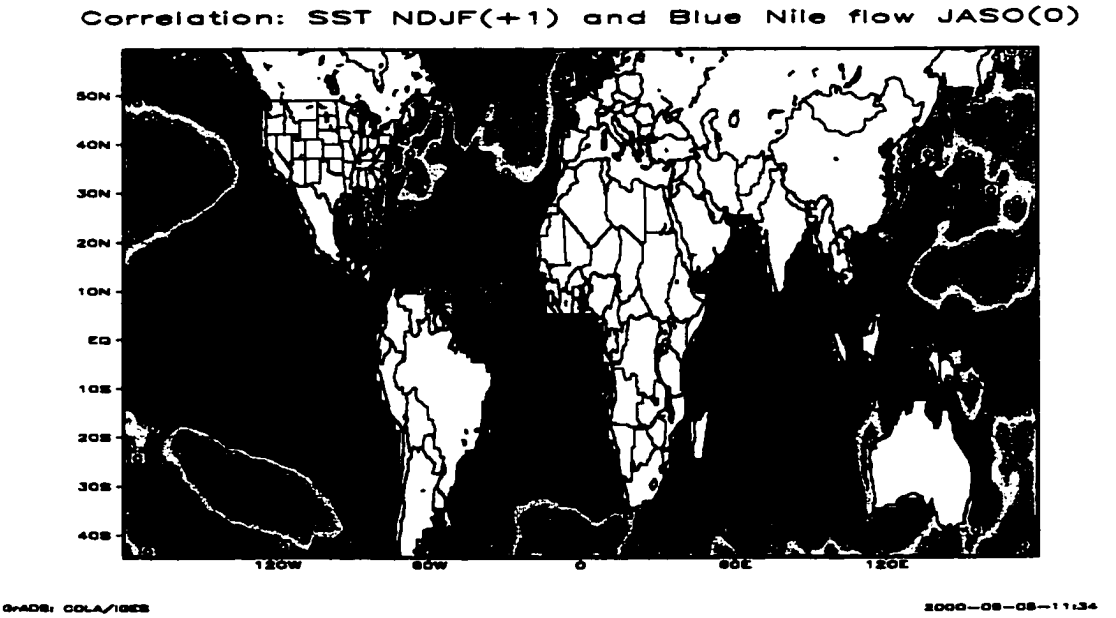

Fig. A_2 Cont.

Correlation: SST MAMJ(+1) and Blue Nile flow JASO(0)

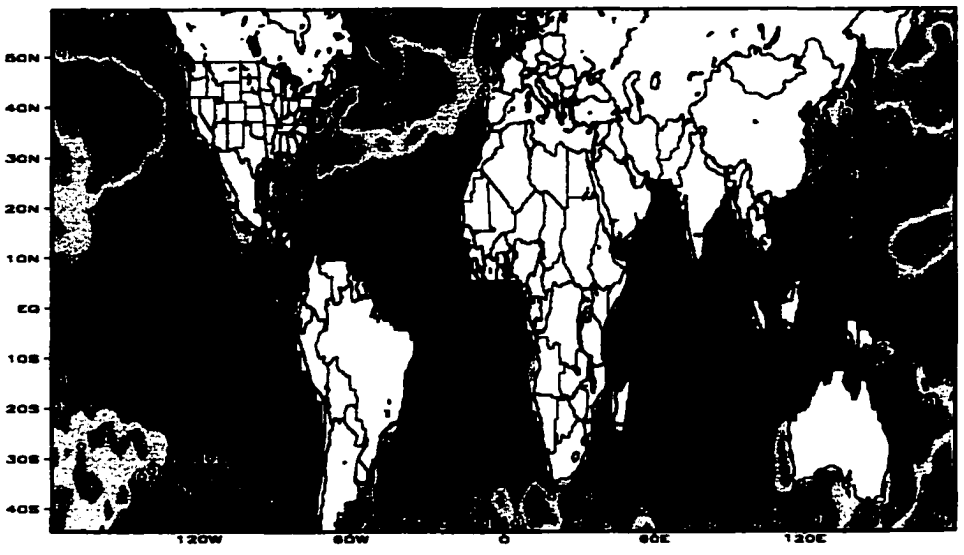

GrADS: COLA/IGES 1998-10-24-00:14

Correlation: SST JASO(+1) and Blue Nile flow JASO(0)

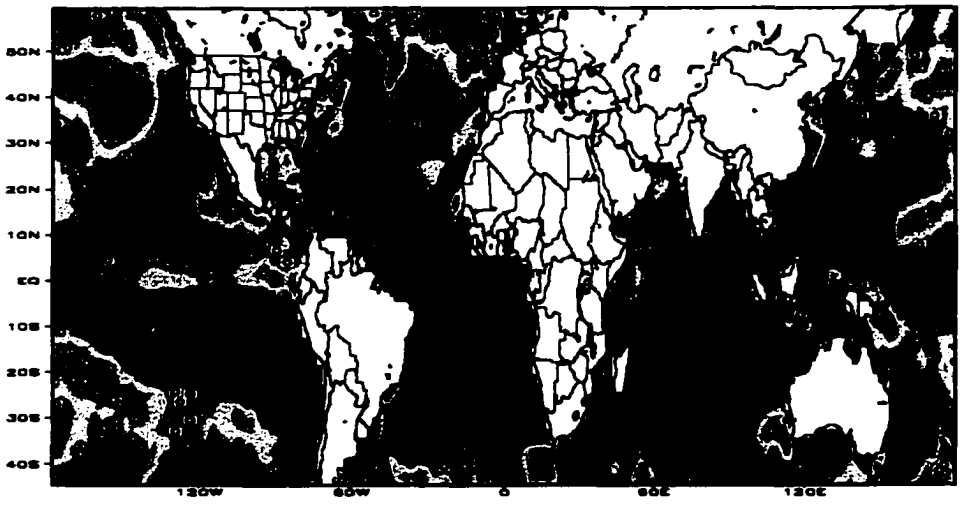

GrADS: COLA/IGES 1998-10-24-00:23

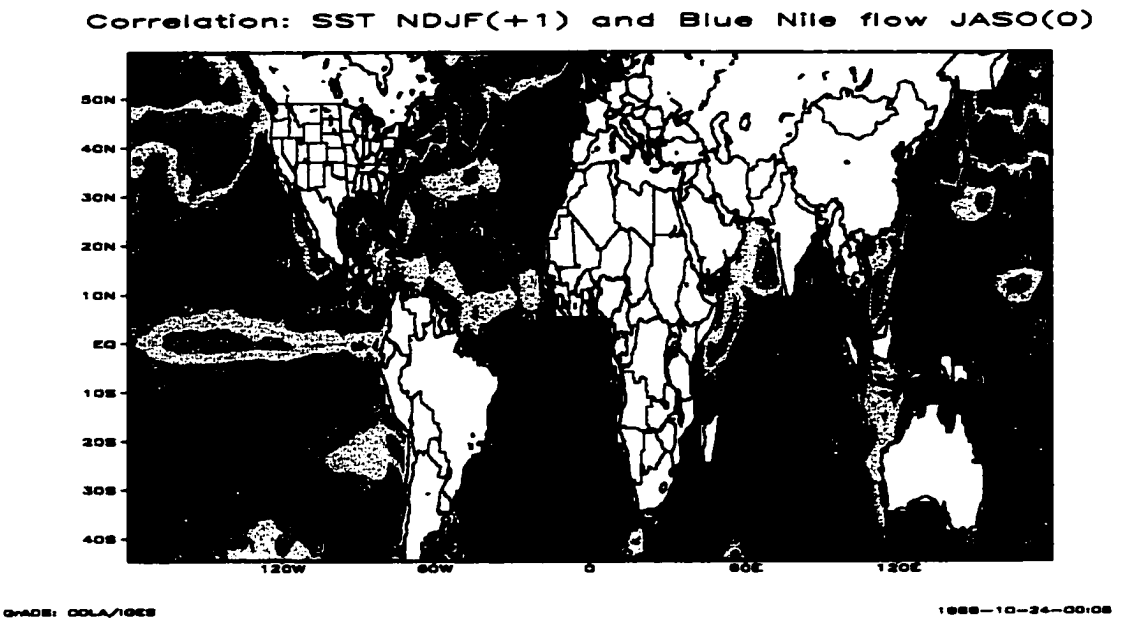

Fig. A_2 Cont.

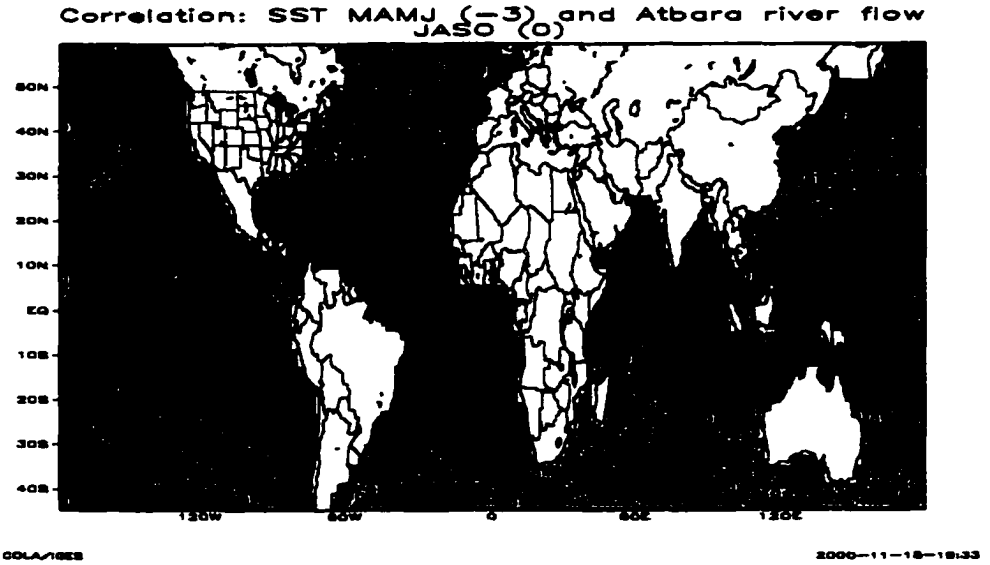

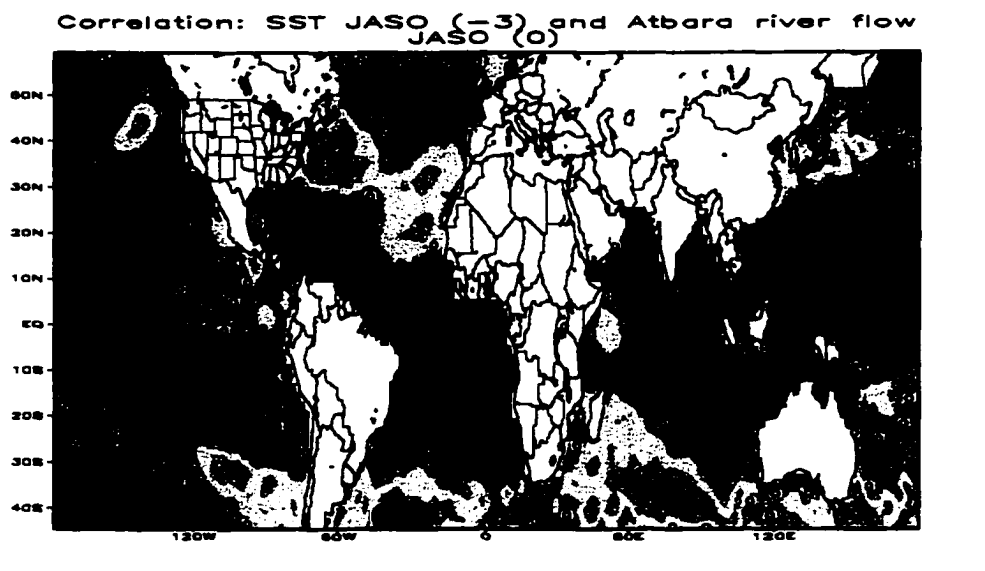

Fig. A_3 Correlation maps for the Atbara River flows (July to October) and the SST at various lead seasons shown at the top of each graphs

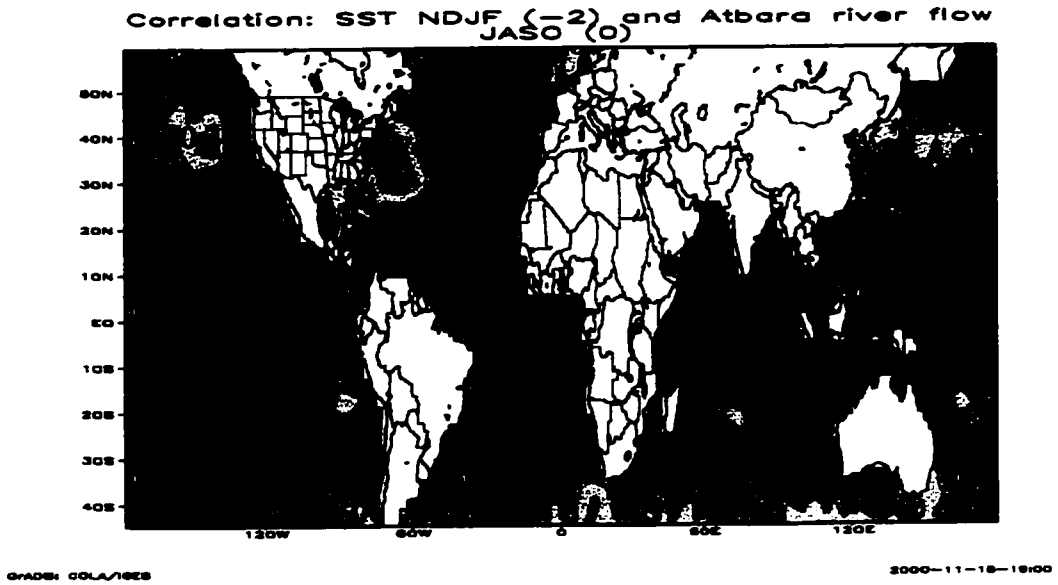

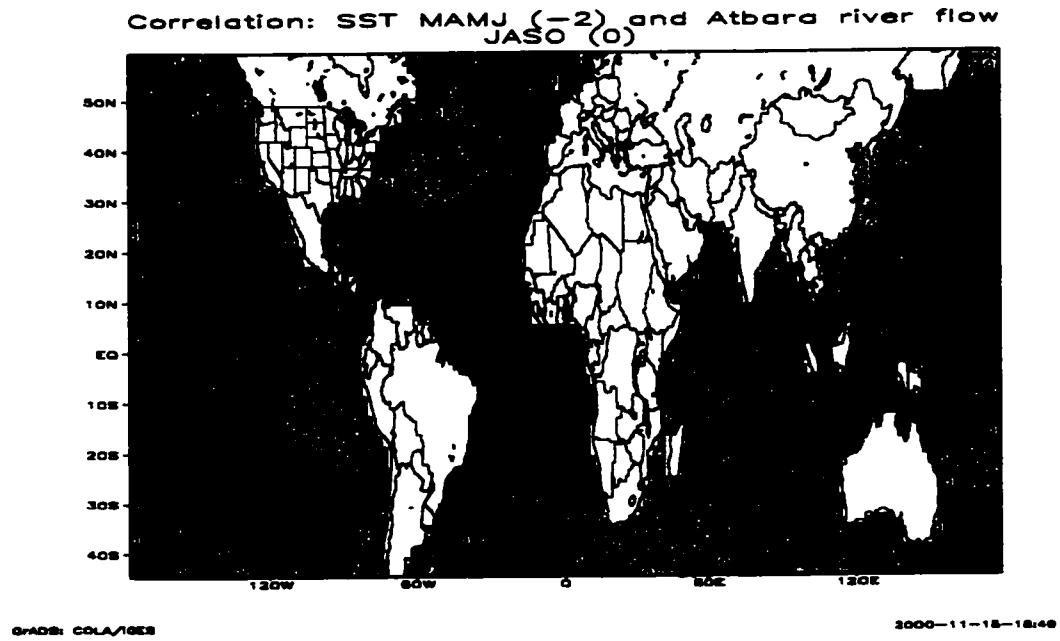

Fig. A_3 Cont.

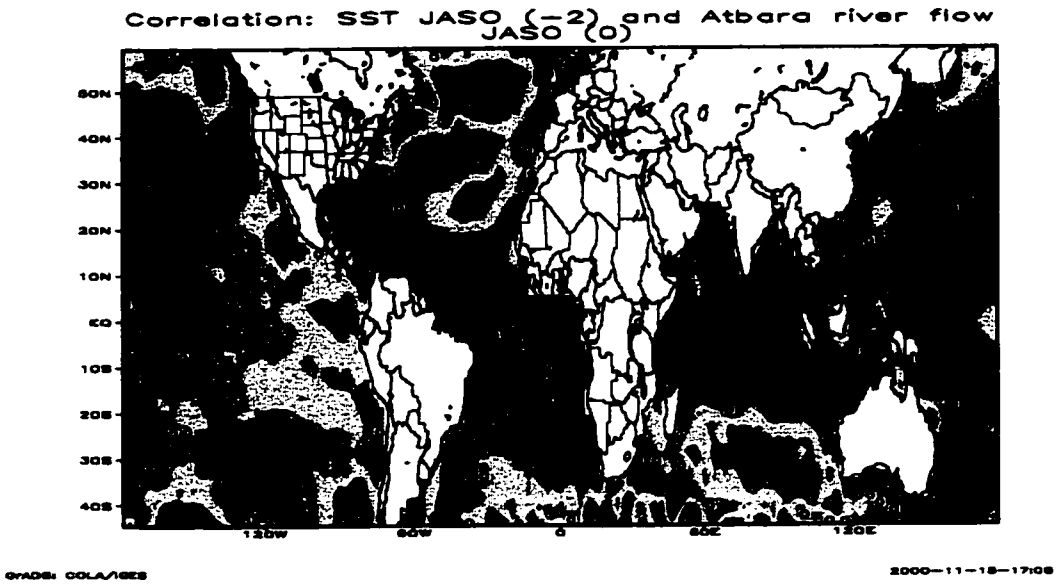

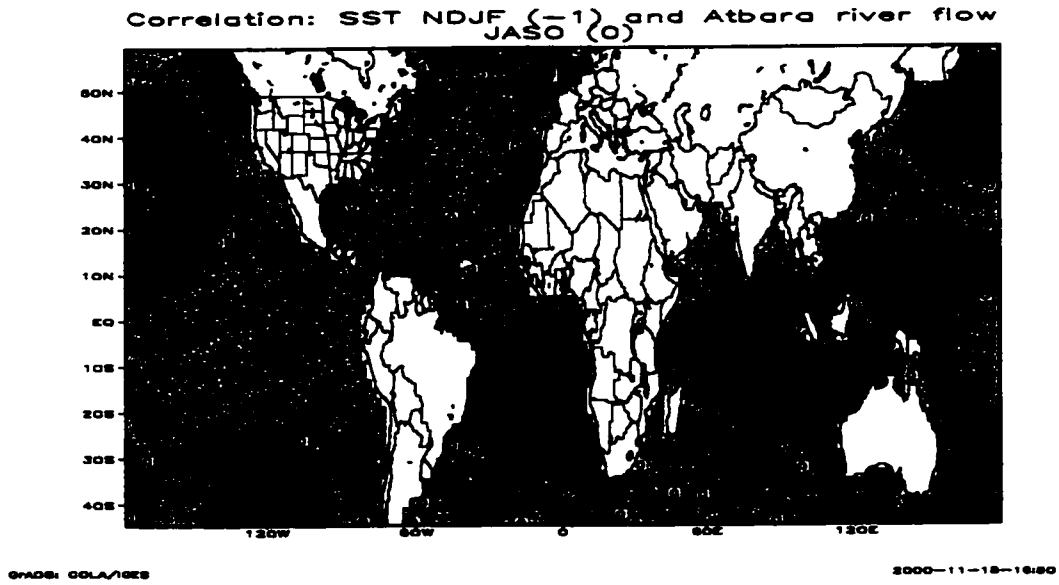

Fig. A_3 Cont.

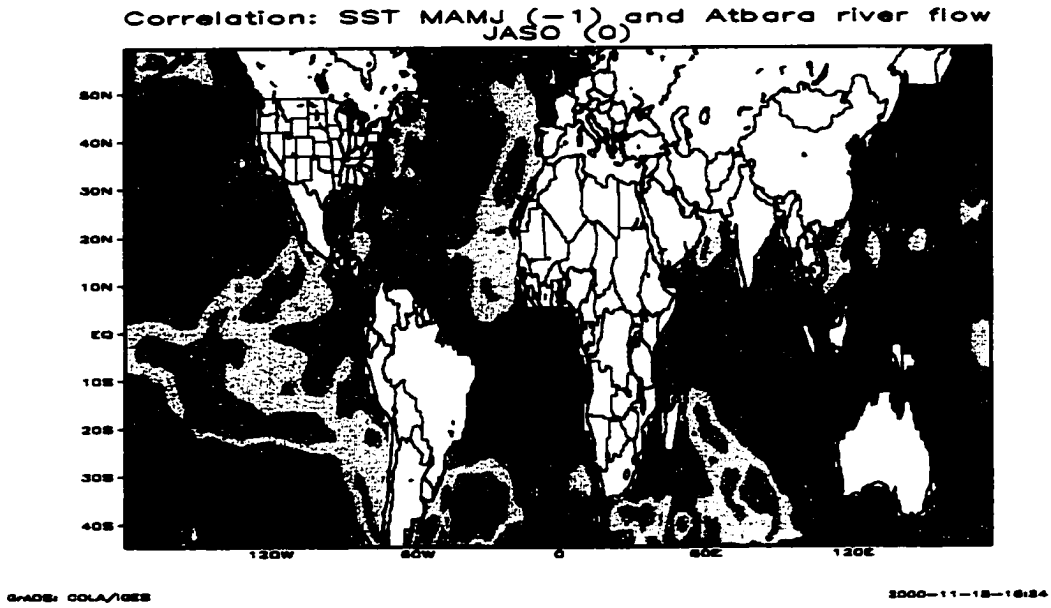

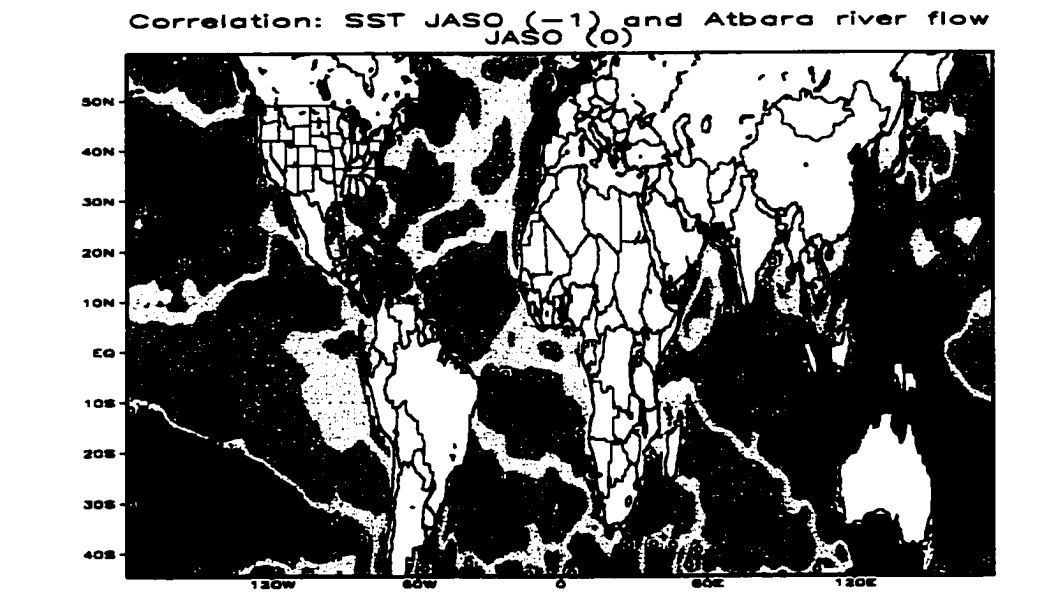

Fig. A_3 Cont.

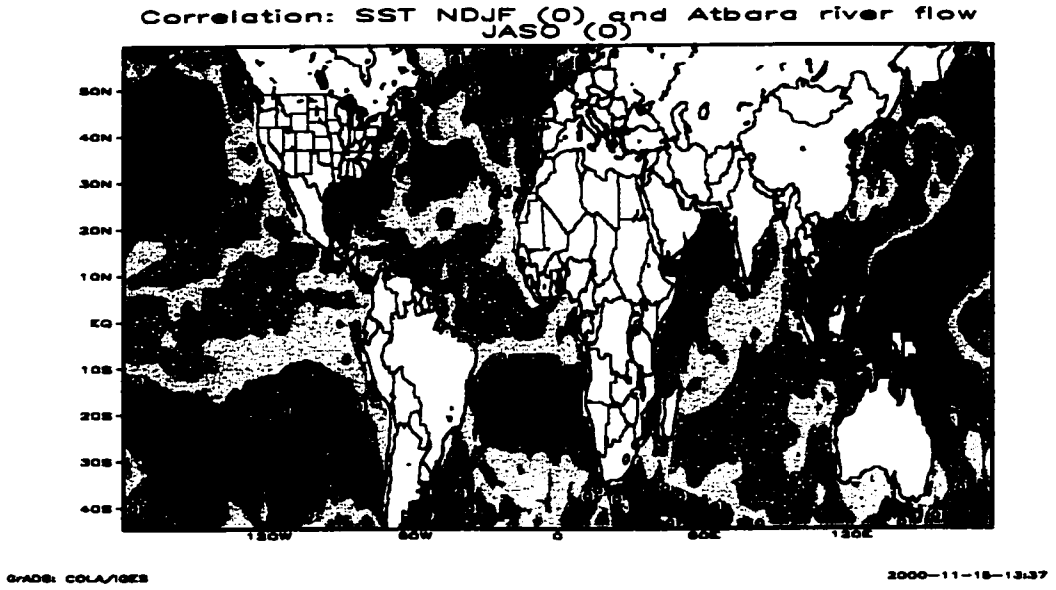

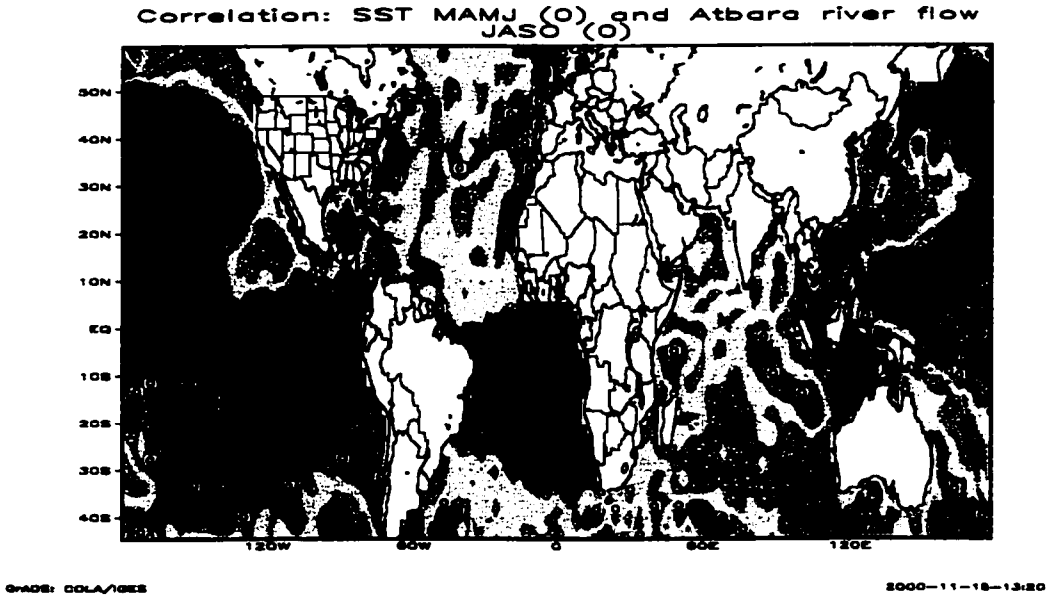

Fig. A_3 Cont.

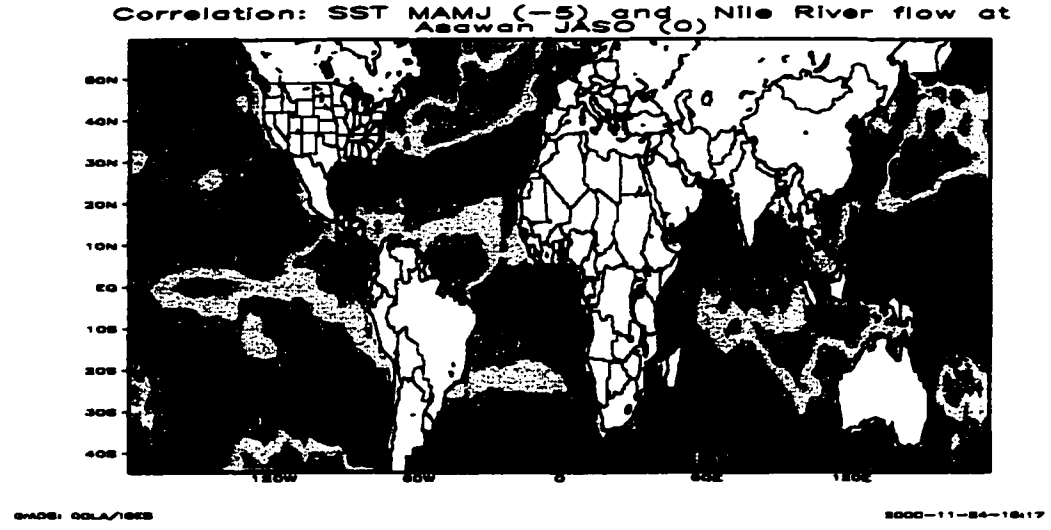

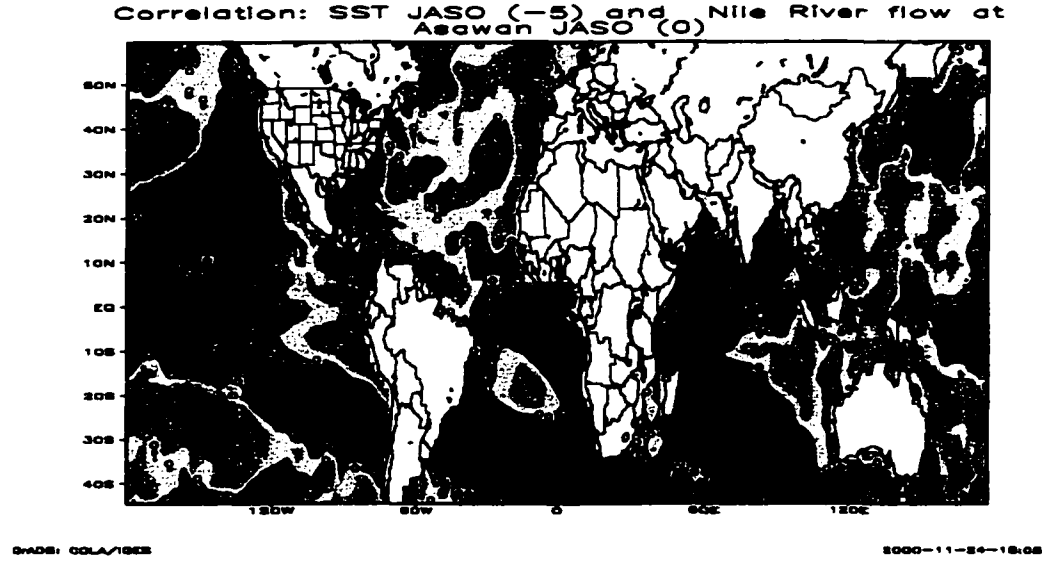

Fig. A_4 Correlation maps for the Main Nile River flows at Aswan (July to October) and SST at various lead seasons shown at the top of each graphs

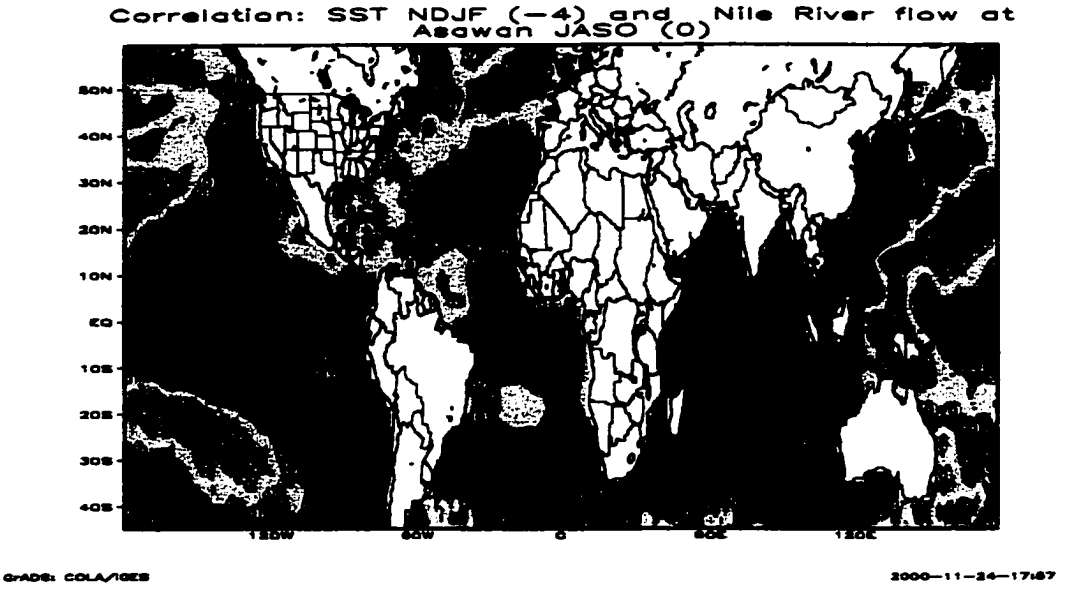

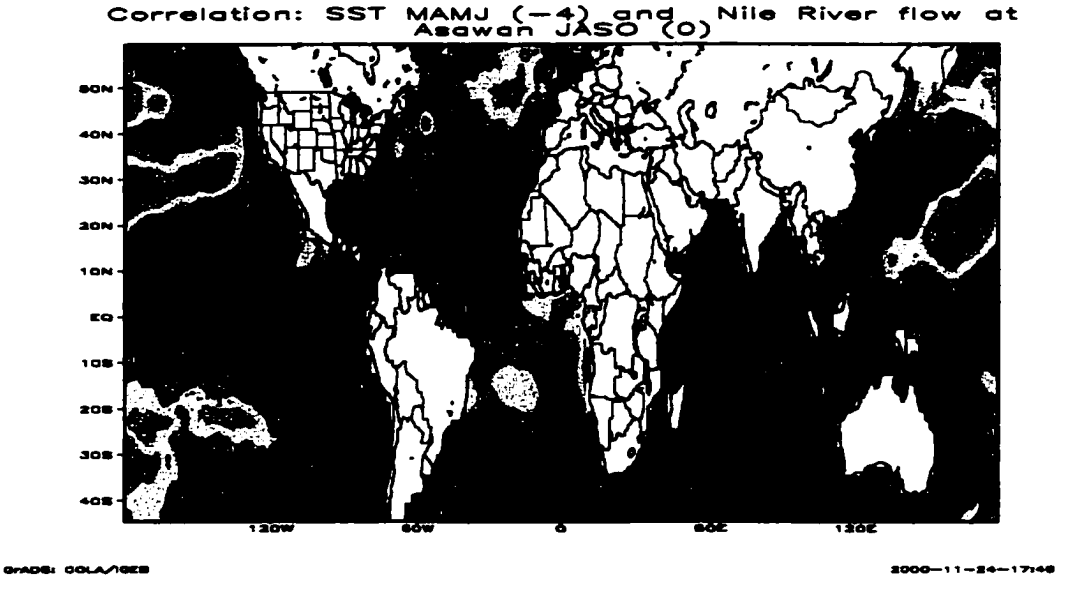

Fig. A_4 Cont.

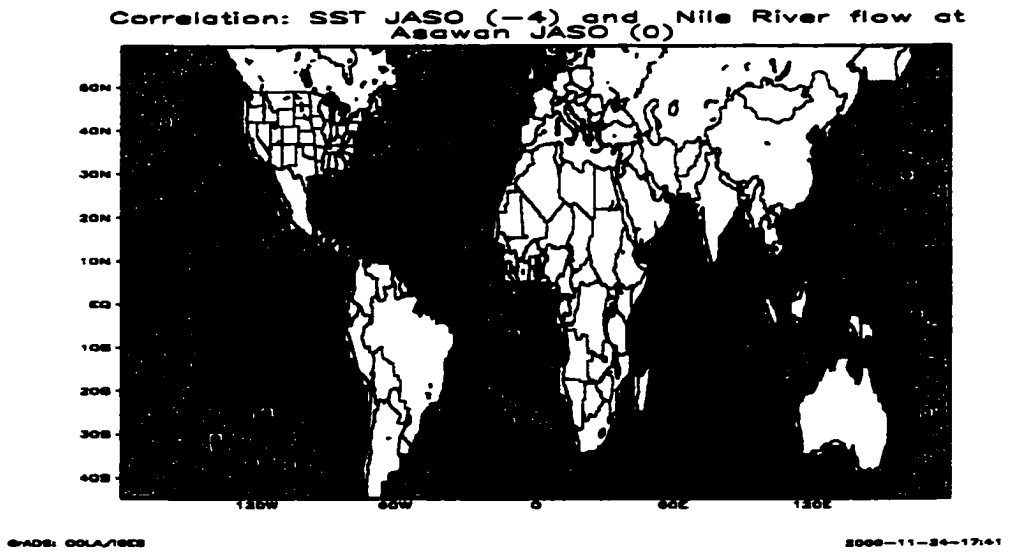

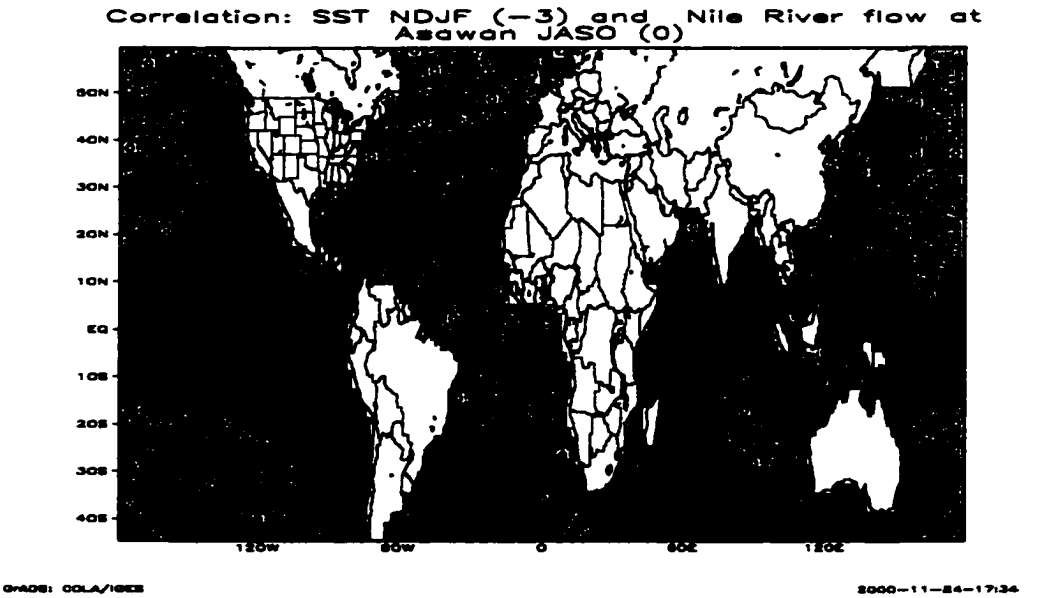

Fig. A_4 Cont.

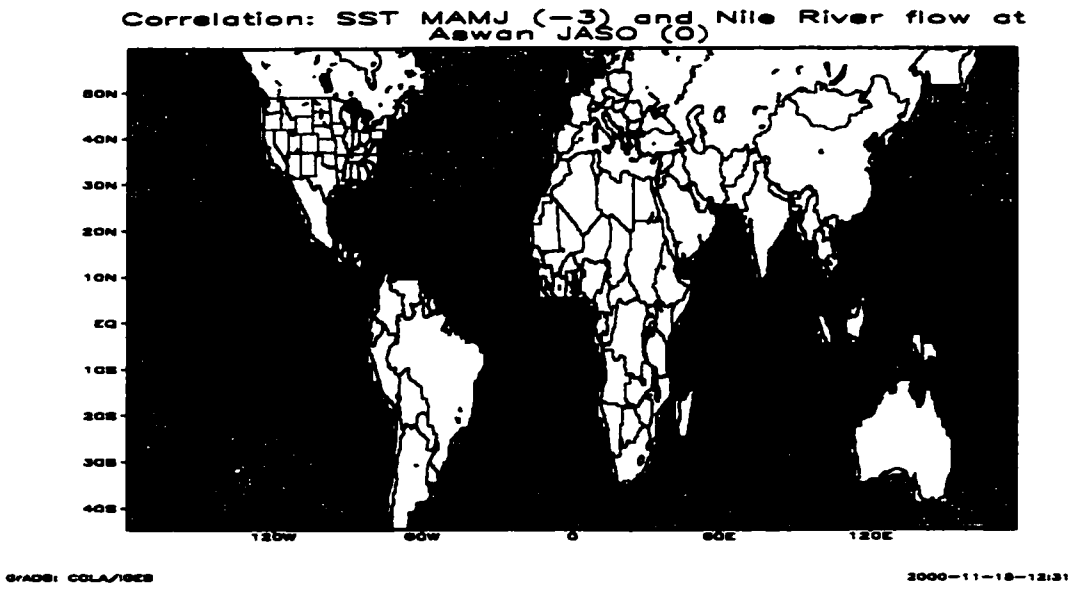

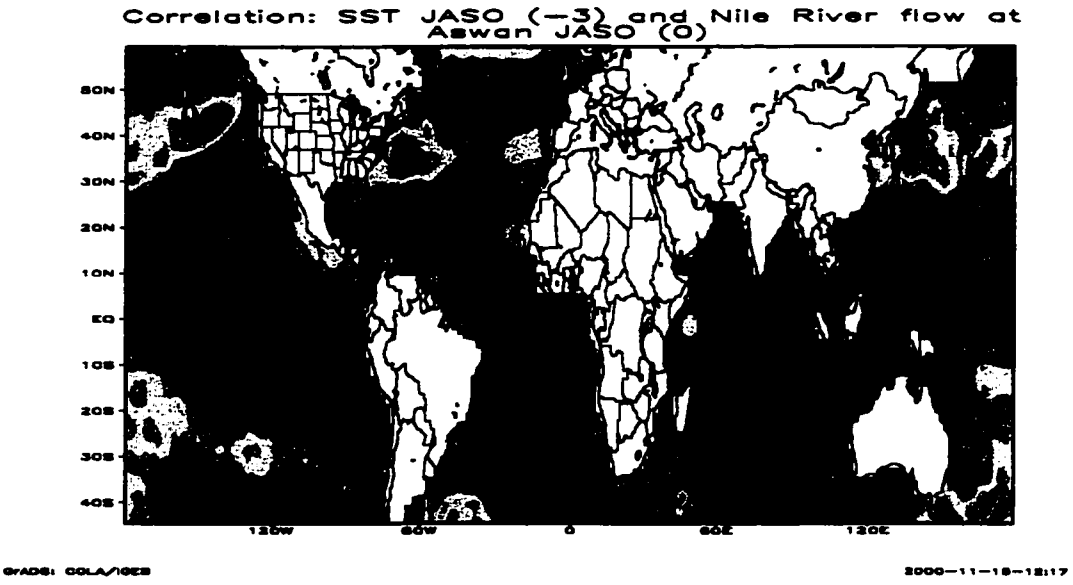

Fig. A_4 Cont.

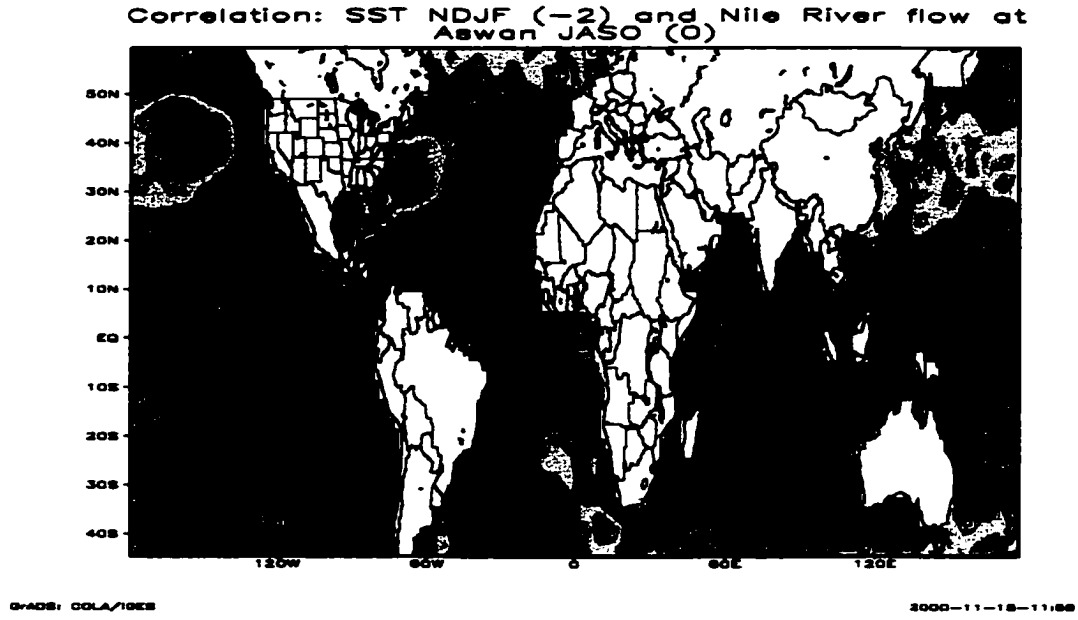

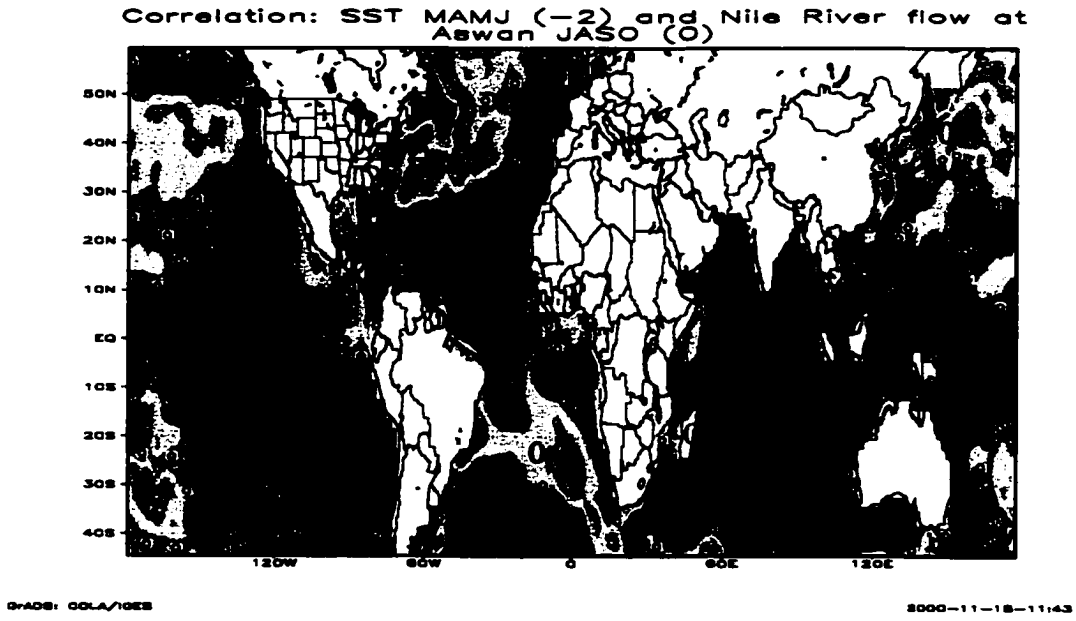

Fig. A_4 Cont.

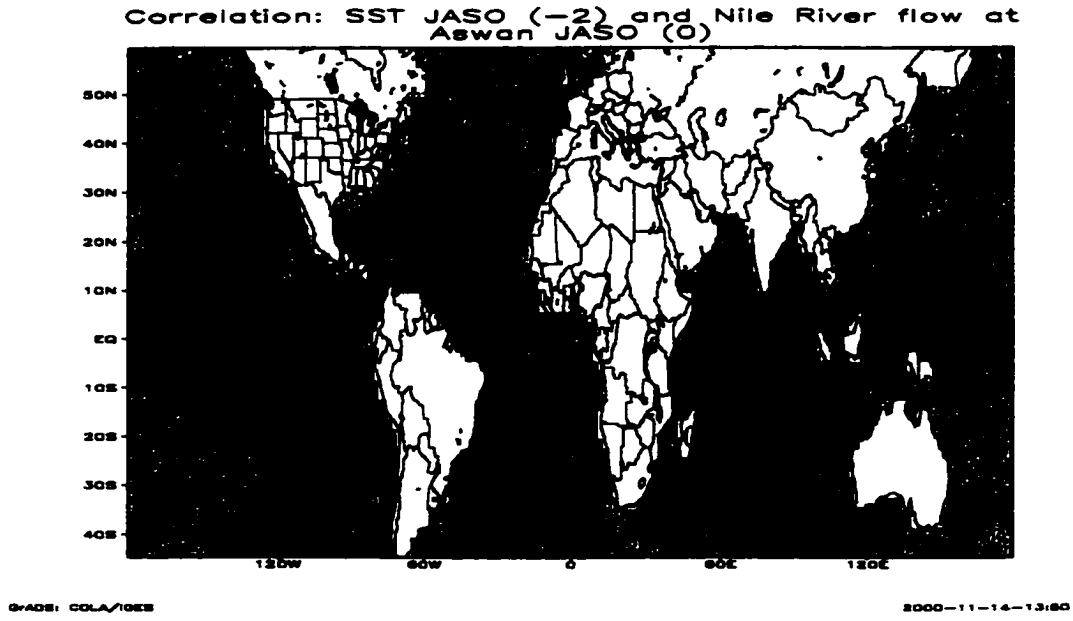

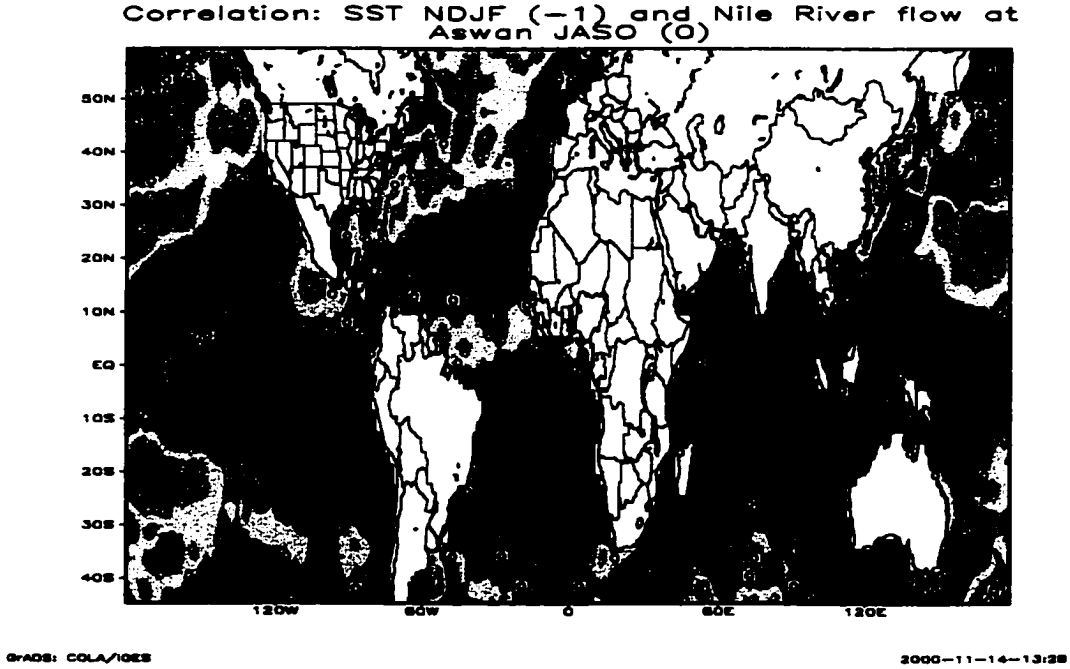

Fig. A_4 Cont.

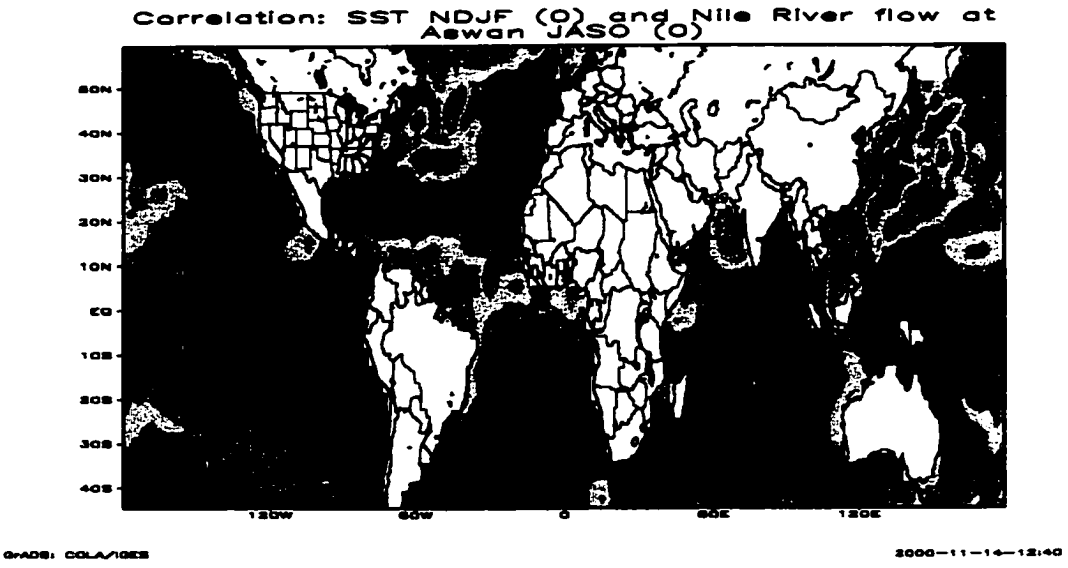

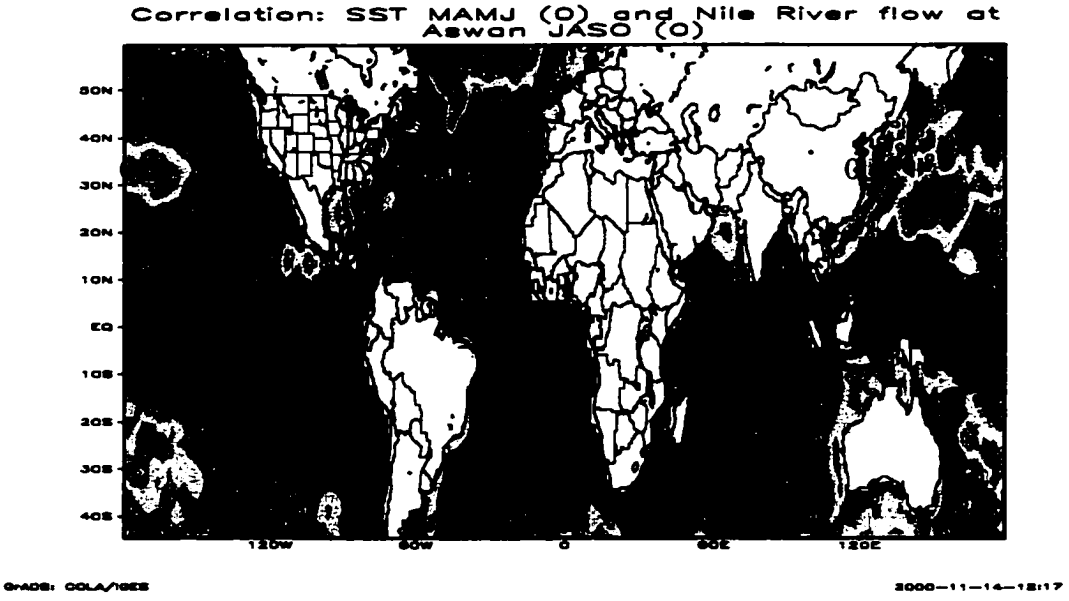

Fig. A_4 Cont.

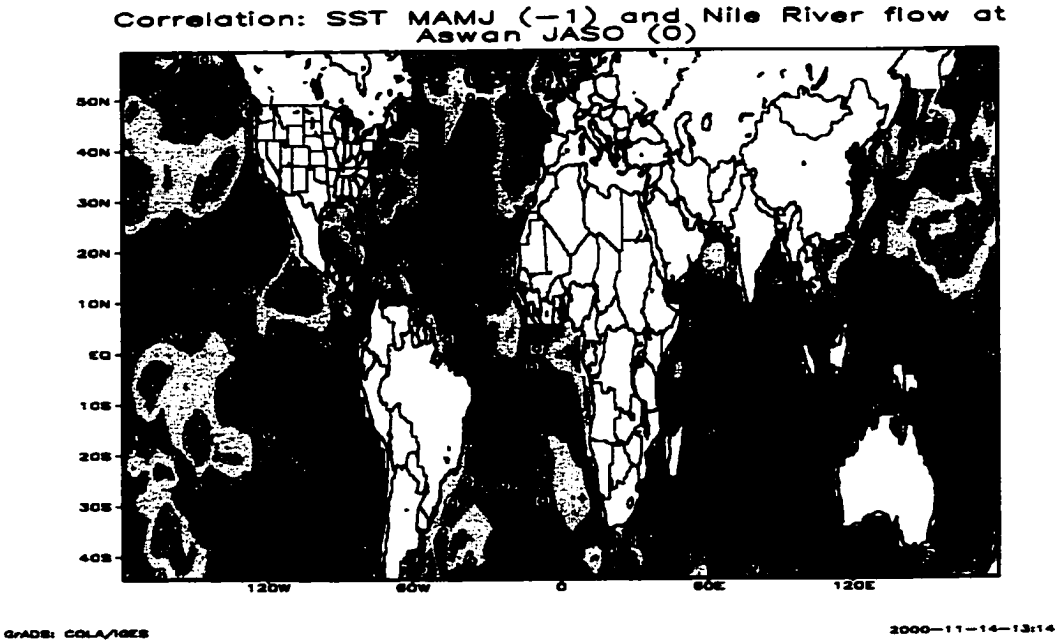

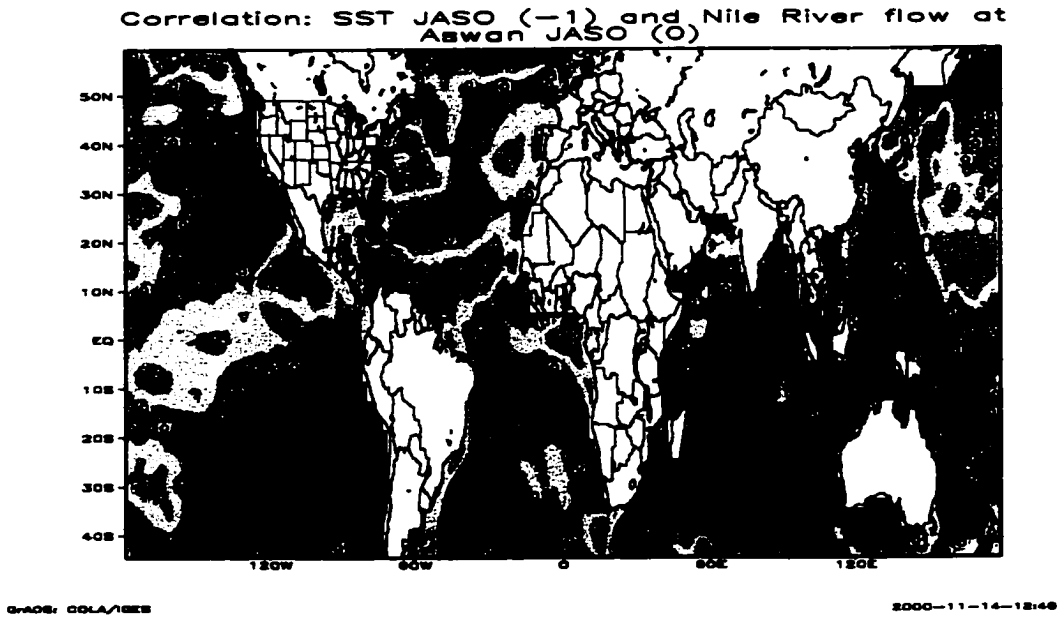

Fig. A_4 Cont.

APPENDIX B

TABLES OF PREDICTORS FOR THE NILE RIVER AND IT'S TRIBUTARIES USED IN TABLES 5-5, 5-6, 5-7 and 5-8

Appendix B_1 Locations of the stable predictors and their respective correlation coefficient with the Sobat River flows for (JASO) for various leading seasons for the models developed in Tables 5-5.

NO.	LEAD-SEASON	LOCATION	LATITUDE	LONGITUDE	CORR	LOCATION	LATITUDE	LONGITUDE	CORR	SEESAW CORR.
1	February (-3)	N. .P. Pattern	65° N→30° N	100° E→140° W	-0.36					
2	April (-3)	P. Delgada			-0.42					
3	July (-3)	NAO1_stdG			-0.41					
4	JASO (-3)	Pacific	35° S	145° W	-0.47	Indian	00°	50° E	0.35	-0.56
5	JASO (-3)	Atlantic	00°	00°	-0.42					
6	JASO (-3)	Indian	00°	50° E	0.35					
7	OND (-3)	S. Atlantic	00° →20° S	30° W→10° E	0.44	Atlantic	40° N→30° N	70° W→60° W	0.46	-0.54
8	January(-2)	S. Atlantic	00° →20° S	30° W→10° E	0.47					
9	NDJF (-2)	Indian	05° N→05° S	20° W→05° E	0.51					
10	NDJF (-2)	Atlantic	40° N	30° W	-0.37	Atlantic	05° N→05° S	20° W→05° E	0.51	-0.54
11	NDJF (-2)	Atlantic	40° N	30° W	-0.37	Atlantic	25° N	70° W	0.44	-0.52
12	MAMJ (-2)	Atlantic	40° N	30° W	-0.37	Atlantic	10° S	20° W	0.39	-0.53
13	MAMJ (-2)	Atlantic	40° N	30° W	-0.42					
14	MAMJ (-2)	Atlantic	10° S	20° W	0.39					
15	MAMJ (-2)	Pacific	40° S	150° E	0.41					
16	MAMJ (-2)	Indian	00° →10° S	40° W→20° W	0.37					
17	June (-2)	Jakarta-SLP			-0.35					
18	July (-2)	SW-iceland			-0.43					
19	JASO (-2)	Pacific	30° S→40° S	179° W→165° W	0.42					
20	MAMJ (-1)	Pacific	30° S→40° S	150° W→160° W	0.44					
21	JASO (-1)	Pacific	20° N	130° W	-0.49					
22	JASO (-1)	Pacific	40° S	140° E	-0.60					

Appendix B_1 (Cont.)

NO.	LEAD-SEASON	LOCATION	LATITUDE	LONGITUDE	CORR	LOCATION	LATITUDE	LONGITUDE	CORR	SEESAW CORR.
23	NDJF (0)	Indian	20° S	60° E	-0.33	Pacific	50° N	160° E	0.43	-0.48
24	NDJF (0)	Indian	20° S	60° E	-0.33					
25	NDJF (0)	Pacific	25° S	90° W	-0.36					
26	NDJF (0)	Pacific	50° N	160° E	0.43					
27	MAMJ (0)	Indian	08° S→18° S	55° E→65° E	-0.38					
28	April (0)	Jakarta			-0.40					
29	MAMJ (0)	Indian	08° S→18° S	55° E→65° E	-0.38	Pacific	20° S	165° E	0.35	-0.48
30	MAMJ (0)	Pacific	10° S→20° S	90° W→100° W	-0.33	Pacific	20° S	165° E	0.35	-0.43
31	MAMJ (0)	Atlantic	00°	05° E	0.41					
32	MAMJ (0)	Indian	08° S→18° S	55° E→65° E	-0.38					

Appendix B_2 Locations of the stable predictors and their respective correlation coefficient with the Blue Nile River flows for (JASO) for various leading seasons for the models developed in Tables 5-6.

NO.	LEAD-SEASON	LOCATION	LATITUDE	LONGITUDE	CORR	LOCATION	LATITUDE	LONGITUDE	CORR	SEESAW CORR.
1	February (-3)	Jakarta			-0.55					
2	MAMJ (-3)	Atlantic	8 S-12 S	00° →05° E	-0.39	Pacific	50° N→30° N	135° E→179° E	0.37	-0.48
3	MAMJ (-3)	Atlantic	8 S-12 S	00° →05° E	-0.39	Pacific	20° S→30° S	170° W→145° W	0.48	-0.59
4	MAMJ (-3)	Atlantic	8 S-12 S	00° →05° E	-0.39	Pacific	40° N→30° N	179° W→155° W	0.42	-0.57
5	MAMJ (-3)	Pacific	00° →15° S	150° E→165° E	-0.39	Pacific	20° S→30° S	170° W→145° W	0.48	-0.58
6	JASO (-3)	Pacific	08° N→00°	145° E→155° E	-0.42	Pacific	10° S→30° S	175° W→165° W	0.33	-0.49
7	JASO (-3)	Pacific	08° N→00°	145° E→155° E	-0.42	Pacific	50° N→30° N	120° E→150° E	0.43	-0.58
8	JASO (-3)	Pacific	08° N→00°	145° E→155° E	-0.42	Pacific	45° N→40° N	150° W→140° W	0.42	-0.49
9	JASO (-3)	Pacific	20° N→05° N	130° E	-0.52	Pacific	10° S→30° S	175° W→165° W	0.33	-0.62
10	JASO (-3)	Pacific	20° N→05° N	130° E	-0.52	Pacific	50° N→30° N	120° E→150° E	0.43	-0.64
11	JASO (-3)	Pacific	20° N→05° N	130° E	-0.52	Pacific	45° N→40° N	150° W→140° W	0.42	-0.52
12	JASO (-3)	Indian	10° N→05° S	85° E→95° E	-0.47	Pacific	50° N→30° N	120° E→150° E	0.43	-0.55
13	JASO (-3)	Indian	10° N→05° S	85° E→95° E	-0.47	Pacific	45° N→40° N	150° W→140° W	0.42	-0.52
14	JASO (-3)	Atlantic	30° S→40° S	15° W→00°	-0.41	Atlantic	40° N→30° N	70° W→60° W	0.47	-0.56
15	JASO (-3)	Indian	10° N→05° S	85° E→95° E	-0.47	Pacific	45° N→32° N	120° E→140° E	0.47	-0.57
16	JASO (-3)	Indian	10° N→05° S	85° E→95° E	-0.47	Pacific	45° N→40° N	160° W→140° W	0.42	-0.60
17	JASO (-3)	Pacific	08° N→00°	140° E→150° E	-0.42	Pacific	12° S→27° S	179° W→165° W	0.33	-0.53
18	JASO (-3)	Pacific	08° N→00°	140° E→150° E	-0.42	Pacific	45° N→32° N	120° E→140° E	0.47	-0.61
19	JASO (-3)	Pacific	08° N→00°	140° E→150° E	-0.42	Pacific	45° N→40° N	160° W→140° W	0.42	-0.56
20	JASO (-3)	Pacific	22° N→10° N	125° E→130° E	-0.60	Pacific	45° N→32° N	120° E→140° E	0.47	-0.60
21	JASO (-3)	Pacific	22° N→10° N	125° E→130° E	-0.60					
22	NDJF (-2)	Indian	15° S→25° S	50° E→55° E	-0.40	Pacific	45° N→35° N	160° W→140° W	0.57	-0.64

Appendix B_2 (Cont.)

NO.	LEAD-SEASON	LOCATION	LATITUDE	LONGITUDE	CORR	LOCATION	LATITUDE	LONGITUDE	CORR	SEESAW CORR.
23	NDJF (-2)	Indian	20° N→15° N	50° E→60° E	-0.33	Pacific	45° N→35° N	160° W→140° W	0.57	-0.60
24	NDJF (-2)	Indian	20° N→15° N	50° E→60° E	-0.33	Pacific	40° N→30° N	160° E→140° E	0.45	-0.53
25	NDJF (-2)	Pacific	30° S→35° S	90° W→80° W	-0.44	Pacific	45° N→35° N	160° W→140° W	0.57	-0.66
26	NDJF (-2)	Pacific	10° N→00°	148° E→155° E	-0.39	Pacific	45° N→35° N	160° W→140° W	0.57	-0.65
27	NDJF (-2)	Atlantic	30° N→20° N	90° W→75° W	0.48					
28	NDJF (-2)	Pacific	45° N→35° N	160° W→140° W	0.57					
29	NDJF (-2)	Atlantic	40° N→30° N	70° W→60° W	0.54					
30	NDJF (-2)	Pacific	50° N→35° N	160° W→140° W	0.54					
31	NDJF (-2)	Pacific	30° S→35° S	90° W→80° W	-0.44	Pacific	50° N→35° N	160° W→140° W	0.53	-0.65
32	NDJF (-2)	Pacific	30° S→35° S	90° W→80° W	-0.44	Pacific	40° N→30° N	140° E→160° E	0.45	-0.57
33	NDJF (-2)	Indian	15° S→30° S	50° E→70° E		Pacific	50° N→35° N	160° W→140° W	0.53	-0.61
34	NDJF (-2)	Pacific	10° N→00°	148° E→155° E	-0.39	Pacific	50° N→35° N	160° W→140° W	0.53	-0.63
35	NDJF (-2)	Pacific	10° N→00°	148° E→155° E	-0.39	Pacific	40° N→30° N	140° E→160° E	0.45	-0.54
36	NDJF (-2)	Indian	00° →10° S	85° E→95° E	-0.36	Pacific	50° N→35° N	160° W→140° W	0.53	-0.59
37	NDJF (-2)	Indian	00° →10° S	85° E→95° E	-0.36	Pacific	40° N→30° N	160° E→140° E	0.45	-0.51
38	NDJF (-2)	Atlantic	20° N→10° N	30° W→20° W	-0.44	Atlantic	40° N→30° N	70° W→60° W	0.46	-0.54
39	MAMJ (-2)	Atlantic	35° S→44° S	35° W→20° W	-0.36	Pacific	50° N→40° N	130° E→160° E	0.34	-0.49
40	MAMJ (-1)	Pacific	20° N→10° N	110° W→100° W	0.52					
41	MAMJ (-1)	Indian	44° S→35° S	115° E→130° E	-0.43	Pacific	20° N→10° N	110° W→100° W	0.52	-0.56
42	MAMJ (-1)	Indian	05° N→02° S	60° E→70° E	-0.31	Pacific	20° N→10° N	110° W→100° W	0.52	-0.53
43	MAMJ (-1)	Atlantic	32° N→25° N	50° W→40° W	-0.33	Atlantic	45° N→35° N	20° W→00°	0.37	-0.59
44	MAMJ (-1)	Pacific	30° S→44° S	110° W→90° W	-0.46	Pacific	20° N→10° N	110° W→100° W	0.52	-0.53

Appendix B_2 (Cont.)

NO.	LEAD-SEASON	LOCATION	LATITUDE	LONGITUDE	CORR	LOCATION	LATITUDE	LONGITUDE	CORR	SEESAW CORR.
45	MAMJ (-1)	Indian	30° S→40° S	120° E→130° E	-0.50	Pacific	20° N→10° N	110° W→100° W	0.52	-0.59
46	MAMJ (-1)	Indian	00° →05° S	120° E→130° E	-0.41	Pacific	20° N→10° N	110° W→100° W	0.52	-0.54
47	MAMJ (-1)	Indian	00° →05° S	60° E→70° E	-0.28	Pacific	20° N→10° N	110° W→100° W	0.52	-0.51
48	MAMJ (-1)	Pacific	44° S→30° S	110° W→90° W	-0.46	Pacific	20° N→10° N	110° W→100° W	0.52	-0.53
49	JASO (-1)	Indian	35° S→25° S	30° E→60° E	-0.35	Pacific	15° N→10° N	120° W→100° W	0.52	-0.55
50	JASO (-1)	Indian	00° →07° S	90° E→130° E	-0.39	Pacific	20° N→10° N	160° E→179° E	0.35	-0.48
51	JASO (-1)	Indian	00° →07° S	90° E→130° E	-0.39	Pacific	15° N→10° N	120° W→100° W	0.52	-0.52
52	JASO (-1)	Pacific	35° S→20° S	140° W→100° W	-0.43	Pacific	20° N→10° N	160° E→179° E	0.35	-0.53
53	JASO (-1)	Pacific	35° S→20° S	140° W→100° W	-0.43	Pacific	15° N→10° N	120° W→100° W	0.52	-0.60
54	JASO (-1)	Indian	35° S→25° S	30° E→60° E	-0.35	Pacific	15° N→10° N	120° W→100° W	0.52	-0.55
55	JASO (-1)	Indian	00° →07° S	90° E→130° E	-0.39	Pacific	15° N→10° N	160° E→179° E	0.35	-0.47
56	JASO (-1)	Indian	00° →07° S	90° E→130° E	-0.39	Pacific	15° N→10° N	120° W→100° W	0.52	-0.52
57	JASO (-1)	Pacific	35° S→20° S	140° W→100° W	-0.43	Pacific	15° N→10° N	160° E→179° E	0.35	-0.52
58	JASO (-1)	Pacific	35° S→20° S	140° W→100° W	-0.43	Pacific	15° N→10° N	120° W→100° W	0.52	-0.60
59	ASON (-1)	Guinea			0.63					
60	NDJF (0)	Pacific	20° S→12° S	105° W→90° W	-0.45	Pacific	50° N→20° N	120° E→160° E	0.50	-0.56
61	NDJF (0)	Pacific	25° S→40° S	80° W→75° W	-0.45	Pacific	50° N→20° N	120° E→160° E	0.50	-0.56
62	NDJF (0)	Pacific	20° S→12° S	105° W→90° W	-0.45	Indian	22° N→10° N	110° E→115° E	0.47	-0.66
63	NDJF (0)	Pacific	40° S→25° S	80° W→75° W	-0.45	Indian	22° N→10° N	110° E→115° E	0.47	-0.62
64	NDJF (0)	Pacific	20° S→12° S	105° W→90° W	-0.45	Pacific	50° N→20° N	120° E→160° E	0.50	-0.62
65	NDJF (0)	Pacific	40° S→25° S	80° W→75° W	-0.45	Pacific	50° N→20° N	120° E→160° E	0.50	-0.62
66	NDJF (0)	Pacific	50° N→42° N	155° W→145° W	-0.40	Pacific	50° N→20° N	120° E→160° E	0.50	-0.58

Appendix B_2 (Cont.)

NO.	LEAD-SEASON	LOCATION	LATITUDE	LONGITUDE	CORR	LOCATION	LATITUDE	LONGITUDE	CORR	SEESAW CORR.
67	NDJF (0)	Pacific	20° S→12° S	105° W→90° W	-0.45	Pacific	50° N→20° N	120° E→160° E	0.50	-0.56
68	NDJF (0)	Pacific	40° S→25° S	80° W→75° W	-0.45	Pacific	50° N→20° N	120° E→160° E	0.50	-0.56
69	NDJF (0)	Pacific	20° S→12° S	105° W→90° W	-0.45	Atlantic	10° N→00°	60° W→40° W		-0.56
70	AprMay(0)	Darwin	12° S	131° E	-0.50					
71	AMJ (0)	Jakarta			-0.59					
72	AMJ (0)	SOI			0.44					
73	AMJ (0)	CTI (SST)	06° N→06° S	180° W→90° W	-0.58					
74	MayJun (0)	G. Tropics	10° N→10° S	00° →360°	-0.53					
75	MAMJ (0)	Pacific	05° N→05° S	130° W→90° W	-0.55					
76	MAMJ (0)	Pacific	05° N→20° S	120° W→80° W	-0.52					
77	MAMJ (0)	Pacific	30° N→25° N	140° E→160° E	0.57					
78	MAMJ (0)	Pacific	10° S→20° S	100° W→90° W	-0.49	Pacific	20° S	165° E	0.31	-0.53
79	MAMJ (0)	Indian	30° S→40° S	30° E→65° E	-0.46	Pacific	30° N→25° N	140° E→160° E	0.55	-0.67
80	MAMJ (0)	Indian	30° S→40° S	30° E→65° E	-0.46	Pacific	38° N→30° N	179° W→165° W	0.40	-0.58
81	MAMJ (0)	Pacific	02° N→05° S	130° W→90° W	-0.52	Pacific	30° N→25° N	140° E→160° E	0.55	-0.69
82	MAMJ (0)	Pacific	02° N→05° S	130° W→90° W	-0.52	Pacific	38° N→30° N	179° W→165° W	0.40	-0.59
83	MAMJ (0)	Pacific	02° N→05° S	120° W→80° W	-0.52	Pacific	30° N→25° N	140° E→160° E	0.55	-0.67
84	MAMJ (0)	Pacific	02° N→05° S	120° W→80° W	-0.52	Pacific	38° N→30° N	179° W→165° W	0.40	-0.55
85	MAMJ (0)	Pacific	02° N→20° S	120° W→80° W	-0.51	Pacific	30° N→25° N	140° E→160° E	0.55	-0.67
86	MAMJ (0)	Pacific	02° N→20° S	120° W→80° W	-0.51	Pacific	35° N→25° N	179° W→165° W	0.34	-0.54
87	MAMJ (0)	Pacific	02° N→20° S	120° W→80° W	-0.51	Pacific	20° S→35° S	179° W→160° W	0.37	-0.57
88	MAMJ (0)	Pacific	02° N→05° S	130° W→90° W	-0.52	Pacific	30° N→25° N	140° E→160° E	0.55	-0.69

Appendix B_2 (Cont.)

NO.	LEAD-SEASON	LOCATION	LATITUDE	LONGITUDE	CORR	LOCATION	LATITUDE	LONGITUDE	CORR	SEESAW CORR.
89	MAMJ (0)	Pacific	02° N→05° S	130° W→90° W	-0.52	Pacific	35° N→25° N	179° W→160° W	0.40	-0.57
90	MAMJ (0)	Pacific	02° N→05° S	130° W→90° W	-0.52	Pacific	20° S→35° S	179° W→160° W	0.44	-0.58
91	MAMJ (0)	Indian	30° S→40° S	30° E→65° E	-0.46	Pacific	30° N→25° N	140° E→160° E	0.55	-0.64
92	MAMJ (0)	Pacific	02° N→05° S	130° W→90° W	-0.52	Indian	10° S→20° S	110° E→125° E	0.41	-0.60
93	MAMJ (0)	Pacific	02° N→05° S	120° W→80° W	-0.51	Indian	10° S→20° S	110° E→125° E	0.41	-0.63

Appendix B_3 Locations of the stable predictors and their respective correlation coefficient with the Atbara River flows for (JASO) for various leading seasons for the models developed in Tables 5-7.

NO.	LEAD-SEASON	LOCATION	LATITUDE	LONGITUDE	CORR	LOCATION	LATITUDE	LONGITUDE	CORR	SEESAW CORR.
1	MAMJ (-3)	Atlantic	02° N→00°	35° W→30° W	-0.39	Atlantic	44° S	30° W	0.36	-0.48
2	MAMJ (-3)	Atlantic	05° N→12° S	05° W→00°	-0.54	Atlantic	44° S	30° W	0.36	-0.58
3	MAMJ (-3)	Atlantic	08° S→12° S	00° →05° E	-0.49	Atlantic	44° S	30° W	0.36	-0.59
4	MAMJ (-3)	Pacific	20° N→05° N	150° E→160° E	-0.49	Indian	30° S→35° S	70° E→80° E	0.41	-0.53
5	MAMJ (-3)	Pacific	54° N→48° N	179° W→170° W	-0.44	Pacific	28° S→38° S	150° W→100° W	0.35	-0.47
6	MAMJ (-3)	Pacific	20° N→05° N	150° E→160° E	-0.49	Pacific	28° S→38° S	150° W→100° W	0.35	-0.54
7	MAMJ (-3)	Pacific	22° N→15° N	170° E→150° W	-0.49	Indian	30° S→35° S	70° E→80° E	0.41	-0.56
8	MAMJ (-3)	Pacific	22° N→15° N	170° E→150° W	-0.49	Pacific	28° S→38° S	150° W→100° W	0.35	-0.52
9	MAMJ (-3)	Atlantic	05° N→12° S	05° W→00°	-0.54					
10	MAMJ (-3)	Atlantic	08° S→12° S	00° →05° E	-0.49					
11	MAMJ (-3)	Pacific	20° N→05° N	150° E→160° E	-0.49					
12	MAMJ (-3)	Pacific	22° N→15° N	170° E→150° W	-0.49					
13	JASO (-3)	Pacific	20° N→05° N	150° E→160° E	-0.49	Indian	35° S→40° S	60° E→90° E	0.33	-0.53
14	JASO (-3)	Pacific	20° N→10° N	130° E→170° E	-0.51	Indian	35° S→40° S	60° E→90° E	0.33	-0.48
15	JASO (-3)	Atlantic	38° S→44° S	40° W→20° W	-0.40					
16	JASO (-3)	Pacific	25° N→20° N	170° E→150° W	-0.47					
17	JASO (-3)	Pacific	20° N→10° N	130° E→170° E	-0.51					
18	NDJF (-2)	Atlantic	20° N→10° N	30° W→20° W	-0.44					
19	NDJF (-2)	Pacific	25° N→18° N	160° W→140° W	-0.37					
20	NDJF (-2)	Pacific	20° N→10° N	150° E→179° E	-0.42					
21	NDJF (-2)	Atlantic	20° N→10° N	30° W→20° W	-0.44	Atlantic	40° N→30° N	70° W→60° W	0.46	-0.59
22	January (-2)	Ponta Delgada			0.62					

Appendix B_3 (Cont.)

NO.	LEAD-SEASON	LOCATION	LATITUDE	LONGITUDE	CORR	LOCATION	LATITUDE	LONGITUDE	CORR	SEESAW CORR.
23	MAMJ (-2)	Atlantic	25° N→15° N	25° W→15° W	-0.35	Atlantic	45° N→35° N	65° W→50° W	0.47	-0.62
24	JASO (-2)	Indian	30° S	90° E	0.41					
25	NDJF (-1)	Pacific	30° S→40° S	90° W→75° W	0.36					
26	NDJF (-1)	Pacific	50° N→35° N	170° E→160° W	-0.34					
27	NDJF (-1)	Pacific	50° N→35° N	170° E→160° W	-0.34	Pacific	30° S→40° S	90° W→75° W	0.36	-0.41
28	MAMJ (-1)	Pacific	35° S→44° S	120° W→100° W	-0.46	Indian	35° S	80° E	0.37	-0.56
29	MAMJ (-1)	Atlantic	35° S→40° S	50° W→30° W	0.56					
30	MAMJ (-1)	Indian	35° S	80° E	0.37					
31	AMJ (-1)	Tahiti	18° S	150° W	-0.58					
32	ASO (-1)	Tahiti	18° S	150° W	-0.52					
33	JASO (-1)	Atlantic	12° N	35° W	0.50					
34	JASO (-1)	Pacific	25° S→35° S	150° W→130° W	-0.64					
35	JASO (-1)	Pacific	25° S→35° S	150° W→130° W	-0.64	Indian	25° S→35° S	30° E→60° E	0.34	-0.58
36	JASO (-1)	Pacific	25° S→35° S	150° W→130° W	-0.64	Pacific	10° N	110° W	0.45	-0.63
37	JASO (-1)	Pacific	25° S→35° S	150° W→130° W	-0.64	Pacific	59° N→54° N	179° E→140° E	0.38	-0.64
38	JASO (-1)	Pacific	25° S→35° S	150° W→130° W	-0.64	Pacific	15° N→10° N	120° W→100° W	0.45	-0.64
39	NDJF (0)	Pacific	45° N→35° N	160° W→140° W	-0.41	Pacific	10° N	115° E	0.52	-0.54
40	MAMJ (0)	Pacific	10° S→20° S	110° E→125° E	0.46					
41	MayJun (0)	Jakarta-SLP			-0.51					
42	April (0)	NH(00°, 90°)			0.45					
43	MayJun (0)	Darwin	12° S	131° E	-0.50					

Appendix B_4 Locations of the stable predictors and their respective correlation coefficient with the Nile River flows at Aswan for (JASO) for various leading seasons for the models developed in Tables 5-8.

NO.	LEAD-SEASON	LOCATION	LATITUDE	LONGITUDE	CORR	LOCATION	LATITUDE	LONGITUDE	CORR	SEESAW CORR.
1	MAMJ (-3)	Atlantic	08° S→12° S	00° →05° E	-0.37	Pacific	20° S→30° S	170° W→145° W	0.48	-0.57
2	MAMJ (-3)	Pacific	00° →15° S	150° E→165° E	-0.33	Pacific	20° S→30° S	170° W→145° W	0.48	-0.54
3	MAMJ (-3)	Pacific	00° →15° S	150° E→165° E	-0.33	Pacific	40° N→30° N	179° W→155° W	0.40	-0.45
4	JASO (-3)	Pacific	08° N→00°	140° E→150° E	-0.42	Pacific	12° S→27° S	179° W→165° W	0.32	-0.48
5	JASO (-3)	Pacific	08° N→00°	140° E→150° E	-0.42	Pacific	45° N→32° N	120° E→140° E	0.48	-0.60
6	JASO (-3)	Indian	10° N→05° S	85° E→95° E	-0.43	Pacific	45° N→32° N	120° E→140° E	0.48	-0.56
7	JASO (-3)	Pacific	45° N→32° N	120° E→140° E	0.48					
8	JASO (-3)	Pacific	20° N→05° N	130° E	-0.44	Pacific	10° S→30° S	175° W→165° W		-0.56
9	JASO (-3)	Pacific	20° N→05° N	130° E	-0.44	Pacific	50° N→30° N	120° E→150° E	0.45	-0.62
10	JASO (-3)	Indian	10° N→05° S	85° E→95° E	-0.43	Pacific	50° N→30° N	120° E→150° E	0.45	-0.54
11	JASO (-3)	Pacific	08° N→00°	145° E→155° E	-0.42	Pacific	10° S→30° S	175° W→165° W		-0.46
12	JASO (-3)	Pacific	08° N→00°	145° E→155° E	-0.42	Pacific	50° N→30° N	120° E→150° E	0.45	-0.58
13	NDJF (-2)	Atlantic	30° N→20° N	90° W→75° W	0.47					
14	NDJF (-2)	Atlantic	40° N→30° N	70° W→60° W	0.57					
15	NDJF (-2)	Indian	20° N→15° N	50° E→60° E	-0.38					
16	NDJF (-2)	Atlantic	30° N→20° N	30° W→20° W	-0.37	Atlantic	40° N→30° N	70° W→60° W	0.57	-0.61
17	NDJF (-2)	Indian	15° S→25° S	50° E→55° E	-0.38	Pacific	45° N→35° N	160° W→140° W	0.54	-0.61
18	NDJF (-2)	Indian	20° N→15° N	50° E→60° E	-0.38	Pacific	45° N→35° N	160° W→140° W	0.54	-0.60
19	NDJF (-2)	Indian	20° N→15° N	50° E→60° E	-0.38	Pacific	40° N→30° N	160° W→140° W	0.38	-0.51
20	NDJF (-2)	Pacific	30° S→35° S	90° W→80° W	-0.39	Pacific	45° N→35° N	160° W→140° W	0.54	-0.61
21	NDJF (-2)	Pacific	10° N→00°	148° E→155° E	-0.40	Pacific	45° N→35° N	160° W→140° W	0.54	-0.62
22	NDJF (-2)	Pacific	10° N→00°	148° E→155° E	-0.40	Pacific	40° N→30° N	140° E→160° E	0.38	-0.50

Appendix B_4 (Cont.)

NO.	LEAD-SEASON	LOCATION	LATITUDE	LONGITUDE	CORR	LOCATION	LATITUDE	LONGITUDE	CORR	SEESAW CORR.
23	NDJF (-2)	Pacific	45° N→35° N	160° W→140° W	0.54					
24	NDJF (-2)	Pacific	30° S→35° S	90° W→80° W	-0.39	Pacific	50° N→35° N	160° W→140° W	0.38	-0.60
25	NDJF (-2)	Pacific	10° N→00°	148° E→155° E	-0.40	Pacific	40° N→30° N	140° E→160° E	0.38	-0.50
26	NDJF (-2)	Indian	00° →10° S	85° E→95° E	-0.33	Pacific	50° N→35° N	160° W→140° W	0.38	-0.55
27	NDJF (-2)	Indian	00° →10° S	85° E→95° E	-0.33	Pacific	40° N→30° N	140° E→160° E	0.39	-0.45
28	JASO (-2)	Pacific	10° N→00°	140° E→150° E	-0.31	Pacific	30° S→40° S	170° W→160° W	0.43	-0.54
29	NDJF (-1)	Pacific	10° N→00°	120° E→160° E	-0.36	Pacific	15° S→25° S	175° W→165° W	0.43	-0.64
30	MAMJ (-1)	Indian	30° S→40° S	120° E→130° E	-0.46	Pacific	20° N→10° N	110° W→100° W	0.43	-0.52
31	MAMJ (-1)	Indian	00° →05° S	120° E→150° E	-0.43	Pacific	20° N→10° N	110° W→100° W	0.43	-0.50
32	MAMJ (-1)	Indian	00° →05° S	70° E→60° E	-0.35	Pacific	20° N→10° N	110° W→100° W	0.43	-0.51
33	MAMJ (-1)	Pacific	30° S→44° S	110° W→90° W	-0.43	Pacific	20° N→10° N	110° W→100° W	0.43	-0.47
34	MAMJ (-1)	Pacific	05° N→05° S	110° E→150° E	-0.35	Pacific	20° N→10° N	110° W→100° W	0.43	-0.46
35	MAMJ (-1)	Indian	05° N→02° S	60° E→70° E	-0.36	Pacific	20° N→10° N	110° W→100° W	0.43	-0.52
36	JASO (-1)	Pacific	20° S→35° S	140° W→100° W	-0.44	Pacific	15° N→10° N	120° W→100° W	0.43	-0.54
37	ASON (-1)	Guinea			0.61					
38	NDJF (0)	Pacific	25° S→40° S	80° W→75° W	-0.46	Pacific	50° N→20° N	120° E→160° E	0.47	-0.56
39	NDJF (0)	Pacific	12° S→20° S	105° W→90° W	-0.47	Indian	22° N→10° N	110° E→115° E	0.45	-0.66
40	NDJF (0)	Pacific	25° S→40° S	80° W→75° W	-0.46	Indian	22° N→10° N	110° E→115° E	0.45	-0.62
41	NDJF (0)	Pacific	12° S→20° S	105° W→90° W	-0.47	Pacific	50° N→20° N	120° E→160° E	0.47	-0.63
42	NDJF (0)	Pacific	25° S→40° S	80° W→75° W	-0.46	Pacific	50° N→20° N	120° E→160° E	0.47	-0.62
43	NDJF (0)	Pacific	50° N→42° N	155° W→145° W	-0.37	Pacific	50° N→20° N	120° E→160° E	0.47	-0.54
44	NDJF (0)	Pacific	12° S→20° S	105° W→90° W	-0.47	Atlantic	10° N→00°	60° W→40° W	0.46	-0.55

Appendix B_4 (Cont.)

NO.	LEAD-SEASON	LOCATION	LATITUDE	LONGITUDE	CORR	LOCATION	LATITUDE	LONGITUDE	CORR	SEESAW CORR.
45	MAMJ (0)	Indian	30° S→40° S	30° E→65° E	-0.46	Pacific	30° N→25° N	140° E→160° E	0.52	-0.62
46	MAMJ (0)	Pacific	02° N→05° S	130° W→90° W	-0.52	Pacific	30° N→25° N	140° E→160° E	0.52	-0.66
47	MAMJ (0)	Pacific	02° N→05° S	130° W→90° W	-0.52	Pacific	38° N→30° N	179° W→165° W	0.37	-0.55
48	MAMJ (0)	Pacific	05° N→20° S	120° W→80° W	-0.51	Pacific	30° N→25° N	140° E→160° E	0.52	-0.66
49	MAMJ (0)	Pacific	05° N→20° S	120° W→80° W	-0.51	Pacific	38° N→30° N	179° W→165° W	0.37	-0.53
50	MAMJ (0)	Pacific	05° N→20° S	120° W→80° W	-0.51	Pacific	20° S→35° S	179° W→160° W	0.37	-0.54
51	MAMJ (0)	Pacific	02° N→05° S	130° W→90° W	-0.52	Pacific	30° N→25° N	140° E→160° E	0.52	-0.66
52	MAMJ (0)	Pacific	02° N→05° S	130° W→90° W	-0.52	Pacific	35° N→25° N	179° W→160° W	0.34	-0.53
53	MAMJ (0)	Pacific	02° N→05° S	130° W→90° W	-0.52	Pacific	20° S→35° S	179° W→160° W	0.37	-0.54
54	MAMJ (0)	Pacific	02° N→05° S	130° W→90° W	-0.52	Indian	10° S→20° S	110° E→125° E	0.33	-0.55
55	MAMJ (0)	Pacific	05° N→20° S	120° W→80° W	-0.51	Indian	10° S→20° S	110° E→125° E	0.33	-0.59
56	MAMJ (0)	Pacific	02° N→05° S	130° W→90° W	-0.52					
57	MAMJ (0)	Pacific	05° N→20° S	120° W→80° W	-0.52					
58	MayJune (0)	Glob. Tropics	10° N→10° S	00° →360° W	-0.51					
59	AMJ (0)	CTI	06° N→06° S	180° W→90° W	-0.54					
60	AprMay (0)	Darwin	12° S	131° E	-0.47					
61	MAMJ (0)	Pacific	10° S→20° S	100° W→90° W	-0.49	Pacific	20° S	165° E	0.25	-0.50

APPENDIX C

CORRELATION OF SLIDING WINDOWS

Fig. C_1. The changes in correlation coefficients as a function of time between the Sobat River flows and various predictors (predictors are numbered as in Table 6-1). Correlations were computed in 31-, 25-, and 21-year running windows. Horizontal dotted line shows correlation significant at 5% level. Note that all correlations have been plotted downward regardless of their signs.

Correlations of Predictor (1) and Sobat river flows 31-year sliding windows

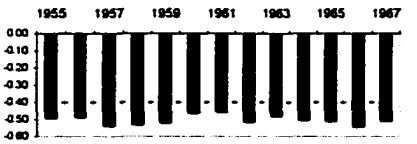

Correlations of Predictor (1) and Sobat river flows 25-year sliding windows

Correlations of Predictor (1) and Sobat river flows 21-

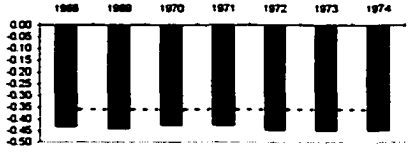

Correlations of Predictor (2) and Sobat river flows 31-year sliding windows

Correlations of Predictor (2) and Sobat river flows 25-year sliding windows

Correlations of Predictor (2) and Sobat river flows 21-year sliding windows

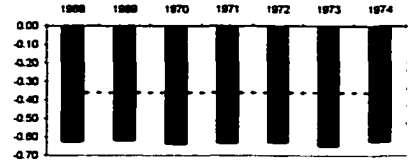

Correlations of Predictor (3) and Sobat river flows 31-year sliding windows

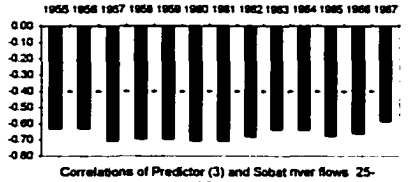

Correlations of Predictor (3) and Sobat river flows 25-year sliding windows

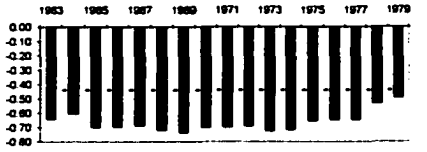

Correlations of Predictor (3) and Sobat river flows 21-year sliding windows

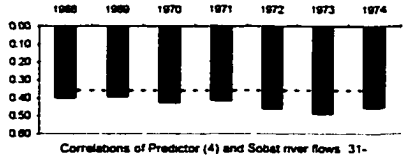

Correlations of Predictor (4) and Sobat river flows 31-year sliding windows

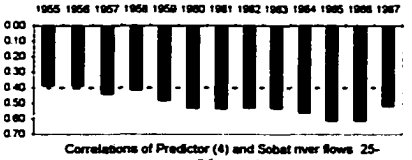

Correlations of Predictor (4) and Sobat river flows 25-year sliding windows

Fig. Correlations of Predictor (4) and Sobat river flows 21-year sliding windows

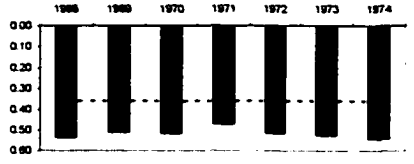

Correlations of Predictor (5) and Sobat river flows 31-year sliding windows

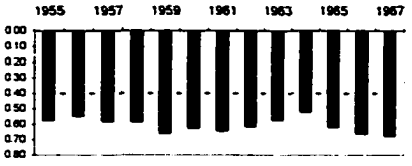

Correlations of Predictor (5) and Sobat river flows 25-year sliding windows

Correlations of Predictor (5) and Sobat river flows 21-year sliding windows

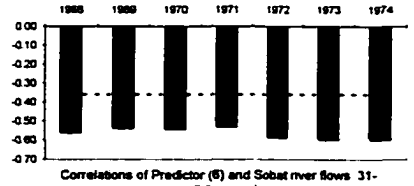

Correlations of Predictor (6) and Sobat river flows 31-year sliding windows

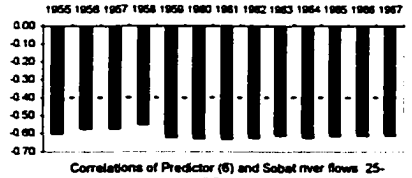

Correlations of Predictor (6) and Sobat river flows 25-year sliding windows

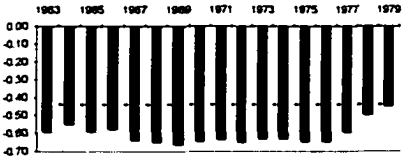

Correlations of Predictor (6) and Sobat river flows 21-year sliding windows

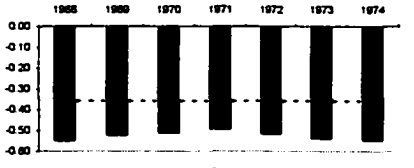

Correlations of Predictor (7) and Sobat river flows 31-year sliding windows

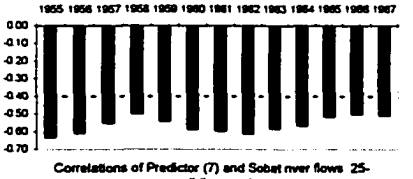

Correlations of Predictor (7) and Sobat river flows 25-year sliding windows

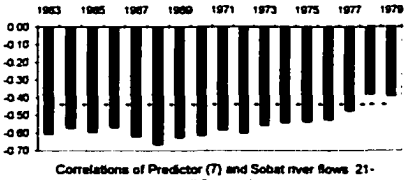

Correlations of Predictor (7) and Sobat river flows 21-year sliding windows

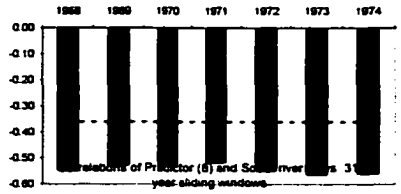

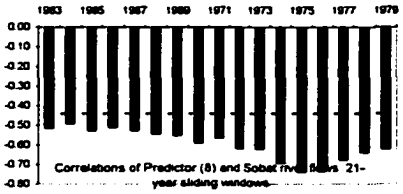

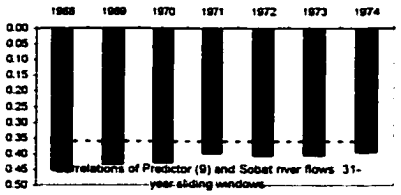

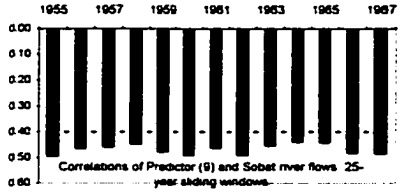

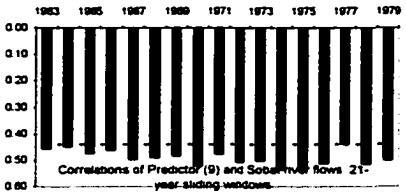

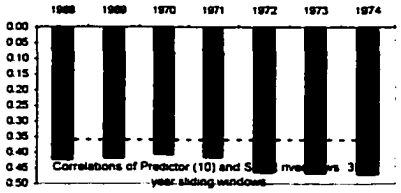

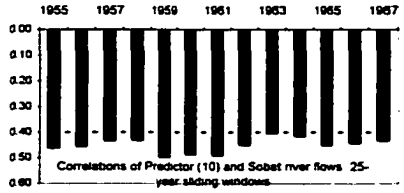

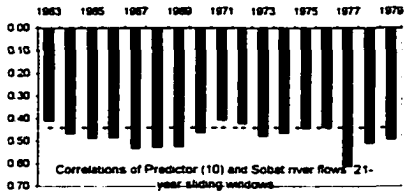

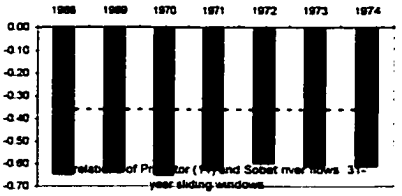

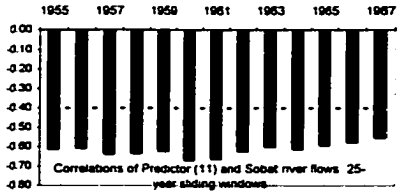

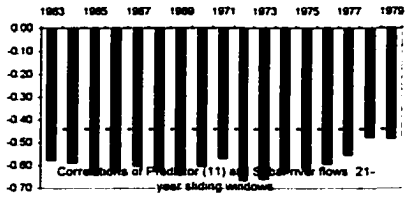

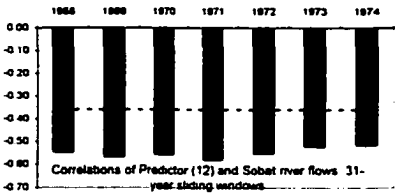

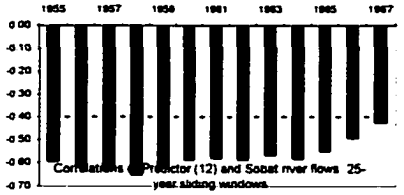

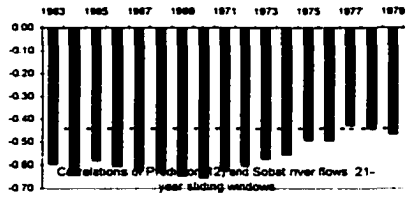

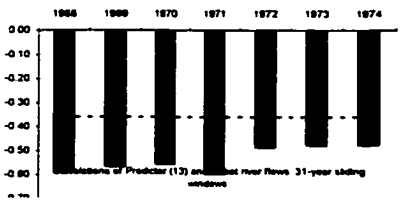

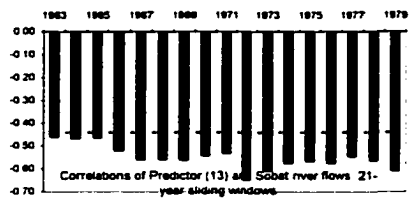

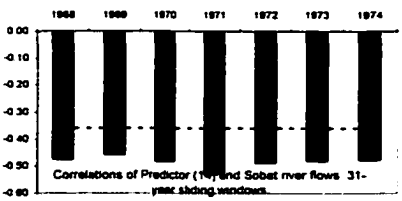

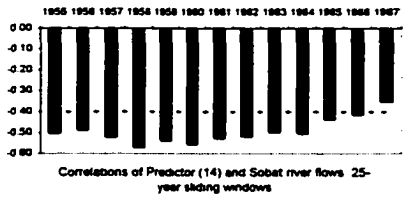

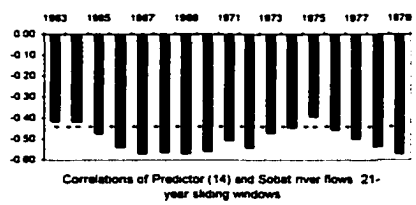

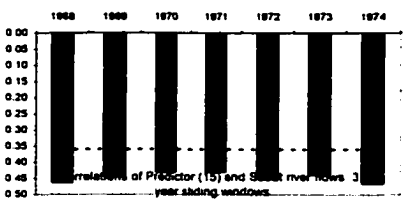

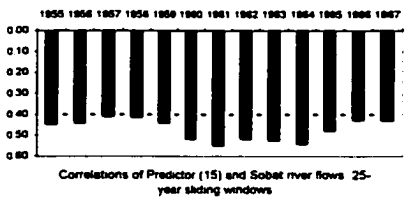

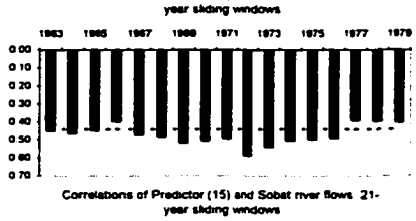

Fig. C_2. The changes in correlation coefficients as a function of time between the Blue Nile River flows and various predictors (predictors are numbered as in Table 6-2). Correlations were computed in 31-, 25-, and 21-year running windows. Horizontal dotted line shows correlation significant at 5% level. Note that all correlations have been plotted downward regardless of their signs.

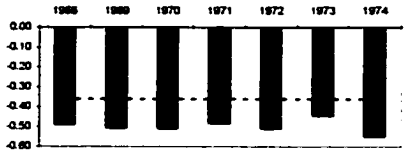

Correlations of Jakarata SLP and Blue Nile flows 31-year sliding windows

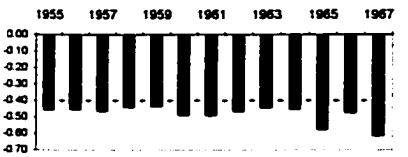

Correlations of Jakarata SLP and Blue Nile flows 25-year sliding windows

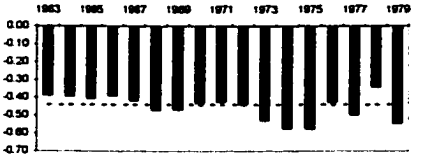

Correlations of Jakarata SLP and Blue Nile flows 21-year sliding windows

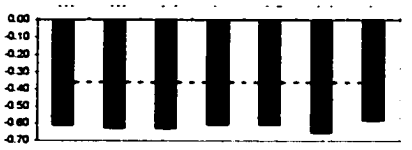

Correlations of Predictor (2) and Blue Nile flows 31-year sliding windows

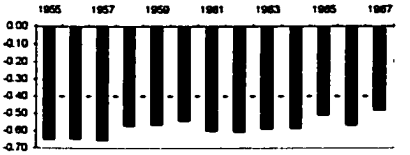

Correlations of Predictor (2) and Blue Nile flows 25-year sliding windows

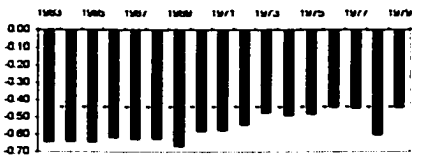

Correlations of Predictor (2) and Blue Nile flows 21-year sliding windows

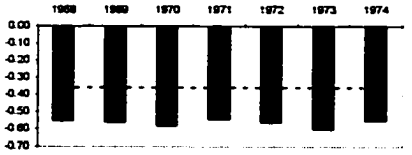

Correlations of Predictor (3) and Blue Nile flows 31-year sliding windows

Correlations of Predictor (3) and Blue Nile flows 25-year sliding windows

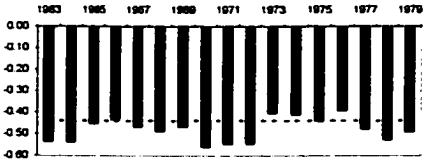

Correlations of Predictor (3) and Blue Nile flows 21-year sliding windows

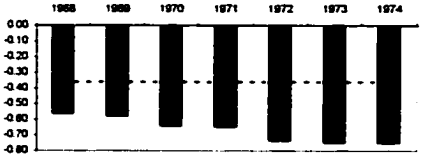

Correlations of Predictor (4) and Blue Nile flows 31-year sliding windows

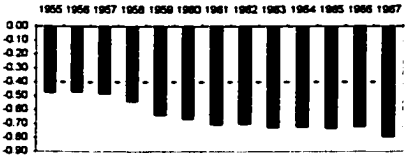

Correlations of Predictor (4) and Blue Nile flows 25-year sliding windows

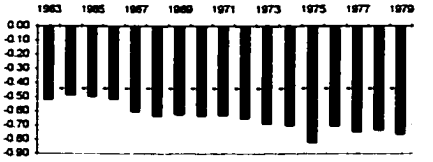

Correlations of Predictor (4) and Blue Nile flows 21-year sliding windows

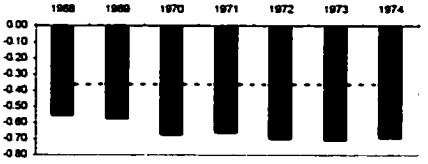

Correlations of Predictor (5) and Blue Nile flows 31-year sliding windows

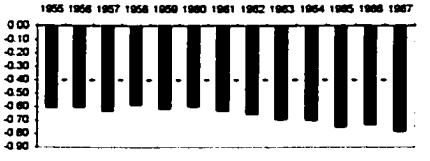

Correlations of Predictor (5) and Blue Nile flows 25-year sliding windows

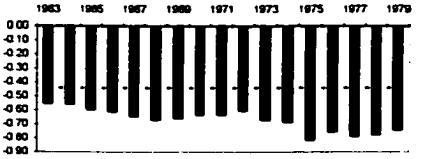

Correlations of Predictor (5) and Blue Nile flows 21-year sliding windows

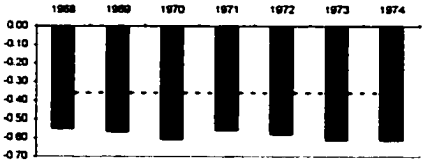

Correlations of Predictor (6) and Blue Nile flows 31-year sliding windows

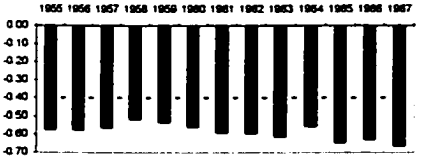

Correlations of Predictor (6) and Blue Nile flows 25-year sliding windows

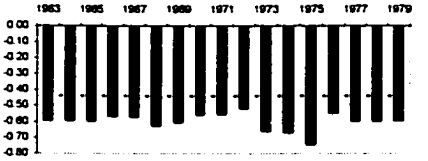

Correlations of Predictor (6) and Blue Nile flows 21-year sliding windows

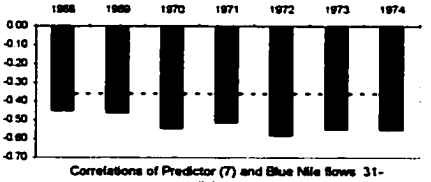

Correlations of Predictor (7) and Blue Nile flows 31-year sliding windows

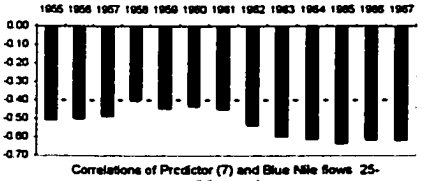

Correlations of Predictor (7) and Blue Nile flows 25-year sliding windows

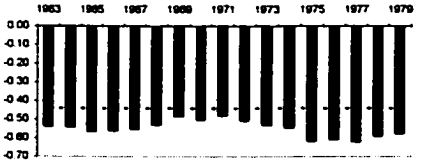

Correlations of Predictor (7) and Blue Nile flows 21-year sliding windows

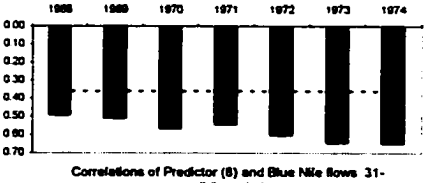

Correlations of Predictor (8) and Blue Nile flows 31-year sliding windows

Correlations of Predictor (8) and Blue Nile flows 25-year sliding windows

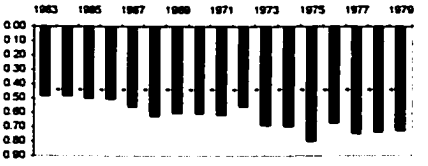

Correlations of Predictor (8) and Blue Nile flows 21-year sliding windows

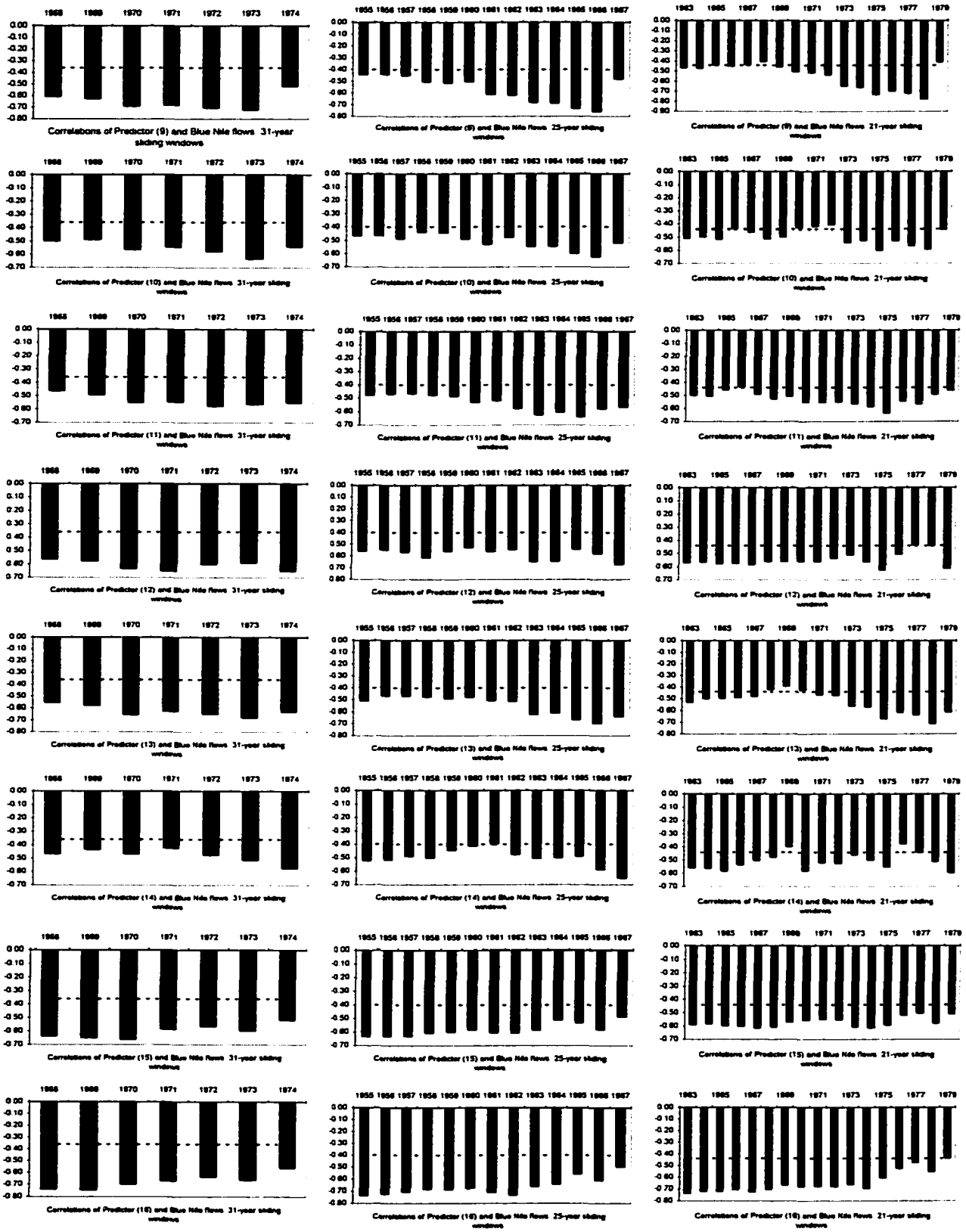

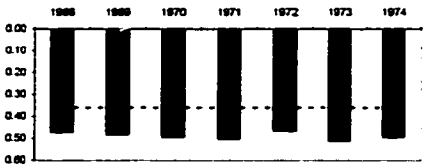

Correlations of Predictor (17) and Blue Nile flows 31-year sliding windows

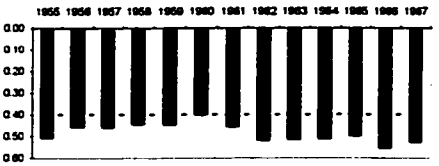

Correlations of Predictor (17) and Blue Nile flows 25-year sliding windows

Correlations of Predictor (17) and Blue Nile flows 21-year sliding windows

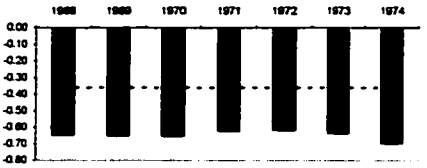

Correlations of Predictor (18) and Blue Nile flows 31-year sliding windows

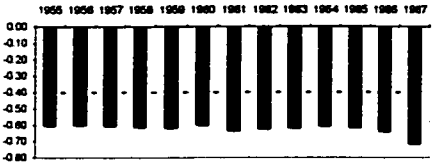

Correlations of Predictor (18) and Blue Nile flows 25-year sliding windows

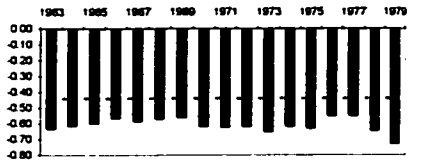

Correlations of Predictor (18) and Blue Nile flows 21-year sliding windows

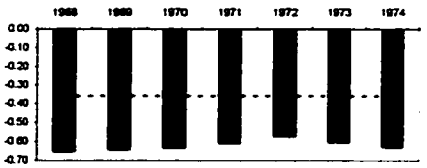

Correlations of Predictor (19) and Blue Nile flows 31-year sliding windows

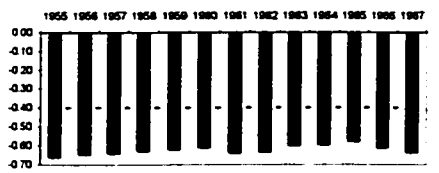

Correlations of Predictor (19) and Blue Nile flows 25-year sliding windows

Correlations of Predictor (19) and Blue Nile flows 21-year sliding windows

Correlations of Predictor (20) and Blue Nile flows 31-year sliding windows

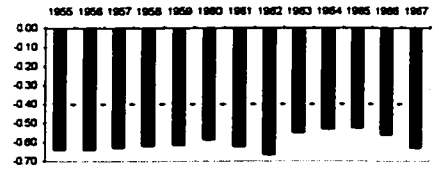

Correlations of Predictor (20) and Blue Nile flows 25-year sliding windows

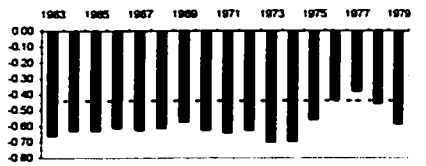

Correlations of Predictor (20) and Blue Nile flows 21-year sliding windows

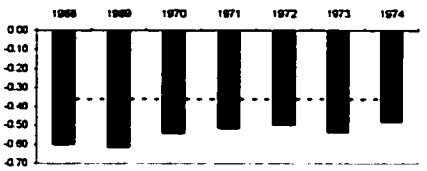

Correlations of Predictor (21) and Blue Nile flows 31-year sliding windows

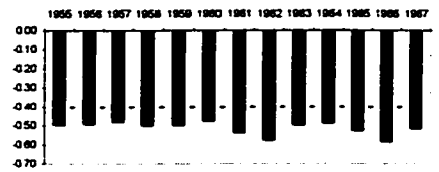

Correlations of Predictor (21) and Blue Nile flows 25-year sliding windows

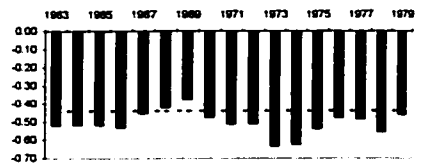

Correlations of Predictor (21) and Blue Nile flows 21-year sliding windows

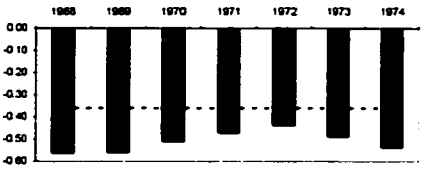

Correlations of Predictor (22) and Blue Nile flows 31-year sliding windows

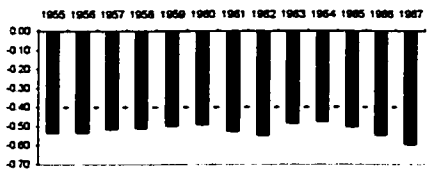

Correlations of Predictor (22) and Blue Nile flows 25-year sliding windows

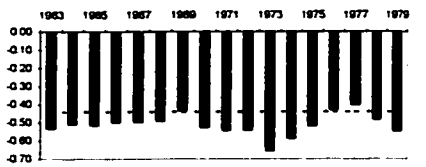

Correlations of Predictor (22) and Blue Nile flows 21-year sliding windows

Fig. C_3. The changes in correlation coefficients as a function of time between the Atbara River flows and various predictors (predictors are numbered as in Table 6-3). Correlations were computed in 31-, 25-, and 21-year running windows. Horizontal dotted line shows correlation significant at 5% level. Note that all correlations have been plotted downward regardless of their signs.

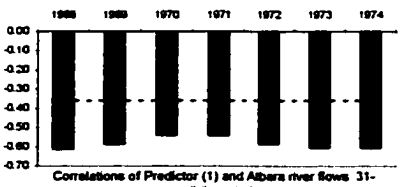

Correlations of Predictor (1) and Albara river flows 31-year sliding windows

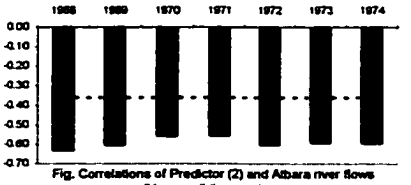

Fig. Correlations of Predictor (2) and Albara river flows 31-year sliding windows

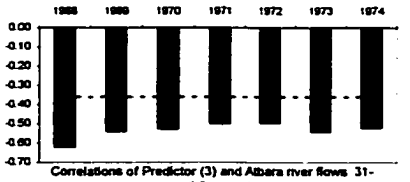

Correlations of Predictor (3) and Albara river flows 31-year sliding windows

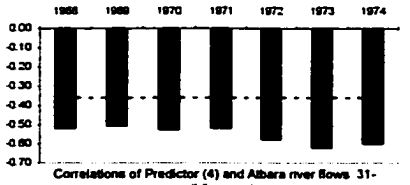

Correlations of Predictor (4) and Albara river flows 31-year sliding windows

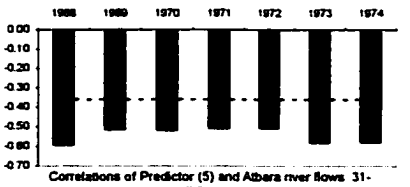

Correlations of Predictor (5) and Albara river flows 31-year sliding windows

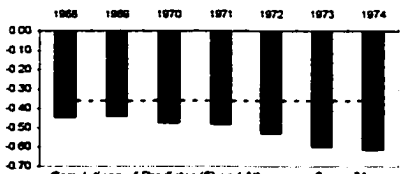

Correlations of Predictor (6) and Albara river flows 31-year sliding windows

Correlations of Predictor (7) and Albara river flows 31-year sliding windows

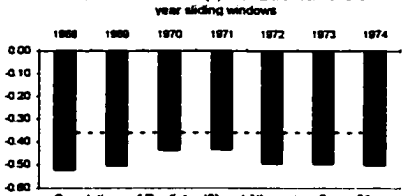

Correlations of Predictor (8) and Albara river flows 31-year sliding windows

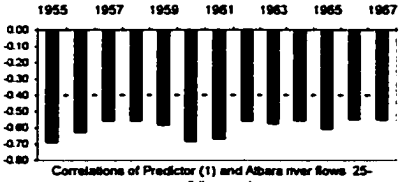

Correlations of Predictor (1) and Albara river flows 25-year sliding windows

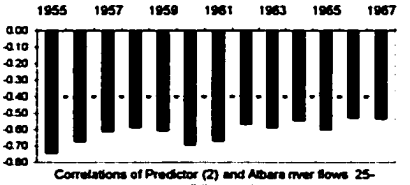

Correlations of Predictor (2) and Albara river flows 25-year sliding windows

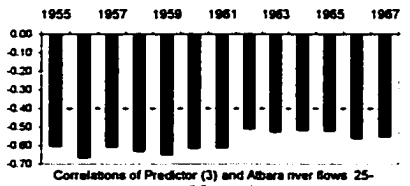

Correlations of Predictor (3) and Albara river flows 25-year sliding windows

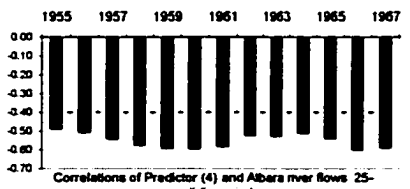

Correlations of Predictor (4) and Albara river flows 25-year sliding windows

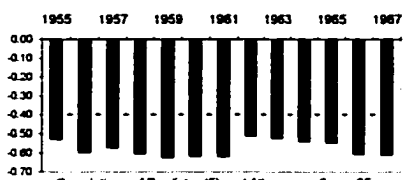

Correlations of Predictor (5) and Albara river flows 25-year sliding windows

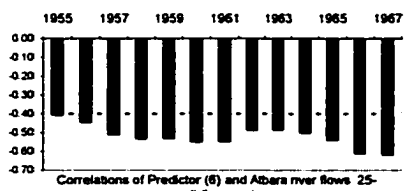

Correlations of Predictor (6) and Albara river flows 25-year sliding windows

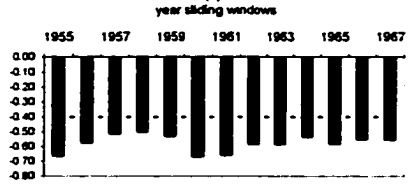

Correlations of Predictor (7) and Albara river flows 25-year sliding windows

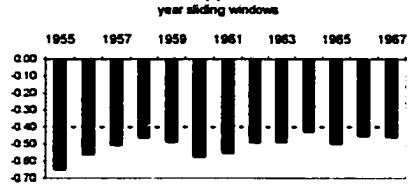

Correlations of Predictor (8) and Albara river flows 25-year sliding windows

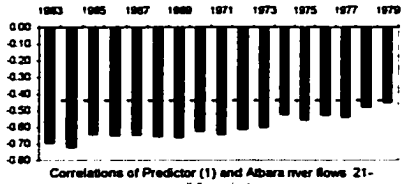

Correlations of Predictor (1) and Albara river flows 21-year sliding windows

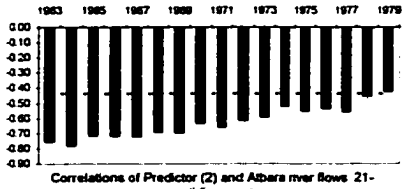

Correlations of Predictor (2) and Albara river flows 21-year sliding windows

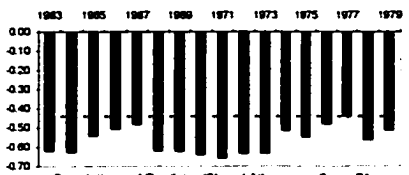

Correlations of Predictor (3) and Albara river flows 21-year sliding windows

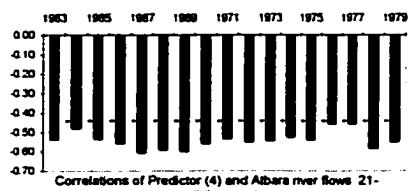

Correlations of Predictor (4) and Albara river flows 21-year sliding windows

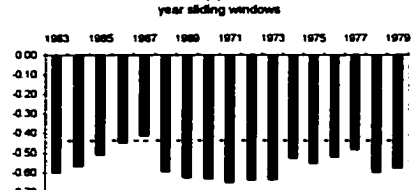

Correlations of Predictor (5) and Albara river flows 21-year sliding windows

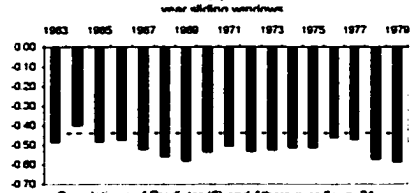

Correlations of Predictor (6) and Albara river flows 21-year sliding windows

Correlations of Predictor (7) and Albara river flows 21-year sliding windows

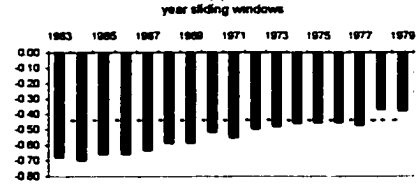

Correlations of Predictor (8) and Albara river flows 21-year sliding windows

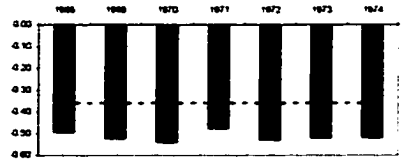

Correlations of Predictor (9) and Atbara river flows 31-year sliding windows

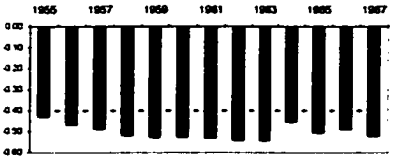

Correlations of Predictor (9) and Atbara river flows 25-year sliding windows

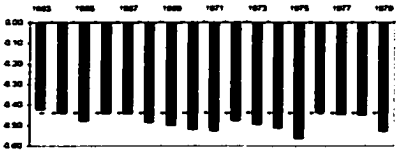

Correlations of Predictor (9) and Atbara river flows 21-year sliding windows

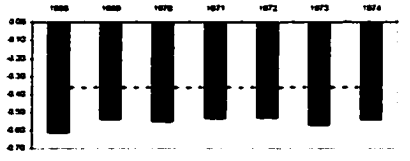

Correlations of Predictor (10) and Atbara river flows 31-year sliding windows

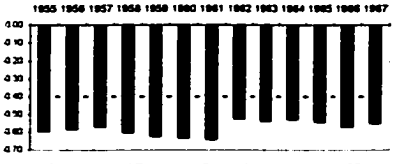

Correlations of Predictor (10) and Atbara river flows 25-year sliding windows

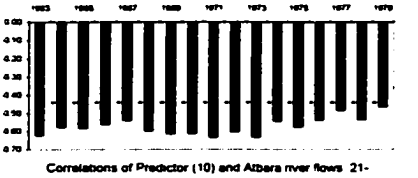

Correlations of Predictor (10) and Atbara river flows 21-year sliding windows

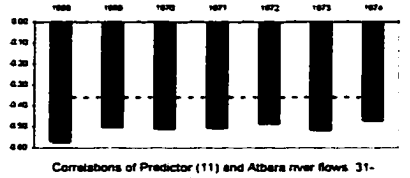

Correlations of Predictor (11) and Atbara river flows 31-year sliding windows

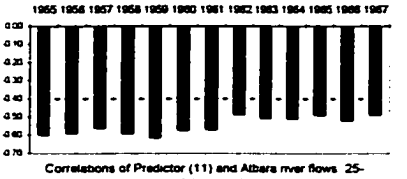

Correlations of Predictor (11) and Atbara river flows 25-year sliding windows

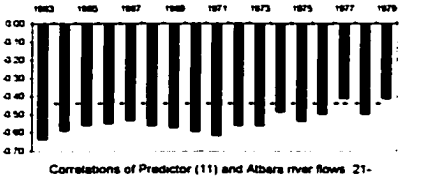

Correlations of Predictor (11) and Atbara river flows 21-year sliding windows

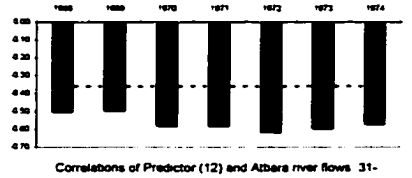

Correlations of Predictor (12) and Atbara river flows 31-year sliding windows

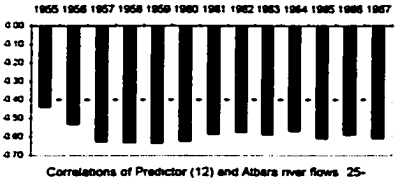

Correlations of Predictor (12) and Atbara river flows 25-year sliding windows

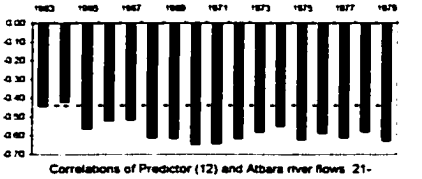

Correlations of Predictor (12) and Atbara river flows 21-year sliding windows

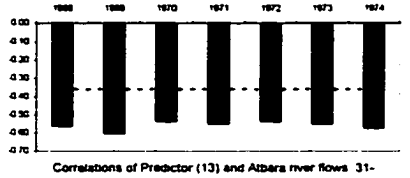

Correlations of Predictor (13) and Atbara river flows 31-year sliding windows

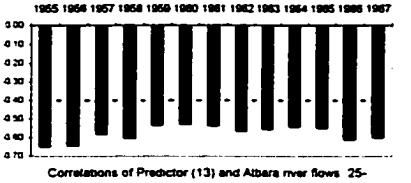

Correlations of Predictor (13) and Atbara river flows 25-year sliding windows

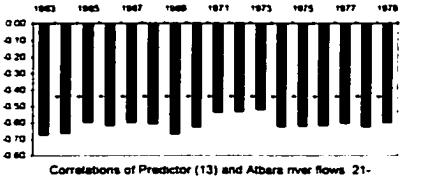

Correlations of Predictor (13) and Atbara river flows 21-year sliding windows

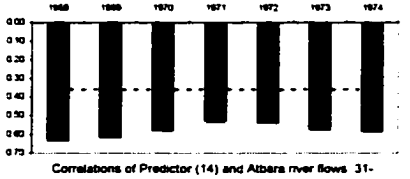

Correlations of Predictor (14) and Atbara river flows 31-year sliding windows

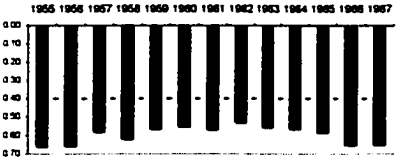

Correlations of Predictor (14) and Atbara river flows 25-year sliding windows

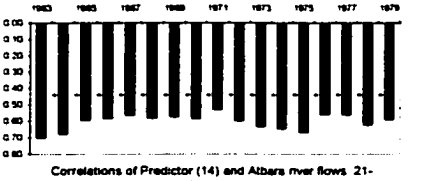

Correlations of Predictor (14) and Atbara river flows 21-year sliding windows

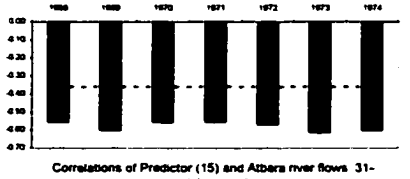

Correlations of Predictor (15) and Atbara river flows 31-year sliding windows

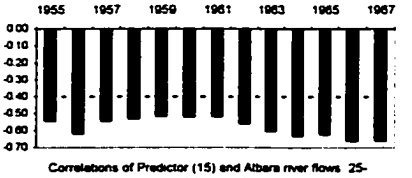

Correlations of Predictor (15) and Atbara river flows 25-year sliding windows

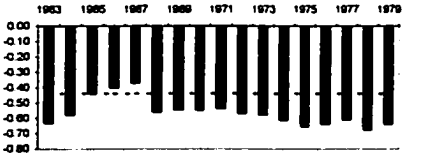

Correlations of Predictor (15) and Atbara river flows 21-year sliding windows

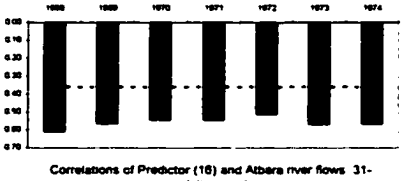

Correlations of Predictor (16) and Atbara river flows 31-year sliding windows

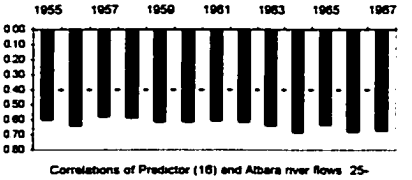

Correlations of Predictor (16) and Atbara river flows 25-year sliding windows

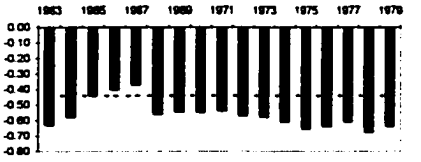

Correlations of Predictor (16) and Atbara river flows 21-year sliding windows

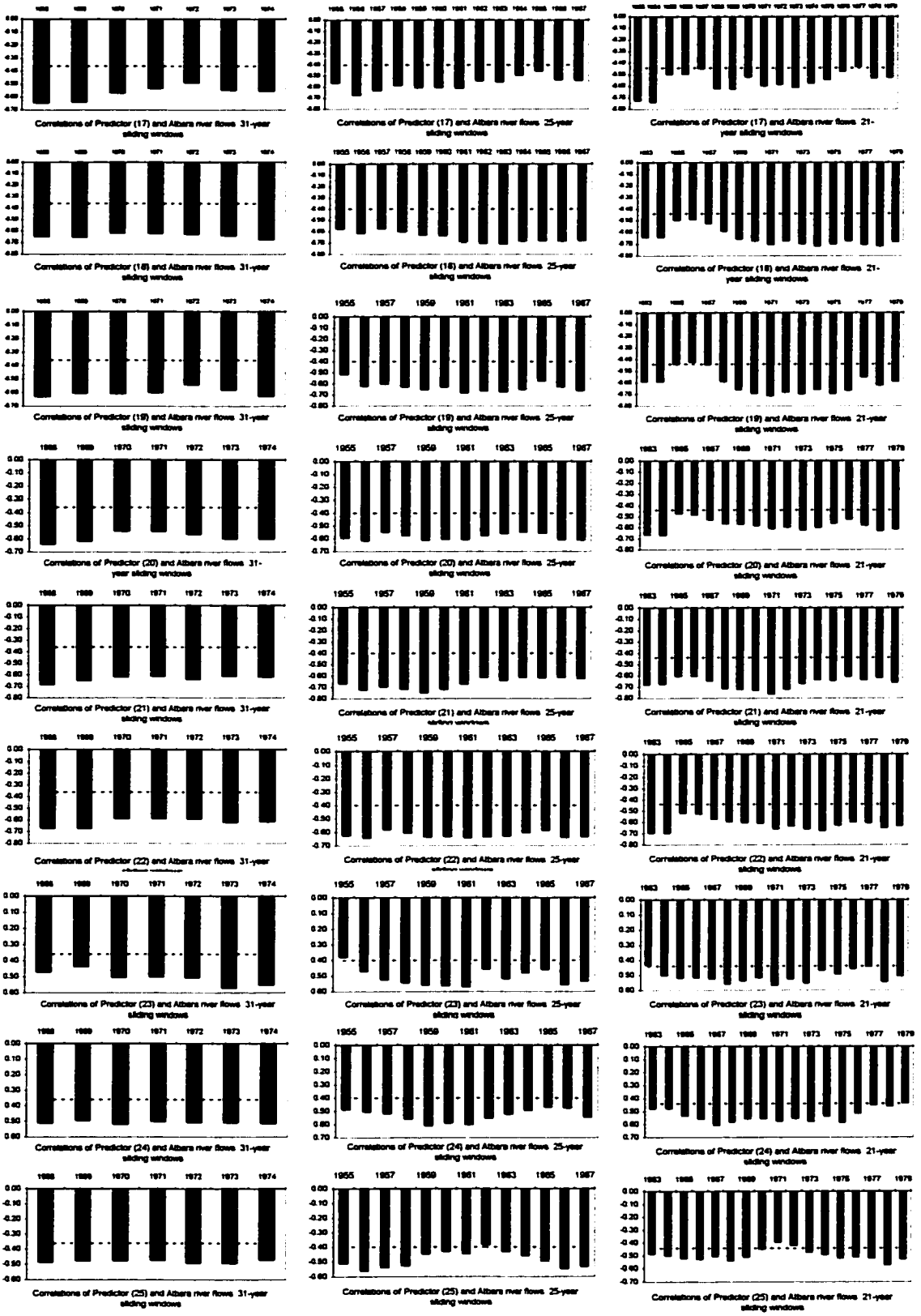

Fig. C_4. The changes in correlation coefficients as a function of time between the Nile river at Aswan flows and various predictors (predictors are numbered as in Table 6-4). Correlations were computed in 31-, 25-, and 21-year running windows. Horizontal dotted line shows correlation significant at 5% level. Note that all correlations have been plotted downward regardless of their signs.

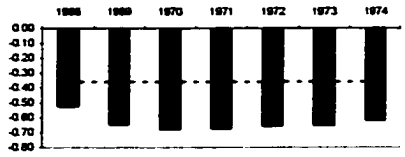

Correlations of Predictor (1) and Main Nile flows 31-year sliding windows

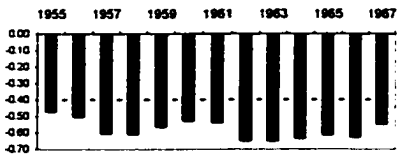

Correlations of Predictor (1) and Main Nile flows 25-year sliding windows

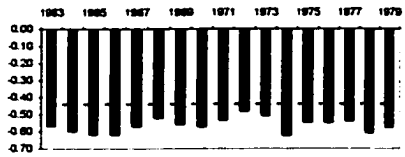

Correlations of Predictor (1) and Main Nile flows 21-year sliding windows

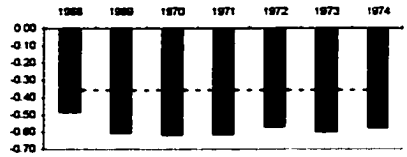

Correlations of Predictor (2) and Main Nile flows 31-year sliding windows

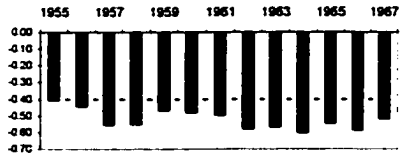

Correlations of Predictor (2) and Main Nile flows 25-year sliding windows

Correlations of Predictor (2) and Main Nile flows 21-year sliding windows

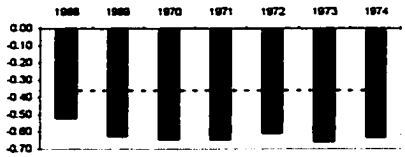

Correlations of Predictor (3) and Main Nile flows 31-year sliding windows

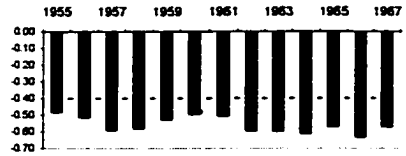

Correlations of Predictor (3) and Main Nile flows 25-year sliding windows

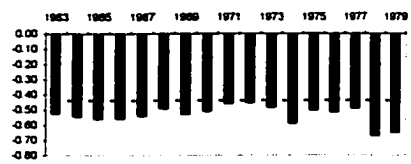

Correlations of Predictor (3) and Main Nile flows 21-year sliding windows

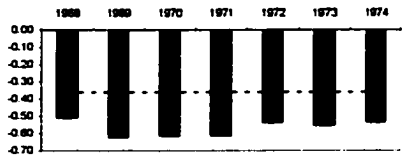

Correlations of Predictor (4) and Main Nile flows 31-year sliding windows

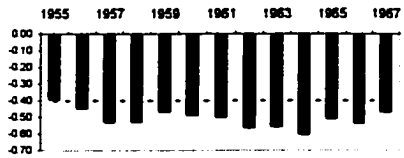

Correlations of Predictor (4) and Main Nile flows 25-year sliding windows

Correlations of Predictor (4) and Main Nile flows 21-year sliding windows

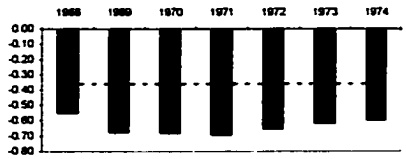

Correlations of Predictor (5) and Main Nile flows 31-year sliding windows

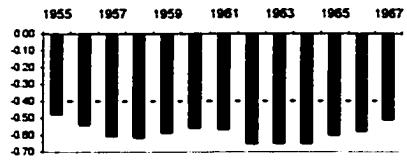

Correlations of Predictor (5) and Main Nile flows 25-year sliding windows

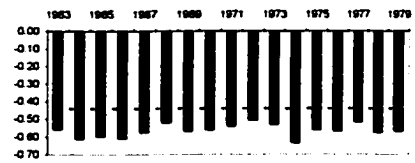

Correlations of Predictor (5) and Main Nile flows 21-year sliding windows

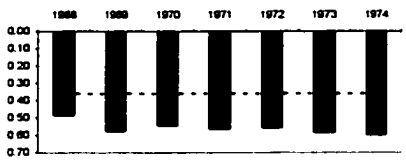

Correlations of Predictor (6) and Main Nile flows 31-year sliding windows

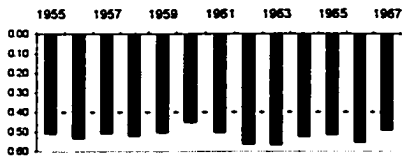

Correlations of Predictor (6) and Main Nile flows 25-year sliding windows

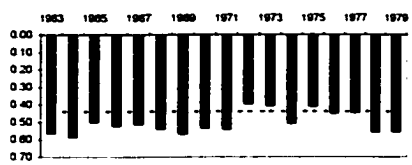

Correlations of Predictor (6) and Main Nile flows 21-year sliding windows

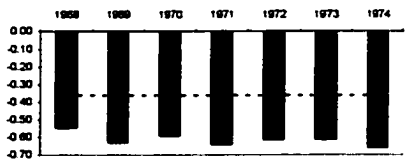

Correlations of Predictor (7) and Main Nile flows 31-year sliding windows

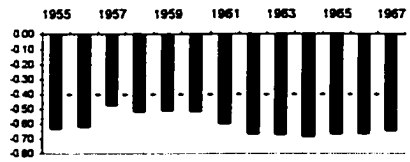

Correlations of Predictor (7) and Main Nile flows 25-year sliding windows

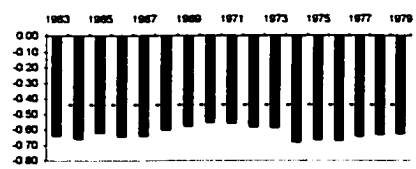

Correlations of Predictor (7) and Main Nile flows 21-year sliding windows

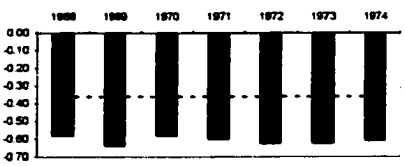

Correlations of Predictor (8) and Main Nile flows 31-year sliding windows

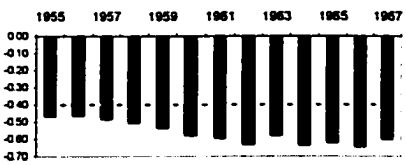

Correlations of Predictor (8) and Main Nile flows 25-year sliding windows

Correlations of Predictor (8) and Main Nile flows 21-year sliding windows

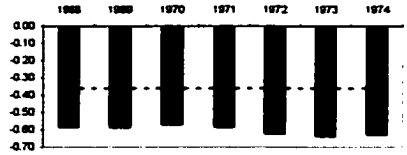

Correlations of Predictor (9) and Main Nile flows 31-year sliding windows

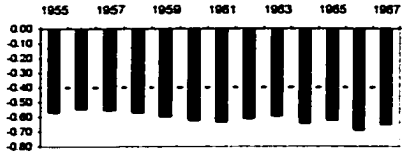

Correlations of Predictor (9) and Main Nile flows 25-year sliding windows

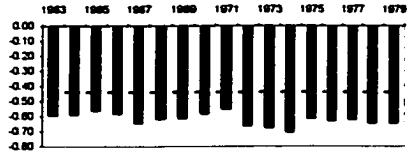

Correlations of Predictor (9) and Main Nile flows 21-year sliding windows

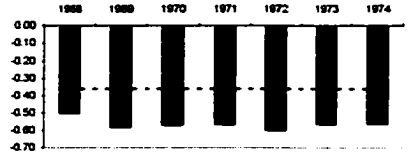

Correlations of Predictor (10) and Main Nile flows 31-year sliding windows

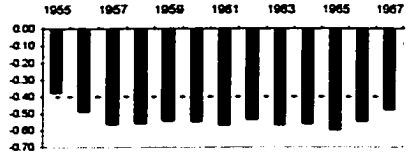

Correlations of Predictor (10) and Main Nile flows 25-year sliding windows

Fig. Correlations of Predictor (10) and Main Nile flows 21-year sliding windows

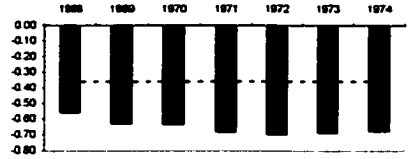

Correlations of Predictor (11) and Main Nile flows 31-year sliding windows

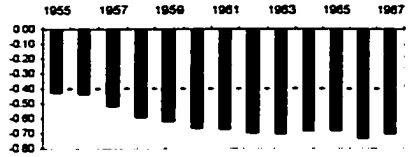

Correlations of Predictor (11) and Main Nile flows 25-year sliding windows

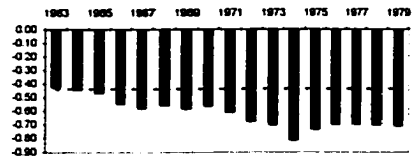

Correlations of Predictor (11) and Main Nile flows 21-year sliding windows

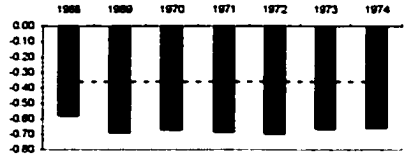

Correlations of Predictor (12) and Main Nile flows 31-year sliding windows

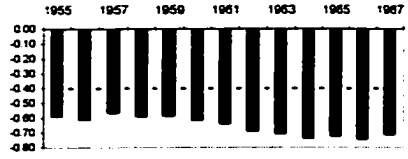

Correlations of Predictor (12) and Main Nile flows 25-year sliding windows

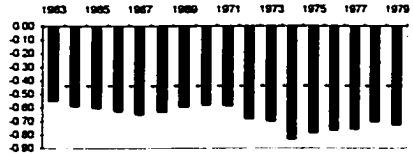

Fig. Correlations of Predictor (12) and Main Nile flows 21-year sliding windows

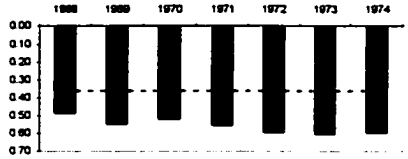

Correlations of Predictor (13) and Main Nile flows 31-year sliding windows

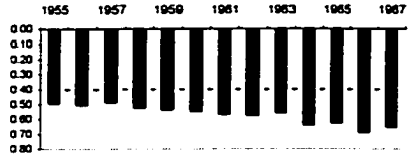

Correlations of Predictor (13) and Main Nile flows 25-year sliding windows

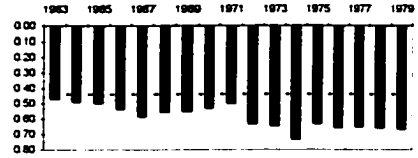

Correlations of Predictor (13) and Main Nile flows 21-year sliding windows

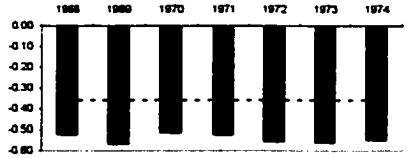

Correlations of Predictor (14) and Main Nile flows 31-year sliding windows

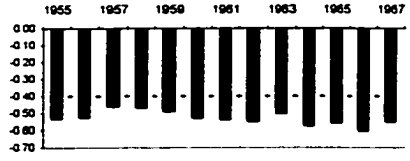

Correlations of Predictor (14) and Main Nile flows 25-year sliding windows

Correlations of Predictor (14) and Main Nile flows 21-year sliding windows

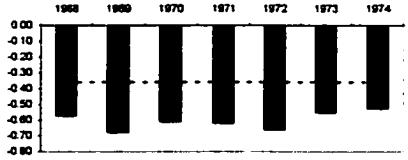

Correlations of Predictor (15) and Main Nile flows 31-year sliding windows

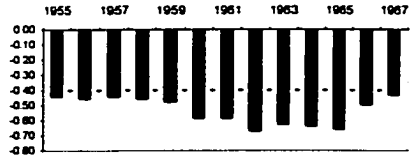

Correlations of Predictor (15) and Main Nile flows 25-year sliding windows

Correlations of Predictor (15) and Main Nile flows 21-year sliding windows

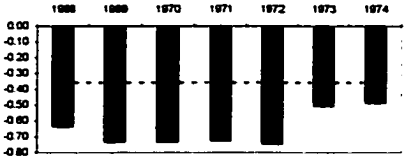

Correlations of Predictor (16) and Main Nile flows 31-year sliding windows

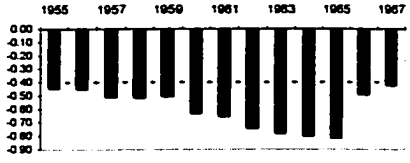

Correlations of Predictor (16) and Main Nile flows 25-year sliding windows

Correlations of Predictor (16) and Main Nile flows 21-year sliding windows

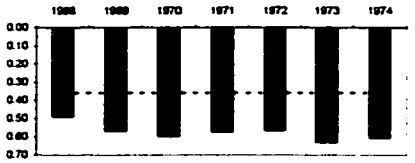

Correlations of Predictor (17) and Main Nile flows 31-year sliding windows

Correlations of Predictor (17) and Main Nile flows 25-year sliding windows

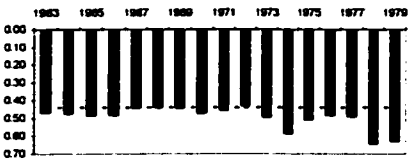

Correlations of Predictor (17) and Main Nile flows 21-year sliding windows

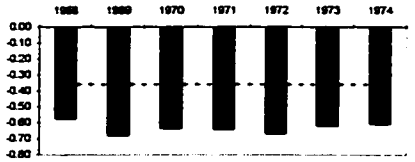

Correlations of Predictor (18) and Main Nile flows 31-year sliding windows

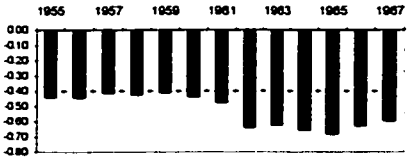

Correlations of Predictor (18) and Main Nile flows 25-year sliding windows

Fig. Correlations of Predictor (18) and Main Nile flows 21-year sliding windows

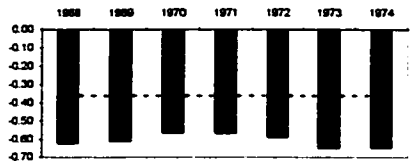

Correlations of Predictor (19) and Main Nile flows 31-year sliding windows

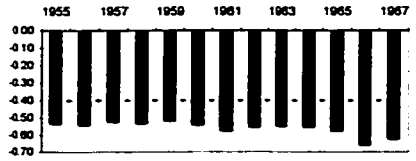

Correlations of Predictor (19) and Main Nile flows 25-year sliding windows

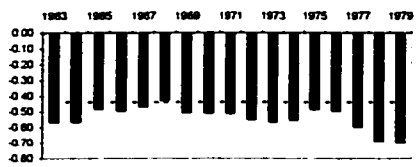

Correlations of Predictor (19) and Main Nile flows 21-year sliding windows

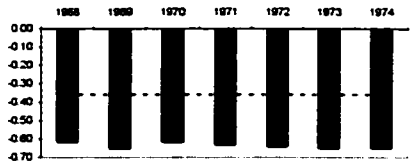

Correlations of Predictor (20) and Main Nile flows 31-year sliding windows

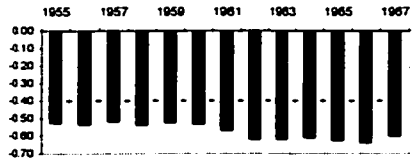

Correlations of Predictor (20) and Main Nile flows 25-year sliding windows

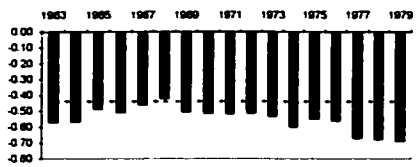

Correlations of Predictor (20) and Main Nile flows 21-year sliding windows

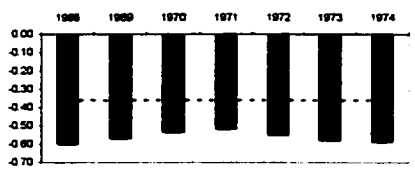

Correlations of Predictor (21) and Main Nile flows 31-year sliding windows

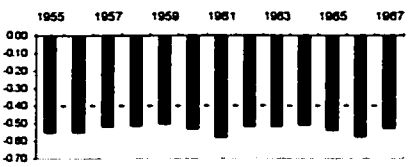

Correlations of Predictor (21) and Main Nile flows 25-year sliding windows

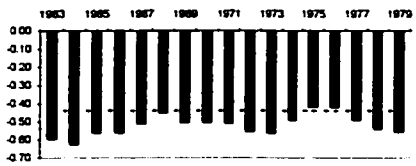

Correlations of Predictor (21) and Main Nile flows 21-year sliding windows

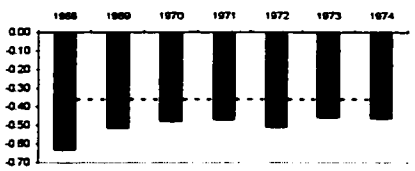

Correlations of Predictor (22) and Main Nile flows 31-year sliding windows

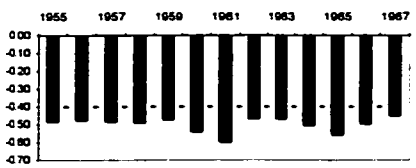

Correlations of Predictor (22) and Main Nile flows 25-year sliding windows

Correlations of Predictor (22) and Main Nile flows 21-year sliding windows

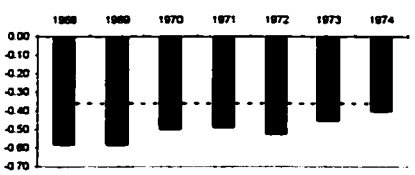

Correlations of Predictor (23) and Main Nile flows 31-year sliding windows

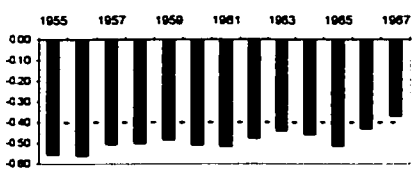

Correlations of Predictor (23) and Main Nile flows 25-year sliding windows

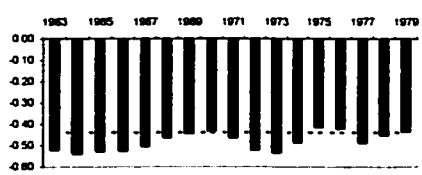

Correlations of Predictor (23) and Main Nile flows 21-year sliding windows